

The interplay between surface processes and tectonics in the actively extending central Italian Apennines

Anneleen H. Geurts

Thesis for the degree of Philosophiae Doctor (PhD)
University of Bergen, Norway
2020

UNIVERSITY OF BERGEN



The interplay between surface processes and tectonics in the actively extending central Italian Apennines

Anneleen H. Geurts



Thesis for the degree of Philosophiae Doctor (PhD)
at the University of Bergen

Date of defense: 08.06.2020

© Copyright Anneleen H. Geurts

The material in this publication is covered by the provisions of the Copyright Act.

Year: 2020

Title: The interplay between surface processes and tectonics in the actively extending central Italian Apennines

Name: Anneleen H. Geurts

Print: Skipnes Kommunikasjon / University of Bergen

I dedicate this work to the memory
of my supervisor, Patience Cowie



Preface

This thesis for the degree of Philosophiae Doctor (PhD) has been submitted to the Department of Earth Sciences at the University of Bergen (Bergen, Norway). The research presented herein has been funded by Bergen University where it was carried out under the principal supervision of Prof. Patience Cowie, and co-supervision of Prof. Ritske Huisman and Prof. Rob Gawthorpe between February 2013 and March 2020. Additional financial support has been provided by the University of Bergen, the Meltzer Research Fund and the *Akademiaavtalen* for expenses related to fieldwork and international conferences and workshops.

The thesis is structured according to the Norwegian guidelines for doctoral dissertations in natural sciences, where the main part of the thesis consists of scientific papers that have been either published or submitted to international peer-reviewed journals. The thesis is divided into three parts: The first part provides the introduction to the research project, an outline of the research objectives and the geological setting of the main study area (Chapters 1 and 2). Part two of the thesis contains the main research results, which are presented in three scientific papers (Chapters 3, 4 and 5). The first two papers have already been published in the journals of *Basin Research* and *Geomorphology*. The third paper is prepared to be submitted to the journal of *Earth and Planetary Science Letters*. The main findings from these papers are summarised and synthesised in part three of the thesis, where also prospects for future research are provided (Chapters 6, 7 and 8). Because the three papers making up the main body of the thesis have been published in or will be submitted to different scientific journals, the template of literature references and figures varies between them.

Anneleen Geurts

Bergen, March 23rd, 2020

Contents

Preface	5
Contents	7
Acknowledgements	9
Abstract	13
1 Thesis introduction	15
1.1. Rationale	15
1.2. The central Apennines continental rift	17
1.3. Surface processes and normal fault activity in continental rifts	20
1.4. Research aims and approach	22
1.5. Thesis outline	23
2 The Central Italian Apennines	27
2.1. Geological setting	27
2.2. Extensional faulting, regional uplift, and high topography	28
2.3. Lithosphere structure and mantle dynamics	33
2.4. Spatial-temporal variability in fault activity	35
2.5. Drainage network and basin stratigraphy	36
3 Paper 1	41
Drainage integration and sediment dispersal in active continental rifts: A numerical modelling study of the central Italian Apennines	
3.1. Abstract	42
3.2. Introduction	43
3.3. Geological setting	45
3.4. Methodology	47
3.5. Results	54
3.6. Discussion	65
3.7. Conclusions	79
3.8. Acknowledgements	82
4 Paper 2	83
Transient landscape and stratigraphic responses to drainage integration in the actively extending central Italian Apennines	
4.1. Abstract	84
4.2. Introduction	85

4.3. Geological setting	89
4.4. Data and methodology	93
4.5. The Aterno River system and associated rift basins	97
4.6. Evolution of the Aterno River system in response to drainage integration	112
4.7. Discussion	115
4.8. Conclusions and implications	128
4.9. Acknowledgements	130
5 Paper 3	131
Dynamic normal fault behaviour and surface uplift in response to mantle lithosphere removal: A numerical modelling study motivated by the central Italian Apennines	
5.1. Introduction	132
5.2. Methodology	134
5.3. Results	138
5.4. Discussion	152
5.5. Conclusions	163
5.6. Acknowledgements	164
6 New insights with focus on the central Apennines	165
6.1. Introduction	165
6.2. Drainage integration: patterns and driving mechanisms	166
6.3. Implications of overspill-driven drainage integration	170
6.4. Mantle-related surface uplift and fault activity	174
7 Wider implications and future perspectives	179
7.1. Towards a process-based understanding of drainage integration in active continental rifts	179
7.2. The impact of drainage integration on sediment dispersal, basin stratigraphy, and transient landscape evolution	184
7.3. Extensional faulting in areas of mantle-induced surface uplift	190
7.4. Future perspectives	192
8 Main conclusions	195
References	197
Appendix I – Supplement to Chapter 3 (Paper 1)	
Appendix II – Supplement to Chapter 4 (Paper 2)	
Appendix III – Supplement to Chapter 5 (Paper 3)	

Acknowledgements

This PhD project started, unofficially, in a mountain cabin in one of Norway's national parks during the international ACDC summer school of 2012. The theme of the summer school was the interaction between surface processes, tectonics and climate, and it was during this awesome summer school that I became fascinated for the fact that rivers not only respond to tectonics, but that sediment displacement and climate can actually affect the structural development of whole mountain ranges. During this summer school I met Ritske Huisman, Vivi Pedersen and Philippe Steer from Bergen University who told me about the open PhD position on the central Apennines. Because Vivi and Philippe told me that I could not imagine a better first supervisor than Patience Cowie, I decided to apply, even though I wasn't sure if my background in lowland river systems was sufficient for this strongly interdisciplinary project.

And yes, Vivi and Philippe were completely right. Patience, I definitely owe most thanks to you. You have been an amazing daily supervisor to me, with your enormous enthusiasm for the Apennines and your interest in and experiences with so many different fields in earth sciences. You taught me how to combine field data analysis with numerical modelling, and made me find out that models with only a limited number of processes could be actually quite useful, even if they didn't really look like the Apennines. It wasn't possible for you to join me during most field seasons, but I regard those three days with you in the Apennines as the highlight of my project. Patience, thanks so much for giving me flexibility while pointing me in the right direction, for teaching me to think more critically, and most of all, for your endless support.

I also want to acknowledge my co-supervisors. First of all, I want to thank Ritske for always making time for me for discussing modelling results, and for his enormous help in run-up to thesis submission. I learned a lot from you and always enjoyed your out-of-the-box 'Why not?' question when unexpected results came out of my model experiments and I presumed these outcomes were not realistic at all. Rob Gawthorpe,

thanks so much for your supervision and great support, in particular with my two drainage integration papers, but also during the final stage of finishing this thesis. I feel very privileged to have been able to work with you and hope there will be an opportunity to learn more from you in the future. Alex Whittaker, thanks so much for your enormous help and great supervision with my field paper. In general, I would like to thank all my supervisors for being patient with my work progress and being supportive during times the combination of work and kids became quite challenging for me.

I was lucky to have been part of a very friendly and supportive research environment at the Department of Earth Science at Bergen University. Many thanks to everyone for their support, varying from short coffee-machine chats to very enjoyable field excursions and courses. Vivi, Guillaume, and Sofia, thanks so much for being such nice office mates, for all good chats and funny moments. Guillaume, also may thanks for joining and helping me in the field, that was really great! Furthermore I owe many thanks to Leo Zijerveld for his tremendous help with setting up and running my models, with finding model bugs, and for his endless interest in my work. Sebastian, Thomas, and Gang, thanks so much for the morning coffee breaks and for regular help with all kinds of modelling issues. Furthermore I want to thank Henk Keers for helping me with my Fourier transform analyses and for cheering me up either with supportive chats, or by bringing me Dutch cheese and cookies!

A general thank you to all international colleagues that I got to know over the last years, and who all contributed in some way to this thesis through scientific discussions. In particular, I would like to thank Luke Wedmore and Laura Gregory for their shared passion for the central Apennines and great discussions. Gerald Roberts, thanks for introducing me into the Apennines during my first field season and Stefano Pucci and Fabio Villano, thanks for your warm welcome at the INGV in Rome. I also want to acknowledge Tomasso Piacentini, for joining me in the field and for sharing your enormous expertise in landscape evolution in the central Apennines. Vivi, Zoltan Erdos and Philip Minderhoud, thanks for great discussions but also for a lot of fun and relaxing (non-scientific) breaks during conference visits.

Finishing this PhD project would not have been possible without the long-distance support from my family and friends in the Netherlands. In particular, I am immensely thankful to my parents and parents in law for regularly entertaining my kids at times I was travelling or simply during other busy moments during my PhD. I also would like to thank friends in Norway who have started to feel like family over the years, in particular Liselotte and Ivo for their continued support. I also want to thank the staff from the daycare in Norheimsund who allowed me to focus on my work, knowing that my kids were not only safe but were having a lot of fun too!

Last but not least I want to thank my husband Bas and our two small boys Espen and Bjarne for reminding me that there is also a life outside of university. Bas, thanks so much for your love and endless support over the last years and for taking me on so many nice trips into the Norwegian nature and mountains. I am looking forward to so many more nature adventures with you to come. Without your support and help with the kids, this PhD project would never have been accomplished. Espen and Bjarne, I hope my thesis inspires you, not necessarily for an academic career, but for following your heart wherever it takes you.

Abstract

The overall objective of this project is to improve our understanding of the interplay between surface processes and tectonics in active continental rifts, based on the central part of the Italian Apennines. Three key aspects are investigated:

- i) The impact of dynamic mantle-induced surface uplift on normal fault activity and topographic development in active continental rifts.
- ii) The evolution of drainage networks in response to extensional faulting and regional uplift and the main controlling mechanisms.
- iii) The impact of drainage network evolution on sediment dispersal, basin stratigraphy and transient landscape evolution.

These three aspects are investigated through a combined field and numerical modelling approach. This approach allows for the direct use of field data for constraining numerical models, as well the direct testing of model-based findings. Synthesised published basin stratigraphic, fault slip and geomorphic data together with new geomorphic and sedimentological fieldwork provide high quality and detailed datasets of stratigraphic and landscape evolution in the central Apennines.

Regional drainage network evolution in the central Apennines is primarily controlled by the balance between the rates of filling and subsidence of normal fault-bounded basins. Basin filling occurs through the supply of sediment and water, whereas basin subsidence is mainly controlled by slip on the main basin-bounding normal fault. Drainage integration occurs when initially underfilled, endorheic basins become overfilled with sediment and water allowing basins to overflow. Because basin overflow, in turn, allows water and sediment to cascade downstream to adjacent basins where it can trigger a next drainage integration event, drainage integration predominantly follows a top-down pattern. Furthermore, drainage integration acts as a first-order control on basin stratigraphy and geomorphic development in the central

Apennines, and produces a highly dynamic landscape evolution with transient conditions that can persist in the landscape for several millions of years.

Two-dimensional thermo-mechanical modelling results demonstrate how the removal of mantle lithosphere leads to regional surface uplift and the localisation of extensional strain in the area of high topography. This is because the upwelling of hot buoyant sub-lithospheric mantle within the lithospheric gap causes both isostatic surface uplift and considerable weakening of the crust. Pre-defined (inherited) fault structures in this area of uplift and weakened crust become activated if the area is subject to a low rate of far-field extension. Faults interact, causing the locus of fault activity to migrate across-strike, and fault slip rates to vary markedly over 10^4 - 10^5 year timescales. Overall, these experiments show that mantle lithosphere removal can explain many first-order characteristics of the central Apennines, such as the correlation between fault strain rates, topography and surface uplift, enhanced surface heat fluxes, negative gravity anomalies and low P-wave velocities in the upper mantle.

CHAPTER 1

Thesis introduction

1.1 Rationale

How do erosion and deposition contribute to the topography of actively evolving continental rifts? These types of questions concerning the interaction between surface processes and tectonics have intrigued many earth-scientists over the last couple of decades. The interest follows from a scientific revolution during the eighties and nineties of last century, which led to the new insight that surface processes can profoundly affect the structural evolution of tectonically active areas through the redistribution of mass and, in turn, modification of the stress state of the crust (see historical review by Merritts and Ellis, 1994). The large number of new insights that have been gained since the onset of this scientific revolution forced us to consider tectonically active areas as systems in which tectonic forcing, surface processes, but also climate feedback on one another (e.g., Molnar and England, 1990; Beaumont et al., 1992, 1999; Burov and Cloetingh, 1997; Pinter and Brandon, 1997; Burbank and Pinter, 1999; Willett, 1999). This thesis is also concerned with the interplay between surface processes and tectonics, and focuses on the evolution of elevated (mountainous) continental areas that are affected by active extensional faulting (Fig. 1.1).

There is special need for combined field-numerical modelling studies focussing on natural systems for which good constraints exist on both fault development and

geomorphic-stratigraphic evolution (Gupta and Cowie, 2000; Tucker and Hancock 2010; Briant et al., 2018). Such a combined field-numerical modelling approach enables the direct application of field data in numerical models, on one hand, as well as the direct testing of model-based findings in the tectonic, geomorphic, and stratigraphic record. One elevated continental rift for which a wealth of data exists on fault activity, basin stratigraphy, and geomorphological evolution is the central part of the Italian Apennines that has been the main motivation for this project (Figs. 1.2-1.4). This area has been used as study area and template, respectively, in the different field-based and numerical modelling studies presented in this thesis.

Improving our understanding of continental rift evolution is, first of all, important for advancing our still limited understanding of the early stages of continental rifting in run-up to continental break-up, as well as extension resulting from complex mantle dynamics in subduction (back-arc) settings (Gawthorpe and Leeder, 2000). Secondly, rift basins are increasingly receiving interest because of their high preservation potential for environmental and climatic records. Thirdly, rift basin studies are important in light of their storage capacity for economic hydrocarbon reserves as well as their potential for the future storage of green house gasses. Finally, as seismic hazard in many densely populated areas worldwide is controlled by normal fault activity, a better understanding of long-term fault development is crucial for improving seismic hazard assessment (Faure Walker et al., 2012).

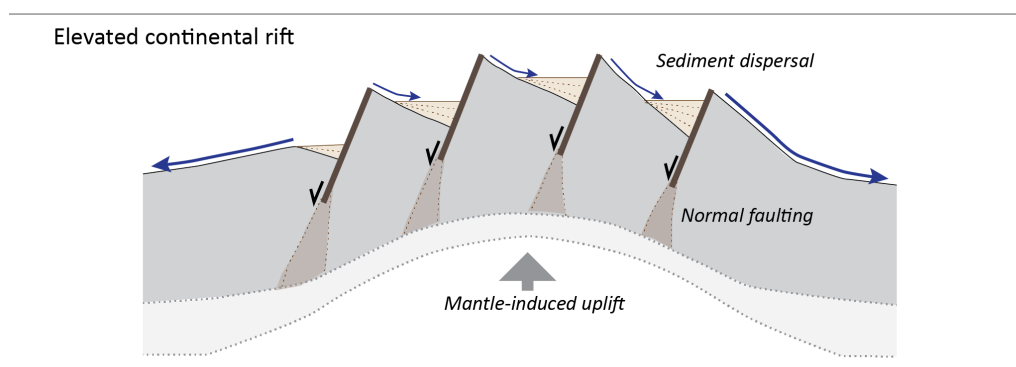


Fig. 1.1 Schematic cross-section across a mantle-supported elevated continental rift and an overview of the different aspects of the system that are thought to interact and feedback on one another.

1.2 The central Apennines continental rift

There are many regions around the globe that are currently affected by active crustal extension (Fig. 1.2). However, all these active continental rifts vary markedly with regard to many factors like their onset of rifting, tectonic setting, fault development, topography, stratigraphic evolution, and dimensions. Compared to most of the other extensional basins shown in Fig. 1.2, the central Apennines is one of the narrowest and youngest continental rifts as extension only commenced ~ 3 Myr. A notable characteristic of the central Apennines is the combination of active normal faulting (~ 3 mm/yr), high topography (< 2900 m; Fig. 1.4) and rapid regional (dome-shaped) uplift ($< 1-2$ mm/yr; D'Anastasio et al., 2006; Serpelloni et al., 2013). Strong evidence exists that the elevated topography in this area is supported by buoyancy variations in the upper mantle (e.g., D'Agostino et al., 2001; Faccenna et al., 2014). Because of the strong correlation between topography, surface uplift, and upper crustal strain rates, it has been hypothesised that not only topography, but also extension and regional uplift are all driven by the same underlying mechanisms related to upper mantle dynamics (e.g., D'Agostino and McKenzie, 1999; D'Agostino et al., 2001; Faure Walker et al., 2012; Cowie et al. 2013; Faccenna et al., 2014).

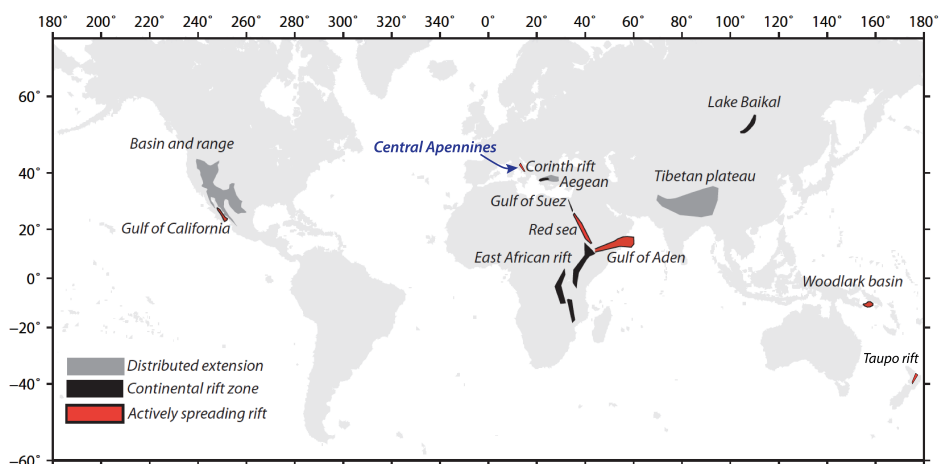


Fig. 1.2 Examples of currently active continental rifts around the globe (modified from Bell, 2008).

The combination of regional uplift and normal faulting has resulted in dynamic landscape evolution over the last 2.5-3 Myr. D’Agostino et al. (2001) were first in discussing long-term drainage network development in the central Apennines in light of its history of extension and mantle-driven uplift. Based on the relationship between gravity admittance data and long-wavelength topography they concluded that “*mantle upwelling beneath the central Apennines has been the dominant geodynamical process during the Quaternary, controlling both the geomorphological evolution and the distribution of active deformation*”. D’Agostino et al. (2001) related the initial isolation (internal drainage) of most of the intramontane basins to extensional faulting. They argued that subsequent progressive integration of these basins occurred because they got captured by aggressively headward eroding river systems cutting down on the flanks of the growing topographic bulge. Their hypothetical model implied that drainage network and basin filling histories were primarily a function of distance from the coast (Figs. 1.3, 1.4). The work from D’Agostino et al. (2001) was one of the main motivations underlying this PhD project.

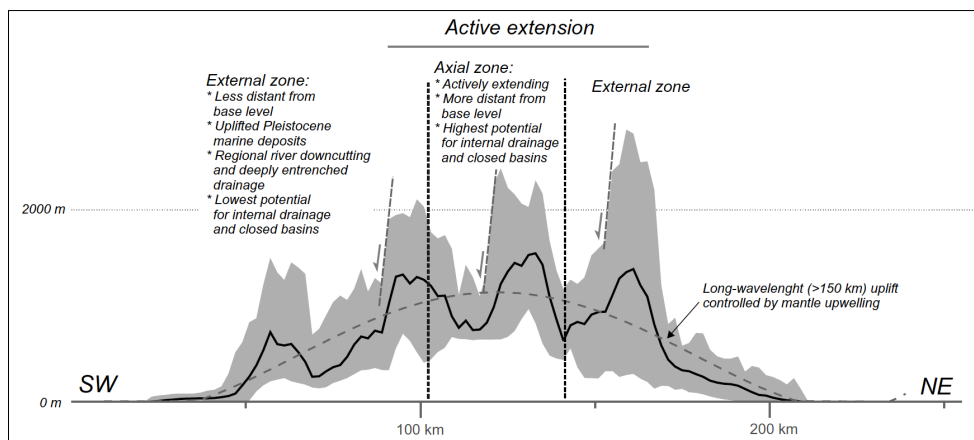


Fig. 1.3 Topographic cross-section across the central Apennines (from D’Agostino et al., 2001) showing the hypothesised interactions between regional mantle-controlled uplift, normal faulting, and drainage network evolution.

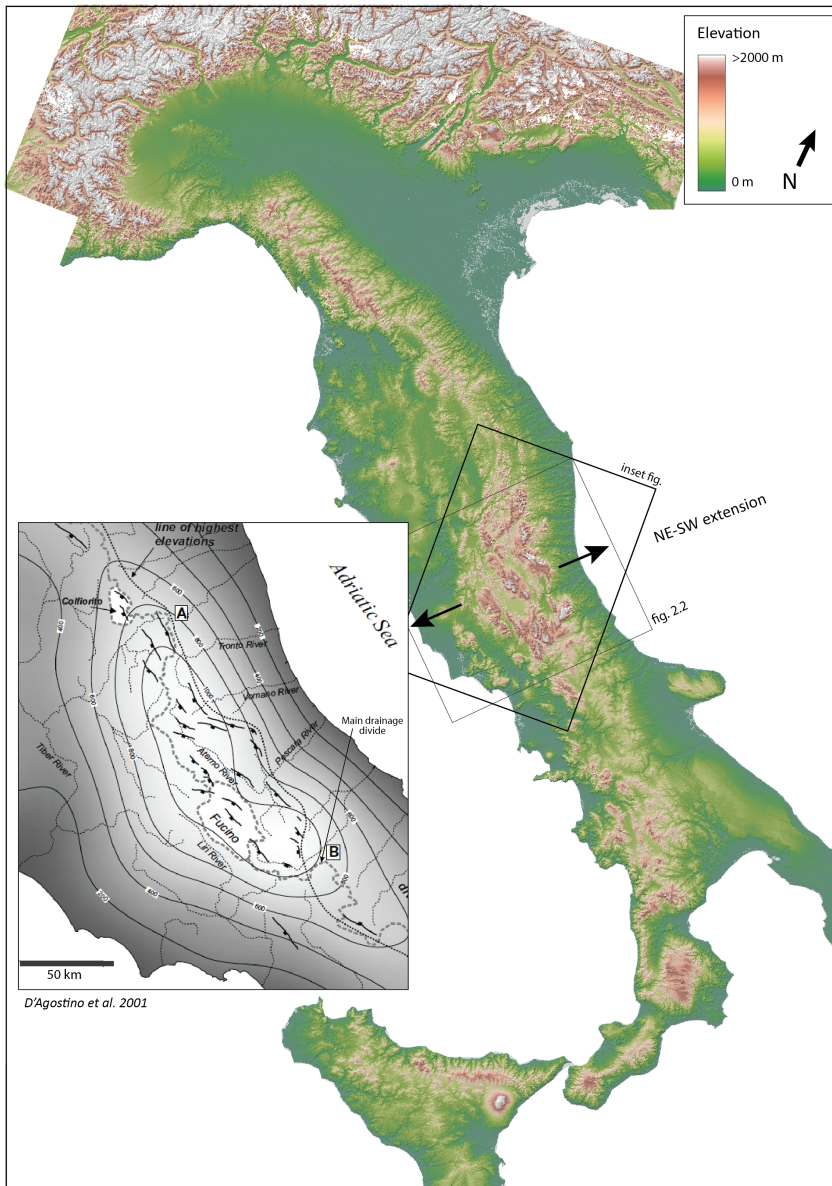


Fig. 1.4 Digital elevation model (SRTM) of the Italian peninsula, showing the overall topography of the Italian Apennines. The central part of the Apennines (within framework) are the main focus of this thesis. For this area, D'Agostino et al. (2001) hypothesised that long-wavelength topography is supported by the mantle, and that regional uplift results in aggressive headward erosion by river systems cutting down on the flanks of the mountain range (see inset figure). They used this to explain why the initially isolated basins in the area became progressively integrated (captured) over time, and for explaining why only the Fucino basin (located right at the drainage divide) is still internally drained (see also Fig. 1.3).

1.3 Surface processes and normal fault activity in continental rifts

1.3.1 *Normal fault development*

Many decades with studies of ancient and active normal fault systems are at the base of our current understanding of fault array evolution. Systematic analysis of the fault lengths and their (along-strike varying) displacement has led to the first ideas about the growth of normal faults and their capability of mechanically interacting and linking with their neighbours (e.g., Walsh and Watterson, 1991; Cowie and Scholz, 1992). These studies have demonstrated that in various settings and over widely varying spatial scales, faults tend to keep a constant displacement-length scaling and that deviations from this scaling are indicative for the transient evolution of the fault array. Numerical and analogue modelling studies (e.g., Sornette et al., 1994; Cowie et al., 1993, 1995) have explored the long-term (10^5 - 10^6 yrs) evolution of normal fault arrays and demonstrated that strain becomes progressively localised over time. Cowie (1998a) was first in showing that fault arrays develop from distributed faults systems consisting of large numbers of small-displacement faults (rift initiation or nucleation stage) into fault systems in which only a small number of large-displacement through-going faults has remained (rift climax stage). Going from the rift initiation to the rift climax stage, involves a time interval of fault growth, interaction and linkage (fault interaction stage). Faults located in the centre of the fault array can most easily interact with their neighbours and tend to become the largest fault systems over time, at the expense of other smaller faults that become inactive (Cowie, 1998a). On top of these long-term developments, distributed normal faults systems reveal shifts in activity over 10^3 - 10^4 year timescales between different faults due to fault interaction (e.g., Nicol et al., 2010; Cowie et al., 2017).

1.3.2 *Drainage development and basin stratigraphy*

Progressive strain localisation during continental rifting affects drainage network development, sediment dispersal and the depositional environments in the fault-

bounded basins. Gawthorpe and Leeder (2000) discuss stratigraphic observations in light of progressive strain localisation and present conceptual models for the different stages of combined tectono-sedimentary rift development. For the early stage of continental rift evolution, they suggest that the large number of relative small hanging wall basins largely develop in isolation from one another and support either lacustrine or fluvial environments depending on local sediment supply. Due to fault segment interaction and linkage, adjacent depocentres merge into larger ones over time, allowing larger axial river systems to develop. Due to the much more limited number of across-strike fluvial connections, i.e., between parallel fault systems, a rectangular (fault-controlled) so-called ‘trellis’ drainage network develops that is characteristic for continental rifts (Twidale, 2004).

Besides the structural development of the rift, basin stratigraphy additionally depends on the prevailing climatic conditions and lithology as these mostly control sediment supply and runoff (Gawthorpe and Leeder, 2000). However, also the degree in which basins are connected with one another is of key importance, as this controls the existence of local base levels, sediment dispersal across the rift and the type of depositional environments within the basins. While the locations of the main river valleys are largely fault-controlled, the degree of connectivity between different basins (or valley segments) often changes over time (e.g., D’Agostino et al., 2001; Connell et al., 2005; Menges, 2008; Duffy et al., 2015).

1.3.3 Interplay between surface processes and fault activity

Whereas fault activity exerts a first-order control on erosion-deposition patterns and sediment fluxes in continental rifts (e.g., Whittaker et al., 2010; Pechlivanidou et al., 2019), sediment redistribution in turn affects upper crustal stresses and normal fault activity. The impact of depositional loading and erosional unloading has mainly been demonstrated by numerical and analogue modelling studies, not only applying to sediment redistribution, but also for climate-related variations in water and ice loads (e.g., Hetzel and Hampel, 2005; Hampel et al., 2009; Zwaan et al., 2018). For individual normal faults it has been demonstrated that footwall erosion and hanging

wall deposition enhance long-term slip rates and basin depths but reduce footwall elevations (e.g., Maniatis et al., 2009; Turpeinen et al., 2008, 2015). Moreover, surface processes can prolong the time interval of fault activity, even up to millions of years after cessation of regional extension (Olive et al., 2014; Turpeinen et al., 2015). Also thermo-mechanical models with dynamic fault development demonstrate that sediment loading leads to strain localisation (e.g., Buitter et al., 2008; Theunissen and Huismans, 2019; Beucher and Huismans, in press.). However, it is much more challenging to demonstrate sediment-controlled loading-or unloading effects on the fault activity in natural rift systems, explaining the much more limited number of field studies demonstrating the existence of such a feedback (Fernández-Ibáñez et al., 2010; Calais et al., 2010). The scarcity of rift systems with sufficient spatial coverage and temporal resolution of data and thorough understanding of the different aspects dominating their landscape dynamics, explains the pioneering character of this type of study. This means that despite the relative good theoretical understanding of potential interactions from modelling studies, they have rarely been identified and their strength has rarely been constrained for real rift systems.

1.4 Research aims and approach

The overall aim of this PhD project was to improve our process-based understanding of the interplay between surface processes and tectonics in active, elevated continental rifts. The work particularly focussed on the following three questions:

- iv) How do river networks evolve over time in response to extensional faulting and regional uplift and what are the main controlling factors?
- v) What is the impact of drainage network evolution on sediment dispersal, basin stratigraphy and transient landscape evolution?
- vi) What is the impact of mantle-induced surface uplift on normal fault and topographic development in active continental rifts?

The first two questions were addressed by means of field-data analysis and numerical modelling, and both at a river-system and regional (rift-wide) scale. Published constraints on regional uplift and fault activity from the central Apennines were used to parameterise a landscape evolution model to investigate the combined impact of faulting and regional uplift on long-term drainage network evolution and sediment dispersal (Chapter 3). This study led to a fundamental change in our view on which mechanisms control drainage network evolution, and these new ideas were subsequently tested in a field-based geomorphic-stratigraphic study (Chapter 4). This follow-up study focussed on integrating stratigraphic and geomorphic observations with constraints on fault development for one of the largest river systems in the central Apennines, the Aterno river system. Because this river system drains the area hit by devastating the 2009 L'Aquila earthquake, a wealth of data on fault activity and basin stratigraphy has been published. Chapter 4 integrates these published data with new geomorphic observations in order to reconstruct the long-term evolution of this river system and for evaluating the main factors controlling its development.

The third research question was approached by means of a geodynamic modelling study (Chapter 5). Strong evidence has been published that indicates that extensional faulting and regional uplift in the central Apennines are controlled by the same dynamic development of the underlying upper mantle (e.g., D'Agostino et al., 2001; Faure Walker et al., 2012; Faccenna et al., 2014). We used a thermo-mechanical model for exploring one of the hypothesised scenarios, namely the removal of mantle lithosphere (e.g., Di Luzio et al., 2009; Chiarabba and Chiodini, 2013). Published observations from the central Apennines were again used to constrain the model, allowing model results to be compared with field observations.

1.5 Thesis outline

This thesis consists of three parts. Chapters 1 and 2 together are the first part of this thesis. This introduction chapter is followed by Chapter 2, which provides an overview of the geological setting of the central Italian Apennines. The second part of this thesis

consists of three ‘paper-chapters’ (Chapters 3, 4, and 5) for which a short description of their contents is given below. In the final part of the thesis (Chapters 6 and 7) the findings from the three ‘paper-chapters’ are synthesised. Chapter 6 discussed those results that are most relevant for the scientific literature focussing on the central Apennines. In Chapter 7, on the other hand, the key findings are integrated and discussed within the wider context of the literature on continental rift development. Here, also outstanding research questions and recommendations for future research directions are provided.

Paper 1: *‘Drainage integration and sediment dispersal in active continental rifts: A numerical modelling study of the central Italian Apennines’* (Chapter 3)

This paper approaches the first two research questions by means of numerical landscape evolution modelling using field constraints on both normal faulting and regional uplift. This work demonstrates that even in the case of constant slip and uplift rates, the combination of normal faulting and regional uplift produces a dynamic landscape evolution. This is because, together, faulting and uplift produce changes in the interconnectivity of the drainage network over time, with relative small and isolated drainage basins progressively becoming interconnected with one another and with the regional drainage network. While this phenomenon of drainage integration was previously described for the central Apennines, the results of this study provide a process-based understanding of the underlying mechanisms and controlling factors. Furthermore, this study demonstrates the large impact of drainage integration on sediment dispersal and transient landscape evolution.

Paper 2: *‘Transient landscape and stratigraphic responses to drainage integration in the actively extending central Italian Apennines’* (Chapter 4)

The second paper (Chapter 4) is a field study that focuses on the evolution the Aterno river system in the central Apennines. The Aterno river system is one of the largest river systems in the region, with a drainage basin area of $\sim 1300 \text{ km}^2$. By integrating published stratigraphic and fault slip data with new geomorphic observations the progressive integration of the different fault-bounded basins and the birth of the

through-going Aterno River have been reconstructed. This drainage integration reconstruction allowed us to test some of the ideas developed in paper 1 of this thesis. This study demonstrates that basins became integrated with one another because they became overfilled with sediment and water, allowing them to spill over. This dataset also suggests that rates of sedimentation and basin subsidence are similar in magnitude, explaining why tipping points between under- and overfilled conditions in the different basins can be easily reached. This work also describes the impact of drainage integration on basin stratigraphy and long-term transient landscape evolution.

Paper 3: *‘Dynamic normal fault behaviour and surface uplift in response to mantle lithosphere removal: A numerical modelling study motivated by the central Italian Apennines’* (Chapter 5)

Paper 3 (Chapter 5) explores one of the potential mechanisms driving both uplift and extension in the central Apennines, namely the removal of mantle lithosphere (e.g., Di Luzio et al., 2009). Two-dimensional thermo-mechanical numerical modelling experiments are used, in which mantle lithosphere is removed in a simplistic, but dynamic manner. The results of this work show the impact of lithospheric thinning on surface uplift and the long-term development of an array of pre-defined normal fault zones. The results demonstrate that heating and thinning of the lithosphere causes isostatic uplift and the localisation of extensional strain within a narrow zone that has a similar width as observed in the central Apennines. The model also shows dynamic fault interaction resulting in temporally varying slip rates and shifts in fault activity across-strike. Overall this work demonstrates that mantle lithosphere removal can explain many first-order observations from the central Apennines.

CHAPTER 2

The Central Italian Apennines

2.1 Geological setting

The Italian Apennines are located in the highly complex zone of north-south convergence between the African and Eurasian plates that occurred at a rate of a few millimetres per year over the last 20 Myr (Fig. 2.1; e.g., Faccenna et al., 2001b; Lucente et al., 2006). Subduction of Tethyan crust and east-southeast migration of the active subduction zone over the last ~20-30 Myr resulted in the formation of the northeast verging fold-thrust belt of the Italian Apennines and the opening of the western-central Mediterranean (e.g., Malinverno and Ryan, 1986; Lucente et al., 2006). Sinking and rollback of the slab is thought to have been the main driving force behind back-arc extension (e.g., Malinverno and Ryan, 1986; Faccenna et al., 2001b; Lucente et al., 2006). In the central (Lazio-Abruzzo) part of the Apennines, orogenesis led to the uplift of Mesozoic-Paleogene limestones above sea level and the deposition of flysch during the Miocene. Limestone and flysch are the two main bedrock types in this area (Fig. 2.2a). Whereas thrusting is still active in the Northern Apennines, it ceased during the mid-Pliocene ~6 Ma in the central Apennines (Patacca et al., 1990).

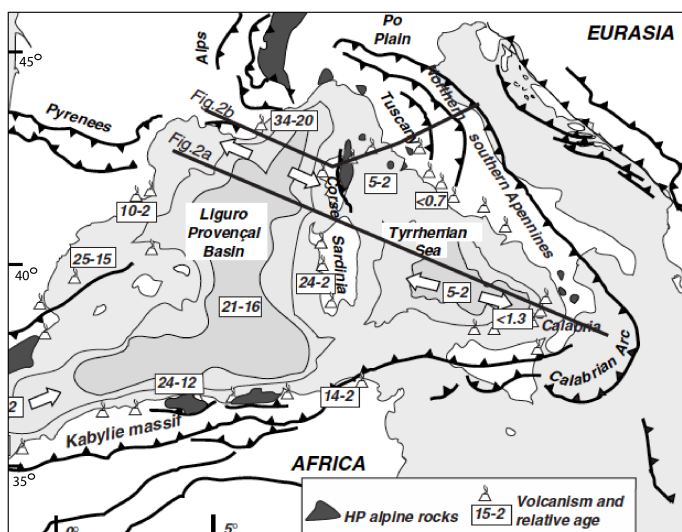


Fig. 2.1 Simplified tectonic map of the central Mediterranean from Faccenna et al. (2001a), showing the main subduction fronts in the zone of convergence between Africa and Eurasia. HP stands for 'high pressure' alpine metamorphism. The map also shows the average ages of volcanism in different regions, showing that volcanism in the Tyrrhenian foreland area directly west of the central Apennines mostly occurred after 0.7 Ma (see also Fig. 2.2a).

2.2 Extensional faulting, regional uplift and high topography

Subsequently, NE-SW extension commenced in the central Apennines around 3-2.5 Ma (e.g., Patacca et al., 1990; Bosi and Messina, 1991; Lavecchia et al. 1994; Cavinato and DeCelles, 1999; Cosentino et al., 2017). GPS velocities indicate a current regional extension rate of $\sim 3 \text{ mm yr}^{-1}$ (Hunstad et al., 2003; Serpelloni et al. 2013; D'Agostino et al., 2009, 2011). Extension is accommodated by numerous active SE striking normal faults, organised in a 60-80 km wide fault array located along the crest of the mountain range (Fig. 2.2b). Striated fault scarps have been preserved since the demise of last glacial ($15 \pm 3 \text{ ka}$), which offset planar hillslopes that are preserved due to the climate-induced ten-fold reduction in hillslope erosion rates (Fig. 2.3; Tucker et al., 2011; Cowie et al., 2017). The vertical height of these fault scarps typically varies between 3 and 24 m, indicating Holocene-averaged throw rates in between 0.2 and 1.6 mm yr^{-1} (Roberts and Michetti, 2004; Papanikolaou et al., 2005, Papanikolaou and Roberts, 2007; Faure Walker 2012). Maximum total throws, i.e., the estimated vertical offset between pre-rift geological horizons, vary between ~ 600 and 2200 m (Roberts and Michetti, 2004).

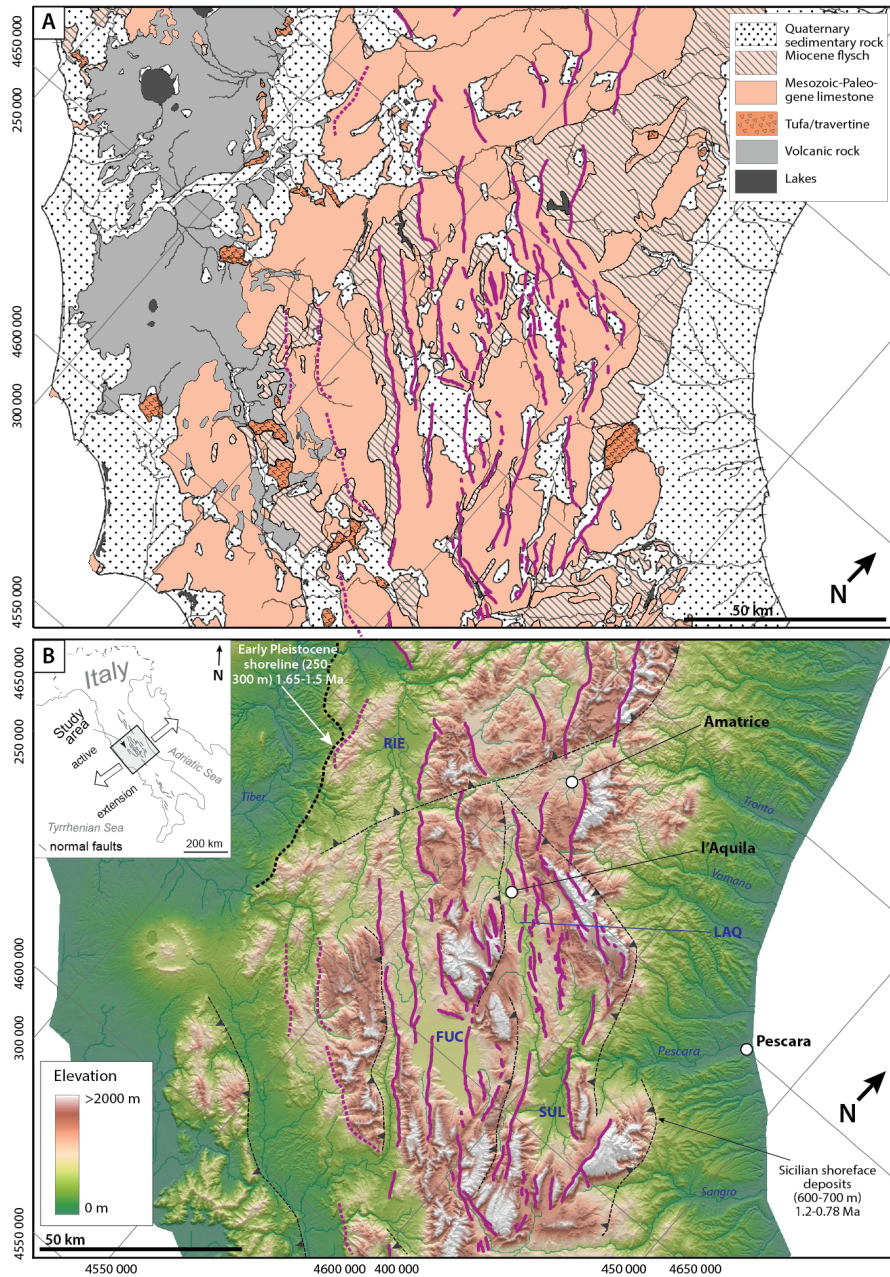


Fig. 2.2 Simplified geological map (A) and topographic map (B; 10-m DEM from Tarquini et al., 2007) of the central Apennines. The main normal faults are projected on top as purple lines (dashed means inactive during the Holocene), principally after Roberts and Michetti (2004). SUL = Sulmona basin, FUC = Fucino basin, LAQ = L'Aquila basin, RIE = Rieti basin. Dashed black lines show (inactive) thrust faults (after Miccadei et al., 2017).

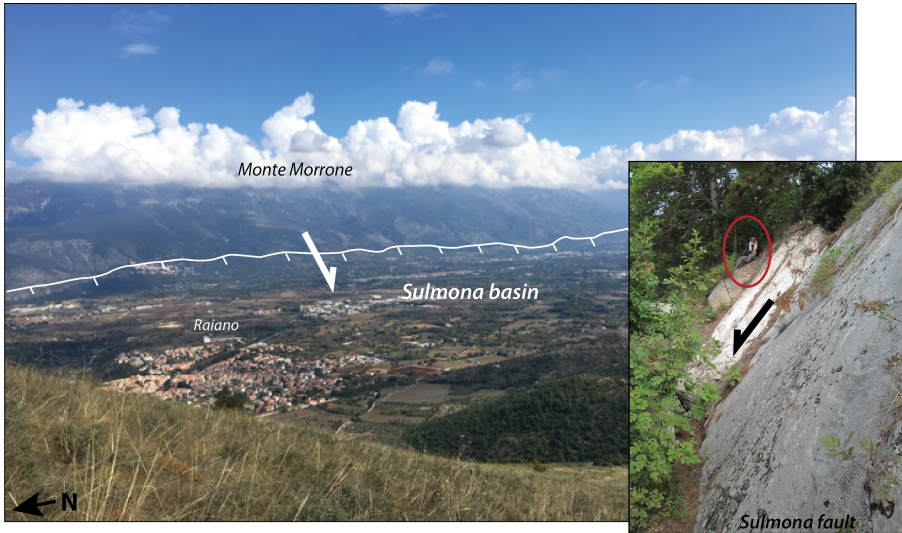


Fig. 2.3 Example of one of the major basins in the central Apennines. Pictures of the Sulmona basin (looking east) and the main basin-bounding fault system (Sulmona or Monte Morrone fault). Note person in the background for scale.

The mainly high-angle normal faults have lengths of the order of 20-40 km, a dominant SW dip direction and produce intense seismicity down to ~15-17 km depth (Roberts and Michetti 2004; Papanikolaou and Roberts 2007; Faure Walker 2012; Chiarabba and Chiodini, 2013). These faults mainly upthrow Mesozoic-Paleogene limestone in their footwalls, whereas their hanging walls are filled with Quaternary fluvial and lacustrine sediment. Active NE-SW extension is also evidenced by the regional stress field reconstructed from focal mechanisms and borehole breakout data (e.g., Montone et al., 2004). Active normal faulting explains the strong seismicity in the region that frequently produces earthquakes with magnitudes up to 7 Mw, including the 1915 Avezzano, 2009 L'Aquila and 2016-2017 Norcia-Amatrice earthquakes (e.g., Wedmore et al., 2017, 2019). Co-seismic fault displacements are typically of the order of $\llsim 1$ m.

Besides extension, the central Apennines experienced pronounced regional uplift from approximately 2 Ma onwards, as evidenced by Early Pleistocene shorelines and shoreface deposits perched over several hundreds of meters above sea level (e.g.,

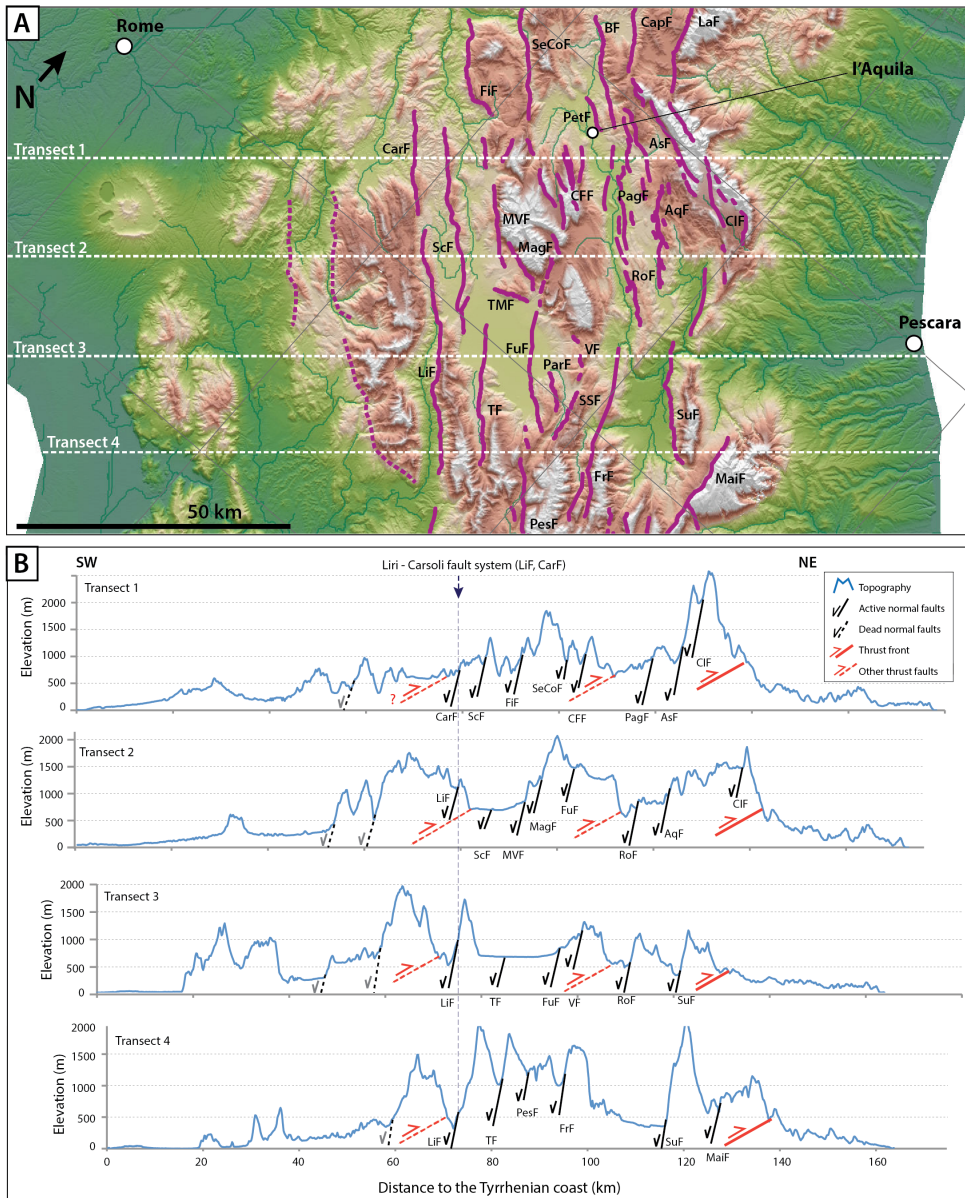


Fig. 2.4 A) Topographic map (10 m DEM from Tarquini et al., 2007) and B) four topographic cross-sections. The name of the normal faults are as follows: AqF = L'Aquila f., AsF = Assergi f., BF = Barete f., CarF = Carsoli f., CapF = Capitignano f., CFF = Campo Felice f., CIF = Campo Imperatore f., CMF = Cinque Miglia f., FiF = Fiamignano f., FrF = Frattura f., FuF = Fucino f., LaF = Laga f., LeF = Leonessa f., LiF = Liri f., MagF = Magnola f., MaiF = Maiella f., MVF = Monte Velino f., PagF = Paganica f., ParF = Parasano-Pescina f., PesF = Pescasseroli f., PetF = Pettino f., RiF = Rieti f., RoF = Roccapreturo f., ScF = Scurcola f., SeCoF = Sella di Corno f., SSF = San Sebastiano f., SuF = Sulmona f., TF = Trasacco f., TMF = Tre Monti f., VF = Ventrino f.

D'Agostino et al., 2001). Uplift mainly affected the mountain range interior, which has been uplifted by >800 m, whereas the surface near today's coastlines remained more or less stable over time (e.g., Bordoni and Valensise, 1998; Pizzi, 2003; Ascione et al., 2008; Mancini et al., 2007). This produced an up-doming pattern of long-term regional surface uplift that is also reflected by geodetic surface uplift rates (D'Anastasio et al., 2006; Serpelloni et al., 2013). Today, the highest mountain peaks (located at elevated footwalls in the Gran Sasso range) reach up to ~2900 m elevation (Fig. 2.2b).

The combination of regional surface uplift and extension has created a topographic bulge with, near its crest, an array of active normal faults bounded by high footwall areas and low-lying half grabens (Figs. 2.2b, 2.4). However, due to pre-rift inherited topography, the topography is not characterised by a relative simple and systematic 'Basin-and-Range type of morphology' but has a strongly 3-dimensional character (Figs. 2.2b, 2.4). Though, in an across-strike direction, the area reveals topography over three dominant spatial scales, which are most clearly visible in transect 2 in figure 2.3. Firstly, long-wavelength (100-150 km) topography resulting from long-term regional up-doming of the area (D'Agostino et al., 2001). Secondly, the central Apennines are characterised by ~30 km wide (across-strike) topographic blocks consisting of Mesozoic limestone that line up with mapped thrust faults and are inherited from the phase of compression (Figs. 2.2b, 2.4). Thirdly, normal fault-related topography consisting of elevated footwall ranges and hanging wall basins controlled by a semi-regular, across-strike fault spacing of ~7-15 km (Roberts and Michetti, 2004).

Compared to other parts of the Apennines, its central part (Lazio-Abruzzo, between 41.5 and 42.5 °N) is the widest and highest part of the mountain range with the highest rates of regional surface uplift, highest upper-crustal strain rates, and the widest array with active normal faults (Fig. 2.1; e.g., Faure Walker et al., 2012).

2.3 Lithosphere structure and mantle dynamics

The depth of the Moho beneath the Italian peninsula is well constrained by S receiver function analysis (Piano Agostinetti and Amato, 2009; Miller and Piano Agostinetti, 2012) and shallow tomography (Di Stefano et al., 2011). These studies suggest that, from east to west across central Italy, the crustal thickness changes from ~30-35 km in the Adriatic domain to ~35-38 km beneath the Apennines, and subsequently decreases down to ~20-25 km in the Tyrrhenian domain. The slight thickening of the crustal wedge cannot explain the high topography of the central Apennines through crustal isostasy (D'Agostino and McKenzie, 1999; D'Agostino et al., 2001; Faccenna et al., 2014). Moreover, because the timing of regional uplift (<2 Ma) post-dates the change from shortening to extension (~6-3 Ma), crustal thickening can be ruled out as an explanation for the high topography and support from the mantle is required (D'Agostino et al., 2001; Faure Walker et al., 2012). Faccenna et al. (2014) calculated the pattern of residual topography along the Apennines (based on the difference between the observed and Airy isostatic topography), and demonstrated that the mean elevation of the central Apennines should be ~600 m lower if it would be only supported by variations in crustal thickness.

P-wave tomography studies demonstrate the presence of the subducting Adriatic slab underneath the northern and southern parts of the Apennines (e.g., Rosenbaum et al., 2008; Di Stefano et al., 2009). However, the same studies also show a broad strongly negative P-wave anomaly in the uppermost mantle (~40-50 km depth) underneath the central Apennines that is interpreted as a window in the slab that allows for the upwelling of hot asthenosphere material (Fig. 2.5; Wortel and Spakman, 2000; Rosenbaum et al., 2008; Di Stefano et al., 2009). Anomalous low densities in the upper mantle (Di Luzio et al., 2009) and free-air gravity data (D'Agostino et al., 2001) additionally support the presence of a slab window beneath central Italy. The upwelling of hot sub-lithospheric mantle can also explain the long-wavelength surface uplift in the area and elevated temperatures and CO₂ contents of groundwater (Fig. 2.5; Chiarabba and Chiodini, 2013; Chiodini et al., 2013). However, it is still debated

whether it is isostatic adjustment due to lithosphere thinning or mantle convection-induced stresses that support the topography (e.g., Faccenna et al., 2014). Decompressional melting of asthenosphere related to slab breakoff has been inferred to explain the youngest phase of volcanism (<0.7 Ma) in the Tyrrhenian coastal areas of central Italy (Peccerillo, 2005; Rosenbaum et al., 2008).

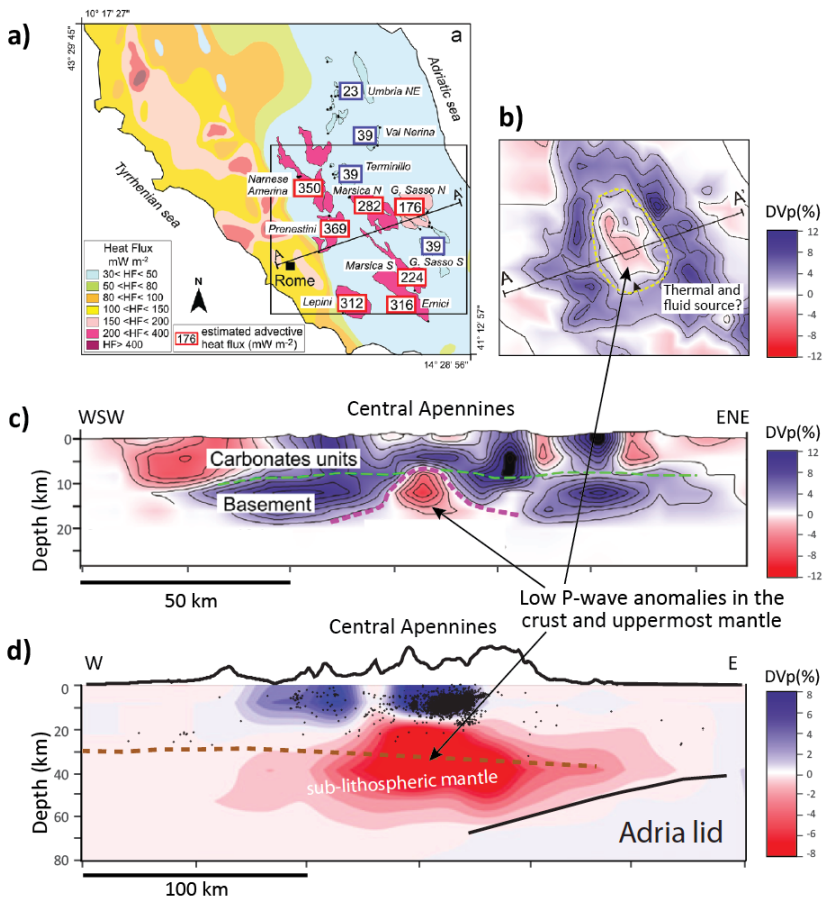


Fig. 2.5 a) Conductive heat flux map of central Italy (Cataldi, 1995) compared to advective heat fluxes estimated from spring water temperatures (from Chiodini et al., 2013). While conductive heat fluxes are highest in the volcanic region along the Tyrrhenian coast, advective heat fluxes reach even higher (>300 mWm⁻²) in the central Apennines interior. b,c) Seismic velocity anomalies V_p for the crust beneath the central Apennines (from Chiodini et al. 2013, based on data from Chiarabba et al., 2010). d) Seismic velocity anomalies V_p down to the uppermost mantle underneath the central Apennines (from Chiarabba and Chiodini 2013, based on data from Di Stefano et al., 2009).

2.4 Spatial-temporal variability in fault activity

During extension, development of the fault array took place through fault growth, elastic interaction and fault linkage resulting in long-term changes in slip rates (Cowie and Roberts 2001). Evidence for fault development comes from comparison of the estimated postglacial (younger than 15 ± 3 ka) slip rates with the long-term (2.5-3 Ma) averaged slip rates. Some of the faults located near the centre of the fault array currently slip at rates that are too high to explain their relative small total displacements, suggesting that they have increased their slip rate over time. Other faults located closer to the edges of the fault array have postglacial slip rates that are consistent with their total displacement, suggesting that they have kept an approximately constant slip rate (Cowie and Roberts, 2001; Roberts and Michetti 2004; Papanikolaou and Roberts 2007; Faure Walker et al. 2010, 2012; Whittaker et al., 2008). This observed pattern of progressive localisation of extensional strain in the centre of the fault array compares well with fault development reproduced in numerical experiments (Cowie et al., 1993; Cowie, 1998a). Modelling and empirical data together suggest strain localisation and slip acceleration on the central faults to have occurred somewhere between 1 and 0.5 Ma, possibly accompanied by the death of some faults located furthest southwest (Fig. 2.2b; Roberts and Michetti 2004).

There is also strong evidence for temporal variations in fault slip rates over shorter timescales (10^3 - 10^4 yr). Variations in cosmogenic ^{36}Cl measured on fault scarps reveal that faults in central Italy typically slip relative rapidly over several thousands of years, separated by equally long periods when slip rates are relative low (Cowie et al., 2017). Like for other extensional settings (e.g., Nicol et al., 2010), these shifts in fault activity in the central Apennines have been attributed to across-strike fault interaction (Cowie et al. 2012, 2017).

2.5 Drainage network and basin stratigraphy

The central Apennines are drained by a few large river systems that start in the mountain interior and flow either to the Adriatic (Aterno-Pescara river system) or Tyrrhenian (Salto-Velino-Nera and Liri river systems) coast (Fig. 2.6). These rivers predominantly follow an along-strike (fault-parallel) course, but start flowing in an across-strike direction where they managed to cross actively uplifting footwall topography and enter the foreland area. However, there are also parts of the mountain interior that are not externally drained by river systems. Most important is the large, underfilled endorheic Fucino basin, which has a watershed of $\sim 860 \text{ km}^2$ and is located right at the main drainage divide (Fig. 2.6a; D'Agostino et al., 2001). Basin subsidence is controlled by the Fucino fault system that is the largest fault system in the area and located in the centre of the active normal fault array (Roberts and Michetti, 2004). While the Fucino basin has received most attention, there are a large number of smaller underfilled depressions ($< \sim 50 \text{ km}^2$) mostly at higher elevations in elevated footwall areas (Fig. 2.6a). Some of them are truly endorheic, others are drained by subsurface (karst) systems that developed in the limestone bedrock (e.g., Boni, 2000).

During the early Pleistocene, not only the Fucino basin, but also most of the other major normal fault-bounded basins were internally drained (e.g., D'Agostino et al., 2001; Piacentini and Miccadei, 2014), as evidenced by the dominance of lacustrine sediment in the older parts of their stratigraphy that formed under endorheic conditions (Figs. 2.7a,c; e.g., Cavinato, 1993; Cavinato and DeCelles, 1999; Cavinato et al., 1994; Miccadei et al., 2002; Pucci et al., 2014; Piacentini and Miccadei, 2014; Nocentini et al., 2017, 2018). Over time, these basins became progressively connected with one another by a through-going river system. As first proposed by D'Agostino et al. (2001), this process of drainage integration has been generally thought to be driven by headward eroding rivers in the coastal areas that progressively elongate their course in a landward direction through the step-wise capturing of intramontane basins. The transient response of today's large through-going river systems to long-term drainage integration is likely at least partly responsible for the large knickzones that

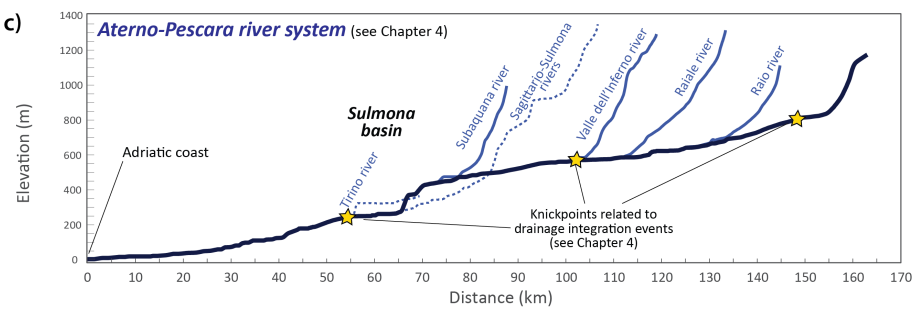
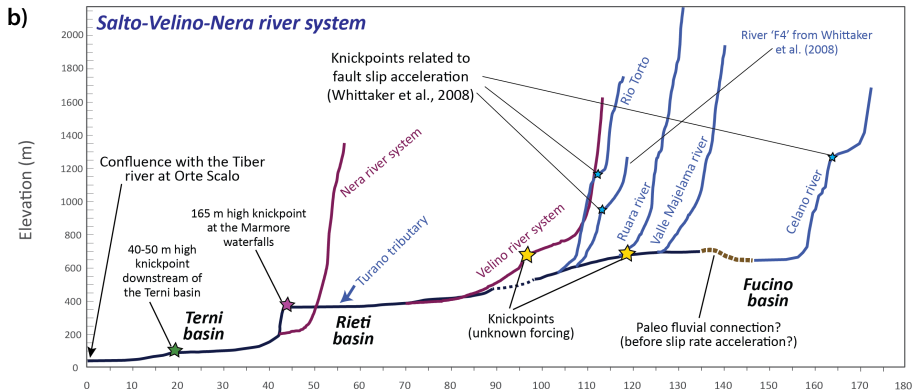
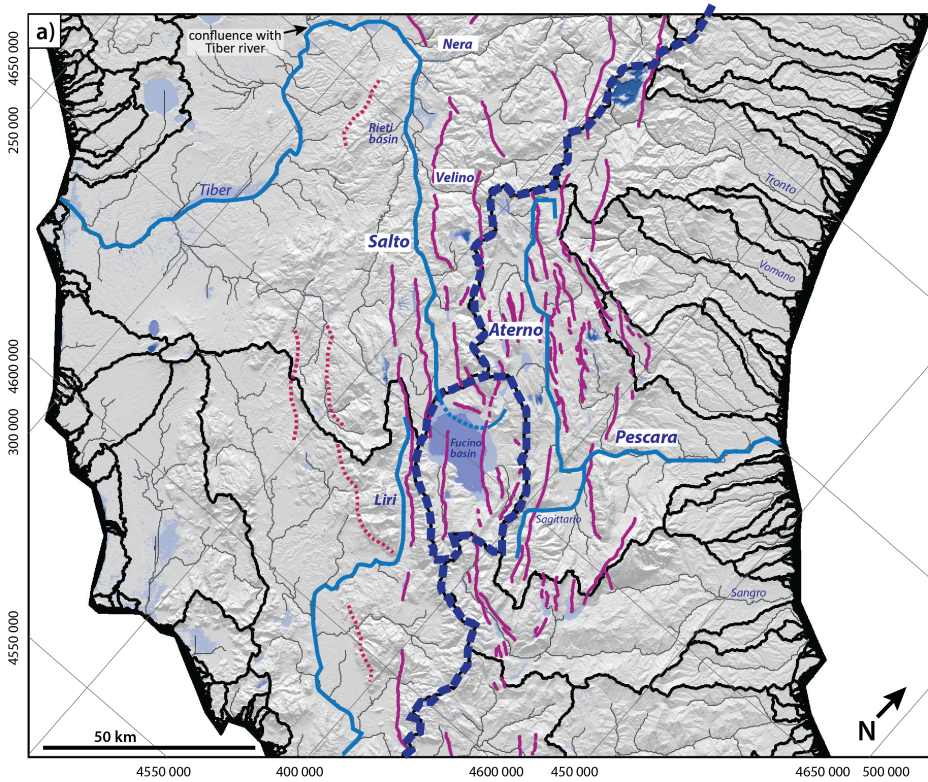


Fig. 2.6 (shown on previous page) a) Drainage network and watersheds extracted from the 10 m DEM of the central Apennines (Tarquini et al., 2007). Blue shaded areas are basins that are underfilled, i.e., have surface areas lower than their spill point. b) Longitudinal profile of the Salto-Velino-Nera river system draining most of the western half of the central Apennines (see a). This profile has been extended in an upstream direction into the endorheic Fucino basin. The Rio Torto and River F4 were taken from (Whittaker et al., 2008). Stars mark the upstream limits of convex reaches. c) Longitudinal profile of the Aterno river (see Chapter 4).

characterise their longitudinal profiles (Fig. 2.6b,c). Also some of footwall draining tributaries crossing active normal faults reveal high knickzones that have been explained by slip acceleration (Fig. 2.6b; e.g., Whittaker et al., 2008).

Since the onset of extension ~ 3 Ma, the extensional intramontane basins in the central Apennines trapped up to <1000 m thick sequences of predominantly lacustrine and fluvial deposits (e.g., Cavinato, 1993; Cavinato and DeCelles, 1999; Cavinato et al., 1994; Miccadei et al., 2002; Pucci et al., 2015; Piacentini and Miccadei, 2014; Nocentini et al., 2017, 2018). Lacustrine sediment in this area comprises whitish laminated to massive calcareous silts and clays, whereas the fluvial deposits typically consist of well-rounded and moderate to well-sorted calcareous gravels and sandy gravels (Fig. 2.7c,d; e.g., Mancini et al., 2012; Giaccio et al., 2012; Nocentini et al., 2017, 2018). Stratigraphic cross-sections have been published for most of the largest basins in the area, which are based on well logs and seismic profiles (Fig. 2.7a). In many basins the youngest (Late Pleistocene-Holocene) stratigraphy can be studied in outcrops in the walls of deeply incised basin-crossing river valleys (e.g., Sulmona and Lower Aterno-Subequana basins, Salto valley). In some basins also (shifts in) fault activity caused basin infill to become partly exposed by footwall uplift (e.g., the Fucino and Castelnuovo basins). For most basins, age constraints exist from a combination of tephra-chronology, biostratigraphy and palaeomagnetism.

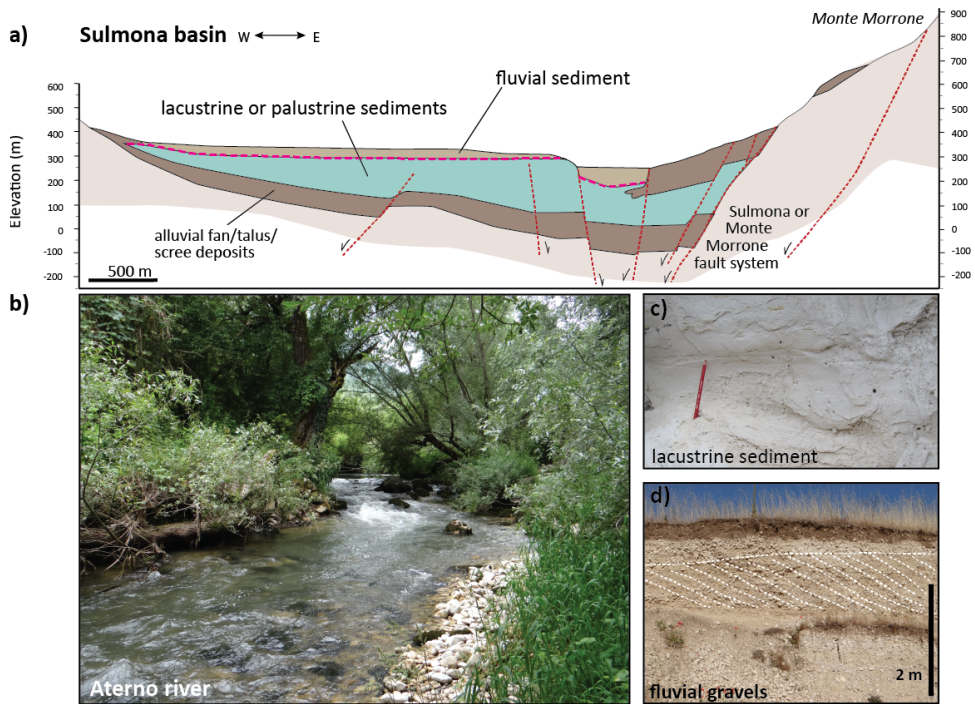


Fig. 2.7 a) Example of a stratigraphic cross-section across one of the main basins in the central Apennines, namely the Sulmona basin. b) Picture of the Aterno River in its middle reaches in the Lower Aterno Valley. c,d) Examples of outcrops with characteristic lacustrine and fluvial deposits as observed in the intramontane basins of the central Apennines.

CHAPTER 3

Paper 1

Drainage integration and sediment dispersal in active continental rifts: A numerical modelling study of the central Italian Apennines

Published in *Basin Research* as:

Geurts, A.H., Cowie, P.A., Duclaux, G., Gawthorpe, R.L., Huisman, R.S., Pedersen, V.K., Wedmore, L.N.J., 2018. Drainage integration and sediment dispersal in active continental rifts: A numerical modelling study of the central Italian Apennines. *Basin Research*, 30, 965-989.

3.1 Abstract

Progressive integration of drainage networks during active crustal extension is observed in continental areas around the globe. This phenomenon is often explained in terms of headward erosion, controlled by the distance to an external base-level (e.g. the coast). However, conclusive field evidence for the mechanism(s) driving integration is commonly absent as drainage integration events are generally followed by strong erosion. Based on a numerical modelling study of the actively extending central Italian Apennines, we show that overspill mechanisms (basin overfilling and lake overspill) are more likely mechanisms for driving drainage integration in extensional settings and that the balance between sediment supply versus accommodation creation in fault-bounded basins is of key importance. In this area drainage integration is evidenced by lake disappearance since the early Pleistocene and the transition from internal (endorheic) to external drainage, i.e. connected to the coast. Using field observations from the central Apennines we constrain normal faulting and regional surface uplift within the surface process model CASCADE (Braun & Sambridge, 1997) and demonstrate the phenomenon of drainage integration, showing how it leads to the gradual disappearance of lakes and the transition to an interconnected fluvial transport system over time. Our model results show that, in the central Apennines, the relief generated through both regional uplift and fault-block uplift produces sufficient sediment to fill the extensional basins, enabling overspill and individual basins to eventually become fluvially connected. We discuss field observations that support our findings and throw new light upon previously published interpretations of landscape evolution in this area. We also evaluate the implications of drainage integration for topographic development, regional sediment dispersal and offshore sediment supply. Finally, we discuss the applicability of our results to other continental rifts (including those where regional uplift is absent) and the importance of drainage integration for transient landscape evolution.

3.2 Introduction

In many continental settings undergoing active extension river network geometries change considerably over time (e.g. Leeder & Jackson, 1993; Jackson & Leeder, 1994). An often-observed trend is the progressive development of fluvial connections between initially isolated, endorheic, drainage basins and the eventual formation of a regional drainage network (e.g. D'Agostino *et al.*, 2001; Connell *et al.*, 2005; Menges, 2008; Smith, 2013; Dickinson, 2015; Duffy *et al.*, 2015). This phenomenon, so-called drainage integration, explains why lake sediments often characterise older parts of the stratigraphy of fault-bounded extensional basins, while fluvial sediments are observed higher up in the record (e.g. D'Agostino *et al.*, 2001; Connell *et al.*, 2005; Cavinato & De Celles, 1999; Miccadei *et al.*, 2002). An area where drainage integration has clearly occurred is the central part of the Italian Apennines (Fig. 3.1), which has been affected by active extension since approximately the beginning of the Pleistocene (Cavinato & De Celles, 1999; Roberts & Michetti, 2004). While lakes were widespread during the Early-Middle Pleistocene in this area, most of them disappeared in the course of the Middle-Late Pleistocene as tectonic basins became progressively fluvially connected (e.g. D'Agostino *et al.*, 2001; Piacentini & Miccadei, 2014). Understanding the mechanisms that control drainage integration is clearly important for interpreting the stratigraphic record preserved in such extensional settings.

In the central Apennines, drainage integration has previously been explained in terms of headward erosion from the coast, i.e. the capturing of basins at higher elevations by major streams that enlarge their catchments in an upstream direction (D'Agostino *et al.*, 2001). However, there are other mechanisms that can lead to drainage integration between adjacent extensional basins. Drainage integration may partly be explained by the structural evolution of normal fault systems as adjacent fault segments propagate and link (Cowie *et al.*, 1998). This leads to the structural lowering of topographic thresholds between these basins so they can become fluvially connected in an along-strike direction (Gawthorpe & Leeder, 2000; Connell *et al.*, 2005; Menges, 2008; House *et al.*, 2008). Another structural mechanism allowing integration to occur can

be a reduction of fault slip rates over time (Connell *et al.*, 2005). However, for explaining drainage integration across-strike and at a regional scale, as observed in the central Italian Apennines, additional mechanisms based on the dynamics of the fluvial system itself are required. Besides headward erosion (e.g. D'Agostino *et al.*, 2001; Dickinson, 2015), other important mechanisms, proposed mainly for other areas, are the spilling over of lakes (e.g. Bishop, 1995; Douglass *et al.*, 2009; Smith, 2013; Garcia-Castellanos *et al.*, 2003) and the complete infilling of tectonic basins with sediment (e.g. Bishop, 1995; D'Agostino *et al.*, 2001; Douglass *et al.*, 2009). Although we have a fairly good understanding of these different mechanisms at a local scale, i.e. for individual basins, many fundamental questions remain regarding the conditions under which the different mechanisms may dominate and the impact of drainage integration on landscape evolution, sediment dispersal and, ultimately, basin stratigraphy in continental rifts (Smith, 2013).

There are additional reasons why improving our understanding of drainage integration is important. First of all, it forms a key aspect of transient landscape development in extensional settings but has, in contrast to the evolution of normal fault systems, received surprisingly little attention (e.g. Bishop, 1995; Stokes *et al.* 2002). Secondly, drainage integration has a profound impact on the volumes and characteristics of sediment supplied to tectonic basins (e.g. Smith, 2013). Thirdly, through its impact on sediment dispersal and hence mass redistribution, it is of great relevance for studies on the feedback between surface processes and tectonics in extensional settings (e.g. Maniatis *et al.*, 2009; Buitter *et al.*, 2008). However, studying drainage integration in the field is complicated due to poor preservation of evidence. This is because drainage integration generally produces a wave of erosion in response to base-level changes. To overcome the problem of limited field evidence we investigate the processes of drainage integration by means of numerical modelling. We use a simple model setup that includes the main features of tectonic deformation in the central Apennines to drive surface processes through time. By applying our modelling approach to this area we make use of a wealth of field observations for calibrating our model and for evaluating our results. While previous modelling studies have demonstrated aspects of drainage reorganization in rifts at a local scale (Cowie *et al.*, 2006; Douglass &

Schmeeckle, 2007; Smith, 2013; Garcia-Castellanos *et al.*, 2003), this approach allows us to address the problem at a regional scale (>100 km), involving a large number of extensional basins and fault-blocks.

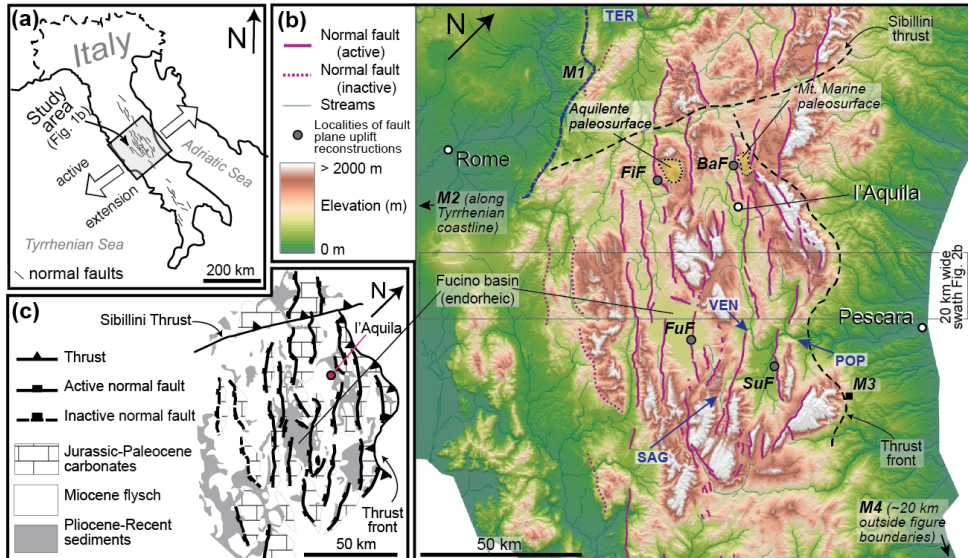


Fig. 3.1 (a) Location map of the study area in the central Apennines, (b) the study area and model domain itself (DEM from Tarquini *et al.* (2007)), and (c) a simplified geological map of the area showing the main lithological units (modified from Whittaker *et al.* 2008). On top of the topographic map in (b) we show active (solid pink lines) and inactive (dashed pink lines) normal faults (principally after Roberts & Michetti, 2004). We also show sea-level markers (M1 = Early Pleistocene shoreline, M2 = Last-interglacial shoreline, M3 = Sicilian shoreface deposits, and M4 = Last-interglacial floodplain, see also Supplementary Materials S2), fault sites (FiF = Fiamignano fault, FuF = Fucino fault, BaF = Barete fault, and SuF = Sulmona fault; see also Fig. 3.2b) and paleosurfaces which were used for estimating long-wavelength uplift (see also Supplementary Materials S3). Other abbreviations used on the map are: TER = Terni basin, SAG = Sagittario gorge, VEN = San Venanzio gorge, and POP = Popoli gorge.

3.3 Geological setting

The central part of the Italian Apennines is the highest (up to ~2900 m) and widest part of the Apennines mountain belt. After cessation of thrusting during the Pliocene (Patacca *et al.*, 1990) its Quaternary landscape evolution (ca. the last 3 million years) has been dominated by a combination of regional uplift and southwest-northeast extension localised on dominantly southwest dipping normal faults (e.g. Roberts & Michetti, 2004; Fig. 3.1b). Brackish marsh deposits at the base of some of the

extensional basins suggest the area was close to sea-level when extension and uplift commenced (Gliozzi & Mazzini, 1998). Regional uplift has produced a topographic bulge as the mountain belt interior has undergone large (>800 m) differential uplift relative to the coastlines (D'Agostino *et al.*, 2001; Centamore & Nisio, 2003; Pizzi, 2003; Ascione *et al.*, 2008; D'Anastasio *et al.*, 2006; Serpelloni *et al.*, 2013; Mancini *et al.*, 2007). Most of the extensional deformation has occurred along the crest of this topographic bulge and is accommodated by a wide (>60 km) array of normal faults (Fig. 3.1b; D'Agostino *et al.*, 2001; Roberts & Michetti, 2004; Faure Walker *et al.*, 2010). Over time these faults have generated large footwall uplifts mainly consisting of Mesozoic limestone and have trapped thick sequences of continental deposits in their hanging-wall basins (Fig. 3.1c; Cavinato, 1993; Cavinato *et al.*, 1994; Cavinato & De Celles, 1999; Miccadei *et al.*, 2002; Cavinato *et al.*, 2002). Total throw estimates along the (up to 40 km long) faults vary across the area but tend to be greatest (up to 2200 m) across the more centrally located, higher elevation, faults (Cowie & Roberts, 2001; Roberts & Michetti, 2004).

The elevated topography in the central part of the Apennines cannot be explained by crustal or lithospheric isostasy (Faccenna *et al.*, 2014). However, a clear correlation exists between topography, surface uplift and regional extension rates, suggesting that uplift and extension are driven by the same underlying mechanism (Faure-Walker *et al.*, 2012). Although the exact mechanism is debated (see review provided by Faccenna *et al.*, 2014) uplift and extension are likely related to either flow or buoyancy variations in the uppermost mantle and removal of mantle lithosphere (e.g. D'Agostino & McKenzie, 1999; D'Agostino *et al.*, 2001; Bartolini *et al.*, 2003; Cowie *et al.*, 2013; Faccenna *et al.*, 2014).

As first discussed by D'Agostino *et al.* (2001), many field observations demonstrate the combined impact of uplift and faulting on the geomorphologic development of the central Apennines and on the evolution of the drainage network (see also D'Alessandro *et al.*, 2003, 2008; Ascione *et al.* 2008). A key observation is that most of the major fault-bounded basins contain lake sediments in the older parts of their stratigraphy (Cavinato, 1993; Cavinato *et al.*, 1994; Cavinato & De Celles, 1999;

Miccadei *et al.*, 2002; Cavinato *et al.*, 2002). Based mainly on these sediments it has been concluded that many large lakes co-existed during the Lower-Middle Pleistocene suggesting that endorheic drainage was prevalent at that time (D’Agostino *et al.*, 2001; Piacentini & Miccadei, 2014). Today, most of these basins are fluvially dissected and connected to one another and to the coast. In other words, a temporal transition is inferred to have occurred from internal to external drainage leading to the integration of previous isolated basins with the regional river network (D’Agostino *et al.*, 2001; Bartolini *et al.*, 2003; Piacentini & Miccadei, 2014). Developing a better understanding of this transition via numerical modelling is the focus of this study.

3.4 Methodology

For simulating regional landscape evolution for the setting of the central Apennines we use the surface process model CASCADE developed by Braun and Sambridge (1997). Its suitability has been demonstrated for modelling landscape development in extensional settings, where both fluvial erosion and deposition occur and where lakes are common features in the landscape (Cowie *et al.*, 2006). There is a one-way coupling in our model in that we allow surface processes to respond to surface deformation due to tectonics, but there is no feedback of surface processes on the tectonics. Besides extensional faulting our model also includes regional uplift, and both are simulated by means of simple surface deformation functions (see below).

Table 3.1. Overview of parameter values used in the surface process model CASCADE.

Parameter	Description	Values	Units
dx,dy	Grid resolution	1000	m
dt	Calculation timestep (adjusted dynamically)	~ 100	yr
$endtime$	Length of model run	$3 \cdot 10^6$	yr
v	Effective precipitation rate	1	m/yr
K_f	Dimensionless fluvial transport parameter	0.08 – 0.12	-
L_f	Fluvial erosion length scale	$30 - 70 \cdot 10^3$	m
ϕ	Scaling exponent for channel width $W = c \cdot Q^\phi$	0.5	-
c	Scaling factor for channel width $W = c \cdot Q^\phi$	1	-

The model domain covers all land area between the modern coastlines in central Italy (Fig. 3.1b). The region is rotated 45° clockwise relative to true North so that the dominant SW-NE direction of extension coincides with the x-direction in the model domain (Figs 3.1a-b). The model domain is 170 x 170 km and has a spatial resolution of 1 km in both directions (Table 3.1). The left and right boundaries of the model domain represent the Tyrrhenian and Adriatic coastlines, respectively. These coastal boundaries are fixed in order to keep base-level constant, as climatically induced sea-level oscillations are small compared to the tectonic deformation we impose. We return to this assumption in the Discussion section. The other two boundaries of the model domain delimit our study area in the along strike direction, i.e. along the Apennines (y-direction in the model), and are free to slip vertically. All four boundaries are open in the sense that water and sediment can cross them. There is a free surface above for enabling topography to develop and vertical surface displacements are imposed from below. We run all our experiments for 3 million years, i.e. the estimated duration of extension (Roberts & Michetti, 2004). Although some authors suggest that regional uplift may have commenced more recently (e.g. Pizzi, 2003) we impose regional uplift from the beginning of the model runs for the sake of simplicity. The calculation time step in the model is adjusted dynamically but is ca. 100 years on average. We do not assume any pre-existing topography, except for 1 m-scale random noise to initiate flow, even though the central Apennines were likely characterised by some relief at the time extension commenced (e.g. D'Alessandro *et al.*, 2003). This means that there is no inheritance effect on drainage network development. We evaluate the potential implications of our zero pre-existing topography assumption in the Discussion section.

3.4.1 Normal faulting surface deformation and regional uplift function

For our calculations of vertical surface deformation in response to normal faulting we use the elastic dislocation model Coulomb 3.4 (Toda *et al.*, 2005; Lin & Stein, 2004), which is based on linear elasticity laws and a half-space assumption (Okada, 1992; for more details see *Supplementary Materials S1*). The main input to the elastic

dislocation model is a fault map that includes all normal faults thought to have accommodated extension in the central Apennines since the Early Pleistocene (principally based on Roberts & Michetti, 2004 and Wedmore *et al.*, 2017). Except for some faults located in the southwestern part of the area, they are all considered as active today and throughout the modelling period (Fig. 3.1b). In order to focus on the main topographic features only, the fault map was simplified by removing faults shorter than 5 km and by straightening the fault traces (compare Figs 3.1b and 3.2a). The simplified fault map comprises 50 faults with lengths between 5 and 40 km. Nearly all faults dip to the southwest (towards the left in the model domain) and we assume pure dip-slip for all of them. Rarely observed minor strike-slip motions do not contribute to relief and are thus ignored.

Table S1 (*Supplementary Materials S1*) shows the parameter values used in the elastic dislocation model. Parameters for which no field area-specific data exist are assigned published values and are kept constant in all our calculations (Poisson's ratio, Young's modulus and coefficient of friction). The three fault-related parameters dip angle ('*dip*'), fault root depth ('*root*'), and a linear fault length-displacement scaling factor (γ or '*gamma*') are most important for our study. The latter scales maximum fault displacement D (experienced by the central part of the fault) linearly to fault length L as given by: $D = \gamma \cdot L$ (Cowie & Scholz, 1992). For each of these parameters, we test the impact on the vertical surface displacement field for three different values (two extremes and one intermediate value) based on published data from the central Apennines (Table S1; *Supplementary Materials S1*). The parameter γ has the greatest impact on the vertical surface displacement field. Our intermediate value for γ (0.07) produces total throws which correspond best to those estimated in the field (Roberts & Michetti, 2004), and we use this surface deformation field as our standard faulting scenario in all of our experiments (Fig. 3.2a). For transforming the fault map into surface deformation rates used in the landscape evolution model, we divide the total uplift and subsidence values by 3 million years (see Fig. 3.2a for the resulting uplift and subsidence rates). This implies that fault offsets accumulate linearly over time (with $\gamma = 0.07$, maximum uplift and subsidence rates are ca. 0.24 and -0.54 mm yr⁻¹,

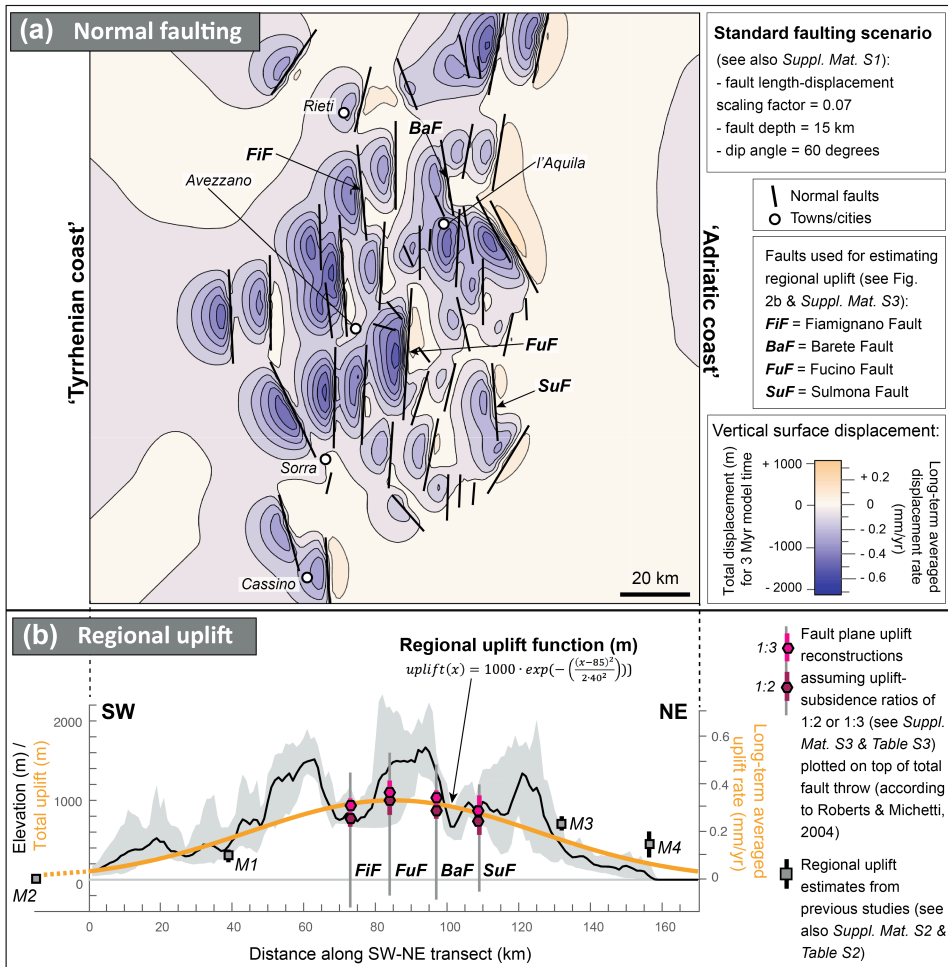


Fig. 3.2. (a) Vertical surface displacement map produced by the elastic dislocation model *Coulomb 3.4* based on a simplified fault map from the central Apennines (modified from Wedmore et al., 2017). It shows our ‘standard faulting scenario’ using dip = 60°, root = 15 km, and $\gamma = 0.07$ (see Methodology section and Supplementary Materials S1). This displacement field is assumed to represent the accumulated impact of normal faulting after 3 Myr. Uplift and subsidence rates (mm/yr) are the total uplift and subsidence values divided by 3 million years. (b) Regional uplift curve showing the total amount of long-wavelength surface uplift along a coast-to-coast transect projected on top of a 20 km wide topographic swath (in grey) across the central Apennines (see Fig. 3.1b for swath location). Regional uplift rates (mm/yr) are the total regional uplift values divided by 3 million years (see vertical axis on the right). Also shown are localities and elevations of field observations that were used to constrain the amplitude and shape of the regional uplift function. These observations comprise four different sea-level markers (M1-M4; see also Supplementary Materials S2) and the localities of four faults (FiF, FuF, BaF, and SuF) where the amount of regional uplift was estimated (see also Supplementary Materials S3).

respectively). Because field evidence suggests that some faults in the central Apennines experienced an increase in slip rate around 0.5-1.0 Ma (Cowie & Roberts, 2001; Roberts & Michetti, 2004; Whittaker *et al.*, 2008) we address the potential implications of changes in fault slip rates in the Discussion section.

We simulate long-wavelength regional uplift across the mountain belt and its forelands using a Gaussian function (coast-to-coast transect; Fig. 3.2b). In the direction parallel to the mountain range, i.e. parallel to the y-axis in our model domain, we assume regional uplift to be uniform. We scaled our Gaussian function based on published field observations and some new estimates of regional uplift for the mountain range interiors, in order to obtain the right order of magnitude of total Pleistocene plus Holocene uplift (Fig. 3.2b). Because of the limited number of well-dated regional uplift estimates and their considerable spatial variability across our study area, we emphasise that our regional uplift function is only a first-order approximation. However, most important for our modelling study is that it accounts for the strongest uplift in the mountain range interiors and a gradual decline when moving across the foreland areas towards the Tyrrhenian and Adriatic coastlines. The published data that we used for constraining our uplift function in the foreland areas are paleoshorelines and exposed shoreface deposits (e.g. D'Agostino *et al.*, 2001; Pizzi, 2003). The data from the different sites is provided in Fig. 3.2b and described in more detail in *Supplementary Materials S2* (Table S2). Besides these published observations we use structural data from four normal faults to provide some additional constrains on our regional uplift function in the interior part of the central Apennines. For these four normal faults (see Figs 3.1b and 3.2a for their locations) we estimate the amount of uplift of their fault planes by assuming typical long-term ratios of footwall uplift to hanging-wall subsidence and by assuming that the land surface was close to sea-level before regional uplift started. A detailed description of our method, the data, and our regional uplift estimates are provided in *Supplementary Materials S3* (Table S3). These new uplift estimates suggest a total amount of regional uplift of around 1000 m in the innermost part of the central Apennines that corresponds well with reconstructions made by others (Ascione *et al.*, 2008; Pizzi, 2003). It is important to note that we use a symmetrical uplift function in most of our numerical experiments

even though some studies suggest the Adriatic flank of the mountain range may have experienced more uplift than its Tyrrhenian counterpart (e.g. Pizzi, 2003). We assume a symmetric function for simplicity and because there seems to be no general agreement about the exact pattern of regional uplift. The potential implications of this assumption are addressed in the Discussion section. Regional uplift rates are kept constant through time in our model (see Fig. 3.2b for regional uplift rates).

3.4.2 Surface process model

We use CASCADE for simulating fluvial erosion and sediment deposition in lakes (Table 3.1). The fluvial erosion algorithm follows the ‘under-capacity model’ and can generate both erosion and deposition (Kooi & Beaumont, 1996; Van der Beek & Bishop, 2003):

$$\frac{dh}{dt} = \frac{1}{W \cdot L_f} (Q_c - Q_s) \quad (1)$$

where $\frac{dh}{dt}$ is elevation change. Transport capacity Q_c is the volume of sediment that is theoretically possible to be carried by the flowing water and its magnitude depends on discharge Q_w and local channels slope S :

$$Q_c = K_f \cdot Q_w \cdot S \quad (2)$$

This linear dependency is scaled by the dimensionless transport capacity constant K_f . The sediment volume Q_s in equation (1) is determined by integrating all the elevation changes that are occurring upstream and represents the sediment passed to every node in each time step:

$$Q_s = \int_0^A \frac{dh}{dt} da \quad (3)$$

where A is the total upstream drainage area and da is the downstream increment of upstream area. According to equation (1) the rate of erosion or deposition $\frac{dh}{dt}$ is primarily a function of the disequilibrium between the transport capacity Q_c of the

river and the volumetric sediment flux Q_s . If $Q_c > Q_s$ there is erosion, if $Q_c < Q_s$ there is deposition, and the difference between them controls the rate of erosion or deposition. However, erosion and deposition rates are additionally controlled by the width of the channel W and the fluvial length-scale parameter L_f , which both reduce erosion rates as their values increase. Because of the large dimensions of our study area we assume channel width to vary as a function of discharge ($W = \sqrt{Q_w}$). Both parameters K_f and L_f affect the erosive conditions in our model. Simply stated, higher values for K_f generate higher erosion rates and vice versa, whereas lower values for L_f generate higher erosion rates and vice versa. However, as discussed in detail by Cowie *et al.* (2006), L_f additionally controls the way in which rivers respond to changes in base-level, either in a more transport-limited or in a more detachment-limited manner. We systematically varied K_f and L_f between 0.08 – 0.12 and 30 – 70 km, respectively, in order to test the sensitivity of our model (see *Supplementary Materials S4*). We do not consider spatial lithological differences and temporal changes in climate in this study, and K_f and L_f are consequently kept constant in space and time. We address the potential implications of assuming a uniform lithology in the Discussion section. Climate variability is out of the scope of our study as it is not possible to resolve its crucial aspects (e.g. storm intensity) on geological time-scales (e.g. Whittaker, 2012). Land-sliding is locally important for landscape evolution in the central Apennines (Whittaker *et al.*, 2010) but we do not include it because the spatial resolution (1000m) of our regional scale model means that no slopes exceed the critical angle for landslide initiation (typically $\geq 21^\circ$). The fluvial algorithm in CASCADE does not distinguish fluvial channels from the interfluvial areas and thus erosion occurs across the entire landscape not only along channels.

Important for this study is the treatment of water and sediment when a stream enters a local minimum in an extensional basin. First of all, the model calculates the lowest point on the rim of the basin (i.e. the spill-point) and defines all nodes in the basin at lower elevation as lake nodes. All sediment entering a basin is trapped as long as the basin is under-filled and supports a lake. The sediment is deposited in nodes closest to the river mouth, causing basins to become progressively filled from their edges. With

regard to water conservation we simulate truly endorheic drainage, i.e. closed basins where water loss through evaporation or seepage (including karst) exceeds water supply. This is chosen because at least two large lakes in central Italy, i.e. the historical Fucino lake (which is now artificially-drained) and the Trasimeno lake (Umbria; Ludovisi *et al.*, 2013), demonstrate the occurrence of truly endorheic drainage under modern-day (interglacial) climatic conditions. Additionally, some studies on Italian lakes have demonstrated the important role of evaporation in controlling their hydrological balance also in glacial times (e.g. Zanchetta *et al.*, 2007). Finally, by comparing model experiments in which we implemented either endorheic or non-endorheic (water 100 % conserved) drainage we found that characteristic topographic features of the central Apennines and important aspects of its evolution are only reproduced by means of the endorheic type of drainage (see *Supplementary Materials S5*).

3.5 Model results

3.5.1 Topographic development

Here we present results mainly from our ‘reference model’ (using $K_f = 0.10$ and $L_f = 50$ km) as it shows the general behaviour of the system we model. Varying erosional conditions produces slightly different patterns and rates of landscape development but does not change the main trend of landscape evolution (see *Supplementary Materials S4*). The surface displacement field (faulting (Fig. 3.2a) and regional uplift (Fig. 3.2b) together) produces +1600 m and -900 m of maximum uplift and subsidence, respectively, corresponding to maximum rock uplift and subsidence rates in between -0.3 and $+0.6$ mm yr⁻¹ over 3 Myr. The steady-state concavity of major river systems crossing both the faulted domain and the foreland area lies between ca. 0.35 and 0.6 for the K_f and L_f values used in our reference model (*Supplementary Materials S6*). This range encompasses concavity values that are typical for steady-state river profiles in general and also corresponds well with those observed in the central Apennines (Whittaker *et al.*, 2008).

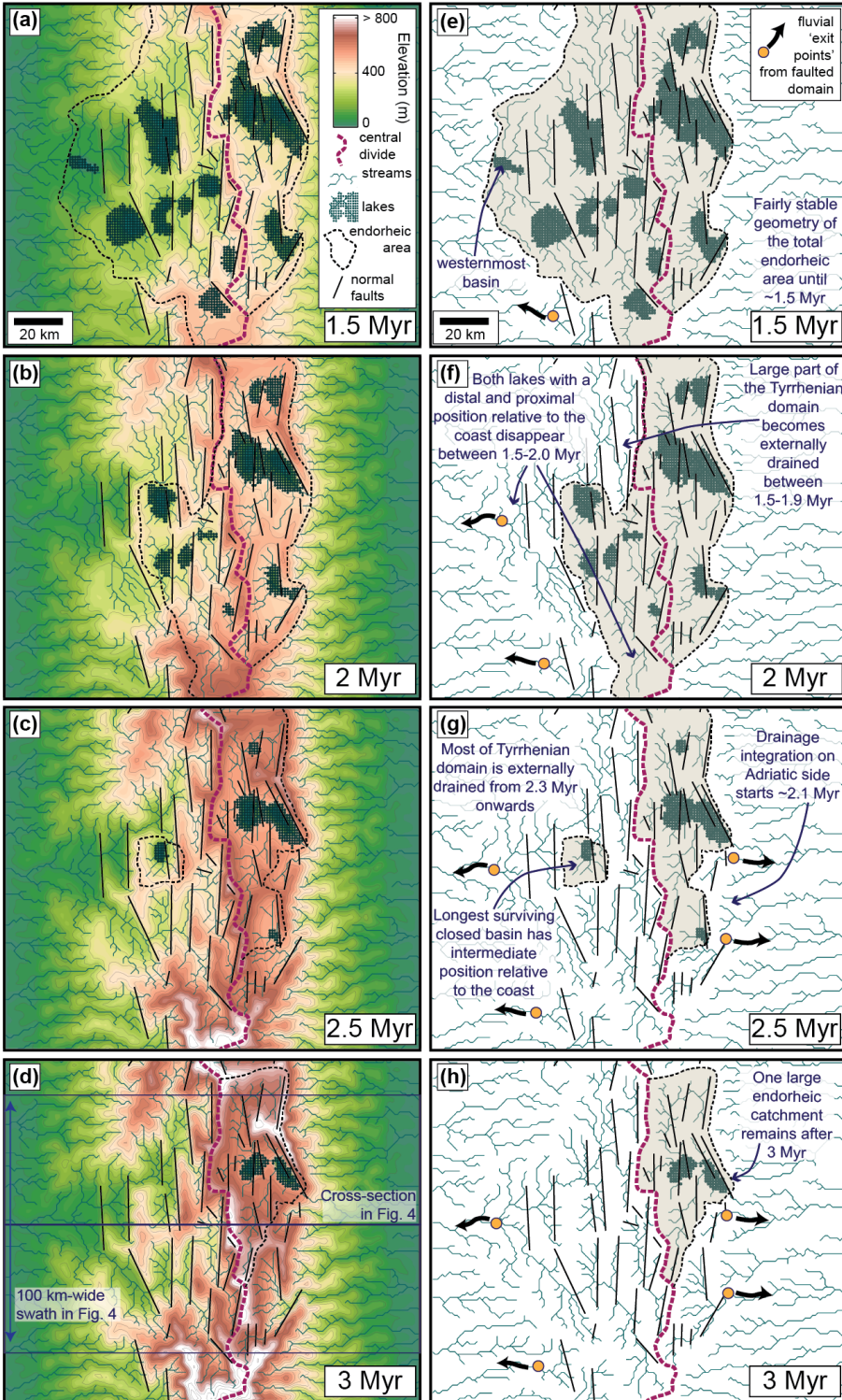


Fig. 3.3. (shown on previous page) Time evolution maps from our reference model (see main text) showing the main landscape features after 1.5, 2, 2.5 and 3 Myr. (a-d) Topographic evolution. (e-h) Development of the drainage network. The maps show only lakes $> 10 \text{ km}^2$, associated with the fault-bounded basins. By fluvial 'exit points' we mean localities on the edges of the faulted domain where the intermountain drainage network becomes integrated with streams draining towards the coast. At these localities water and sediment exits the mountainous area affected by normal faulting. For model sensitivity tests, see Supplementary Materials S4.

Figures 3.3a-d illustrate over four time steps how the topography evolves through time in the reference model. Initially, elevations remain low everywhere ($< \sim 500 \text{ m}$ during the first 1.5 Myr of run-time), since we do not assume any pre-existing topography. However, with time, mean elevations in the central part of the model domain increase as a consequence of regional uplift (Figs 3.3a-d). Our reference model produces just over 1000 m of topography after 3 Myr run-time (Figs 3.3d, 3.4). A local-scale morphology of longitudinal ridges and basins develops due to the normal faulting superimposed on the regional topography (Figs 3.3d, 3.4). This gradual increase in relief at two different spatial scales (regional vs. local-scale) is characteristic of the topographic development in our model and is consistent with the topography of central Italy today (see Discussion section). While the final regional relief is approximately 1000 m, the local-scale ($\sim 10\text{-}20 \text{ km}$) fault-related relief is of the order of hundreds of meters, but varies greatly throughout the model (Fig. 3.4). This large spatial variation in fault-related relief in our model is caused by variations in fault length, fault spacing, the orientation of faults relative to one another, and the position of faults relative to the regional uplift field. This is because surface deformation at any location in our model is the sum of all surface deformation fields produced by the individual faults plus the regional uplift field (Fig. 3.2). Local relief is additionally affected by the degree of basin infilling. Because most basins experience, successively, sedimentation and incision, the degree of infilling is strongly time-dependent. Another striking feature of the final topography is its asymmetry (higher topography on the Adriatic side) even though our regional uplift function is symmetrical (lower part of Fig. 3.4). This asymmetry is partly due to the SW preferential fault dip in combination with the relative small fault spacing (so that the uplift-subsidence fields of individual faults overlap), generating higher fault-related topography on the Adriatic side (Fig. 3.2a).

However, as discussed below in ‘Regional-scale sediment dispersal’, the asymmetry in topography additionally results from different rates of erosion and overall landscape evolution between the Adriatic and Tyrrhenian domains.

Both spatially averaged mean and maximum elevations continue to increase even at the end of each model run (Fig. 3.5a). In other words, the landscape does not reach a topographic steady state within the 3 Myr time period we consider here. This is consistent with the transient landscapes observed today in the central Apennines (e.g. Whittaker *et al.*, 2008) and on-going surface uplift (D’Anastasio *et al.*, 2006; Serpelloni *et al.*, 2013). In our reference model, steady state is reached approximately after 6 Myr, i.e. after twice the normal model run-time. In the central Apennines today elevations can exceed 2000 m, while in the model the highest elevations are around 1000 m. This difference can be attributed to pre-existing topography, something we come back to in the Discussion section.

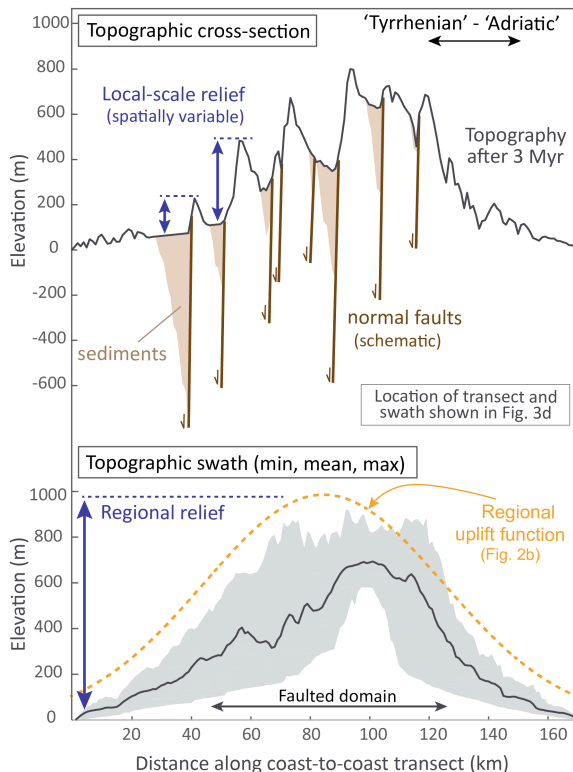


Fig. 3.4. Topographic profile (top panel) and 100-km wide topographic swath profile (bottom panel) across the final (3 Myr) topography of the reference model (transect and swath shown in Fig. 3.3d) together with normal faults (schematic) and basin deposits. Vertical arrows demonstrate regional and local scale relief (see main text). The regional uplift function is shown as reference in the bottom panel (see also Fig. 3.2b).

3.5.2 Drainage network evolution

At the beginning of the experiments, small stream networks initiate over the entire model domain. A large number of lakes form particularly in the faulted domain where local topographic minima develop in the hanging-wall basins. Each of the drainage basins that support lakes are endorheic, i.e. internally drained (see ‘Surface process model’). The lakes act as local base-levels and trap all the sediment delivered from upstream. Initially, the whole area affected by normal faulting is internally drained, i.e. circa 40-50% of the total model domain (Figs 3.3e, 3.5b). However, through time we observe a consistent trend of progressive integration of the drainage network, resulting in the disappearance of lakes and shrinkage of the total endorheic area (Figs 3.3e-h, 3.5b). Although both lake and endorheic area show a progressive change over time it is important to note that the total surface area occupied by lakes (‘total-lake-area’) declines in a different way compared to the total area that is internally drained (compare Figs 3.5b and 3.5c). The total-lake-area shrinks from the beginning of the model run, with the most drastic decline occurring during the first 1.5 Myr of the experiment (from ~24% down to ~7% of the total model domain, see Fig. 3.5c). On the other hand, the total endorheic area remains fairly constant until 1.5 Myr and successively shrinks in a step-wise manner (Fig. 3.5b). The reason why the total-lake-area decline is so different from that of the endorheic area (Figs 3.5b-c) is because the extent of the endorheic area is determined by the presence of lakes most proximal to the coast. For instance the westernmost basin (e.g. Fig. 3.3e) keeps the Tyrrhenian flank internally drained until ~1.6 Myr although many lakes upstream have already disappeared. The transition from internal to external drainage means that sediment produced in the upland area is henceforth transported out of the faulted domain, and thus exported to the coast, at localities that we define as fluvial ‘exit points’ (Figs 3.3e-h).

Characteristic of the drainage network in general is the strong contrast in drainage network geometry, within and outside the central area affected by normal faulting. Outside the faulted domain the network has a parallel to slightly dendritic appearance,

formed by channels that follow the regional slope of the land surface towards both coastlines (Fig. 3.3). Within the central area, however, many streams or stream segments flow axially, parallel to fault strike, forming a trellis-like drainage pattern (Twidale, 2004). The planview geometry of the drainage network and the position of the central drainage divide are established early on and remain fairly stable over time (Fig. 3.3). The position of this drainage divide is controlled by the regional uplift field (see also *Supplementary Materials S7*).

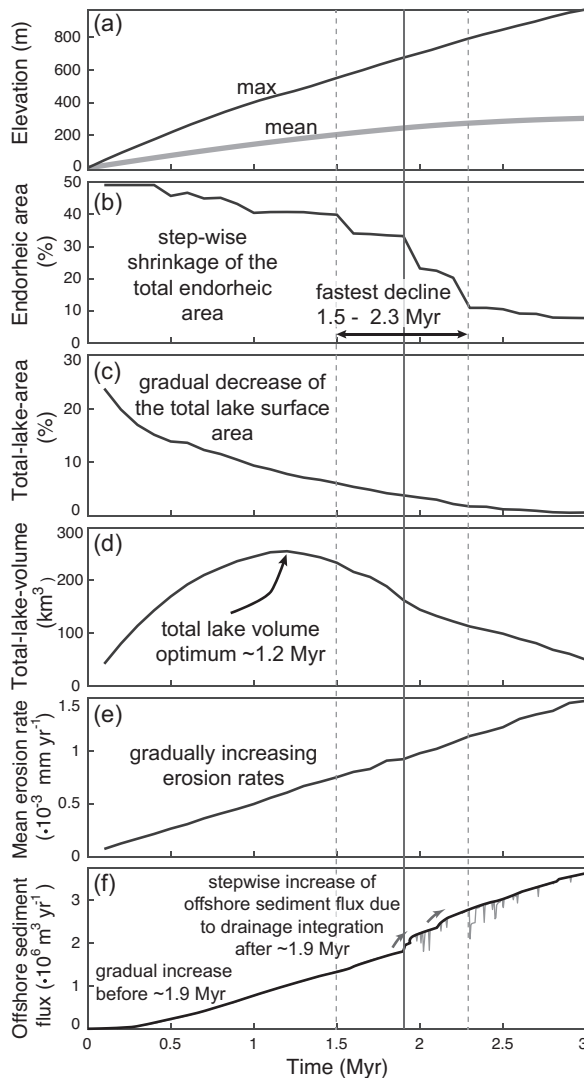


Fig. 3.5. Time evolution plots showing different aspects of modelled landscape evolution. (a) Maximum and mean elevation calculated for the total model domain. (b) Size of the total area that is internally drained (as a percentage of the total model domain), as indicated by the grey area in Figs 3.3e-h. (c) Total surface area occupied by lakes (as a percentage of the total model domain). (d) Total volume of all lakes together. The volume of each individual lake is determined by calculating the volume of water that is needed to fill a topographic depression up to its spill point. (e) Mean erosion rate, based on the total area experiencing erosion (excluding depocentres). (f) Sediment flux crossing the coastal (left and right) boundaries of the model.

3.5.3 *Drainage integration*

The dominant mechanism that causes drainage integration in our model is what we call ‘basin overfilling’. By this we mean the filling of basins with sediment up to the elevation of their spill-point, i.e. the lowest point on their morphological boundaries. When a basin becomes overfilled with sediment the water can spill over and the lake environment is replaced by a through-going river system (Fig. 3.6a). From this moment onwards, some sediment is still deposited within the basins to balance newly created accommodation due to fault-controlled basin subsidence, but most sediment is now transported downstream towards other basins (Figs 3.6a, c) or all the way to the coast. The long-term regional-scale tendency of basins to become overfilled demonstrates that sedimentation rates gradually start to outpace the rate at which accommodation is created through basin subsidence. This happens over time as mean erosion rates increase owing to an increase in both fault-related and regional relief (Fig. 3.5e). This increase in mean erosion rates, in turn, causes a gradual shift in the balance between sediment supply and accommodation creation within the basins. Using lake volume as a proxy for how undersupplied a basin is we can demonstrate this shift (Fig. 3.6b). Lake volumes firstly tend to increase, meaning that the basins become increasingly undersupplied. However, this trend reverses as soon as sediment supply outpaces accommodation creation causing the lake to shrink and the supporting basin to become progressively less undersupplied. It is important to note that each individual basin/lake follows its own curve (Fig. 3.6b). In our reference model, the total volume of all lakes together increases until circa 1.2 Myr and successively decreases thereafter (Fig. 3.5d).

The order in which the individual basins become overfilled does not follow any clear spatio-temporal pattern. For instance within the Tyrrhenian part of the chain interior, lakes with either a proximal or distal location relative to the coast disappear early on in time (e.g. Fig. 3.3f). Moreover, the longest surviving endorheic basin on the Tyrrhenian side has an intermediate position and is not located closest to the central drainage divide (Fig. 3.3g). A clear spatio-temporal pattern is lacking because basin overfilling is a function of a large number of local factors that affect the balance

between sediment supply and accommodation creation. The rate at which accommodation is created is not only a function of fault length and slip-rate, but is also affected by the position of faults relative to one another. Sediment supply on the other hand is controlled by the size of the source area and its internal relief, which are also strongly controlled by the pattern of faulting. Furthermore, sediment supply to individual basins depends on the infilling histories of basins located upstream.

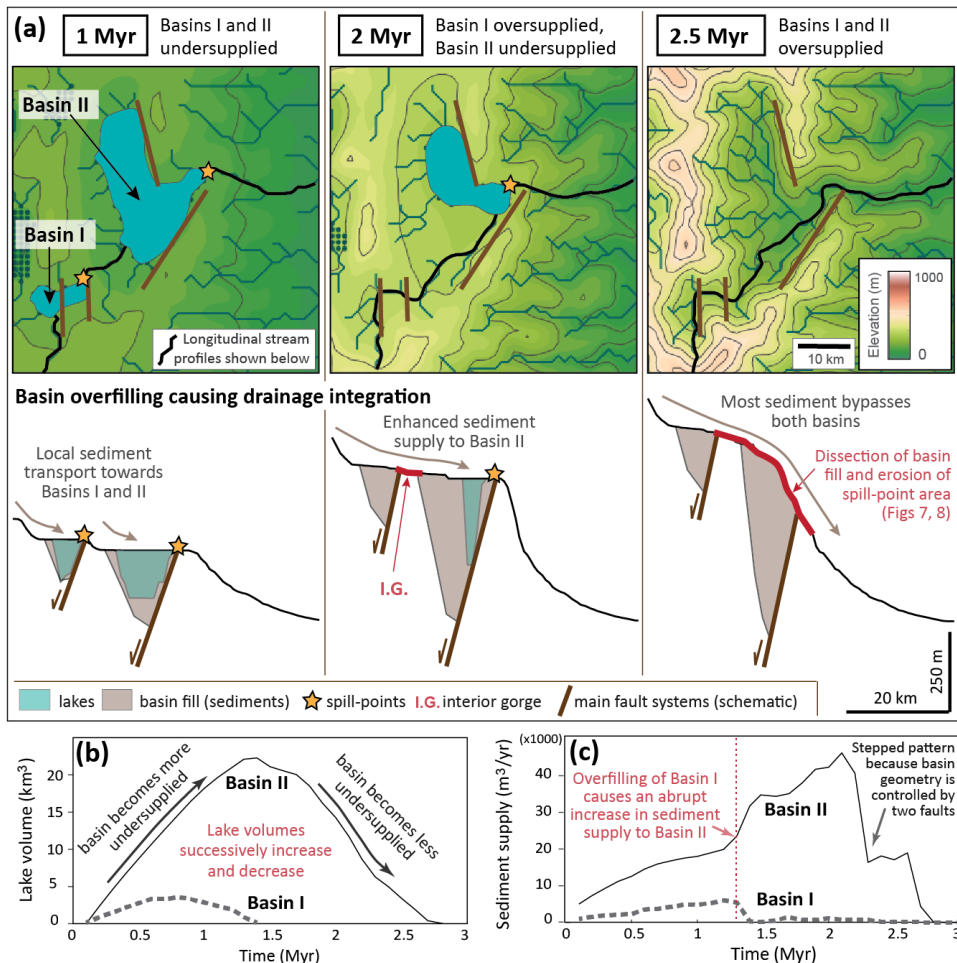


Fig. 3.6. (a) Maps and cross-sections of two fault-bounded basins in the model illustrating the gradual filling of basins through time and the mechanism of basin overfilling (for location see Fig. 3.7a). Basin I and basin II become overfilled around 1.3 and 2.2-2.8 Myr, respectively. I.G. = Interior gorge, located in between basin I and II. (b) Lake volume curves of basin I and II shown in (a). These curves show that basins initially tend to become more under-supplied but later on less under-supplied due to constant fault-slip rates but increasing erosion rates. (c) Sediment supply to basin I and II, showing that overfilling of basin I generates a sudden increase in sediment supply to basin II.

3.5.4 *Regional-scale sediment dispersal*

Erosion rate maps (Figs 3.7a-c) show the general pattern of erosion and deposition in our reference model: Sediment is mainly produced at the footwall highs and along the major river valleys and is deposited in the fault-controlled basins or offshore (outside the model boundaries). However, the three different time windows (Figs 3.7a-c) also show how sediment dispersal changes over time. The most important regional trends are: 1) The gradual increase in erosion rates and hence sediment production due to increasing relief, and 2) the progressive decline in deposition in tectonic basins due to drainage integration (e.g. compare Figs 3.7a and c). Because less sediment is trapped within the basins over time, progressively more sediment becomes removed from the faulted domain as the landscape evolves. In other words, there is a delayed export of sediment out of the mountain range towards the offshore.

At a local scale, on the other hand, we observe abrupt shifts between erosion and deposition. These shifts are again related to drainage integration that acts as a threshold phenomenon. While most basins firstly experience a relative stable phase of lake sedimentation (e.g. Fig. 3.7a), they abruptly switch to a fluvial environment with strong incision as soon as they become overfilled. Incision initiates in the area of the spill-point as a new base-level is established at a lower level and there is an abrupt increase in discharge (Figs 3.7b, 3.8a) as the fluvial system becomes connected. Lowering of the spill-point, in turn, generates a wave of erosion that starts to propagate upstream and deeply dissects the basin fill (Figs 3.7c, 3.8b). In other words, in our model, sedimentary basins themselves and their spill-point areas are most prone to abrupt local changes in erosion or deposition. All the surrounding terrain successively adapts in a more gradual manner. However, it is important to note that these local developments, due to drainage integration, strongly affect the downstream parts of the catchment. For instance when a basin becomes overfilled, the sediment is no longer trapped and is henceforth transported to another basin downstream (Figs 3.6a, c). Additionally, strong incision commences in the valley in between the basins causing the sediment supply to the downstream basin to become enhanced even more.

As such, the infilling history of each basin is a function of the infilling histories of all the other basins located upstream.

After 3 Myr of landscape evolution, the Tyrrhenian and Adriatic domains (i.e. measured from the central divide) have experienced approximately the same amount of erosion (respectively 49 and 51 %; Fig. 3.7d), implying that both offshore areas have received similar sediment volumes overall. However, Fig. 3.7d clearly shows that erosion is most intense on the Adriatic flank of the central Apennines in our model. This is because the SW preferential fault dip is opposite to the regional slope in the Adriatic domain, generating higher relief along the flank of the mountain range and thus higher erosion rates (Fig. 3.9). The reason why this does not produce a higher total sediment output to the Adriatic offshore compared to the Tyrrhenian offshore, is that a large part of Adriatic faulted domain is still internally drained after 3 Myr in our model (Fig. 3.7c). This latter effect can also be attributed to the structural setting of the Adriatic domain (fault dip opposite to regional slope) as it slows down basin overfilling and therefore drainage integration. In other words, within the Adriatic faulted domain, local relief and therefore sediment delivery to hanging-wall basins are relatively low while the rate of accommodation creation is relatively high compared to its Tyrrhenian counterpart (Fig. 3.9).

The offshore as a whole, i.e. the Tyrrhenian and Adriatic coasts together, experiences a long-term progressive increase in sediment supply in our model (Fig. 3.5f). At around 1.9 Myr an abrupt increase in the offshore sediment flux is observed when most of the internally drained area on the Tyrrhenian flank becomes fluviially connected to the coast (Fig. 3.3f). Every time a significant part of the faulted domain becomes externally drained, a step-wise increase is observed in the offshore sediment flux (Fig. 3.5f).

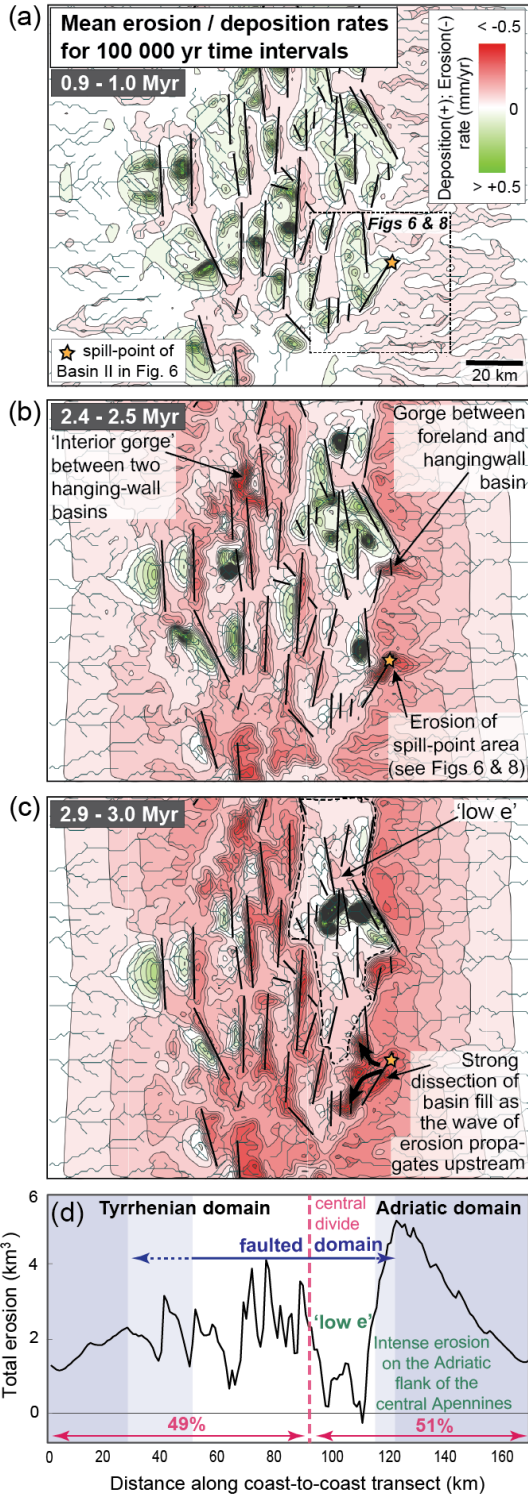


Fig. 3.7. (a-c) Erosion-deposition maps showing the total amount of erosion and deposition that occurred in the model during 100 kyr periods, namely 0.9-1 Myr, 2.4-2.5 Myr and 2.9-3 Myr. Yellow stars correspond to the spill point of Basin II in Fig. 3.6a. 'low e' = reduced erosion within the endorheic area. (d) Cumulative erosion (for the total 3 Myr time period) summed along-strike and projected on a coast-to-coast transect. The transect has been divided into a Tyrrenian flank domain (dark shaded zone on left-hand side), a faulted domain (white zone in the middle), and an Adriatic flank domain (dark shaded zone on right-hand side) based on the extent of the area affected by normal faulting. The two light shaded zones are transition zones owing to the 3D geometry of the fault array that is projected on a 2D cross-section. 'low e' = reduced erosion because of endorheic drainage (see also Fig. 3.7c). Percentages show the relative contribution of the total Tyrrenian and Adriatic domains (both including a faulted domain and mountain flank part) to the overall amount of eroded material delivered to the coastlines.

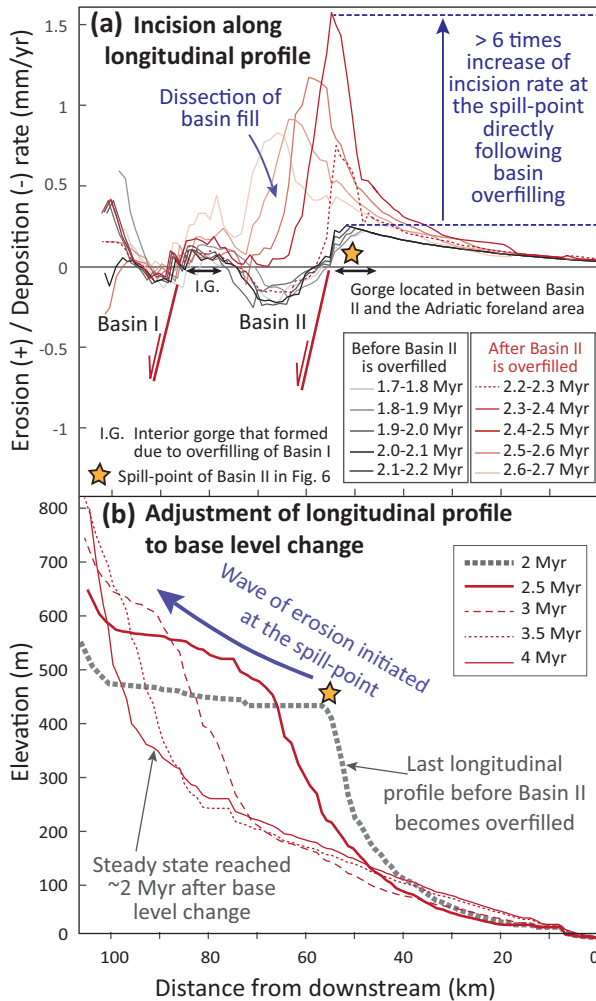


Fig. 3.8. (a) Erosion/Deposition rate along the stream shown in Fig. 3.6 (crossing 2 distinct basins) for the time period in between 1.7 and 2.7 Myr. This period encloses the event of basin overfilling for Basin II (Fig. 3.6) for which its spill point is marked by means of a yellow star (corresponding to yellow stars in Fig. 3.7). Black lines show erosion rates before overfilling of Basin II takes place, and red lines do the same for after basin overfilling. (b) Longitudinal profile along the same stream as analysed in (a) and Fig. 3.6 at different model time-steps, showing the way in which the stream profile adapts to base-level change following basin overfilling. Although our standard model time is 3 Myr, we also show longitudinal profiles developed after 3.5 and 4 Myr when steady-state is approximately reached.

3.6 Discussion

In this study, surface process modelling is used to investigate the impact of regional uplift and normal faulting on long-term landscape evolution across the central Apennines. Our model results enable us to improve our general understanding of drainage integration in extensional continental areas and allow field observations from the Apennines to be evaluated in a temporal perspective. The benefit of our study lies in the simplicity of our model set up. However, it may not explain detailed field observations on a local scale.

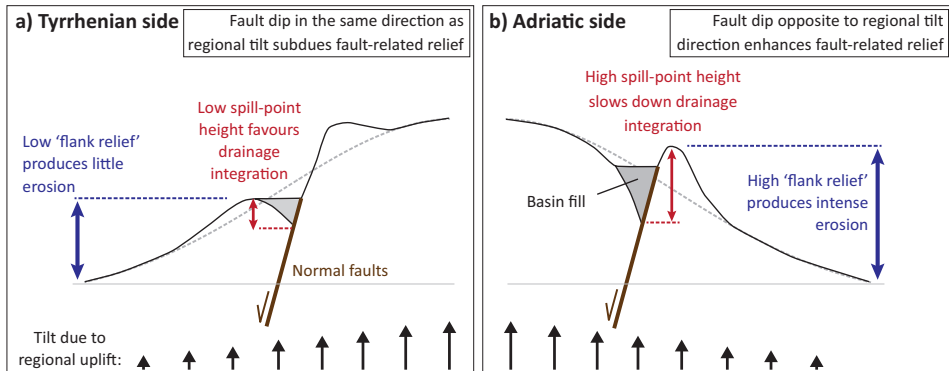


Fig. 3.9. Cartoon explaining the structural asymmetry between the Tyrrhenian (a) and Adriatic (b) sides of the central Apennines (due to the dominant southwest dip direction of the normal faults) and its implications for the rate of drainage integration and erosion on the mountain flanks.

3.6.1 Model versus observations

The drainage integration trend seen in our model explains the commonly observed transition from lacustrine to fluvial sedimentation in basin stratigraphy in the central Apennines, followed by strong incision of the basin fill (Cavinato, 1993; Miccadei *et al.*, 2002; Pucci *et al.*, 2014). While widespread lacustrine deposition characterised the Lower-Middle Pleistocene, progressively more basins became externally drained post late Middle Pleistocene (Piacentini & Miccadei, 2014). Our modelling results are therefore in general agreement with D'Agostino *et al.* (2001) in concluding that drainage integration in the central Apennines is related to the development of a topographic bulge in combination with normal faulting along its crest. However, our results allow us to investigate the processes controlling this transition in more detail.

We compare the final topography (after 3 Myr) from our model with the *Digital Elevation Model* (Tarquini *et al.*, 2007) from the central Apennines (Figs 3.10a, c). Both show a combination of long-wavelength and more local-scale fault-related topography, demonstrating the importance of both normal faulting and regional uplift for landscape evolution in the central Apennines. In addition, our model reproduces the observed strong tectonic imprint on the stream network (Figs 3.10b, d). The river network has a dominantly along-strike orientation within the faulted domain and exhibits a parallel drainage pattern in the tilted foreland areas. Although the modelled

and observed stream networks overlap to great extent, the exact catchment geometry differs in detail (compare Figs 3.10b and d). This is because catchment geometry in extensional settings is strongly controlled by the localities where streams find their way across fault-related topography. Because these transverse reaches are sensitive to many factors that are not included in our model (e.g. pre-existing topography, lithological differences, fault propagation and rock damage, karst drainage, etc.), some are not exactly reproduced. An important example is the Popoli gorge that receives water from the large Pescara catchment, and is the locality where most surface water exits the faulted domain on the Adriatic side (Figs 3.10b, 3.11, 3.12f). In our model, there are instead two smaller catchments, one supplying the Sulmona basin (catchment ‘Y’ in Fig. 3.10d) and the other one in the area around l’Aquila and Campo Imperatore (catchment ‘X’ in Fig. 3.10d). This is because the model predicts the presence of two main ‘exit points’ instead of one near Popoli (Figs 3.10d, 3.11). Although this is an obvious mismatch, we believe it provides some interesting insights. First of all, our simple model setup always produces high topography in the area around Popoli instead of producing a relative low area that can become an exit point. This suggests that active tectonics alone probably cannot explain the Popoli gorge and another factor is needed to explain it, e.g. pre-existing topography (Fig. 3.10e, see below) and possibly karstification processes (Boni, 2000). Secondly, the localities of the two exit points produced by the model actually do coincide with a deeply incised valley that receives water from Campo Imperatore and a large windgap in between Maiella and Sulmona (Fig. 3.11). Although this valley and windgap may have other explanations our results clearly demonstrate that these two localities are favoured as potential exit points based on faulting and regional uplift only.

Evidence for pre-existing topography is clear from the difference in maximum elevation (~2000 versus 1000 m) between our model and observations (note different colour bar scaling in Figs 3.10a and c, see also Fig. 3.10f). In addition, there is an intermediate-scale morphology in the central Apennines consisting of 20-30 km wide ridges that cannot be explained by normal faulting alone (Fig. 3.10a). These differences are clearly visible in our calculated residual topography (present-day topography minus our tectonic uplift function) shown in Fig. 3.10e. Because the

landscape morphology in Fig. 3.10e lines up with mapped thrust faults it confirms that the central Apennines were likely characterised by significant thrust-related topography and deformation structures from the earlier phase of compression prior to Quaternary extension. In other words, our model results support the idea that inherited thrust-related topography has also contributed to the modern-day landscape, (e.g. D'Alessandro *et al.*, 2003) and possibly influenced the extensional fault pattern (D'Agostino *et al.*, 1998; Scisciani *et al.*, 2002). However, here we show that inherited topography is not a necessary ingredient to produce drainage integration.

Even though local peak elevations >1000 m are not reproduced in our model, the hypsometric distributions show a striking similarity between model and reality marked by a local maximum around 600 m (Fig. 3.10f). In the model this local maximum cannot be explained only by the tectonic uplift function, as demonstrated by the hypsometric distribution produced by normal faulting and regional uplift only (pink line in Fig. 3.10f). It can be explained, however, by the prevalence of internal drainage for a considerable part of the 3 Myr model time and the existence of local (perched) base-levels. As long as there is internal drainage, rivers transport material towards the altitude of their local base-level, leading to the development of a local maximum in the hypsometric distribution. The real local maximum in the central Apennines corresponds to the elevation of the internally drained Fucino basin, at circa 650 m. The Fucino basin remains internally drained today because there is insufficient sediment supply compared to the high rate of accommodation creation (see 'Overspill versus headward erosion from the coast' below). In our model run, the local hypsometric maximum corresponds to the local base-level elevation of the l'Aquila - Campo Imperatore area that is still internally drained after 3 Myr (Fig. 3.10d). The primary reason why drainage integration in this area of the model is slowed down is the structural setting of the Adriatic part of the faulted domain where the dominant fault dip direction is opposite to the regional slope (Fig. 3.9; see 'Regional-scale sediment dispersal' in the Model results section).

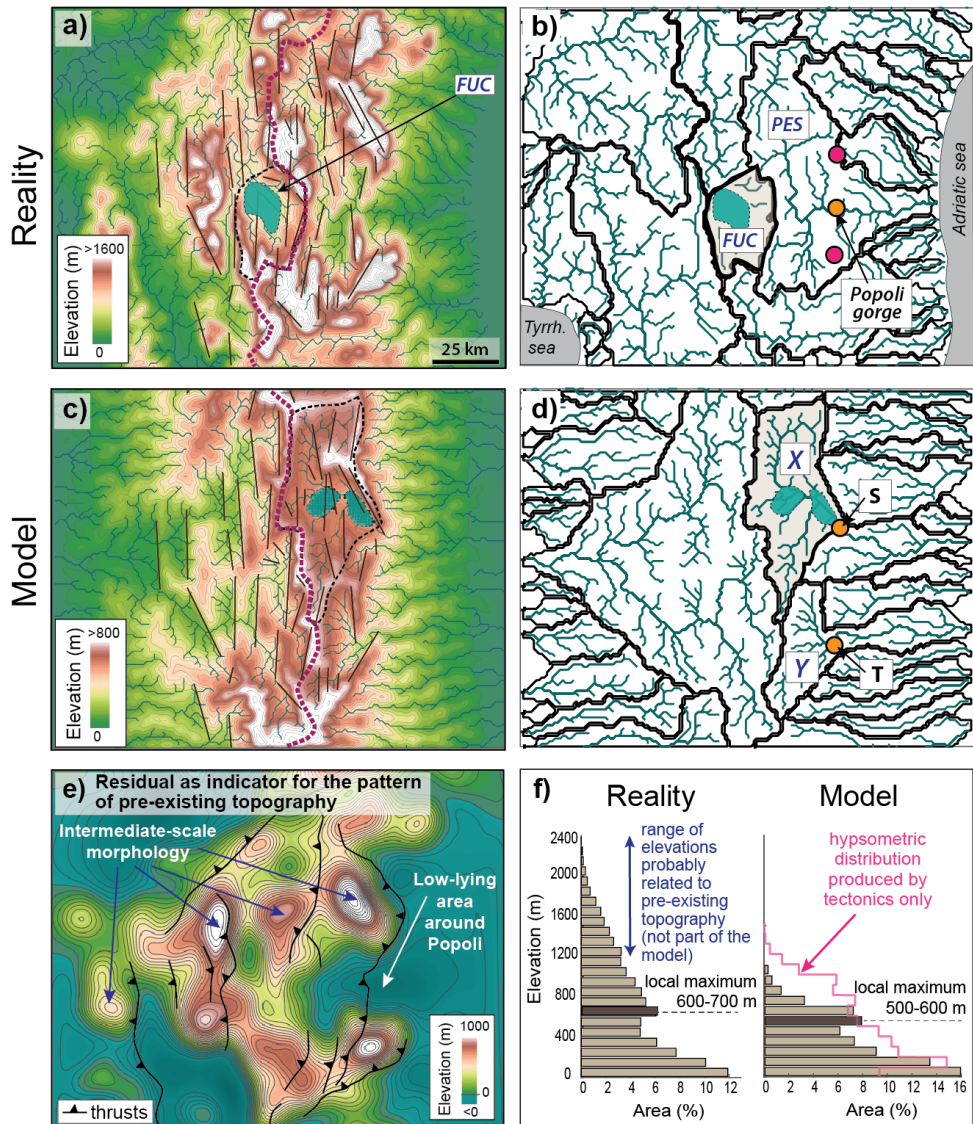


Fig. 3.10. Comparison of the topography and stream network of the central Apennines with our reference model. (a) 10 m-DEM of the central Apennines (Tarquini et al., 2007) interpolated at 1 km resolution, similar to the model resolution, together with normal faults, the stream network, the central water divide (for legend see also Fig. 3.3) and the internally drained Fucino basin ('FUC'). (b) Stream network and catchment geometry of the central Apennines, derived from the DEM shown in (a). The yellow dot shows the Popoli gorge that is the main locality where surface water exits the Adriatic side of the faulted domain. For comparison, we also show the localities of the two fluvial 'exit points' produced by our reference model ('S' and 'T' in (d)) by means of pink dots. Also shown are the Pescara ('PES') and Fucino ('FUC') catchments. (c) and (d) show the same type of data as shown in (a) and (b) but from our reference model after 3 Myr. Yellow dots show the two fluvial 'exit points' ('S' and 'T') on the Adriatic side and in grey the area that is still endorheic after 3 Myr. The model catchments marked 'X' and 'Y' show alternative geometries for the real Sulmona and l'Aquila-Campo

Imperatore catchments, and emerge in the absence of an influence from pre-existing topography (see also (e)). These model catchments are connected to the Adriatic foreland area through fluvial exit points 'S' and 'T'. (e) Residual between the DEM and the surface displacement field used in our model. The residual is derived by subtracting the 3 Myr surface deformation field (including both normal faulting and regional uplift; Figs 3.2a, b) from the DEM (Fig. 3.10a) and has been smoothed by means of a Gaussian kernel ($\sigma = 4$ km) in order to reveal the main topographic features. Main thrust faults (modified from Miccadei et al., 2017) are shown on top. The morphological pattern shown by the residual most likely reflects pre-existing, thrust-related, topography. (f) Hypsometric distributions for both the DEM and the final (3 Myr) topography of our reference model shown in (a) and (c), respectively.

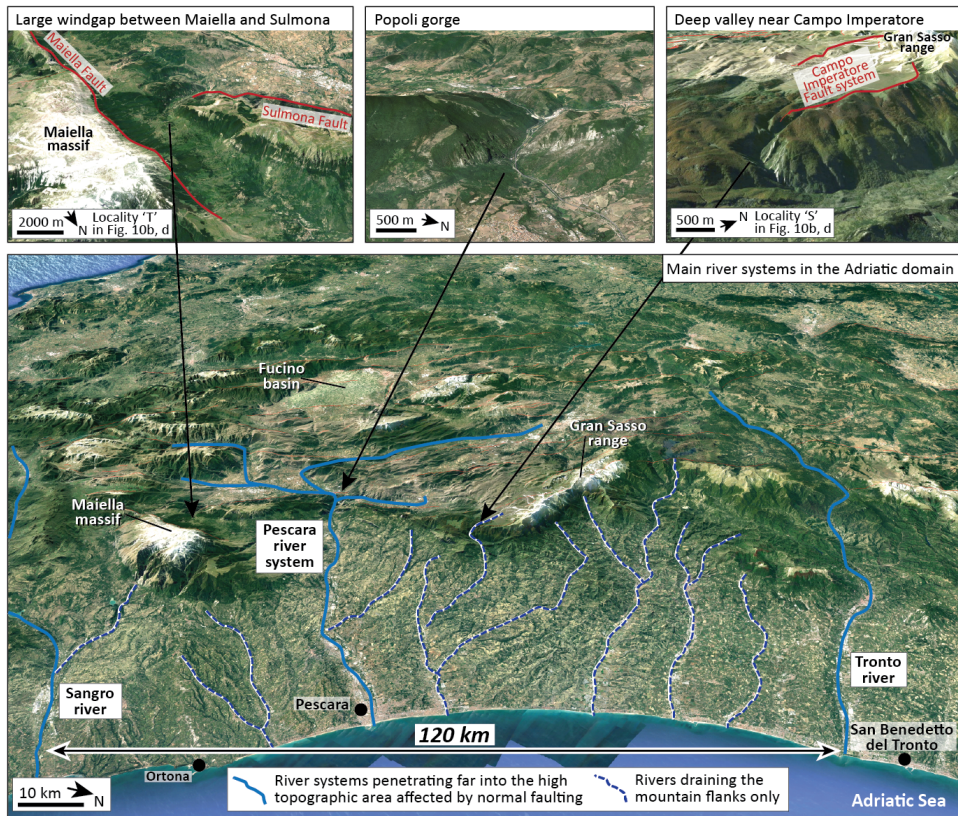


Fig. 3.11. Top figures: Google Earth images of the Popoli gorge and the two modelled fluvial 'exit points' on the Adriatic side produced by our reference model (see also Fig. 3.10b, d). Main fault systems (according to Roberts & Michetti, 2004) shown by means of red lines. Bottom figure: Google Earth image of the Adriatic foreland area and the central Apennines in the background, also showing the main river systems. Over a distance of 120 km only one river system penetrates far into the high topographic area (the Pescara river system), while most rivers drain the mountain range flank and foreland area only.

3.6.2 *Overspill versus headward erosion from the coast*

Our model results demonstrate that an important mechanism driving drainage integration is basin overfilling, i.e. the progressive filling of basins with sediment up to the level of their spill-point enabling water to spill over (Fig. 3.6a). We note, however, that our endorheic model setup (see Methodology section) does not allow us to distinguish basin overfilling from lake overspill, i.e. the spill over of water when the lake surface (and not the sediment surface) reaches the altitude of the spill-point. In theory the potential for lake overspill is mainly climate-dependent, likely making lake overspill more important under wetter climatic conditions (e.g. Heidarzadeh *et al.*, 2017; House *et al.*, 2008; Garcia-Castellanos *et al.*, 2003). Even though our model cannot distinguish between basin overfilling and lake overspill, we can consider them both as ‘overspill mechanisms’ (Bishop, 1995; Smith, 2013), as they both act in a downstream or ‘top-down’ direction and are mainly controlled by sediment and water supply from upstream. Therefore, in turn, we believe our model suggests that overspill mechanisms mainly drive drainage integration in the central Apennines (Figs 3.12a, c). This finding contradicts previous field-based studies on the central Apennines that suggest headward erosion from the coast to be the dominant driving mechanism (Figs 3.12b, d; D’Agostino *et al.*, 2001; Bartolini *et al.*, 2003), i.e. ‘bottom-up’ fluvial integration (Bishop, 1995; Smith, 2013). We do observe headward erosion from the coast in our model, but its contribution to drainage integration is negligible, and this result is irrespective of the erosional parameters that we use (see *Supplementary Materials S4*).

It is important to note that there is no reason to expect the contribution of overspill in our model to be over-estimated relative to headward erosion. First of all, increased sediment supply to hanging-wall basins can only be generated under more erosive conditions, which in turn also increases headward erosion. Their relative importance thus remains the same and explains why overspill remains the dominant process driving drainage integration when varying erosional parameters K_f and L_f (*Supplementary materials S4*). Secondly, we do not expect the dominant role of

overspill to be related to major assumptions underlying our model setup. If lithology is not uniform, as we assume, overspill would most likely become even more important as the main lithological contrast between basin alluvium and the more resistant bedrock ridges would lead to more rapid excavation of sediment from the basins and more rapid incision at the spill-point directly following a drainage integration event (e.g. Cowie *et al.*, 2008). Initiating the model with pre-existing topography, on the other hand, is likely to increase the rate of basin filling and hence overspill. Increasing the model resolution also would not affect our main results because of the strong control on the scale of the local relief exerted by the fault pattern. Climatically induced sea-level low stands could theoretically enhance headward erosion but are small compared to the tectonic uplift. Finally, using an asymmetric regional uplift function instead of a symmetric function does not affect the dominant role of overspill in long-term drainage integration, even though it produces a significantly different landscape after 3 Myr (*Supplementary Materials S7*).

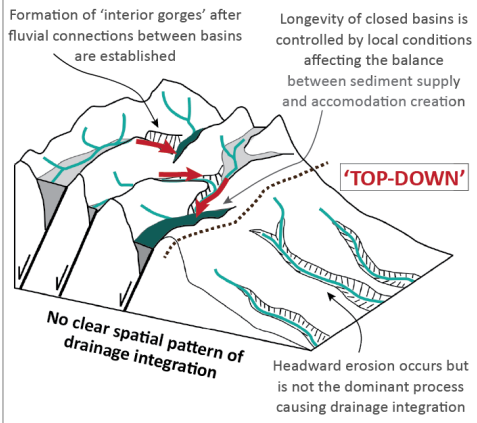
There are a number of field observations from the central Apennines that point towards basin overfilling, or lake overspill, being an important process. The most direct evidence comes from the Terni basin in the northwest corner of our study area (Fig. 3.1b). Here continental deposits are preserved on top of the adjacent Narnese-Amarina ridge, marking the location of the former outlet of the Terni basin. The high elevation of this former outlet relative to the present-day basin surface shows that the basin has been totally filled up to its spill-point and that basin overfilling caused it to become interconnected with the Tyrrhenian foreland area (D'Agostino *et al.*, 2001).

Based on the position of the closed Fucino basin on the central drainage divide and at greatest distance to the Tyrrhenian and Adriatic coasts (Fig. 3.10a), previous work has argued for headward erosion from the coast to be the main mechanism driving drainage integration (D'Agostino *et al.*, 2001). D'Agostino *et al.* (2001) hypothesise that over time all other major and initially endorheic basins have been captured except for the Fucino basin, which has 'survived' and remained internally drained because of its distal position relative to regional (marine) base-level. However, based on our results we suggest that the Fucino basin is internally drained today due to an

insufficient sediment supply that has been outpaced by fast accommodation creation (see also Whittaker *et al.*, 2008). Its stratigraphy does not support the ‘survival-concept’ as it shows a transition from overfilled to underfilled conditions over time (Cavinato *et al.*, 2002) that can be explained by a x3 to x5 increase in slip rate at around 1-0.5 Ma along the main basin-bounding fault (Roberts & Michetti, 2004; Cowie & Roberts, 2001; Whittaker *et al.*, 2008; *Supplementary Materials S8*). Our study suggests that the main reason why the Fucino basin is endorheic today is simply because its central position within the fault array caused the Fucino fault to become the largest and most active fault in the area (Cowie & Roberts, 2001; Roberts & Michetti, 2004). In other words, the preservation of the Fucino basin confirms the importance of accommodation creation versus sediment supply and hence the major role of overspill mechanisms rather than headward erosion from the coast in controlling drainage integration.

Another reason why we do not expect headward erosion from the coast to be important for drainage integration in the central Apennines is the small number of fluvial connections of significant size between the foreland area and the interior of the mountain range. For instance, in the Adriatic domain only one such connection, i.e. the Popoli gorge, exists over a total along-strike distance of ~120 km, i.e. between the Sangro and Tronto river valleys (Fig. 3.11). Moreover, the young age of the Popoli gorge (~400-350 ka according to Miccadei *et al.*, 2002) implies that for most of the Pleistocene no fluvial connections existed at all between the mountain range interior and the Adriatic foreland area. Although fluvial incision in the foreland areas is clearly significant, these field observations suggest that most foreland draining streams have not been successful in enlarging their catchments into the faulted domain. Moreover, our modelling results support the idea that the Popoli gorge is more likely controlled by other local factors like pre-existing topography (Fig. 3.10e), perhaps in combination with the collapse of underground drainage (Piacentini & Miccadei, 2014; Boni, 2000), rather than by efficient headward erosion from the coast.

a) OVERSPILL
(basin overflowing / lake overflow)



b) HEADWARD EROSION
from the coast

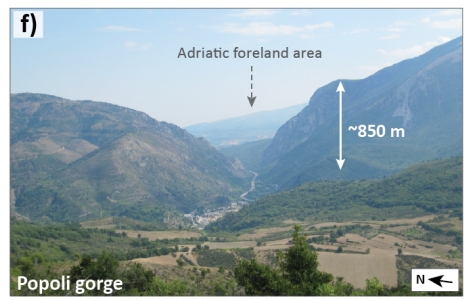
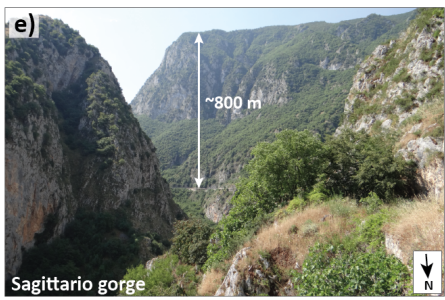
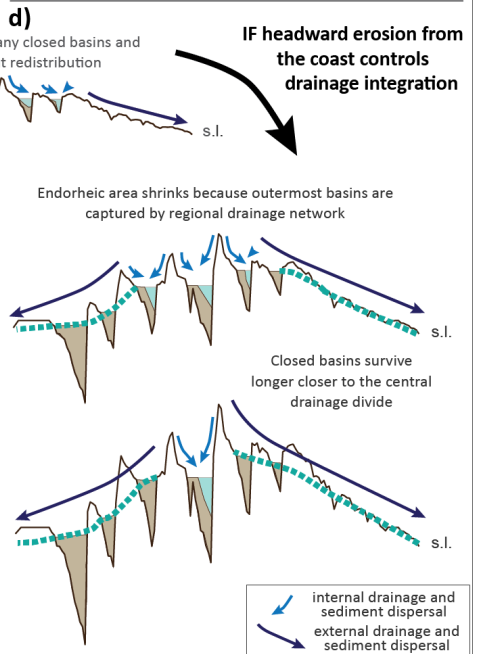
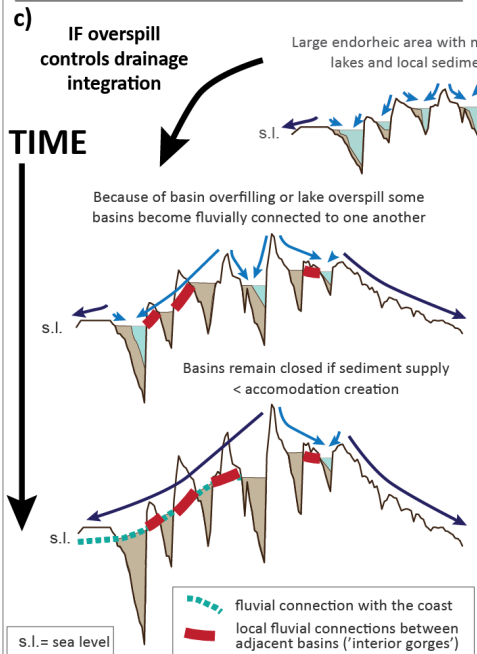
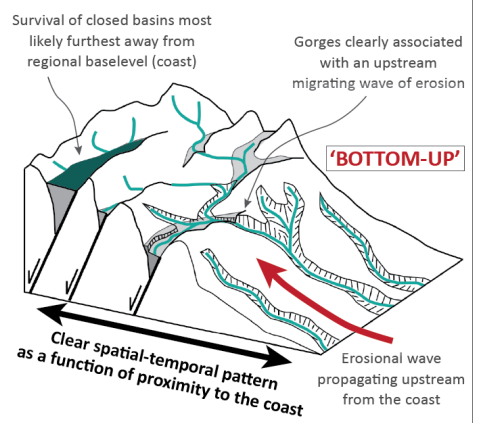


Fig. 3.12. (previous page) Main features in extensional systems where drainage integration is either dominated by overspill mechanisms (a) and (c) or headward erosion from the coast (b) and (d) based on our model results. (e) Picture of the Sagittario gorge (see Fig. 3.1b for locality), example of an ‘interior gorge’ located in between two fault-bounded basins. It cannot be explained by headward erosion from the coast but might have formed as a consequence of basin overfilling (f) Picture of the Popoli gorge (see Fig. 3.1b for locality), located in between the Sulmona basin and the Adriatic foreland area. Our model results suggest that it cannot be explained by faulting, regional uplift and fluvial incision only, but it might be explained by pre-existing topography perhaps in combination with karst.

A type of field observation that we also consider as indicative of overspill is what we call ‘interior gorges’, i.e. deeply incised river valleys located in the interior part of the faulted domain that are not related to an erosional wave propagating upstream from the coast (Figs 3.7b, 3.12). Theoretically, this kind of gorge could be produced by headward erosion at a more local scale, e.g., by a first-order stream draining an individual hanging-wall basin margins. For example, Smith (2013) suggests that inter-basin headward erosion is favoured when a lower-elevated fault-bounded basin (the one containing the headward eroding stream) subsides at a faster rate than an adjacent higher-elevated basin (the one becoming captured). Even where these tectonic conditions occur (e.g. Fig. 3.6a), overspill can still dominate and can lead to local incision and gorge formation between adjacent basins (e.g. Fig. 3.8a). Therefore, based on our model results, we expect interior gorges in the central Apennines to be mainly produced through overspill-driven drainage integration. One example of such an interior gorge is the San Venanzio gorge located between the Lower Aterno valley and Sulmona basin (Fig. 3.1b). The fact that alluvial fan deposits at the outlet of the gorge interfinger with lacustrine deposits in the Sulmona basin (Cavinato & Miccadei, 2000) implies that this gorge was formed before the Sulmona basin was captured by headward eroding rivers that drain to the coast. Another example is the Sagittario river gorge, also located upstream of the Sulmona basin, but downstream of Lake Scanno (Figs 3.1b, 3.12e). The dimensions of this gorge suggest that it cannot be explained by an upstream propagating wave of erosion considering its position in the hanging-wall of a large normal fault (Fig. 3.1b) and the much more limited amount of incision in the downstream Sulmona basin. Therefore, based on our model results, we suggest both gorges most likely formed due to overspill from basins located directly upstream,

leading to the formation of fluvial connections with the downstream located Sulmona basin followed by rapid local incision.

Finally, our model results are consistent with an increasing number of studies that call into question headward erosion as being an important drainage integrating process (e.g. Bishop, 1995; Spencer & Pearthree, 2001; Connell *et al.*, 2005; Douglass *et al.*, 2009; Heidarzadeh *et al.*, 2017). Theoretically, true headward erosion, i.e. the uphill lengthening of first-order streams, is expected to be a relatively inefficient process as discharge and consequently stream power are low close to the water divide (Bishop, 1995; Spencer & Pearthree, 2001; Connell *et al.*, 2005). It is potentially relevant at the scale of gully systems for which headward erosion has been mainly described, where erosion is strongly associated with high runoff events and therefore relatively large amounts of water entering the gully heads due to sheet flow (e.g. Bocco, 1991; Bishop, 1995). We think that the relative inefficiency of headward erosion is clearly demonstrated by the drastic increase in incision rate that is generally observed directly following a drainage integration event (Fig. 3.8a; see also e.g. Stokes *et al.*, 2002). As long as the basin is still internally drained, erosion affecting the basin margins proceeds typically at a low rate and can only be explained by headward erosion by first order streams. However, as soon as a fluvial connection becomes established, the spill-point area experiences an increase in discharge and slope causing a rapid increase in erosion rates (e.g. Stokes *et al.*, 2002; Smith, 2013; Garcia-Castellanos *et al.*, 2003). For instance, for the model river analysed in Figs 3.6 and 3.8, drainage integration results in a >6 times increase in incision rate (Fig. 3.8a). Our conclusion is that headward erosion may have been invoked too often in regional or catchment-scale landscape evolution studies because drainage integration events are usually followed by intense erosion so that field evidence necessary for distinguishing between bottom-up and top-down integration mechanisms tends to become lost (Douglass *et al.*, 2009).

3.6.3 *Impact of drainage integration on sediment dispersal*

Our model results also have important implications for studying regional-scale sediment dispersal in the central Apennines and comparable settings. Top-down (basin

overflowing and lake overspill) and bottom-up (headward erosion) mechanisms clearly produce different spatio-temporal patterns of sediment dispersal (Fig. 3.12). In the case of headward erosion a systematic pattern emerges which is a function of distance to the coast (Figs 3.12b, d). The more proximal to the coast the earlier lake sedimentation ceases, fluvial activity starts and incision of the basin fill commences. In the case of overspill, in contrast, the pattern is complex as local conditions become more important (Figs 3.12a, c): Lacustrine sedimentation ceases first in those basins that either; i) have relatively high sediment input due to a large source area with high relief, ii) have relatively low rates of basin subsidence, or iii) have a relatively low spill-point (e.g. due to pre-existing topography). However, in the case of overspill, sediment dispersal also strongly depends on the geometry of the drainage network and modifications to it over time. For instance, basins experience a significant increase in sediment supply when an upstream basin becomes externally drained and its sediment-fill becomes excavated. In other words, the top-down pattern of drainage integration is more difficult to predict because overflowing of a single basin is the integrated effect of all landscape developments occurring upstream and depends strongly on the regional-scale geometry and temporal evolution of the upstream drainage network. The temporal evolution of the drainage network, in turn, depends strongly on the growth of the extensional fault population (Cowie *et al.*, 2006).

For the offshore area, our numerical experiments suggest a long-term increase in sediment supply due to the progressive increase in regional relief. This corresponds to field observations from the Adriatic where strong progradation started ca. 1.8 Ma (e.g. Artoni, 2013). On top of this gradual trend, however, our model predicts more step-wise increases in sediment supply due to drainage integration events. Considering the age of the Popoli gorge (~0.4-0.35 Ma; Miccadei *et al.*, 2002), which is the main sediment exit point on the Adriatic side of the central Apennines, we would expect a sudden increase in sediment to the Adriatic around this time. Based on the limited data available, no clear evidence exists that could confirm this but it is possible that the increase in sediment supply due to formation of the Popoli gorge is overprinted by effects due to a possible acceleration of regional uplift in the Adriatic foreland area around circa 0.7 Ma (e.g., Pizzi, 2003). Another implication of our model results is

that the Adriatic mountain range flank has likely experienced more intense erosion than its Tyrrhenian counterpart (Fig. 3.7d). This is because the dominant SW dip direction of the normal faults produces enhanced uplift and high relief driving erosion (Fig. 3.9), even though the long-wavelength uplift is symmetric in our model.

3.6.4 Transient landscape evolution as a function of regional uplift and normal faulting

Our model clearly demonstrates that landscape development in the central Apennines is transient even after 3 Myr. Even though the tectonic forcing is constant and climatic oscillations are not considered, we show that the landscape adapts continuously to modifications to the connectivity of the drainage network. This has an important implication because drainage integration represents a transient development that forms the background to other transient responses related to changes in allogenic forcing such as fault slip rate variations (Whittaker *et al.*, 2008) or climate (Wegmann & Pazzaglia, 2009). Therefore we consider drainage integration as an autogenic process inherent to many continental extensional systems and recommend it to be considered as an important element in future transient landscape studies in such settings.

Furthermore, our model results suggest that in the central Apennines, drainage integration can be explained by the unique combination of normal faulting and differential regional uplift. On their own, these individual tectonic processes do not lead to drainage integration, either because no closed basins develop (in the case of regional uplift only) or because they do not become interconnected over time (in the case of normal faulting only). Besides fault development (controlling accommodation creation), we believe that the availability of sediment is a crucial factor in driving drainage integration and is potentially more important than external base-level fall. This means that in settings like the central Apennines where sediment originates only from the extensional domain itself, it is of key importance that there is enough relief to produce enough erosion and thereby sufficient sediment to fill the basins (favouring both basin overfilling and lake overspill). This relief can either be produced by active regional uplift or be inherited from pre-extensional times. Because of the high

amplitude of regional uplift (up to ~1000 m) across relative short distance (~150 km) this requirement is fulfilled in the central Apennines, while the exact pattern of regional uplift is less relevant (see ‘Asymmetric uplift experiment’ in *Supplementary Materials S7*).

In the Basin and Range Province, in contrast, the lack of sufficient relief and hence sediment supply may explain why drainage integration at a regional scale (including across-strike integration) is, in several areas, less advanced. The lack of relief can be overcome if an external sediment source is available (external to the extensional domain), e.g. the Gila river system (Arizona) that transports sediment from the southern edge of the Colorado Plateau to basins in the southern Basin and Range (Dickinson, 2015). Although the Gila river and its tributaries drain most of the fault-bounded basins in this region, there are also a few basins that remain internally drained (Dickinson, 2015). Importantly, these endorheic basins all have a distal position relative to the Colorado Plateau (the main sediment source), supporting the idea that sediment supply and overspill play a key role in controlling drainage integration.

Finally our study shows that drainage integration occurs even if both faulting and regional uplift accumulate uniformly over time. Although changes in tectonic deformation, for example due to fault propagation and interaction (Cowie *et al.*, 2006), likely affected the evolution of the central Apennines river network, our model shows they are not needed to explain drainage integration. In other words, our simple model setup demonstrates that landscape evolution is highly dynamic even if the tectonic forcing is not. We expect changes in tectonic conditions over time to have made long-term drainage integration even more dynamic and to have enabled some basins to go through multiple cycles of internal and external drainage (e.g. Galli *et al.*, 2010; see also *Supplementary Materials S8*). Therefore, we expect the trend of lake disappearance seen in our model to be even more complex in reality.

3.7 Conclusions

We have used a surface process model to investigate the phenomenon of drainage integration in the actively extending central Italian Apennines. By using a simple model setup that accounts for the main aspects of tectonic deformation in this area, i.e. regional uplift and normal faulting, we investigated the evolution of drainage integration, the roles of the main controlling mechanisms, and its impact on regional-scale sediment dispersal. Based on our modelling, our specific conclusions are:

- 1) Both regional uplift and extensional deformation are important for long-term landscape evolution in the central Apennines. Together they reproduce the main landscape features and essential transient aspects of its evolution, in particular, the cessation of lake sedimentation and drainage integration.
- 2) Basin overfilling, and hence overflow and drainage integration occur in our model because of the increasing relief at both fault-block and regional scales that generates more erosion and in turn more sediment supply to basins over time. Even for the case of constant fault slip rates, this causes basins to become progressively overfilled and eventually a through-going river system to develop (e.g. Fig. 3.6).
- 3) Our model suggests overflow (basin overfilling and lake overflow) rather than headward erosion from the coast to be the dominant fluvial mechanism driving drainage integration in the central Apennines, i.e. ‘top-down’ rather than ‘bottom-up’ integration (Fig. 3.12). These results are consistent with field observations from the central Apennines, in particular the formation of ‘interior gorges’ (Fig. 3.12), and with an increasing number of other studies that call into question headward erosion as being an important process for regional-scale drainage integration.
- 4) Overflow depends largely on the balance between sediment supply and accommodation creation in individual fault-bounded basins. Because both of them depend on many local factors and developments along the drainage network upstream, basin overfilling does not produce a clear spatio-

temporal pattern of drainage integration - unlike in the case of headward erosion where it depends primarily on distance to the coast in the case of Italy (Fig. 3.12).

- 5) We show that landscape evolution can be highly dynamic even if the tectonic forcing and climate are uniform over time. This is because drainage integration causes the landscape to adapt continuously to modifications in connectivity of the drainage network. Other processes like fault interaction are likely to make drainage integration even more dynamic in reality (e.g. enabling some basins to go through multiple cycles of internal and external drainage), although it is not needed in order to explain the phenomenon itself.
- 6) Over long timescales of millions of years, drainage integration produces a delayed export of sediment out of the area affected by normal faulting and a step-wise increase in sediment supply offshore. At a local scale it leads to abrupt changes in erosion/deposition patterns, marked variation in sediment supply to basins and hence sedimentary environment (lacustrine vs. fluvial), and strong incision following drainage integration events (e.g. Figs 3.7 and 3.8).
- 7) According to our model results, the dominant SW dip of the normal faults in the central Apennines favours overspill and therefore drainage integration within the Tyrrhenian part of the faulted domain, compared to its Adriatic counterpart. The Popoli gorge is an exception that is probably explained by local factors. Moreover, this structural asymmetry generates more intense erosion on the Adriatic flanks than on the Tyrrhenian flanks of the mountain range (e.g. Fig. 3.9).
- 8) We suggest that the most important factor for drainage integration to occur in continental extensional systems is the availability of sufficient sediment relative to the accommodation being created through normal faulting (more important than proximity to the coast, or other external base-levels). The important role that normal faulting plays both through the uplift of source areas and the accommodation creation in hanging-wall basins leads to the

conclusion that better understanding of the underlying geodynamic mechanism(s) for fault growth is vital. In the case of the central Apennines this is likely related to either flow or buoyancy variations in the uppermost mantle and associated with surface uplift at a regional-scale (e.g. Faure Walker *et al.*, 2012; Cowie *et al.*, 2013; Faccenna *et al.*, 2014). Sufficient sediment, on the other hand, can alternatively be provided through (pre-extensional) inherited relief, strong regional uplift (in case of the central Apennines) or an external sediment source (e.g. high topography adjacent to the continental rift).

- 9) Finally, our results reveal abrupt and complex shifts in patterns of erosion/deposition at the fault block scale, suggesting that feedbacks between surface processes and fault development may be enhanced, potentially contributing to temporal variations in fault slip rates and/or fault activity over time (e.g. Maniatis *et al.*, 2009).

3.8 Acknowledgements

We thank Jean Braun for providing the numerical code and for his help during the early stage of setting up the model experiments. We thank Gerald Roberts and Alessandro Michetti for providing the fault data and sharing their ideas at the time of constraining our model setup. We also acknowledge Alberto Pizzi, Elsa Gliozzi, and Tommaso Piacentini for providing more details on their data or publications. This study greatly benefitted from stimulating discussions with Alex Whittaker, Stefano Pucci, and Fabio Villani, and from constructive comments from Peter van der Beek and an anonymous reviewer on an earlier draft of our manuscript. AHG acknowledges Bergen University for supporting her PhD research and RLG acknowledges support from VISTA.

CHAPTER 4

Paper 2

Transient landscape and stratigraphic responses to drainage integration in the actively extending central Italian Apennines

Published in *Geomorphology* as:

Geurts, A.H., Whittaker, A.C., Gawthorpe, R.L., Cowie, P.A., 2020. Transient landscape and stratigraphic responses to drainage integration in the actively extending central Italian Apennines. *Geomorphology*, 353, 107013.

4.1 Abstract

Drainage networks in continental rifts are generally reported as dynamic features that produce transitions between endorheic and exorheic conditions. While this is of major importance for landscape development, sediment dispersal, and basin stratigraphy, the controls of drainage network evolution across an array of normal fault bounded basins are still not well understood. In this study we use the central Italian Apennines – an area that has been affected by active normal faulting and regional uplift over the last ~3 Myrs – to determine the controls on drainage network evolution and its impact on transient landscape evolution and basin stratigraphy. We compile previously published stratigraphic and fault-related data with new geomorphological constraints for the Aterno River system (~1300 km²), for which a wealth of data has been collected following the destructive L'Aquila earthquake in 2009. We use this compilation to demonstrate how the different basins along the river system were initially isolated during the Early Pleistocene but became fluviially integrated with one another and the Adriatic coast between ca. 1.2 and 0.65 Ma. We conclude that the spatial and temporal pattern of drainage integration is mostly explained by a long-term increase in sediment and water supply relative to basin subsidence due to the Early to Middle Pleistocene climatic transition, the progressive increase in fault-related topography, and the transport of sediment and water down-system as drainage integration occurred. Overall we conclude that rates of sedimentation and basin subsidence in the central Apennines are well-matched, allowing tipping points between over- and under-filled conditions to be easily reached. We also show that consecutive drainage integration events produce discrete waves of river incision and terrace formation, and conclude that drainage integration is of major importance, at least equivalent to tectonics and climate, in controlling transient landscape evolution and rift basin stratigraphy.

4.2 Introduction

Extensional basins in continental rifts commonly go through both phases of internal (endorheic) and external (exorheic) drainage related to temporal changes in the connectivity of the river network (e.g., Jackson and Leeder, 1994; Gawthorpe and Leeder, 2000; D'Agostino et al., 2001; Connell et al., 2005; Larson et al., 2014; Reheis et al., 2014; Duffy et al., 2015; Repasch et al., 2017; Geurts et al., 2018). Endorheic basins have their own local base level and support permanent or playa lakes depending on the prevailing climatic conditions. Exorheic basins are fluvially connected with adjacent basins in an often predominantly axial (parallel to fault-strike) direction. For many extensional systems it has been suggested that endorheic drainage predominates during early stages of extension and that these initially isolated basins progressively become integrated over time, either during the period of active extension (Fig. 4.1A; e.g., Gawthorpe and Leeder, 2000; D'Agostino et al., 2001; Duffy et al., 2015; Gawthorpe et al., 2018), or after extension has largely ceased (e.g., Meek, 1989; Connell et al., 2005; House et al., 2008; Menges, 2008; Phillips, 2008; Larson et al., 2014; Reheis et al., 2014; Repasch et al., 2017). Despite the major importance of drainage network evolution for basin stratigraphy, transient landscape evolution, and the propagation of climatic and tectonic signals across the landscape, our understanding of this process remains limited (e.g., Gawthorpe and Leeder, 2000; Allen and Allen, 2013; Larson et al., 2017; Geurts et al., 2018).

Long-term drainage integration can be partly explained by fault growth and structural linkage of adjacent fault segments that affect the topography of intra-basin areas (e.g., Gawthorpe and Leeder, 2000; Cowie et al., 2006). However, it is increasingly recognised that the lacustrine-fluvial system itself plays an important role in establishing fluvial connections between different basins. One way that the drainage of initially isolated basins becomes integrated is by means of upstream-directed (bottom-up) basin capture by headward eroding rivers (e.g., D'Agostino et al., 2001). Another mechanism is the downstream-directed (top-down) successive overfilling and overspill of basins (e.g., Geurts et al., 2018). The relative importance of these opposing

mechanisms of drainage integration, and how they can be differentiated remains contentious (e.g., Bishop, 1995; Douglass et al., 2009; Larson et al., 2017; Geurts et al., 2018; Meek, 2019). This is partly because the process of headward erosion is not well understood and its efficiency is largely unconstrained (e.g., Douglass et al., 2009). Conclusive evidence for basin overspill, on the other hand, is often poorly preserved because of the intense erosion following drainage integration events.

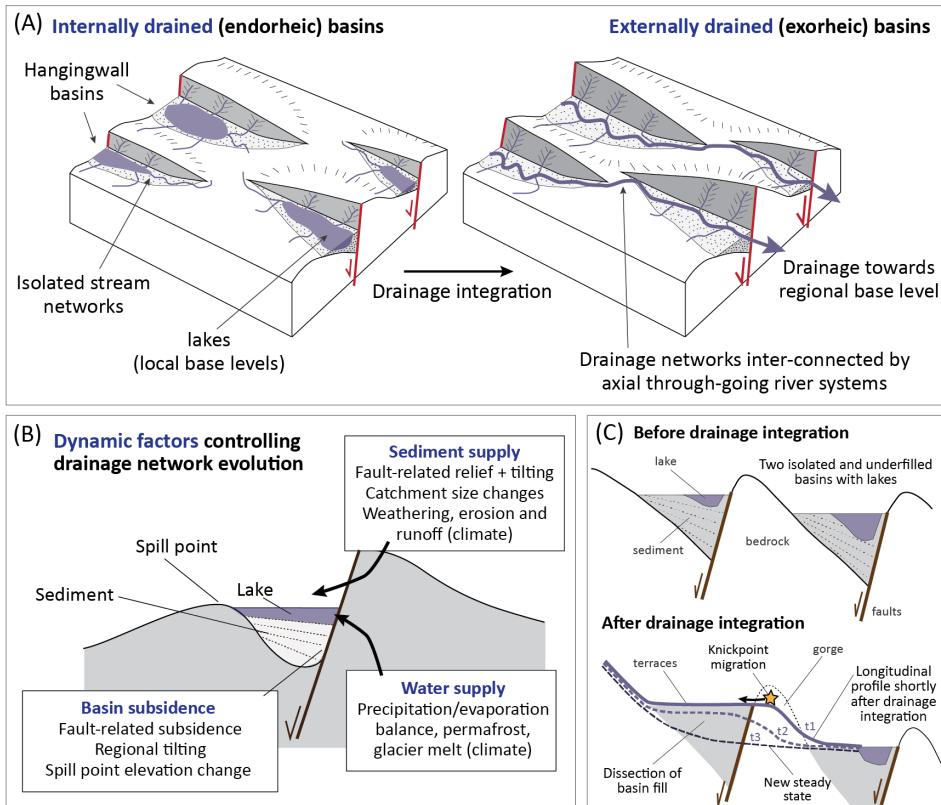


Fig. 4.1. (A) Long-term drainage integration showing the fluvial integration of initially isolated basins with one another during active extension (schematic). (B) Overview of factors that control sediment supply, water supply and basin subsidence and therefore can change the connectivity of the drainage network by means of overspill mechanisms. We only show ‘dynamic factors’, which are factors that can produce changes in sediment supply and water supply and the rate of basin subsidence during the time period of active extension. (C) Schematic cross section through two subsiding basins that are initially isolated from one another (top). Overfilling of the upstream basin leads to the integration of both basins by a through-going river system (bottom). The longitudinal profile of this river contains a knickpoint that migrates upstream as the river adjusts to its new boundary conditions (t_1 , t_2 , t_3 represent different moments in time). This leads to strong incision in the area of the former spill point and in the upstream basin fill, leading the formation of a bedrock gorge and fluvial terraces.

However, in extensional areas for which we have sufficient temporal constraints on basin stratigraphy, the spatio-temporal pattern of drainage integration might allow us to differentiate between them (e.g., Repasch et al., 2017; Geurts et al., 2018).

One extensional area where the connectivity of the drainage network has clearly changed over time is the central part of the Italian Apennines (Fig. 4.2). Since the Late Pliocene, ca. 3 Ma, this region has been affected by both regional uplift and active extensional deformation, which is accommodated by a ~60 km wide fault array located along the crest of the mountain range (Fig. 4.2; e.g., Cowie and Roberts, 2001; D'Agostino et al., 2001; Roberts and Michetti, 2004; Faure Walker et al., 2012). The presence of lacustrine sediment in the deeper parts of the basin fills has been used to argue that most basins were endorheic during early stages of extension, but have become fluvially integrated over time (e.g., Cavinato et al., 2000; D'Agostino et al., 2001; Miccadei et al., 2002; Bosi et al., 2003; Piacentini and Miccadei, 2014). Drainage integration has been mainly explained by the active capture of intermontane extensional basins by means of headward erosion from the coast (e.g., D'Agostino et al., 2001).

More recently, numerical modelling work (Geurts et al., 2018) has been used to argue that drainage network evolution in the central Apennines could alternatively be controlled by basin overspill and thus the balance between fault-related basin subsidence and the supply of water and sediment to basins (Fig. 4.1B). In this model, even when climate is constant, drainage integration results from a long-term increase in sediment supply driven by the increase in footwall topography. The modelling additionally demonstrates how drainage integration leads to deep fluvial incision and terrace formation when the integrated river system geomorphically adjusts to its new base level (Fig. 4.1C).

The aim of this paper is to use field evidence from the central Italian Apennines to evaluate the predictions of drainage network evolution of Geurts et al. (2018). We focus on the Aterno River system because this area, particularly around the city of L'Aquila, has been the focus of substantial research following the major earthquakes

in 2009 (e.g., Giaccio et al., 2012; Mancini et al., 2012; Santo et al., 2014; Pucci et al., 2015; Macri et al., 2016; Porreca, et al., 2016; Nocentini et al., 2017, 2018). We integrate published basin stratigraphic data with new geomorphological constraints in order to reconstruct the evolution of the Aterno River system over the last 3 Myr. We use this dataset to evaluate the main factors and mechanisms controlling drainage evolution, and evaluate the impact that drainage network integration has on basin stratigraphy and transient landscape evolution. This is the first time, to our knowledge, that drainage-network-controlled landscape transience has been evaluated in detail for an extensional province that is highly active (regional extension $\sim 3 \text{ mm yr}^{-1}$) and well-understood in terms of fault development (e.g., Roberts and Michetti, 2004; Cowie et al., 2017) and where other factors such as damming of rivers by volcanic activity (e.g., Repasch et al., 2017) have not played any obvious role.

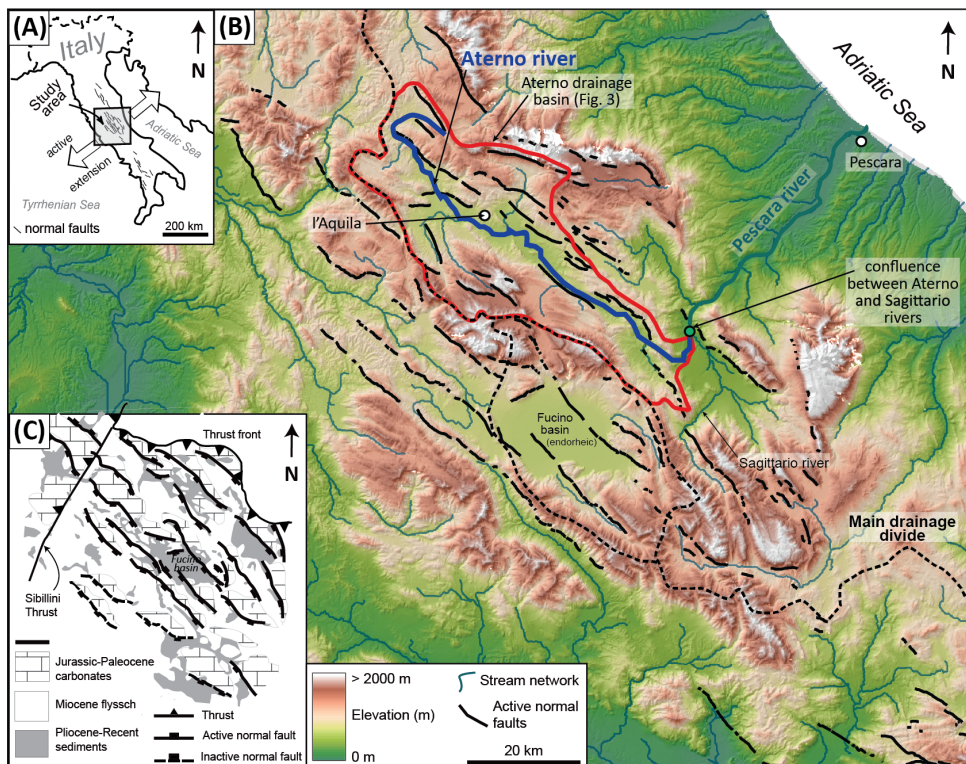


Fig. 4.2. (shown on previous page) (A) Location map of the study area in central Italy. (B) Topography of the central Apennines (DEM from Tarquini et al. (2007)) with the drainage network and active normal faults (modified from Roberts and Michetti, 2004). It also shows the catchment of the Aterno River and the large endorheic Fucino basin located at the main drainage divide separating the Tyrrhenian from the Adriatic domain. (C) Simplified geological map of the research area showing the main lithological units (modified from Whittaker et al., 2008).

4.3 Geological setting

The broad morphology of the Italian Apennines results from convergence between the African, Adriatic and Eurasian plates and has led to the formation of a Neogene NE-verging imbricate fold and thrust belt (e.g., Patacca et al., 1990; Royden, 1993). In the central Apennines subduction of oceanic lithosphere ceased by around 6 Ma, and thrust sheets mainly consisting of Mesozoic platform limestone are locally overlain by syn-tectonic Miocene flysch (Fig. 4.2; Patacca et al., 1990; Montone et al., 2004; Vezzani et al., 2010). Since approximately 3 Ma, the interior part of the central Apennines has been affected by extensional deformation accommodated by a >60 km wide array of mainly southwest dipping normal faults (Lavecchia et al., 1994; Cowie and Roberts, 2001; Roberts and Michetti, 2004; Fig. 4.2). Stratigraphy in the hangingwall basins to these normal faults has been dated using palaeontology and tephrochronology and indicate that extension started in what is now the area of the Central Apennines at ca. 3-2.5 Ma (Cosentino et al., 2017).

Contemporaneously with extension, the central Apennines has also undergone >800 m differential uplift relative to the Adriatic and Tyrrhenian coastlines (e.g., D'Agostino et al., 2001; Centamore and Nisio, 2003; Pizzi, 2003; Ascione et al., 2008). The long-term development of this regional topographic 'bulge' that extends >200 km along-strike along the Italian Peninsula is evidenced by marine shorelines perched at least several hundreds of meters above sea level (D'Agostino et al., 2001; Mancini et al., 2007) and shoreface deposits of Early Pleistocene age, fringing the Tyrrhenian and Adriatic flanks of the central Apennines (Pizzi, 2003; Cantalamessa and Di Celma, 2004; Artoni, 2013). Prior to regional uplift, the area was close to sea level allowing marginal marine and brackish sediment to accumulate at the base of some of the extensional basins (Gliozzi and Mazzini, 1998).

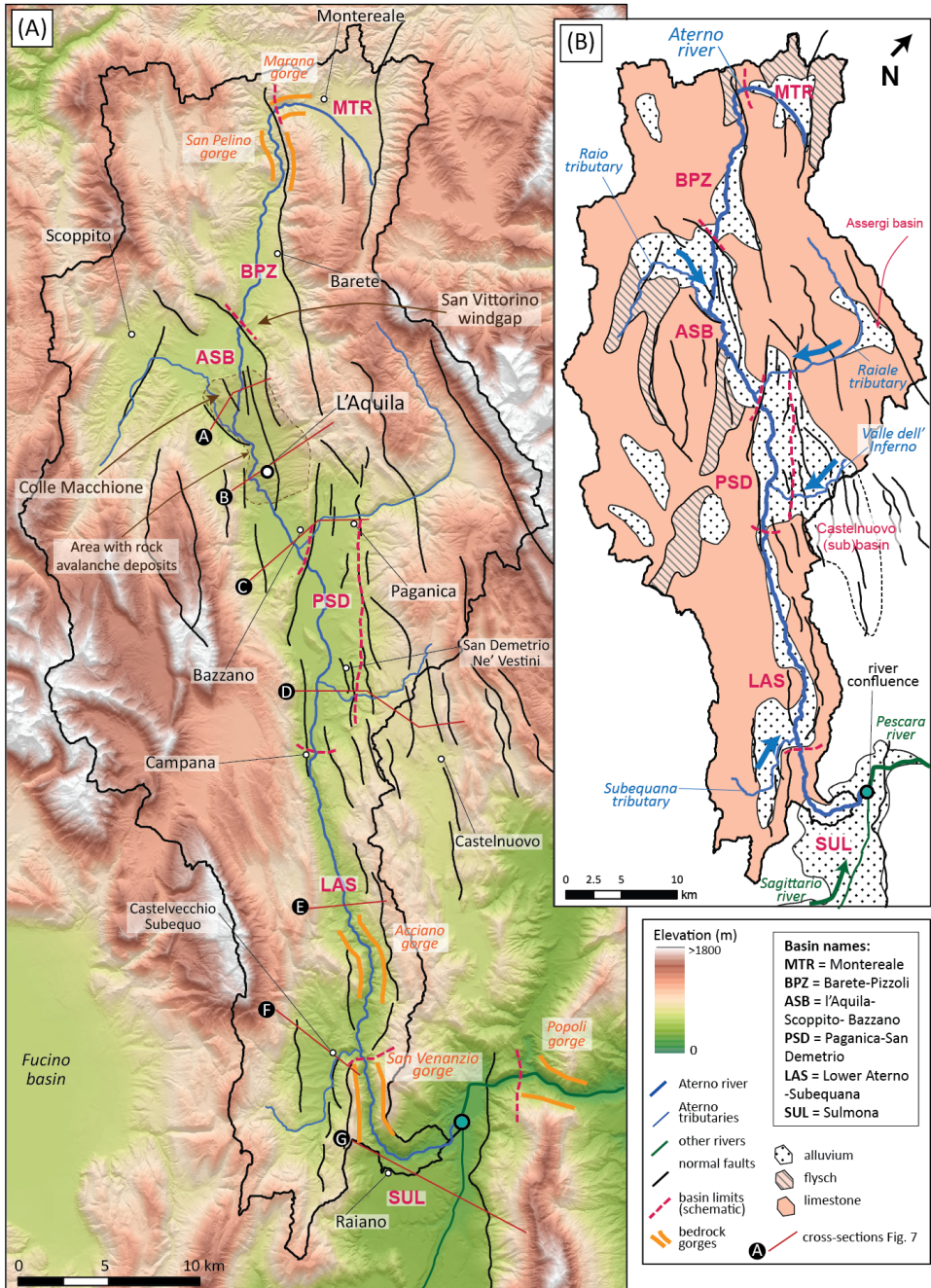


Fig. 4.3. (shown on previous page) (A) Topography of the Aterno River catchment, showing the location of the Aterno River that successively crosses the Montereale (MTR), Barete-Pizzoli (BPZ), L'Aquila-Scoppito-Bazzano (ASB), Paganica-San Demetrio (PSD), Lower Aterno-Subequana (LAS), and Sulmona (SUL) basins. It also shows the location of bedrock gorges and the location of the stratigraphic cross sections shown in Fig. 4.7. (B) Lithology of the Aterno River catchment, the location and geometry of the six major extensional basins, and the main tributaries of the Aterno River.

Today, much of the area lies at a mean elevation >800 m and elevations in the Apennines reach >2500 m in the footwalls of the largest normal faults. Total throw estimates along the faults vary across the area, but tend to be greatest (up to 2200 m) across the more centrally located, higher elevation fault segments, which have lengths of up to 40 km (Cowie and Roberts, 2001; Roberts and Michetti, 2004). Geodetic levelling and GPS velocity measurements over a length scale of 100-150 km suggest a regional extension rate of ~ 3 mm yr⁻¹ and an uplift rate of ~ 1 mm yr⁻¹ in the interior part of the central Apennines (D'Anastasio et al., 2006; D'Agostino et al., 2011; Serpelloni et al., 2013; Faccenna et al., 2014). Surface uplift, regional extension rates, topographic elevation, and also the width of the mountain range are all enhanced compared to along-strike adjacent parts of the Apennines, suggesting that the magnitude of uplift and extension are coupled to the same underlying geodynamic mechanism (Faure Walker et al., 2012). While the broad relationship between thrusting and extension in Italy has been argued to be driven by roll-back of what is now the Calabrian Arc (e.g., Magni et al., 2014), it is generally accepted that the magnitude of active surface uplift and extensional faulting over the last ~ 3 Myr in the Central Apennines must also be the result of dynamic, mantle-driven processes (e.g., Cavinato and De Celles, 1999; D'Agostino et al., 2001; Faccenna et al., 2014).

The highest Holocene throw rate estimates that exist for faults located in the central Apennines reach up to $\sim 1-2$ mm yr⁻¹ (e.g., Roberts and Michetti, 2004; Lavecchia et al., 2012; Cowie et al., 2017). These fault throw rates, combined with the measured geological throws would suggest basin initiation ages that would be substantially younger than 3 Ma. Consequently, Roberts and Michetti (2004) argue that faults in the central Apennines had throw rates in the order of $0.3-0.35$ mm yr⁻¹ during early stages of extension, which then increased for some faults as fault segments evolved, interacted and/or linked. Both structural and geomorphological studies suggest that

faults located in the central and highest elevation areas of the array increased their slip rate at ca. 0.8 Ma, whereas faults nearer the edge of the fault array either kept a more-or-less constant slip rate, or became inactive (Cowie and Roberts, 2001; Roberts and Michetti, 2004; Whittaker et al., 2007, 2008). Along some faults, slip rates decreased because of a shift in the locus of activity to neighbouring faults (e.g., Giaccio et al., 2012; Cosentino et al., 2017).

The numerous hangingwall basins in the central Apennines are filled with up to 900 m of continental deposits (e.g., Cavinato et al., 1993; Cavinato and Miccadei, 2000; Cavinato et al., 2002; Miccadei et al., 2002; Nocentini et al., 2017, 2018). The sedimentological characteristics of these deposits are highly variable, comprising fluvial and proximal deltaic sands and conglomerates, distal lacustrine silts and clays, and poorly sorted basin margin deposits originating from debris flows and various types of mass wasting. Most basin stratigraphies, except from the closed Fucino basin (Fig. 4.2), show a long-term transition from mainly lacustrine to fluvial deposition or fluvial incision, which can be explained by the reorganisation and long-term integration of the drainage network (D'Agostino et al., 2001; Bartolini et al., 2003; Piacentini and Miccadei, 2014; Geurts et al., 2018). Although many basins show this long-term trend, there is considerable variability of stratigraphy and evolution between them that is still largely unexplained (e.g., Bosi et al., 2003; Cosentino et al., 2017).

Various types of palaeoenvironmental records from central Italy in combination with sedimentological and geomorphological observations from the central Apennines demonstrate the impact of Quaternary climatic changes on erosion and sediment transport. Tucker et al. (2011) demonstrate that limestone weathering in the central Apennines occurred more than 10 times faster during the Last Glacial Maximum (LGM) because of frost cracking and reduced vegetation cover, producing enhanced erosion rates up to 30 times higher than Holocene values. While palynological records and hydrological models suggest precipitation during the LGM was similar to today or even slightly reduced (e.g., Ramrath et al., 1999; Jost et al., 2005; Wu et al., 2007), lake-level reconstructions imply considerably wetter conditions (Giraudi, 1989; Giraudi and Frezzotti, 1997). This discrepancy can be explained by the presence of

discontinuous permafrost and glacial meltwaters that increased runoff (Giraudi and Frezzotti, 1997; Bogaart et al., 2003; Kettner and Syvitski, 2008; Tucker et al., 2011). Higher lake levels may have also resulted from a higher precipitation/evaporation ratio during cold glacial conditions. Enhanced discharge for mountain streams is also supported by the coarser calibre of clasts observed in fluvial conglomerates formed during glacial times (Whittaker et al., 2010; Whittaker and Boulton, 2012).

4.4 Data and methodology

Our approach is to integrate geomorphological and stratigraphic data for the present-day Aterno River system (Figs. 4.2 and 4.3). Our focus is to identify changes to the drainage pattern of this river system over the last 3 Myr, in particular drainage integration and isolation events, which influenced the connectivity between the different basins along the Aterno River. We assume the locations of the main valleys and hangingwall depocentres of the Aterno River system were established during the early stages of extension and have remained largely unchanged since then. We base this assumption on the observation that the boundary of the Aterno drainage network today is confined by high topography, by the pattern of active normal faulting (Roberts and Michetti, 2004; Nocentini et al., 2017, 2018) and by the structures inherited from the earlier phase of compressional tectonics (e.g., Piacentini and Miccadei, 2014; Geurts et al., 2018); these structures equally limit the spatial extent of Early to Middle Pleistocene hangingwall lacustrine sediment. Only in the Castelnuovo sub-basin (see below and Fig. 4.3), is there evidence that a valley formerly linked with the Aterno system now drains elsewhere. Consequently, as we discuss in detail in the results, the Aterno River system today spatially integrates these previously endorheic sub-basins via low elevation ‘spill-points’ that lie between them.

4.4.1. River profile and terrace analysis

We used the longitudinal profile of the Aterno River to assess whether the river system is undergoing a transient erosional response to drainage integration over time. We

extracted this from a 10 m DEM of central Italy (Tarquini et al., 2007) and manually identified marked concave reaches and knickzones (i.e., over-steepened or convex reaches). For all knickzones we evaluated whether they could be explained by lithological contrasts using detailed geological maps from the area (e.g., Vezzani and Ghisetti, 1998). For lithological contacts between flysch and limestone in the western part of the central Apennines, Whittaker et al. (2008) estimated a maximum convexity height of ~100 m upstream of these boundaries for small streams with a drainage area of ~10 km². Even though the lithological contrasts in our study area mainly comprise limestone-alluvium alternations, the 10 to 100 times larger drainage area of the Aterno River is expected to strongly limit the heights of lithology-related knickzones as a higher discharge increases stream erosivity (Stock and Montgomery, 1999).

We also evaluated whether the knickzones along the Aterno River could be explained by a transient response to fault slip acceleration. For fault block-scale catchments in the western part of the central Apennines, Whittaker et al. (2007, 2008) demonstrated how streams had steepened and narrowed their channel directly upstream of faults that had been documented to have increased their slip rate ca. 0.8 Ma. Based on the position of knickzones relative to the pattern of active normal faults that are mapped for the Aterno River catchment (Roberts and Michetti, 2004; Nocentini et al., 2017, 2018), we therefore evaluated whether any knickzones could be explained by an increase in slip rate on these faults since their initiation (Cowie and Roberts, 2001).

For knickzones for which a lithological and/or fault-related origin could be excluded, we evaluated whether they could be produced by drainage integration events, i.e., two different river profiles becoming one. First we looked for transitions from lacustrine to fluvial sedimentary facies in the basin located upstream of the knickzone, something we explain in more detail below (in Section 4.5.2). In the case of a drainage integration event, the transition from endorheic to exorheic conditions in the upstream basin is expected to lead to river incision and the formation of a depositional terrace that primarily consists of endorheic (often lacustrine) sediment (e.g., Garcia-Castellanos et al., 2003; Connell et al., 2005; House et al., 2008; Menges, 2008; Larson et al., 2017; Repasch et al., 2017). Therefore we analysed the character of the

main depositional terraces in each basin using geological maps, cross sections and the DEM of the area (Miccadei et al., 2002; Bosi et al., 2004; Chiarini et al., 2014; Piacentini and Miccadei, 2014; Nocentini et al., 2017, 2018) and estimated their top elevation. When estimating the elevation of the individual terraces, we attempted to use only terrace remnants whose elevation relative to the Aterno River was not expected to be significantly affected by active faulting (see Supplementary Materials A for details).

4.4.2. Basin stratigraphy

We compiled and compared the infilling histories of six major fault-controlled basins to reconstruct the development of the Aterno River system, and synthesised published stratigraphic data from these basins into one integrated stratigraphic scheme. These basins comprise the Montereale basin (MTR), the Barete-Pizzoli basin (BPZ), the L'Aquila-Scoppito-Bazzano basin (ASB), the Paganica-San Demetrio basin (PSD), the Lower Aterno-Subequana basin (LAS), and the Sulmona basin (SUL; Fig. 4.3). The data come from numerous detailed studies of individual basins (Miccadei et al., 2002; Bosi et al., 2004; Chiarini et al., 2014; Pucci et al., 2015; Gori et al., 2017; Nocentini et al., 2017, 2018) but also from some studies that compared several basins from the central Apennines with one another (e.g., Bosi et al., 2003). To evaluate the impact of extensional faulting on basin geometry, we additionally compiled data on the total sediment thickness from seismic and borehole studies (Miccadei et al., 2002; Santo et al., 2014; Chiarini et al., 2014; Gori et al., 2017).

We identified in each basin's stratigraphic record units that likely formed when basins were underfilled – indicated by the widespread presence of lacustrine (or palustrine) sediment. We used these units to identify when the basin likely did not have any fluvial outlet (i.e., endorheic drainage). In contrast we assumed the presence of fluvial stratigraphy to reflect phases in a basin's evolution when overfilled and exorheic conditions occurred, i.e., when basins were fluvially connected with their downstream neighbour or with the Adriatic coast. In the central Apennines, lacustrine deposits comprise a number of different facies. Most important for our identification of

underfilled conditions were deep lake deposits that generally comprise white-grey, laminated to massive calcareous clays and silts with occasional intervening layers of sand or gravel (e.g., Miccadei et al., 2002; Gori et al., 2017; Nocentini et al., 2017, 2018). The input of coarser clastic material typically becomes more abundant towards the basin margins where the deep-water facies pass laterally into either delta, alluvial fan or slope deposits. To estimate the timing of these transitions we used age estimates from lacustrine or fluvial units that encompass the transition most precisely. These age estimates are provided by published palaeomagnetic, biostratigraphic and tephra analyses, the latter comprising both lithotype analysis and radioisotope dating (e.g., Galli et al., 2010; Magri et al., 2010; Palombo et al., 2010; Giaccio et al., 2012; Mancini et al., 2012; Chiarini et al., 2014; Gori et al., 2015, 2017; Nocentini et al., 2017, 2018).

In addition, we examined vertical facies successions to provide insight into changes in the balance between sediment supply and basin subsidence (in volumetric terms) and to identify major shifts in depositional environment associated with abrupt lacustrine deepening, shallowing, or with fluvial incision. Most important were shallowing-upward stratigraphic motifs, for instance deep lake facies passing gradually upward into prograding delta deposits, which suggest a change from under- to overfilled conditions. We also integrated information on the sedimentary contact between lacustrine and fluvial units, for instance whether it is an erosional unconformity or a gradual transition. Furthermore, we made a compilation of the stratigraphic cross sections that are available for the four southernmost basins, i.e., the ASB, PSD, LAS and SUL basins, as these provide insight into the stratigraphic position of the different units relative to one another, their geometry, and potential shifts in fault activity over time. These published cross sections are primarily based on well logs, and in some cases, additionally on seismic profiles (Miccadei et al., 2002; Piacentini and Miccadei, 2014; Nocentini et al., 2017, 2018). We used the amount of relief of the top surface of the endorheic basin fill to estimate the amount of incision that followed drainage integration events. The final preserved thicknesses (without decompaction) and ages of the lacustrine units were also used to estimate long-term sedimentation rates. Given

that part of these lacustrine records may have been eroded as a consequence of drainage integration events, these sedimentation rates are minimum estimates.

In general, we focus on the stratigraphic and geomorphological observations that are most closely related to the development of the Aterno River, however, many observations come from incised terraces along the basin margins. Even though this generates uncertainties, we believe the available data from the Aterno River catchment is sufficient to allow us to reconstruct the development of the axial parts of the basins to first order. This approach also explains the way we analysed the Paganica-San Demetrio (PSD) basin that is commonly considered as a sub-basin of the much larger Paganica-San Demetrio-Castelnuovo basin (Fig. 4.3B). We focused mainly on the PSD sub-basin as it has recorded not only the Early (to early Middle) Pleistocene lake that covered both the PSD and Castelnuovo sub-basins, but also the successive development of the Aterno River.

4.5 The Aterno River system and associated rift basins

The Aterno River is the largest river system draining the Adriatic domain of the central Apennines (Figs. 4.2 and 4.3). It has a length of ~100 km, a drainage area of ~1300 km², and flows axially over most of its length (i.e., approximately parallel to fault strike). Within its catchment, elevations vary between ~2500 and 250 m above sea level. Even though the river is perennial and has continuous flow throughout most years, it is characterised by a highly variable, seasonal discharge regime with a modern-day minimum, mean and maximum discharge of ~0.08, 5.2 and 143 m³/s within its downstream reach, near its entrance to the San Venanzio gorge (Lastoria et al., 2008; Fig. 4.3A).

The headwaters of the present-day Aterno River are located in the uplands surrounding the Montereale (MTR) basin (Fig. 4.3). The river first flows across the MTR basin (at ~820 m elevation) and through the Marana gorge in a southwest (across-strike) direction for ~10 km. Downstream of the MTR basin the river starts flowing in a predominantly southeast (along-strike) direction over a distance of ~85 km, across

successively the Barete-Pizzoli (BPZ), L'Aquila-Scoppito-Bazzano (ASB), Paganica-San Demetrio (PSD), and Lower Aterno-Subequana (LAS) basins. Downstream of the LAS basin the river flows through the San Venanzio gorge and continues across the Sulmona (SUL) basin where it turns to the northeast (across-strike) and meets with the Sagittario River at ~250 m elevation. From here the combined Aterno-Sagittario River continues in a northeast direction through the Popoli gorge and into the Adriatic foreland area where it is called the Pescara River (Fig. 4.3).

4.5.1. River profile and terrace analysis

Figure 4.4A shows the DEM-derived longitudinal profile of the Aterno River as well as its downstream continuation as the Pescara River towards the Adriatic coast. The longitudinal profile reveals three large, convex-up knickzones (each >100 m high), which have been ground-truthed by field surveys (yellow in Fig. 4.4B). The most prominent knickzone lies directly upstream of the SUL basin, at ~250 m, where the Aterno River flows through the San Venanzio bedrock gorge from the LAS basin. This knickzone extends approximately 30-35 km upstream, to an elevation of ~550-575 m (Fig. 4.4A and B). In detail, this convex reach itself comprises a number of small-scale convexities, which can be partly attributed to alternations between limestone bedrock and alluvium, e.g., around the Acciano bedrock gorge (Fig. 4.4A and C).

A second, large convex reach with a height and length of ~100 m and 10 km, respectively, is located in between the two most upstream basins, the MTR and BPZ basins (Fig. 4.4A and B). Along this reach the Aterno River crosses both the active Monte Marine Fault (also known as Barete Fault; Roberts and Michetti, 2004) and the Marana and San Pelino bedrock gorges, located in the footwall and hangingwall of the Monte Marine Fault, respectively (Fig. 4.4A and B). Between these two major convex reaches, the overall shape of the Aterno longitudinal profile is concave, except for a number of knickpoints smaller than 30 m (Fig. 4.4A and B). Along the Pescara River, i.e., in between the downstream end of the Aterno River and the Adriatic coast, the longitudinal profile exhibits another convexity that is ~15 km long and 150 m high between the SUL basin and the foreland area (Fig. 4.4A and B). Here the river crosses

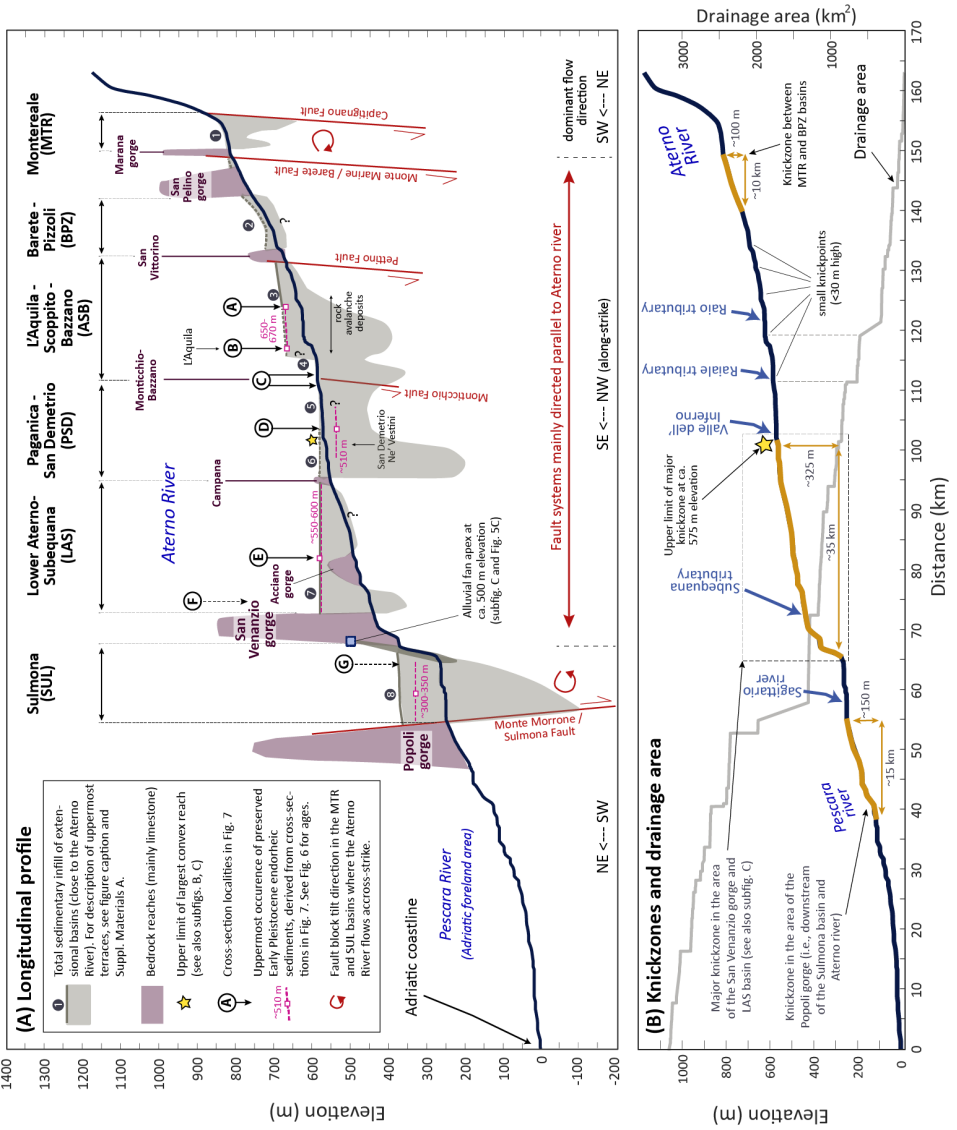


Fig. 4.4. (shown on previous page) (A) Longitudinal profile of the Aterno River, the location of the different extensional basins, and their (bedrock) spill point areas. Most basin-bounding fault systems are orientated parallel to the river and are therefore not shown individually. We do show, however, the position of those fault systems with strike approximately perpendicular to the river. Pink squares and pink dashed lines show the approximate elevation of the sedimentary contact between the endorheic (lacustrine/palustrine/deltaic) and exorheic (fluvial) sediment in the four southernmost basins, based on the cross sections shown Fig. 4.7. Also shown are the approximate upper- and lowermost elevation of the basin sedimentary fills. The upper elevations are based on the top elevation of the uppermost terraces (dark grey lines) that we selected along the river. We selected terraces consisting of fluvial or lacustrine sediment and excluded those consisting of rock avalanche / debris flow deposits in the Colle Macchione-L'Aquila area (see Supplementary Materials A for details): (1) Main (active) fluvial plain of the MTR basin at ~815 m elevation, (2) Early Pleistocene (age poorly constrained) terraces consisting of fluvial and lacustrine sediment. The elevation of its top surface varies considerably across the basin, likely because of differential basin subsidence. (3) Terraces with top elevations of ~650-670 m, consisting of late Middle Pleistocene (~MIS5a) fluvial gravel deposits belonging to the 'Fosso Vetoio Synthem' according to Nocentini et al. (2017). (4) Main (active) fluvial plain in the Bazzano sub-basin at ~590 m elevation. Large elevation difference (>50 m) between uppermost terraces between the areas up- and downstream of L'Aquila can be explained by the temporal blocking of the river valley by >50 m thick rock avalanche deposits during the Middle Pleistocene. (5) Main (active) fluvial plain at ~575 m elevation in the PSD basin, upstream of San Demetrio Ne' Vestini. (6) Fluvial terrace morphology borders the Aterno River on both sides in the PSD basin downstream of San Demetrio Ne' Vestini. However, it is uncertain to what extent these terraces are related to fault activity. Based on the longitudinal profile we expect the wave of incision related to the formation of the San Venanzio gorge to have reached the downstream part of the PSD basin and to explain 25 m high terrace morphology in this area. (7) Terraces consisting of Early Pleistocene lacustrine and fluvial deposits with top elevations at ~550-600 m elevation close to the Aterno River. (8) 'Terrazza Alta di Sulmona' at ~350-400 m elevation consisting primarily of >50 m of fluvial gravel, in turn overlying Early to early Middle Pleistocene lacustrine sediment (Miccadei et al., 2002). (B) Large convex reaches (yellow), smaller convexities, tributary confluences, and drainage area accumulation along the Aterno longitudinal profile. (C) Topography of the area of the major knickzone upstream of the San Venanzio gorge. Based on the longitudinal profile of the Aterno River, we expect that the upper limit of this transient knickzone is located at approximately 575 m elevation, i.e., close to San Demetrio Ne' Vestini in the PSD basin (Fig. 4.4A). However, another option is that the upper limit is located at approximately 550 m, near Campana, i.e., approximately at the border between the PSD and LAS basins. Therefore, we show both the 550 and 575 m contour lines to illustrate the approximate area of fluvial incision caused by knickpoint propagation.

the Popoli gorge and the tip of the Monte Morone Fault (also referred to as the Sulmona Fault; Roberts and Michetti, 2004).

Along much of its course, the modern-day Aterno River has an incised position within the youngest parts of the basin fills (Fig. 4.4A). Either depositional or erosional terraces with top elevations less than 10-20 m above the Aterno thalweg have been described for the ASB, PSD, and SUL basins and are interpreted to be a product of the last glacial-interglacial cycle (Miccadei et al., 2002; Nocentini et al., 2017, 2018).

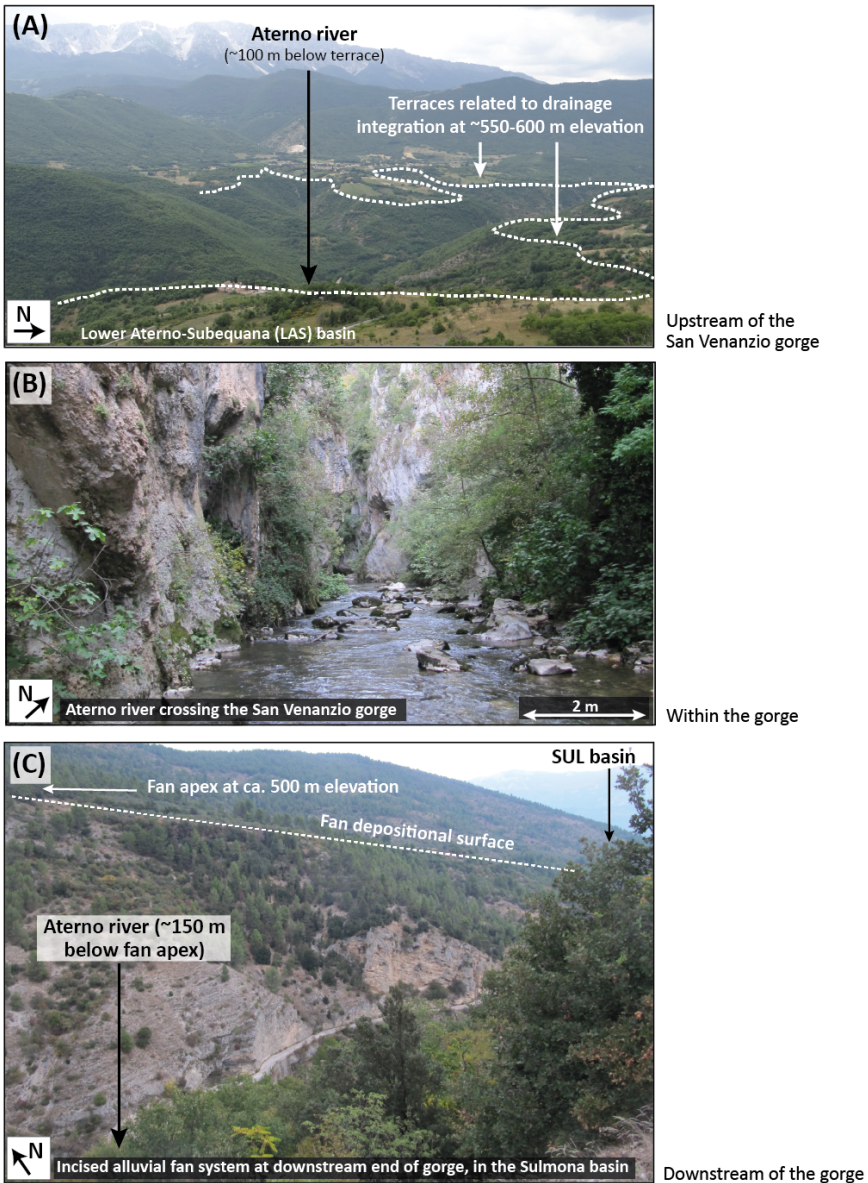


Fig. 4.5. Pictures taken upstream (A), within (B) and downstream (C) of the San Venanzio gorge. (A) Depositional terraces along the Aterno River in the LAS basin that were formed as a consequence of drainage integration between the LAS and SUL basins. These terraces largely consist of lacustrine sediment with fluvial gravels on top, suggesting the basin to have become overfilled. Overspill towards the SUL basin (ca. 0.7 Ma) led to the formation of a through-going river system that started to incise sediment in the LAS basin and to transport sediment towards the SUL basin, where it initially formed a large alluvial fan system where the downstream end of today's San Venanzio gorge is located (shown in C). On-going incision by the Aterno River led to the progressive dissection of the alluvial fan deposits (in C) and the LAS basin fill (in A) and the formation of the San Venanzio gorge (in B).

However, in many basins we also observe at least one significantly higher depositional surface that forms the upper limit of the basin fill and has elevations that vary in between 30 and 150 m above the Aterno River (Fig. 4.4A). The most prominent of these depositional surfaces, varying between ~550 and 600 m elevation, are within the LAS basin (Figs. 4.4A and 4.5A; e.g., Gori et al., 2017), and the extensive ‘*Terrazza Alta di Sulmona*’ at ~350-400 m elevation in the SUL basin (e.g., Miccadei et al., 2002). It is important to note that the age and sedimentological characteristics of these prominent terraces vary among the different basins (Fig. 4.4A; see Supplementary Materials A for details). However, what they have in common is that they may all relate to the integration of the drainage network, and we develop this idea further below.

4.5.2. Basin stratigraphy

The total thickness of syn-rift sediments varies considerably along the Aterno River from zero within the bedrock limestone reaches to more than 400 m within the deepest hangingwall basins (grey shading, Fig. 4.4A). This spatial variability can be largely explained by the pattern of extensional faulting. Within individual basins, there is significant variability in sediment thickness, as for instance within the ASB, PSD, and LAS basins. This intra-basin variability can primarily be explained by the fact that many of these large basins are controlled by multiple faults. Moreover, in some basins, transverse faults (i.e., striking approximately SW-NE) additionally affect basin geometry and hence the pattern and rates of basin subsidence (e.g., Santo et al., 2014; Gori et al., 2017).

Figure 4.6 summarises the stratigraphy for each basin along the Aterno River, and Fig. 4.7 shows stratigraphic cross sections through the four southernmost basins. For most basins the onset of infilling is poorly constrained to the beginning of the Early Pleistocene based on the regional onset of extensional faulting in this area (D’Agostino et al., 2001; Cosentino et al., 2017). In case of the PSD and ASB basins, however, biostratigraphic dating suggest that sedimentation started at, or before, the Pliocene-Pleistocene transition (Cosentino et al., 2017; Fig. 4.6). In this section we

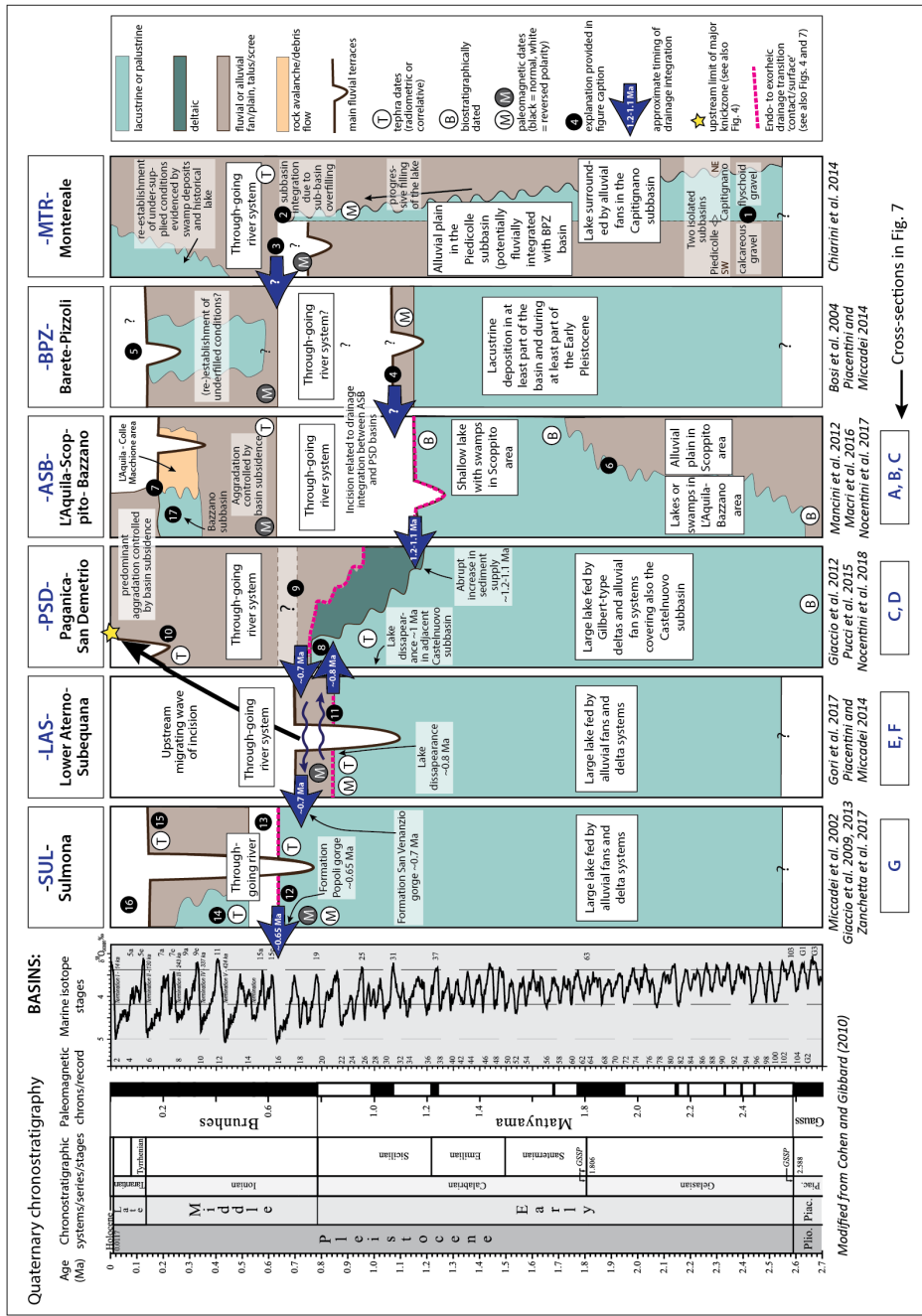


Fig. 4.6. (shown on previous page) Main stratigraphic units for each basin along the Aterno River system and the approximate timing of fluvial integration with their downstream neighbour (see large dark blue arrows). Key references are provided below each individual basin column. (1) Early Pleistocene isolation of sub-basins in the MTR basin evidenced by flyschoid and calcareous sediment in the NE and SW sub-basins, respectively. (2) Sub-basin integration caused by sub-basin overflowing evidenced by the appearance of flyschoid gravel in the SW sub-basin. (3) Deep (>40 m) fluvial incision during the early Middle Pleistocene likely related to integration with downstream BPZ basin. Subsequent infilling of incised channels with tephra- and organic-rich sediment. (4) Fluvial sediment with reversed magnetic polarity in the windgap between BPZ and ASB basins suggest a through-going river system to have formed sometime during the Early Pleistocene, however, exact timing of drainage integration is poorly constrained. (5) Aterno River channel has an incised position (up to ~50 m) within Early-Middle Pleistocene sediment, however, the origin (fluvial or fault-related) and age of these terraces are not constrained. (6) Transition from alluvial fan/slope deposits to lacustrine sediment biostratigraphically dated to 2-1.7 Ma. Locally this transition comprises a period of non-sedimentation and soil development (e.g., on abandoned fan surfaces and fault-related terraces). (7) Rock avalanche activity may explain the differences between the late Middle Pleistocene-Recent stratigraphies in ASB basin areas up- and downstream of L'Aquila. (8) Lake disappearance in the PSD basin estimated to ca. 0.8-0.7 Ma based on developments in the adjacent LAS and Castelnuovo basins (see main text). (9) Lacustrine sedimentation first followed by fluvial sedimentation in the PSD basin. However, the PSD basin may have experienced a short period of (minor) fluvial incision or non-deposition during the early Middle Pleistocene (Giaccio et al., 2012). (10) We suspect at least part of the terrace morphology in the downstream part of the PSD basin to be related to the wave of erosion propagating upstream from the San Venanzio gorge. (11) Lacustrine silts grade upwards into fluvial gravels showing reversed flow direction towards the PSD basin. Around 0.7 Ma, a fluvial connection through the San Venanzio gorge and a normal flow direction across the LAS basin were established, followed by the onset of strong fluvial incision. (12) Top of the Early to early Middle Pleistocene lacustrine unit (unit 'SUL6' according to Giaccio et al., 2013) estimated to ca. 650 ka, assuming a constant sedimentation rate and extrapolating from a $^{40}\text{Ar}/^{39}\text{Ar}$ dated tephra layer from ca. 724 ka (Zanchetta et al., 2017). (13) First main phase of incision in the Sulmona basin, with soil development on the abandoned terraces. End of this phase is well constrained by a thick 527 ka tephra layer observed directly above the palaeosol (Zanchetta et al., 2017). (14 and 15) Strong aggradation between ca. 530 and 135 ka, causing the deposition of lacustrine sediment in the downstream part of the basin (near the Popoli gorge) and >50m of fluvial gravel across the remaining part of the basin (Miccadei et al., 2002). (16) Around 135 ka, a second main phase of incision started in the Sulmona basin, however, which was periodically affected by travertine formation within and downstream of the Popoli gorge (Lombardo et al., 2001) (17) Temporal re-establishment of underfilled / lacustrine conditions during the late Middle Pleistocene in the Bazzano sub-basin (e.g., Macri et al., 2016).

describe the most important aspects of the individual basin stratigraphies that provide insights into when and where endorheic or exorheic conditions existed, and how transitions between them might have occurred. We mostly adopt lithofacies names instead of local formation names in order to increase the readability of the paper, and partly because there is no general agreement on the formation names.

- Predominant lacustrine sedimentation during the Early to early Middle Pleistocene -

In all basins the Early to early Middle Pleistocene stratigraphy consists at least partly of lacustrine sediment (Figs. 4.6 and 4.7). In the most upstream MTR basin, Early to early Middle Pleistocene lake sediments have been observed in its north-eastern sub-basin (Fig. 4.6; Chiarini et al., 2014). Early Pleistocene lake sediments have also been documented for the adjacent basin, the BPZ basin (Bosi et al., 2004; Piacentini and Miccadei, 2014), however, its spatial extent and age is poorly constrained. In all the other basins farther downstream, i.e., the ASB, PSD, LAS and SUL basins, lake sediments are widespread and suggest that lakes covered most of their individual hangingwall basins for some periods during the last 3 Myr (Miccadei et al., 2002; Giaccio et al., 2012; Gori et al., 2017; Figs. 4.6 and 4.7). In the ASB basin, the area around L'Aquila and Bazzano experienced continued lacustrine sedimentation during the Early Pleistocene, whereas the Scoppito area experienced a transition from an alluvial fan-dominated environment to lacustrine sedimentation around 2-1.7 Ma (Fig. 4.6; Mancini et al., 2012; Nocentini et al., 2017). These differences in stratigraphy can be explained by a former geomorphological threshold that might have existed half-way down the ASB basin in the area of Colle Macchione (Fig. 4.3A; Mancini et al., 2012). The lake in the PSD basin was a major lake that also covered the adjacent Castelnuovo basin (cross section D in Fig. 4.7; Giaccio et al., 2012). Water depths in this lake were of the order of 30 m as suggested by the height of Gilbert delta foresets (Giaccio et al., 2012).

No direct constraints on lake depths exist for the other basins. However, the absence of frequent alternations between shallow and deep lake facies suggests most Early to early Middle Pleistocene lakes to have been sufficiently deep to impede glacial-interglacial climate-related oscillations in lake level (e.g., Giraudi and Frezzotti, 1997) from markedly affecting the sedimentary environment. An exception is the Scoppito part of the ASB basin where the characteristic '*Madonna della Strada*' deposits are found between ca. 2-1.7 and 1.2-1.1 Ma (Fig. 4.6 and cross sections A, B in Fig. 4.7). These comprise alternating layers of fine (sandy silts and clays) and sandy gravels, with thick lignite seams up to several meters thick (Mancini et al., 2012; Nocentini et

al., 2017). Some of these lignites have been correlated to Early Pleistocene interglacial periods (e.g., Magri et al., 2010) and likely formed in relatively shallow lake or lake margin environments (Mancini et al., 2012; Nocentini et al., 2017).

- Transition from endorheic to exorheic conditions during the late Early and early Middle Pleistocene -

Our data compilation suggests that either the ASB or BPZ basin was the first to become externally drained. In the ASB basin, lacustrine sedimentation is abruptly followed by fluvial incision (Fig. 4.6; Mancini et al., 2012; Macri et al., 2016; Porreca et al., 2016; Nocentini et al., 2017). Here, biostratigraphic data from the youngest preserved lacustrine sediment suggests this abrupt change to have occurred around 1.1-1.2 Ma (Mancini et al., 2012; Nocentini et al., 2017). In the BPZ basin, located directly upstream of the ASB basin, lacustrine sediment in the southern part of the basin is covered by fluvial terrace gravels with a reversed magnetic polarity (Figs. 4.3A and 4.6; Bosi et al., 2004; Piacentini and Miccadei, 2014). The fact that this fluvial terrace extends into a windgap east of San Vittorino (Fig. 4.3A; also discussed by D'Agostino et al., 2001) suggests that a fluvial connection between the BPZ and ASB basins had been established by the latest part of the Early Pleistocene (Fig. 4.6).

The LAS basin was likely the third basin to become externally drained between 0.8 and 0.7 Ma (Fig. 4.6). This integration event is constrained by two $^{40}\text{Ar}/^{39}\text{Ar}$ dated tephra layers near the top of the lacustrine silts (890 and 805 ka) and a normal magnetic polarity of overlying fluvial gravels (Gori et al., 2015, 2017). In the LAS basin a gradual transition from lacustrine silts into fluvial sands and gravels has been interpreted by Gori et al. (2017) as the basin shallowing and becoming overfilled (Fig. 4.6 and cross sections E and F in Fig. 4.7). These oldest fluvial gravels show a flow direction to the northwest, i.e., towards the PSD basin, opposite to the regional flow of the Aterno River (Fig. 4.3A; Gori et al., 2015, 2017). Thus from at least ca. 1.1-1.2 Ma until ca. 0.8-0.7 Ma, we argue that the PSD basin acted as a local base level, first for the ASB and BPZ basins, and later on, also for the LAS basin. The Castelnuovo basin, which lies parallel, but East of the PSD and LAS basins, started draining towards the

PSD basin from ca. 1 Ma onwards (Fig. 4.3B; Giaccio et al., 2012). In the LAS basin, basin infilling and the establishment of a NW-flowing river was soon followed by deep fluvial incision that is explained by the cutting of the San Venanzio gorge (Gori et al., 2017; Fig. 4.6 and cross sections E and F in Fig. 4.7).

In the PSD basin a strong increase in sediment supply from the north occurred around 1.2-1.1 Ma, causing rapid infilling of the lake by large (up to 30 m high) Gilbert-type deltas that are overlain by braided river deposits (Giaccio et al., 2012; Nocentini et al., 2018; Fig. 4.6 and cross sections C and D in Fig. 4.7). The formation of the San Venanzio gorge around ca. 0.7 Ma (Gori et al., 2015, 2017) terminated endorheic drainage in the combined BPZ-ASB-PSD-Castelnuovo-LAS area and led to the establishment of a through-going river system all the way towards the southernmost SUL basin. The transition from aggradation to a phase of non-deposition or limited fluvial incision in the PSD basin around ca. 0.8-0.7 Ma (Giaccio et al., 2012), suggests that by that time sediment was largely exported out of the basin by the Aterno River flowing through the San Venanzio gorge (Fig. 4.6). A large Pleistocene alluvial fan system in the SUL basin at the downstream end of the gorge has been documented, which was likely formed when large quantities of sediment were transported across the former spill-point between the two basins (Figs. 4.5C, 4.4A and 4.4C; Miccadei et al., 2002; Gori et al., 2015, 2017).

In the SUL basin, lacustrine conditions persisted the longest, until ca. 650 ka, based on radiometric age estimates from multiple tephra layers (Fig. 4.6 and cross section G in Fig. 4.7; Giaccio et al., 2013; Zanchetta et al., 2017). Here the lacustrine phase was followed by a period of localised deep (~50 m) fluvial incision, with soil development on the surrounding abandoned terrace surfaces (Zanchetta et al., 2017). This erosion phase is interpreted to have resulted from the opening and incision of the Popoli gorge and lasted until ca. 530 ka (Fig. 4.3A; Miccadei et al., 2002; Giaccio et al., 2009, 2013; Zanchetta et al., 2017).

The evolution of the MTR basin is the hardest to connect to the other basins. Here external drainage began somewhere during the Middle Pleistocene, as evidenced by

palaeomagnetic analysis of lacustrine sediments (Fig. 4.6) and the abundance of Middle Pleistocene tephra in the oldest fluvial deposits topping the lacustrine deposits (Chiarini et al., 2014). In case of the MTR basin, an erosional unconformity marks the abrupt transition from lacustrine sedimentation to prograding alluvial fan systems that caused the overflowing of the northeastern sub-basin and its integration with the southwestern sub-basin (Chiarini et al., 2014).

- Late Early Pleistocene to Holocene development of the Aterno River -

The late Early Pleistocene to Holocene sections of most of the basin stratigraphies either comprise fluvial sediment, or erosion and terrace formation associated with fluvial incision by the Aterno River (Fig. 4.6). Borehole data from the most upstream located MTR basin suggest that fluvial incision of at least 40 m followed drainage integration with the downstream BPZ basin sometime during the late Early Pleistocene or early Middle Pleistocene (Chiarini et al., 2014). However, the timing of drainage integration as well as the duration of the period of incision in the MTR basin is poorly constrained (Fig. 4.6). In this basin, aggradation has replaced incision and sediment now fully covers the older erosional terrace morphology.

It is uncertain how much fluvial incision occurred in the BPZ basin directly following drainage integration at the end of the Early Pleistocene. However, the basin primarily experienced aggradation during the Middle Pleistocene as sediment with a normal magnetic polarity partly covers Early Pleistocene terraces. This Middle Pleistocene sediment not only consists of fluvial sand and gravel, but also partly of lacustrine silt and clay (Bosi et al., 2004; Fig. 4.6). In the central part of the basin, the active floodplains of the Aterno River are incised 15-20 m into these Middle Pleistocene deposits suggesting renewed fluvial incision to have started sometime during the Late Pleistocene. Maximum Holocene throw rate estimates for the main basin-bounding fault system, i.e., the Monte Marine/Barete Fault, vary between ~ 0.55 and 1 mm yr^{-1} (Roberts and Michetti, 2004; Galli et al., 2011), suggesting that this fault system has accelerated its slip rate over time (see Section 4.3).

Stratigraphic cross-sections across the ASB, PSD, LAS and SUL basins

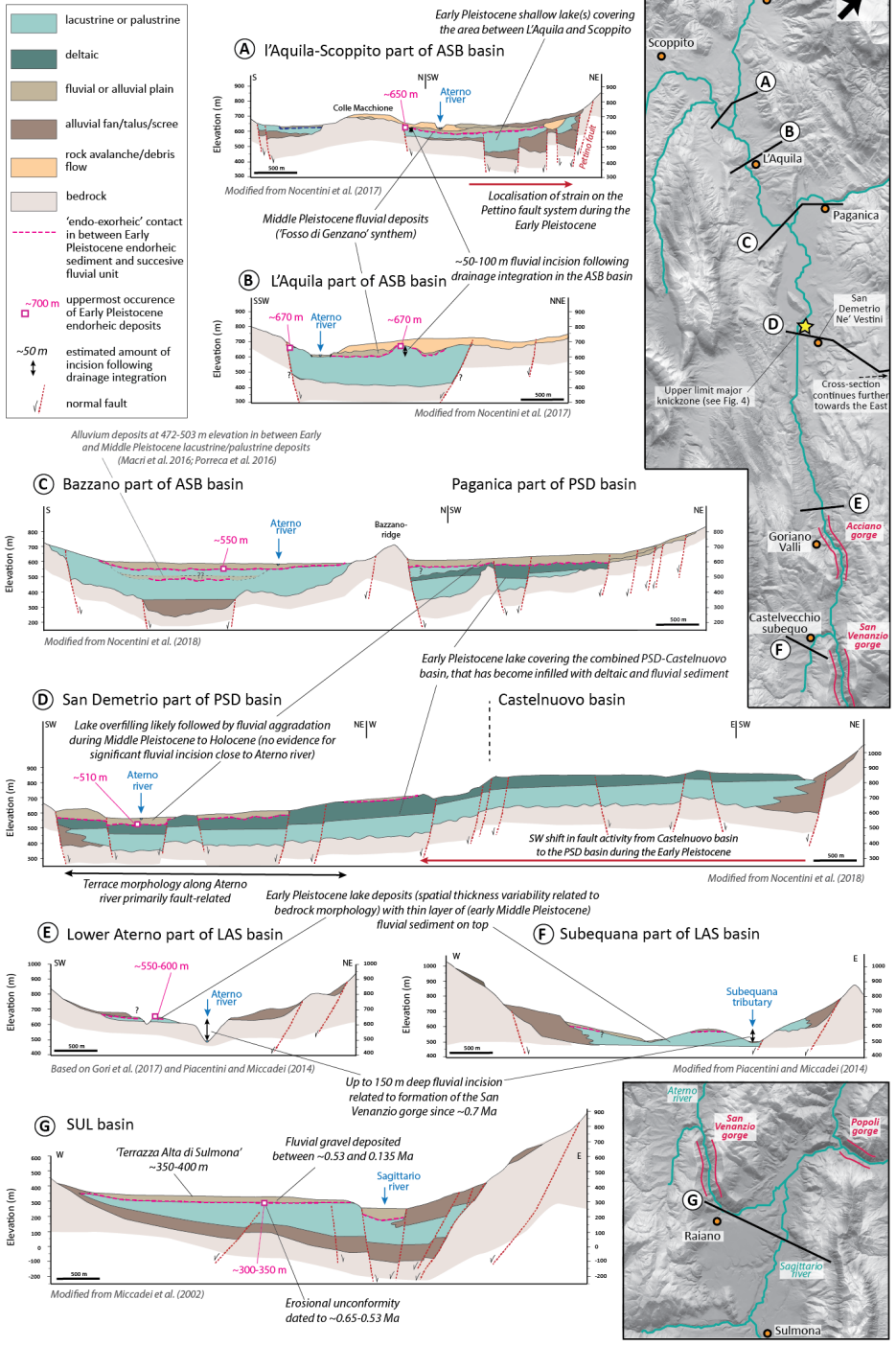


Fig. 4.7. (previous page) Stratigraphic cross sections through the four most downstream located ASB, PSD, LAS and SUL basins (references provided underneath each cross section). Transect positions are also shown in Figs. 4.3A and 4.4A. With pink lines, we marked the contact between the pre-drainage integration endorheic (lacustrine/palustrine/deltaic) sediment and the post-drainage integration fluvial sediment. The pink squares show the uppermost elevation of this contact that we use in Fig. 4.4A. Cross sections A and B and the southern part of C cross the ASB basin. The Early Pleistocene to early Middle Pleistocene parts of these cross sections are similar. However, cross sections A and B show the 50-100 m thick late Middle Pleistocene rock avalanche deposits (in yellow), while cross section C shows a late Middle Pleistocene lacustrine unit (e.g., Macri et al., 2016). Cross section D and the northern part of cross section C show the stratigraphy of the PSD basin. Characteristic for the PSD basin are the up to 100 m thick deltaic deposits overlying the lacustrine unit. While the Early Pleistocene lake covered both the PSD basin and Castelnuovo sub-basin, Middle Pleistocene fluvial activity was limited to the PSD basin from the Middle Pleistocene onwards caused by a SW shift in fault activity (see cross section D). Cross sections E and F cross the LAS basin. They show the variability in thickness of the Early Pleistocene lacustrine sediment along the basin and the thin layer of overlying fluvial deposits related to overflowing of the basin ca. 0.8 Ma. They also show the up to 150 m deep incision that as occurred since the formation of the San Venanzio gorge ca. 0.7 Ma. Cross section G crosses the SUL basin, and shows the thick sequence of Early to Middle Pleistocene (>0.65 Ma) lacustrine sediment, with on top the ~50 m layer of (ca. 530-135 ka) fluvial gravel.

In the ASB basin, drainage integration with the PSD basin around 1.2 Ma was directly followed by fluvial incision of the order of 50-100 m (Mancini et al., 2012; Nocentini et al., 2017; cross sections A, B, and C in Fig. 4.7). Aggradation started again during the early Middle Pleistocene, causing most of the Early Pleistocene lacustrine sediment to become largely covered by Middle Pleistocene fluvial deposits (Nocentini et al., 2017). During the late Middle Pleistocene, the ASB basin additionally experienced major rock avalanche and debris flow events in the L'Aquila-Colle Macchione area (Figs. 4.3A, 4.4A, and 4.6, and see yellow units in cross sections A and B in Fig. 4.7; Nocentini et al., 2017). The Pettino Fault is the main basin-bounding fault system and is inferred to have a Holocene slip rate of approximately 0.6 mm yr^{-1} (Galli et al., 2011).

In the PSD basin, no clear evidence exists for significant fluvial incision adjacent to the Aterno River directly following drainage integration around 0.7 Ma (Fig. 4.6; Giaccio et al., 2012). In this basin, ~50 m of fluvial sediment was deposited on top of the Early (to early Middle) Pleistocene lacustrine deposits during the Middle to Late Pleistocene time interval (Nocentini et al., 2018). Most of the relief in the PSD basin can be explained by activity on the large number of normal fault segments that

together control basin subsidence (Fig. 4.3A, cross section D in Fig. 4.7). However, in the most downstream part of the basin, downstream of San Demetrio Ne' Vestini, some of the terrace morphology may additionally relate to the wave of incision propagating upstream from the San Venanzio gorge and LAS basin (Fig. 4.4A and C). Middle Pleistocene to present-day slip rate estimates for the main fault system controlling the PSD basin are of the order of $\sim 0.5\text{-}0.7\text{ mm yr}^{-1}$ (Galli et al., 2010, 2011; Moro et al., 2013).

In the LAS basin, drainage integration was followed by intense fluvial incision caused by the large drop in local base level caused by incision of the San Venanzio gorge (Figs. 4.4A, 4.4C, 4.5A, and 4.6, and cross sections E and F in Fig. 4.7; Gori et al., 2015, 2017). Incision is still on going and has so far produced around 100-150 m of incision in the downstream part of the LAS basin (Fig. 4.4A and cross sections E and F in Fig. 4.7) and limited incision ($<20\text{-}30\text{ m}$) in the upstream part of the LAS basin (Fig. 4.4A). Maximum Holocene throw rate along the main basin-bounding fault system is estimated to be in between $0.3\text{ and }0.7\text{ mm yr}^{-1}$ (Galadini and Galli, 2000; Faure Walker, 2010).

In the SUL basin, 50-100 m of aggradation occurred between ca. 530 and 135 ka mainly comprising gravels (Miccadei et al., 2002; Giaccio et al., 2009, 2013; Zanchetta et al., 2017). However, in the most downstream (northeastern) part of the basin, mainly lacustrine sediment is observed (Zanchetta et al., 2017). From ca. 135 ka onwards, the Aterno River has been mainly incising, adjusting its profile in response to base level fall across the Popoli gorge. The maximum Holocene throw rate estimated for the basin-bounding Monte Morrone/Sulmona fault system is approximately 1.1 mm yr^{-1} (Roberts and Michetti, 2004), suggesting a significant acceleration in fault slip rate during the Middle Pleistocene.

4.6 Evolution of the Aterno River system in response to drainage integration

The dominant stratigraphic trend observed in all six basins is a transition from primarily lacustrine to fluvial sedimentation that is interpreted to record the progressive integration of the drainage network along the Aterno River system (Fig. 4.8). Long-term drainage integration in the central Apennines has previously been described (e.g., D'Agostino et al., 2001; Bartolini et al., 2003; Piacentini and Miccadei, 2014) and reproduced by means of numerical modelling (Geurts et al., 2018). However, the data compilation for the Aterno River reported here provides detailed insights into the timing, variable character and causes of the individual drainage integration events.

The timing of drainage integration is not a function of distance from the coast (Fig. 4.8). Based on the available evidence, it appears that drainage integration commenced along the middle reaches of the Aterno River system, in the ASB or BPZ basin, and occurred last between the most downstream located SUL basin and the Adriatic coast. Consequently, the spatio-temporal pattern of drainage integration is not consistent with a model where progressive hinterland capture is driven by headward erosion from the coast (e.g., D'Agostino et al., 2001; Dickinson, 2015). As demonstrated by numerical modelling experiments (Geurts et al., 2018) and suggested by drainage integration studies focussing on other areas (e.g., Connell, 2005), the more disordered pattern of drainage integration that we observe for the Aterno River could be expected from overspill mechanisms, i.e., the overfilling of basins with sediment and water (Geurts et al., 2018). We come back to this in more detail in Section 4.7.1.

We interpret the three large-scale convexities along the Aterno longitudinal profile to relate to the progressive, long-term integration of the drainage network (Fig. 4.4B). For all of these convexities, we can exclude a lithology or fault-related origin. We therefore interpret them as transient features reflecting the ongoing adjustment of newly established fluvial connections between initially isolated basins (Fig. 4.1C). Moving in a downstream direction, we explain the three major knickzones along the

Aterno River profile to reflect integration events between the MTR and BPZ basins, between the LAS and SUL basins, and between the SUL basin and the Adriatic foreland (Miccadei et al., 2002; Giaccio et al., 2013; Chiarini et al., 2014; Gori et al., 2017). As these knickzones migrate upstream, they cause incision into the endorheic deposits of the upstream basin fill and terrace formation (Figs. 4.1C and 4.4A). The best examples are the substantial terraces within the LAS basin, which have surface elevations up to 150 m above the present-day Aterno River (Fig. 4.5A). Even though incision is observed in most basins, it is important to note that this does not represent a single wave of erosion, but multiple waves that started at different times in the individual basins.

The transition from internal (endorheic) to external (exorheic) drainage evidently led to a shift from the complete storage of sediment within individual basins towards the partial reworking and export of sediment towards other basins downstream or the Adriatic coast. The export of sediment explains the relatively low thickness of fluvial sediment (of late Early Pleistocene to Recent age) compared to their lacustrine (Early to early Middle Pleistocene) counterparts, taking into account the different duration of the time intervals during which these deposits were formed (Fig. 4.7).

While drainage integration is the dominant long-term trend for the basin evolution along the Aterno River over the last ~3 Myr, the younger stratigraphy of some basins shows intervals that record a transition back from fluvial to lacustrine or to palustrine depositional environments (Fig. 4.6). Examples of these fluvial to lacustrine/palustrine transitions occur in the MTR basin (Chiarini et al., 2014), the BPZ basin (Bosi et al., 2004), the Bazzano part of the ASB basin (Macri et al., 2016; Porreca et al., 2016), and the northeastern part of the SUL basin (Giaccio et al., 2013; Zanchetta et al., 2017). These transitions provide evidence that these basins must have become at least partly underfilled during the Middle to Late Pleistocene or Holocene.

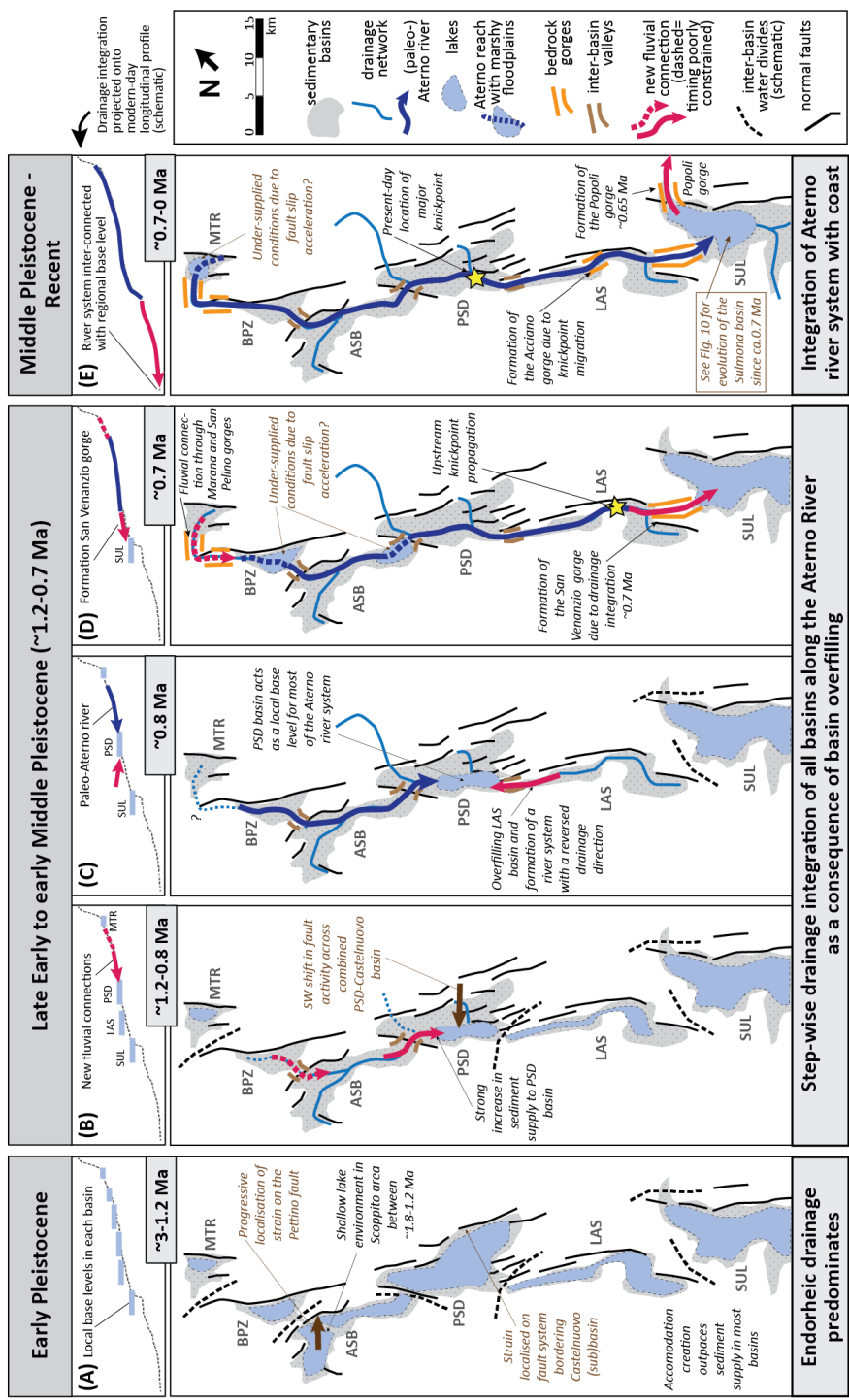


Fig. 4.8. (shown on previous page) Palaeogeographic maps showing the development of the Aterno River system for different time intervals as described in the main text (bottom panels). The long-term trend of drainage integration is also (schematically) projected onto the longitudinal profile of the Aterno River (top panels). (A) All basins were isolated from one another and supported lakes during the greatest part of the Early Pleistocene (ca. 3-1.2 Ma). (B), (C), and (D): Between ca. 1.2 and 0.7 Ma, all basins along the Aterno River became step-wise integrated with one another. Drainage integration started in the area around L'Aquila and occurred because of basin filling and overflow caused by an increase in sediment (and water) supply relative to basin subsidence (see also Fig. 4.9). (E) Approximately 0.65 Ma, a fluvial connection between the fully integrated Aterno River system and the Adriatic foreland became established (see also Fig. 4.10).

4.7 Discussion

The data compilation presented in this paper shows the progressive integration of basins along the Aterno River in the actively extending central Italian Apennines. Here we first discuss the factors that likely primarily controlled the evolution of the Aterno River (Section 4.7.1) and describe the variability in which drainage integration events are expressed in the stratigraphic-geomorphological records of the different basins (Section 4.7.2). Subsequently, we evaluate how long it takes for the landscape to respond to long-term drainage integration (Section 4.7.3), and discuss the general implications of our work in terms of the importance of drainage network evolution for transient landscape evolution and basin stratigraphy in continental rifts (Section 4.7.4).

4.7.1. Potential controls on drainage integration

Factors that controlled the fluvial connectivity between neighbouring extensional basins along the Aterno River are those that can modify the balance between the rate of water supply, sediment supply and the rate of basin subsidence and can in turn cause a basin to switch between underfilled and overfilled conditions (Fig. 4.1B; e.g., Gawthorpe et al., 1994). Where the integrated sediment supply exceeds basin subsidence in volumetric terms, this can cause an endorheic underfilled basin to become overfilled and to form a fluvial connection with its downstream neighbour. If basin subsidence exceeds sediment supply, on the other hand, a fluvially integrated basin may return to underfilled or even endorheic conditions (e.g., Geurts et al., 2018). Further factors that are additionally important are pre-existing topography that sets the

height of the spill point, and the water supply-to-evaporation ratio that controls lake levels (Fig. 4.1B).

Overspill mechanisms are inferred to have controlled drainage integration in other continental extensional settings such as along the Rio Grande (e.g., Connell et al., 2005; Repasch et al., 2017), the lower Colorado River downstream of the Colorado plateau (House et al., 2008), the Salt and Verde rivers in Arizona (Larson et al., 2014), and the Amargosa, Owens, and Mojave rivers in Nevada-California (Meek, 1989, this issue; Menges, 2008; Phillips, 2008). In the central Apennines, the importance of the interplay between sediment supply, water supply and basin subsidence in controlling drainage network evolution has only been suggested at the scale of individual hangingwall basins (e.g., Mancini et al., 2012; Chiarini et al., 2014; Macri et al., 2016). We believe, however, that shifts in balance between sediment supply, water supply and basin subsidence can explain many observations from the Aterno River system as a whole, and for the central Apennines in general.

- Underfilled conditions during the Early to early Middle Pleistocene -

We expect the prevailing trend of drainage integration along the Aterno River to result from a long-term increase in sediment supply relative to basin subsidence, allowing the initially isolated basins to overflow. We test this idea in Fig. 4.9 by generating estimates for the accumulation of basin subsidence and hangingwall sediment thicknesses for basins along the Aterno River. During early stages of extension, faults in the central Apennines are estimated to have had throw rates of the order of 0.3-0.35 mm yr⁻¹ (Roberts and Michetti, 2004). When assuming typical long-term ratios of footwall uplift to hangingwall subsidence in the range of 1:1 to 1:2 (e.g., Bell et al., 2018; De Gelder et al., 2019) these values would correspond to 0.15-0.23 mm yr⁻¹ of accumulating hangingwall volume that could be filled with sediment or water (see blue accumulation curve and inset figure in Fig. 4.9). Uplift-to-subsidence ratios in between 1:1 and 1:1.6 have also been inferred for normal fault systems in the southern Apennines where extension is also accompanied by regional uplift (Roda-Boluda and

Whittaker, 2016, 2017), and we consider the maximum possible value of hangingwall subsidence to be given by a ratio of 1:2.

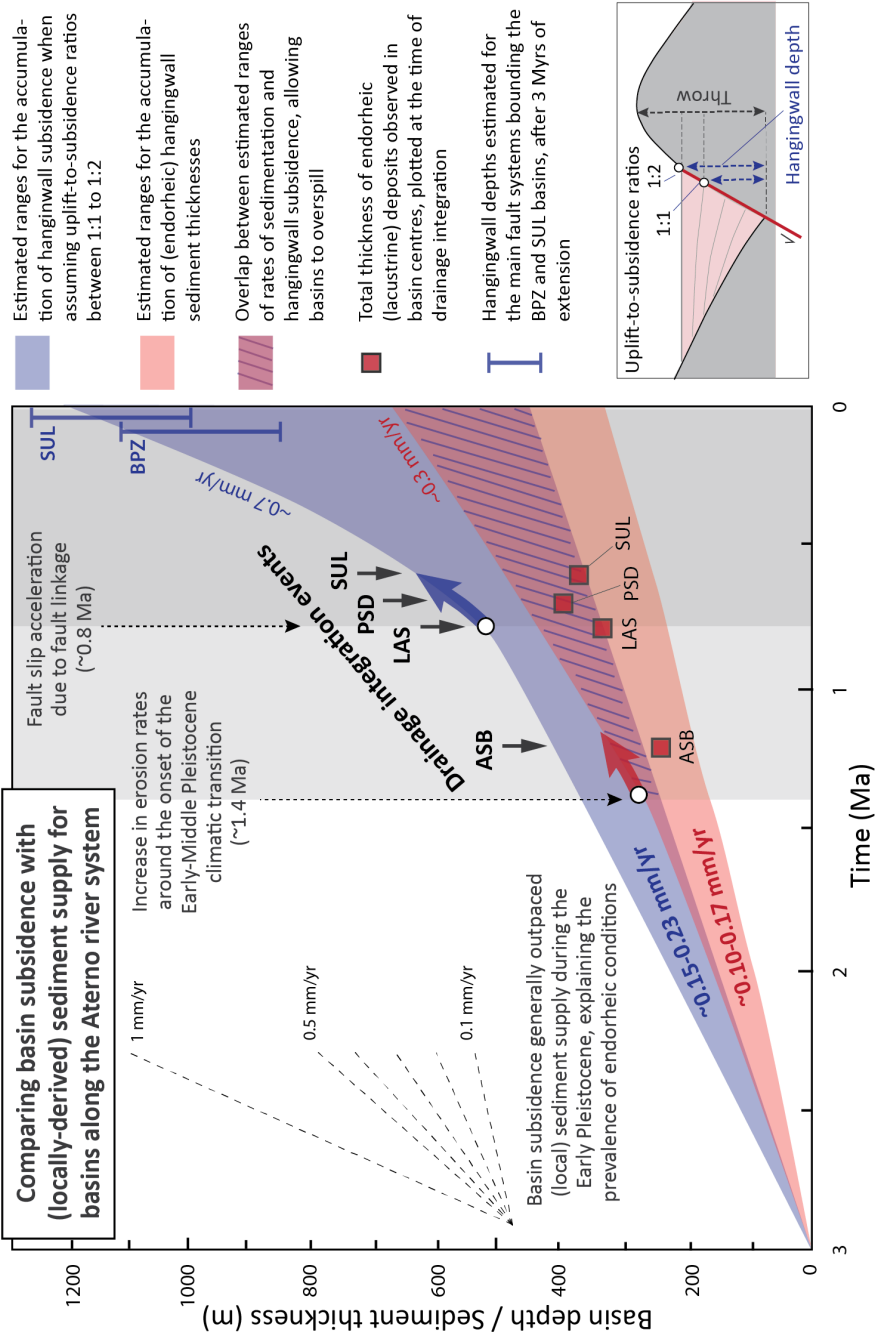


Fig. 4.9. (shown on previous page) The progressive accumulation of basin subsidence (blue shading) and hangingwall sediment thickness (red shading) based on fault slip rate, total throw and stratigraphic data compiled for the basins along the Aterno River and the main basin-bounding faults (see main article text for explanation). When assuming typical long-term ratios of footwall uplift to hangingwall subsidence in the range of 1:1-1:2, we expect approximately half to two-thirds of the accumulated fault throw to represent the basin volume that is available for sediment to accumulate (see inset figure and main text). Basin subsidence outpaced sedimentation during most of the Early to early Middle Pleistocene, explaining the prevalence of endorheic conditions at that time. However, over the long-term we expect sediment supply to have increased because of the progressive increase in fault-related relief and changing climatic conditions related to the Early to Middle Pleistocene climatic transition. Enhanced sediment supply likely led to more overlap between sedimentation and basin subsidence rates (hashed area) and, in turn, to have allowed some basins to overspill. We illustrate the increase in sedimentation rates by means of an approximate doubling of the estimated maximum sedimentation rates from ca. 1.4 Ma onwards (red arrow), however, note that less than a doubling is sufficient to 'tip the balance'. The red squares show the approximate thickness of the sedimentary fills from the central parts of the four southernmost basins at the time of drainage integration. Because part of the endorheic sediment may have been eroded as a consequence of drainage integration events, these thicknesses may have been larger. Fault segment interaction and linkage may have allowed some faults to accelerate their slip rates up to 1.1 mm yr^{-1} around 0.8 Ma (blue arrow), corresponding to a maximum hangingwall subsidence rate of $\sim 0.7 \text{ mm yr}^{-1}$ when assuming a uplift-to-subsidence ratio of 1:2. Such acceleration may for some basins explain a part return to palustrine and lacustrine conditions during the Middle Pleistocene to Holocene time interval. In the upper right corner we show the approximate hangingwall depths of the SUL and BPZ basins, based on their total throw estimates and assuming an uplift-to-subsidence ratio of 1:2.

From the geological cross sections of the ASB, PSD, LAS and SUL basins (Fig. 4.7), and the available chronology, we estimate long-term average sedimentation rates of the order of $0.10\text{-}0.17 \text{ mm yr}^{-1}$ for the Early to early Middle Pleistocene lacustrine units (Fig. 4.9; see Supplementary Materials B for details). These are minimum estimates, as part of the sediment from the endorheic phase may not have been preserved. As a comparison, similar sedimentation rates are suggested by a 0.54 Ma old tephra layer at 100 m depth in the Fucino basin, which is the only large isolated basin that is left in the central Apennines today (Cavinato et al., 2002; Whittaker et al., 2008). A key observation from Fig. 4.9 is that, during the Early to early Middle Pleistocene, our estimated rates of sedimentation ($0.10\text{-}0.17 \text{ mm yr}^{-1}$) are generally less than the initial rates of hangingwall subsidence ($0.15\text{-}0.23 \text{ mm yr}^{-1}$). Even though there is some uncertainty in these estimated ranges, which can differ between the individual basins, the difference in rates is consistent with basins in the central Apennines being predominantly underfilled and isolated during the Early (to early

Middle) Pleistocene (Fig. 4.9; e.g., D'Agostino et al., 2001; Piacentini and Miccadei, 2014).

- Tipping the balance between basin subsidence and 'local' sediment and water supply -

The small difference between the estimated rates of sedimentation and basin subsidence during the Early Pleistocene suggests that only small increases in sediment supply would have been needed to have tipped the balance towards oversupplied conditions and to allow basins to overflow. This is exactly what we interpret to have occurred for the ASB and BPZ basins that were most likely the first basins to become integrated during the late Early Pleistocene (Figs. 4.6 and 4.8). We expect sediment supply to have increased progressively over time, first because of the long-term increase in fault-related topography (Geurts et al., 2018). Second, there was a shift towards more prolonged and intense glaciations during the Early to Middle Pleistocene climatic transition (ca. 1.4-0.4 Ma; Head and Gibbard, 2015). We know that in the central Apennines, glacial conditions strongly enhanced erosion and runoff, so sediment supply is likely to have increased from approximately 1.4 Ma when glacial periods became longer and more intense (Giraudi and Frezzotti, 1997; Tucker et al., 2011; Whittaker and Boulton, 2012). Weathering rates, erosion rates, and runoff have been inferred to have been 30, 10, and 4 times higher, respectively, under glacial conditions compared to interglacial conditions in the central Apennines (Whittaker et al., 2010; Tucker et al., 2011; Whittaker and Boulton, 2012). We depict a conservative increase of ~ 2 times (corresponding to a sedimentation rate of $\sim 0.3 \text{ mm yr}^{-1}$) to illustrate the increase in sediment supply in Fig. 4.9 from the onset of the Early to Middle Pleistocene climatic transition (ca. 1.4 Ma; Head and Gibbard, 2015). Figure 4.9 shows that such a doubling in sedimentation rates is more than sufficient to significantly enhance the overlap (see hashed area in Fig. 4.9) between the estimated ranges of the rates of sedimentation and hangingwall subsidence. Even though these are first-order estimates, it seems a plausible scenario that an increase in sediment (and water) supply around the Early to Middle Pleistocene climatic transition has allowed sedimentation rates in some basins to have matched or overtaken fault-driven

hangingwall subsidence, causing them to overspill, and the long-term trend of drainage integration to commence.

- The role of enhanced down-system sediment and water transport during drainage integration -

As soon as overspilling of the ASB basin and BPZ basin had led to establishment of a through-going river system connecting these adjacent basins, sediment and water were no longer trapped within these basins and could be transported down-system. This means that for those basins located downstream, the balance towards overfilled conditions could, from now onwards, additionally be tipped by increased sediment and water discharge derived from the significantly larger upstream drainage catchment area. The down-system transport of sediment and water across different basins tends to trigger drainage integration in basins located farther downstream, extending the length of axial river systems in a top-down direction. Meek (this issue) discusses this conceptual model in more detail and provides an overview of supporting field evidence from different river systems in the western United States. In the Aterno River system, this model can for instance explain the sudden increase in sediment supply to the PSD basin around 1.2-1.1 Ma (dark blue deltaic unit in cross sections C and D in Fig. 4.7; Giaccio et al., 2012; Nocentini et al., 2018). This increase in sediment supply led to fast progradation of delta systems, particularly from the northern side of the basin, which coincides with lake disappearance and the onset of incision directly upstream in the ASB basin (Mancini et al., 2012; Nocentini et al., 2017). Drainage integration between the ASB and PSD basins increased the source area of the PSD basin by a factor of ~2.5 to 3.5 times (depending on whether the ASB was already integrated with the BPZ basin before that time), generating a large amount of sediment both by erosion of the larger upland area as well as by fluvial incision into the ASB basin (and perhaps also the BPZ basin) infill. This in turn could lead to enhanced sediment input into the PSD basin and enhanced rates of delta progradation into the large Early Pleistocene lake.

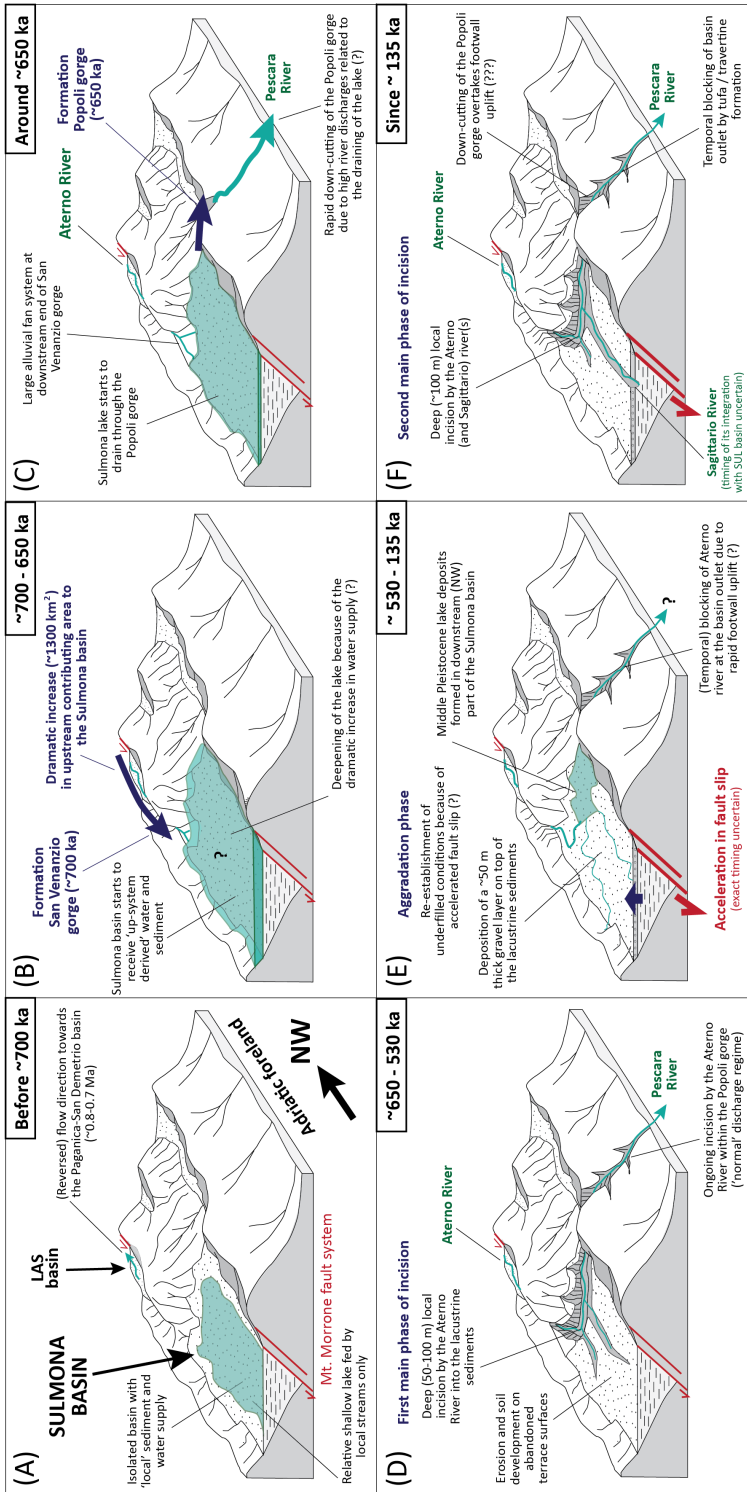


Fig. 4.10. (shown on previous page) Palaeogeographic and tectono-sedimentological reconstruction for the Sulmona basin (looking towards the west). (A) During the Early (to early Middle) Pleistocene, the Sulmona basin was an endorheic basin, fully isolated from the upstream Aterno River system and the Adriatic foreland area. (B) Around 700 ka, overflow of the LAS basin led to the integration of the Aterno River catchment with the Sulmona basin (Gori et al., 2015, 2017). We hypothesise that this drainage integration event produced a dramatic increase in water supply and in turn led to significant deepening of the lake. (C) The emptying of this lake may have had an important role in the formation of the Popoli gorge around 650 ka. (D) Drainage integration across the Popoli gorge produced an upstream propagating wave of (local) fluvial incision between ca. 650 and 530 ka (Zanchetta et al., 2017). (E) Fault slip acceleration can (at least partly) explain the re-establishment of undersupplied conditions between ca. 530 and 135 ka, and the deposition of 50-100 m thick fluvial gravel and lacustrine deposits. (F) Since ca. 135 ka, the Sulmona basin has been mainly affected by fluvial incision, however, during this time interval sedimentation has been additionally affected by tufa or travertine formation in the area of the Popoli gorge (Lombardo et al., 2001).

Another observation that suggests an important role for up-system derived sediment and water is the timing of formation of the Popoli gorge around 0.65 Ma (Giaccio et al., 2013; Zanchetta et al., 2017), which is shortly after the formation of the San Venanzio gorge (ca. 0.7 Ma; Gori et al., 2015, 2017). Drainage integration across the San Venanzio gorge led to a dramatic increase in upstream contributing area to the SUL basin with $\sim 1300 \text{ km}^2$ (size of the Aterno River catchment). Although there is no definitive stratigraphic evidence, we hypothesise that this drainage integration event likely caused significant deepening of the lake in the SUL basin around 0.7-0.65 Ma (Fig. 4.10) caused by the significantly increased water discharge. Considering the position of SUL basin at the very end of the Aterno River system and the timing of drainage integration across the San Venanzio gorge during one of the most extreme glacial periods (MIS16), we might expect this lake to have had at least the volume of the large Early Pleistocene lake in the PSD basin (e.g., Giaccio et al., 2012). We suggest that the emptying of this lake may have had a prominent role in the formation of the Popoli gorge ca. 0.65 Ma (Fig. 4.10) and may have contributed to the basin-wide erosion that is observed into the top of the Early to early Middle Pleistocene lacustrine unit (Miccadei et al., 2002). Because a deep lake in the SUL basin likely existed for a relative short period of time only, there may not have been sufficient time to deposit stratigraphic features such as the large prograding delta systems observed in the PSD basin. In turn, this might explain why enhanced lake levels in the SUL basin around 0.7-0.65 Ma have not been fully discussed before.

- Re-establishment of underfilled conditions during the Middle Pleistocene to Holocene -

Fault segment interaction and linkage are documented to have allowed some faults to accelerate their slip rates at approximately 0.8 Ma (Roberts and Michetti, 2004; Whittaker et al., 2007) and can explain why Holocene throw rate estimates for faults bounding the basins along the Aterno River system reach up to 1.1 mm yr^{-1} . This means that an increase in fault-driven basin subsidence of up to 3 times can be expected to have occurred around 0.8 Ma (Fig. 4.9). Of course, such an increase is not expected for all faults – some faults might have kept a constant slip rate or might even have become inactive. We thus consider a 3 times increase in fault-driven basin subsidence as an upper limit, corresponding to a maximum rate of $\sim 0.7 \text{ mm yr}^{-1}$ assuming a footwall uplift to hangingwall subsidence ratio of 1:2 (Fig. 4.9).

Such an increase in fault slip rate may have led to re-establishment of underfilled lacustrine and palustrine conditions in some of the basins along the Aterno River during the Middle or Late Pleistocene, caused by hangingwall subsidence outpacing sediment supply (Fig. 4.9). However, it is important to note that Fig. 4.9 only shows the ‘local balance’ and does not account for the amount of ‘up-system derived’ sediment originating from the Aterno River catchment upstream. In case of the MTR basin, however, we can exclude significant upstream drainage area enlargement, as it is the most upstream located basin within the Aterno River system. Therefore, for the MTR basin, it is a plausible scenario that acceleration in basin subsidence may have tipped the balance back to undersupplied conditions in the course of the Middle Pleistocene, explaining a renewed phase of lacustrine and palustrine sedimentation (Fig. 4.6). Also, in the case of the next basin downstream, the BPZ basin, the reconstructed strong increase in slip rate of the main basin-bounding fault (Roberts and Michetti, 2004; Galli et al., 2011) may be responsible for the re-appearance of lacustrine conditions during the Middle Pleistocene (Bosi et al., 2004; Piacentini and Miccadei, 2014).

A different scenario, however, may apply to the more downstream basins where the contribution of ‘up-system derived’ sediment was likely much larger, such as the ASB

and SUL basins. In these downstream basins, the re-establishment of underfilled conditions may have required other processes, in addition to accelerated basin subsidence driven by increased rates of faulting. For instance, mass wasting events may have played a role in the case of the ASB basin (e.g., Nocentini et al., 2017; Figs. 4.6 and 4.7) and in the SUL basin, tufa or travertine formation within and directly downstream of the Popoli gorge may also have influenced sedimentation upstream (Lombardo et al., 2001). While we do not exclude the possibility that the re-establishment of underfilled conditions may have coincided with the temporal damming of the Aterno River, we do not have any evidence suggesting prolonged disintegration of the Aterno River system after it was formed.

4.7.2. Variable expression of drainage integration events between basins

A key feature of our data is the variability of expression of each drainage integration event in the sedimentological and geomorphological record of the basin. To some extent, this variability can be explained by the difference in timing at which drainage integration occurred. The longer ago that drainage integration occurred, the more time has been available for the river system to adjust, for instance, in terms of knickpoint propagation. The ASB basin, for example, was likely the first basin that became integrated to its downstream neighbour ca. 1.2-1.1 Ma, resulting in 50-100 m deep dissection of its Early Pleistocene lacustrine deposits. However, around ca. 0.6 Ma, the river had largely adjusted to the fall in local base level and a new phase of fluvial aggradation commenced in response to basin subsidence. The more recently integrated LAS basin (ca. 0.7 Ma), on the other hand, is still adjusting to its fall in local base level.

Another key factor influencing the sedimentological and geomorphological expression of drainage integration is the elevation difference between adjacent basins prior to drainage integration. This determines the magnitude of base level fall experienced by the overspilling basin. For instance, the LAS and SUL basins experienced a large fall in base level (>150 m) that triggered a wave of fluvial incision that deeply dissected the upstream basin forming a pronounced incised valley system (Miccadei et al., 2002;

Gori et al., 2017). Because such a large fall in base level leads to the formation of deep gorges and high terrace morphology, this type of drainage integration event is relatively easily observed and tends to receive most attention (e.g., Geurts et al. 2018). In the PSD basin, on the other hand, fluvial erosion following drainage integration seems to have been limited or absent (Fig. 4.6; Giaccio et al., 2012). Here, aggradation could either continue or rapidly resume because drainage integration occurred simultaneously for the PSD basin and its downstream neighbour, i.e., the LAS basin, which had similar surface elevations, around 0.7 Ma (Fig. 4.8C and D). Consequently there was only one major fall in base level downstream of the LAS basin, which initially did not affect the PSD basin because the wave of erosion had to migrate across the LAS basin first (Fig. 4.8D).

Besides the timing of drainage integration and the magnitude of base level fall there are many more factors that we believe have contributed to the pronounced variability of expression of the different drainage integration events in the different basins. For instance, we also expect the size of the drainage system that is upstream to be of major importance because this determines how much additional sediment and water a basin will receive from upstream. Another factor is the size of the lake or the degree of infilling prior to drainage integration. Overspill of basins with large lakes leads to the abrupt dissection of fine-grained lacustrine sediment (e.g., the ASB and SUL basins) while in basins that are (almost) filled, the fine-grained lacustrine unit is already largely topped by coarse-grained fluvial or deltaic sediment (e.g., the LAS and PSD basins). The data from the Aterno River system would therefore allow for a future comparison of the exact expression of the different drainage integration events given these constraints.

4.7.3. Landscape response times

Our data compilation shows the step-wise development of the Aterno River through a series of drainage integration events (Fig. 4.8). If extension started around 3 Ma, it took ~2.4 Myr in total for this axial river system to develop its course down to the SUL basin, and to form a connection between this most downstream located basin and

the Adriatic coast. Even though the river is now fully integrated, its longitudinal profile suggests that it is far from topographic steady state and is still adjusting to the drainage integration events from which it was formed (Fig. 4.4).

The horizontal distance along the largest convex reach (30-35 km), i.e., the one upstream of the Sulmona Basin (Fig. 4.4B), suggests an average knickpoint migration rate of the order of 43-50 mm yr⁻¹ since drainage integration occurred ca. 0.7 Ma, assuming the upper limit of the knickpoint at an elevation of 575 m is the farthest that the signal of this drainage integration event has propagated. Assuming a unit stream power model and normalising this rate by the square root of drainage area, gives a normalised knickpoint migration rate parameter of 1.4-1.7 · 10⁻⁶ yr⁻¹ following the approach of Whittaker and Boulton (2012; see Supplementary Materials C for details). This value of knickpoint propagation rate overlaps with the upper end of the spectrum of values that have previously been calculated for footwall catchments in the central Apennines that are adjusting to an increase in fault slip rate (0.2-2 · 10⁻⁶ yr⁻¹; Whittaker and Boulton, 2012), but is a factor of 5 to 7 times lower than the value of 1x 10⁻⁵ yr⁻¹ quoted by Loget and Van den Driessche (2009) for knickpoint migration in European catchments during the Mediterranean salinity crisis where the maximum base level change was ~1.5 km. Relatively fast migration rates along the Aterno River relative to footwall catchments in the central Apennines may be explained by the occurrence of relative easily erodible basin sediment compared to the more resistant footwall lithologies and the much larger upstream area of the Aterno River.

Based on our normalised knickpoint propagation parameter of 1.4-1.7 · 10⁻⁶ yr⁻¹, we calculate that it would take at least another 3 Myr for the Aterno long profile convexities to become fully eliminated and for the whole catchment to become geomorphically adjusted to river network integration (see Supplementary Materials C). Importantly, this calculation demonstrates that transient conditions can persist for longer following drainage integration than the time period that needed for the river network to become integrated in the first place. We suggest that this effect is under-recognised in stratigraphic and geomorphological studies in normal fault arrays.

Moreover, local-scale reversals back to endorheic conditions might be able to ‘freeze’ or prolong this process of landscape adjustment to drainage integration considerably.

4.7.4. Drainage network evolution vs. climatic and tectonic forcing

Our data compilation shows that for the greatest part of the total period of extension, i.e., from ca. 3 to ca. 1.2-0.65 Ma, most basins along the Aterno River were isolated from one another. This means that during this time interval, transient climate or tectonic-related signals could not propagate far across the landscape. This has important implications for the interpretation of sedimentary and geomorphological trends observed in the interior of the mountain range. For instance, strong base level fall relative to sea level as a consequence of regional uplift across the central Apennines is generally used for explaining the observation of widespread fluvial incision (e.g., D’Agostino et al., 2001; Bartolini et al., 2003; Giaccio et al., 2012; Chiarini et al., 2014; Gori et al., 2015). However, our dataset shows that the basins associated with the Aterno River were not connected to the coast before ca. 0.65 Ma, and thus fluvial incision in most basins was triggered by a series of local base level falls related to multiple drainage integration events. Because these drainage integration events were initiated at different points in space and time, they need to be considered as individual waves of incision, even though intense incision is a region-wide observed phenomenon at a broad scale.

This study underlines the significant impact of drainage network evolution on transient landscapes and basin stratigraphy. We suggest that the Aterno River system is a strong exemplar of how long-term drainage network integration can be as important as tectonic and climatic forcing in determining the geomorphological and stratigraphic development within extensional settings. Indeed, recent numerical modelling experiments have shown that drainage integration can produce dynamic landscape evolution even if tectonic and climate forcing is held constant (Geurts et al., 2018). Changes in drainage network connectivity can cause marked changes in sediment supply and depositional environments within individual subsiding basins (e.g., Giaccio et al. 2009), for example, causing alternating stages of aggradation and incision, and

the formation of fluvial terrace morphology (e.g., Wegmann and Pazzaglia, 2009). However, an important difference, compared to climate-driven changes in sediment supply and depositional environment, is that changes related to climate should affect different basins across a region more or less similarly and simultaneously, even if they are isolated from one another. In contrast, drainage integration can lead to significant variations between neighbouring basins. Drainage network evolution can also control local base level (e.g., Duffy et al., 2015; Gawthorpe et al., 2018) and can force landscapes to respond to a fall in relative base level by means of upstream propagating waves of erosion (e.g., Whittaker et al., 2007, 2008). However unlike tectonic forcing on individual catchments, the timing and magnitude of the base level fall does not have to correlate directly with the initiation or change in slip rate on a fault. Because of the strong tectonic activity in the central Apennines (and in other normal fault arrays), both at a regional and fault-block scale, stratigraphic and geomorphological observations tend to be mostly approached in terms of tectonic developments (e.g., D'Agostino et al., 2001; Bartolini et al., 2003; Whittaker et al., 2010; Giaccio et al., 2012; Chiarini et al., 2014; Gori et al., 2015) while the contribution of drainage integration along the large axial rivers tends to be overlooked. Our study strongly challenges this assumption.

4.8 Conclusions and implications

This paper synthesises geomorphological and basin stratigraphic data for a large axial river system in the central Apennines – the Aterno River system – in order to reconstruct its development during the time of active extension (since ca. 3 Ma). We use these data to reconstruct drainage network evolution and evaluate how drainage integration controls transient landscape development and basin stratigraphy. Our main conclusions are:

- 1) We observe a long-term trend of drainage integration along the Aterno River, evidenced by a transition from predominantly lacustrine to fluvial sediment in all basin stratigraphic records. All basins were internally drained during the Early (to early

Middle) Pleistocene and have become fluvially integrated with one another and the Adriatic coast between ca. 1.2 and 0.65 Ma. Consecutive drainage integration events produced discrete waves of fluvial incision and terrace formation.

2) Basins with an intermediate location along the Aterno River, around the city of L'Aquila, likely became fluvially integrated with one another first. Drainage integration occurred last between the most downstream located Sulmona basin and the Adriatic foreland. This spatio-temporal pattern of drainage integration is not consistent with a pattern that would be expected from upstream-directed headward erosion from regional base level (e.g., D'Agostino et al., 2001).

3) The spatio-temporal pattern of drainage integration can be explained by an increase in sediment and water supply relative to hangingwall subsidence that caused basins to overflow. On average, rates of sedimentation were lower than rates of hangingwall subsidence during most of the Early to early Middle Pleistocene, explaining why all basins were endorheic at that time. However, because the difference between sedimentation and throw rates was minor, only a small increase in sediment and water supply was sufficient to tip the balance towards oversupplied conditions.

4) The increase in sediment and water supply relative to basin subsidence is explained by the Early to Middle Pleistocene climatic transition and the progressive increase in fault-related relief. As soon as the first basins were integrated, enhanced sediment and water supply additionally resulted from the marked increase in upstream contributing area.

5) Acceleration of slip caused by fault interaction and linkage around 0.8 Ma can explain the re-establishment of palustrine and lacustrine conditions during the Middle Pleistocene to Holocene time interval for some basins along the Aterno River. However, no evidence exists for the full disintegration of the river system during this time.

6) Overall, we conclude that rates of sedimentation and hangingwall subsidence in the central Apennines are well-matched, allowing tipping points between over- and underfilled conditions to be easily reached.

7) Our data show that the step-wise integration of the drainage network took over 2 Myr, and our calculations indicate that the response time for the Aterno River to re-equilibrate following complete drainage integration is at least 3 Myr. Consequently the effects of drainage network evolution can persist in landscapes and sediment routing systems for significant periods following complete integration of the fluvial system.

8) A broader implication of this work is in elevating the importance of the evolution of fluvial connectivity in continental rifts to the level of tectonics and climate in controlling transient landscape evolution and basin stratigraphy. Drainage network evolution in continental rifts is often considered as a simple consequence of tectonics, and in some cases climate change. This study suggests that drainage integration between individual rift basins be looked upon as an important factor in its own right. While drainage network evolution receives a lot of attention in settings where tectonic deformation has largely ceased, its consequences can be easily overlooked in actively extending settings, like the central Apennines, where the combination of active fault development, Quaternary climatic oscillations and regional uplift already produce a spectacular landscape evolution.

4.9 Acknowledgements

AHG acknowledges Bergen University for supporting her PhD research and the Meltzer Research Fund for covering field costs. RLG acknowledges support from VISTA. AHG is grateful to Guillaume Duclaux and Tommaso Piacentini for their help in the field, for sharing ideas and for stimulating discussions from which this work greatly benefitted. We also thank Marco Mancini, Marco Nocentini and Edi Chiarini for sharing ideas and for providing more details about their work. The manuscript benefitted greatly from thorough reviews by two anonymous journal reviewers and from helpful comments by the guest editors Phil Larson and Ronald Dorn.

CHAPTER 5

Paper 3

Dynamic normal fault behaviour and surface uplift in response to mantle lithosphere removal: A numerical modelling study motivated by the central Italian Apennines

To be submitted to *Earth and Planetary Science Letters*.

Geurts, A.H., Huismans, R.S., Cowie, P.A., Wolf, S.G., (in prep.) Dynamic normal fault behaviour and surface uplift in response to mantle lithosphere removal: A numerical modelling study motivated by the central Italian Apennines. To be submitted to *Earth and Planetary Science Letters*.

CHAPTER 6

New insights with focus on the central Apennines

6.1 Introduction

The overall aim of this PhD project was to improve our understanding of the interplay between surface processes, topographic development and normal fault activity in elevated continental rifts affected by mantle-related dynamic surface uplift. The work was motivated by the central Italian Apennines, which was used as a template and as a natural laboratory in respectively the numerical modelling and field-based studies presented in Chapters 3, 4, and 5. In this final part of the thesis, the main findings from the different papers are synthesised and their importance highlighted. In this chapter, Chapter 6, results that are mostly relevant to the central Italian Apennines are discussed. In the following chapter, Chapter 7, the wider implications of this work are discussed and recommendations are provided for future work.

The central Apennines is already known to have experienced a dynamic long-term landscape evolution in response to normal fault interaction and development (Cowie and Roberts, 2001; Roberts and Michetti, 2004; Whittaker et al., 2007, 2008; Faure Walker et al., 2012; Cowie et al., 2012, 2013, 2017; Wedmore et al., 2017), the progressive integration of its drainage network (D'Agostino et al., 2001; Piacentini and Miccadei, 2014), mantle-related surface uplift (D'Agostino et al., 2001; Faure Walker et al., 2012; Faccenna et al., 2014) and Quaternary climatic oscillations (e.g.,

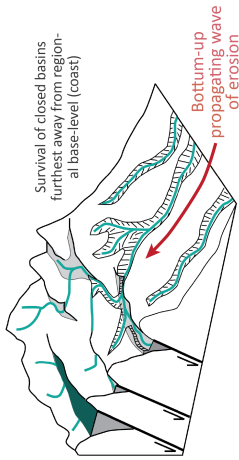
Giraudi and Frezzotti, 1997; Ramrath et al., 1999; Tucker et al., 2011; Whittaker and Boulton, 2012) since approximately 3 Myr. The work presented in this thesis provides a number of new insights into the landscape evolution in the central Apennines, in particular related to the dynamic development of the drainage network (sections 6.2 and 6.3) and mantle-induced fault development and surface uplift (section 6.4).

6.2 Drainage integration: patterns and driving mechanisms

Most fault-bounded basins in the central Apennines were internally drained during the Early- to Middle Pleistocene and became progressively integrated with one another and with the Tyrrhenian and Adriatic coasts over time. The Fucino basin is the only large basin that is still internally drained in the central Apennines today. Because of its position right at the main drainage divide, it seemed generally accepted that drainage integration results from upstream-directed headward erosion starting at the coast (e.g., D'Agostino et al., 2001). Numerical and field data analysis results presented in this thesis, however, demonstrate that drainage integration most likely started in the upstream or middle reaches of today's river systems. This produces a fundamentally different spatial-temporal pattern of drainage integration, both at river system (Chapter 4) and regional scales (Chapter 3). Results from this work demonstrate that the order in which basins in the central Apennines become integrated follows predominantly a top-down (downstream-directed; Fig. 6.1b) rather than bottom-up (upstream-directed; Fig. 6.1a) pattern.

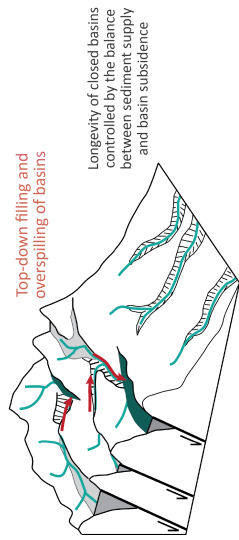
Primarily based on the observed spatial-temporal patterns of drainage integration, we suggest here that a different mechanism controls the progressive integration of extensional basins and the establishment of through-going river systems. Previous work on the Apennines suggests that drainage integration occurred through headward erosion or river piracy, however, results from this thesis suggest that integration occurred because of the overfilling of basins with sediment and water, allowing them to overflow and to establish a fluvial connection with their downstream neighbours (Fig. 6.1a,b; Chapters 3 and 4). While overflow-driven drainage integration is a new

Headward erosion-driven



A

Overspill-driven

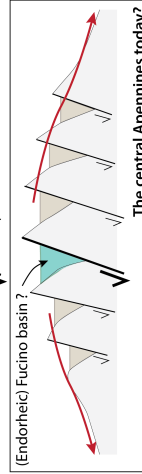
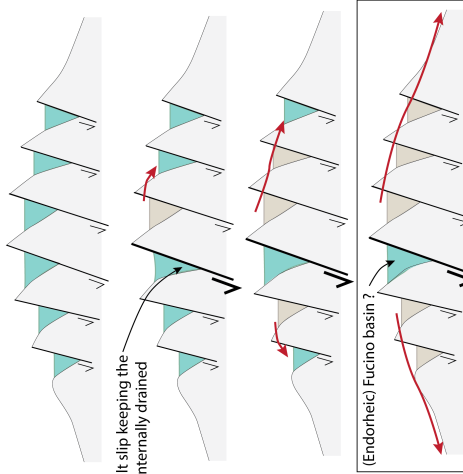
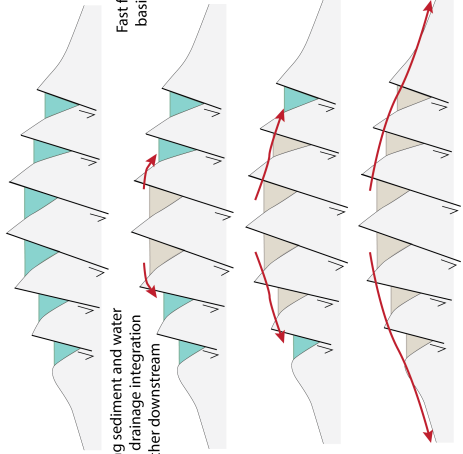
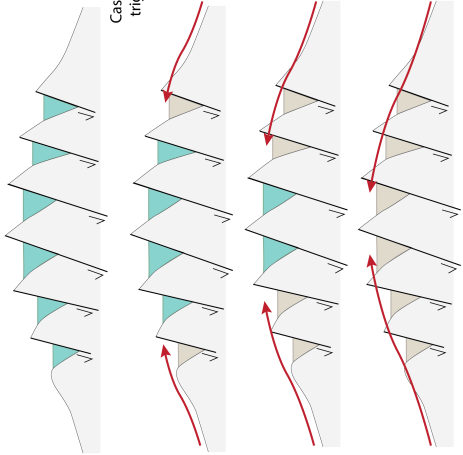
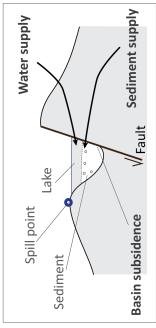


B

('perfect') Top-down

('random') Top-down

Endorheic basin
Exorheic basin



→ Drainage integration (Time)

Fig. 6.1 (shown on previous page) Schematic topographic cross-sections across an elevated continental rift like the central Apennines. Dominant spatio-temporal patterns of drainage integration in case drainage integration is driven by headward erosion (A) or basin overspill mechanisms (B). In case of overspill-driven drainage integration, the overall pattern not necessarily appears as ‘top-down’ at a regional scale but can be more ‘random’ due to active normal faulting or other complexities like inherited pre-rift topography (C).

concept in the central Apennines, it is in line with a large and growing body of field studies from river systems in other extensional areas, in particular from the Basin and Range (e.g., Meek, 1989, 2019; Connell et al., 2005; Menges, 2008; Phillips, 2008; House et al., 2008; Larson et al., 2014; Repasch et al., 2017; Hilgendorf et al., 2020).

At first glance, a top-down directed integration pattern seems inconsistent with the ‘survived’ endorheic Fucino basin located at the main drainage divide. Its internal drainage, however, can be explained by the very high rate of slip on its main controlling fault system ($>2 \text{ mm yr}^{-1}$; Roberts and Michetti, 2004; Whittaker et al., 2008), resulting in fast basin subsidence that outpaces its combined sediment and water supply (Fig. 6.1c). Moreover, considering the generally very similar rates of sedimentation and basin subsidence in this region (Chapter 4), the relative small dimensions of the Fucino source area compared to the size of its depocentre make this a very plausible scenario (Fig. 6.2a). However, an important shortcoming in our knowledge is whether the Fucino basin has been endorheic during its full history (as generally hypothesised), or whether it has been externally drained during the Early Pleistocene before becoming endorheic (Cavinato et al., 2002; Whittaker et al., 2008).

Irrespective of its exact history, the closed conditions of the Fucino basin today illustrate that drainage integration by overspill does not necessarily produce a ‘perfect’ top-down pattern of drainage integration at river-system scale, i.e. from the main drainage divide all the way downslope to the Tyrrhenian and Adriatic coastal areas (as illustrated in Fig. 6.1b). In particular, in the central Apennines where normal faulting is highly active and variable (e.g., Cowie et al., 2017; Chapter 5), and also where other complexities such as inherited topography are prominent, the overspill pattern is likely more random. This is revealed both by the Aterno River dataset (Chapter 4) as well as by the regional-scale landscape evolution model experiments (Chapter 3). However,

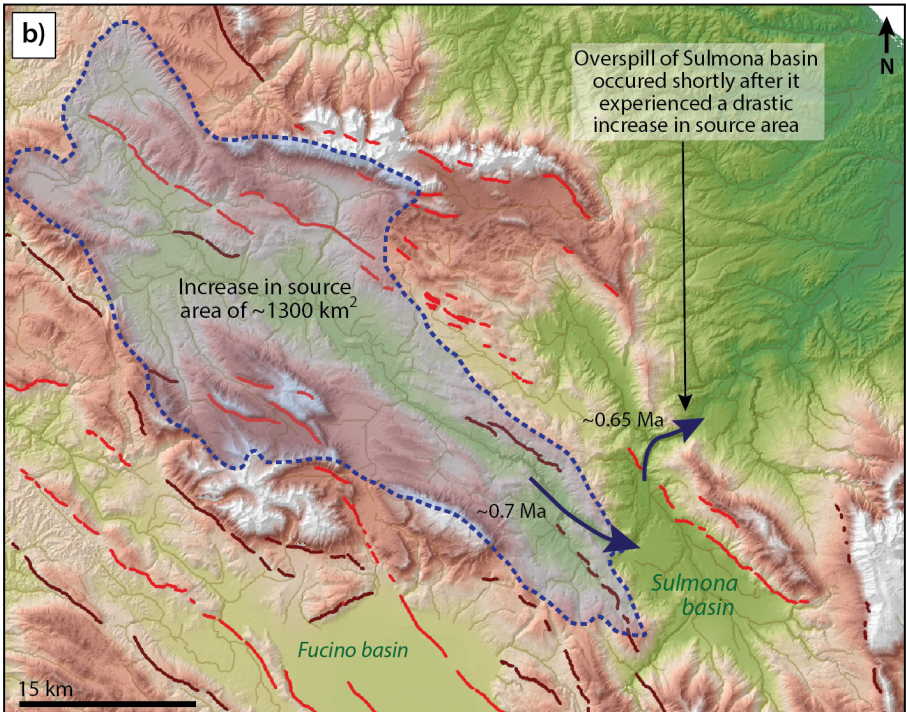
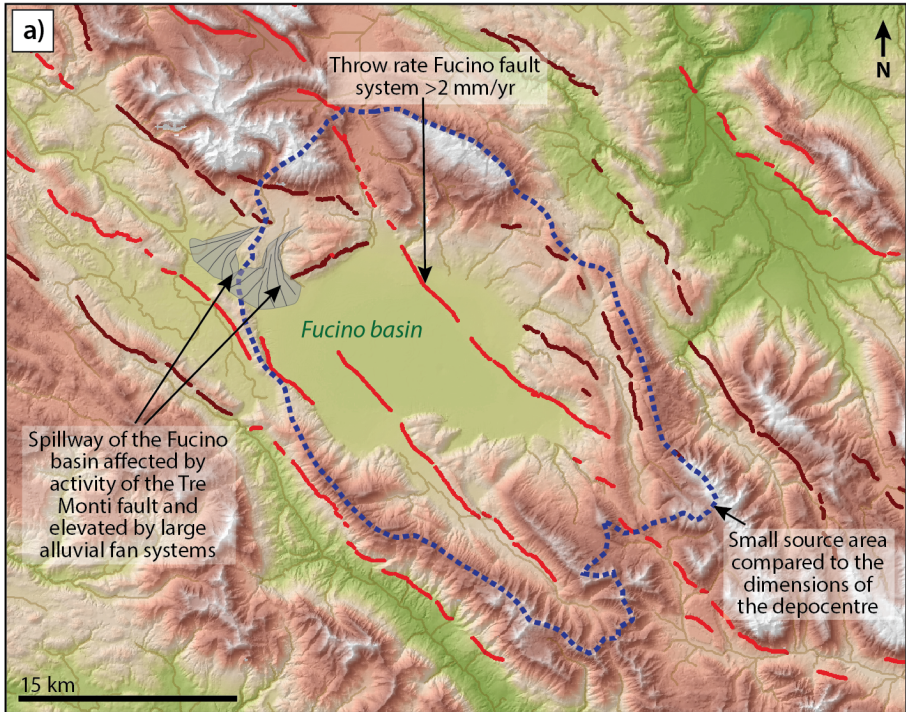


Fig. 6.2 (prev. page) *Topographic maps (10 m DEM Tarquini et al., 2007) of the areas around the Fucino basin (A) and Sulmona basin (B). The blue dotted line in (A) shows the dimensions of the source area of the Fucino basin. The blue dotted line in (B) shows the catchment of the Aterno river that started draining into the Sulmona basin around 0.7 Myr. Red lines show the active normal faults (light red for faults with increased slip rates (around 0.8 Myr); principally after Roberts and Michetti, 2004).*

even drainage integration patterns of more complex continental rifts are expected to reveal top-down integration patterns at a local scale, e.g., for two or three adjacent basins. A good example from the Aterno river system is the Sulmona basin that overspilled shortly after it experienced a massive increase in source area (Fig. 6.2b).

Even though the overspill model presented in this thesis is based on field data from the Aterno river system, it is expected to apply to the central Apennines as a whole. Whereas the Aterno River is the largest river draining the Adriatic domain of the intramontane area, the Salto-Nera-Velino river system is the largest river draining the Tyrrhenian domain (see Fig. 2.6a,b in Chapter 2). For the most downstream located basin along this Tyrrhenian-draining river system, i.e. the Terni basin, continental deposits preserved at high elevation in the area of its former spill-point demonstrate that it became overfilled with sediment during the early Pleistocene and spilled over towards the Tyrrhenian coastal area (D'Agostino et al., 2001; Figs. 2.2 and 2.6a,b in Chapter 2). In other words, even though a complete drainage integration reconstruction for this large Tyrrhenian river system is currently lacking, overspill processes are expected to be the dominant mechanism driving drainage integration in the central Apennines in general.

6.3 Implications of overspill-driven drainage integration

The conceptual model of overspill-driven drainage integration provides a fundamentally different view on various aspects of long-term landscape evolution in the central Apennines. It is first of all considered of key importance for the interpretation of stratigraphic records from the different fault-bounded intramontane basins. While drainage integration is a well-known phenomenon in the central Apennines, its impact on basin stratigraphy has been completely neglected. So far, stratigraphic trends have been only explained in terms of fault activity (e.g., Cavinato,

1993; Cavinato and Miccadei, 2000), changing climatic conditions (e.g., Cavinato and Miccadei, 2000; Miccadei et al., 2002; Giaccio et al., 2012), or regional uplift-induced fluvial incision (e.g., D'Agostino et al., 2001). However, Chapter 4 in this thesis demonstrates that it is the process of drainage integration itself that acts as a first-order control on the main stratigraphic units within each basin along the Aterno River.

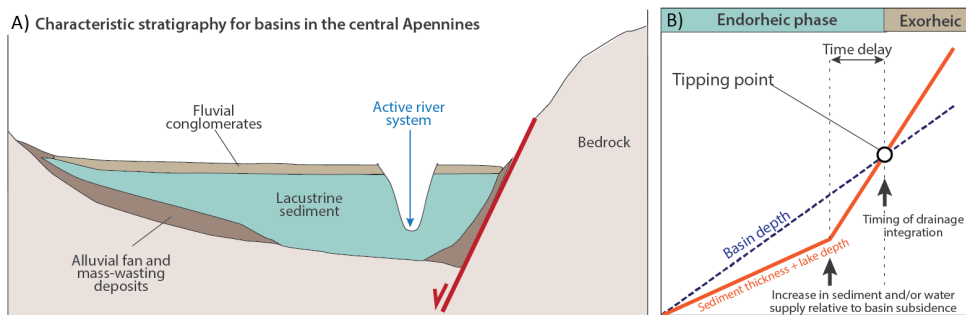


Fig. 6.3 A) Schematic cross-section showing the characteristic stratigraphy of basins in the central Apennines. The major transition from lacustrine sedimentation to fluvial sedimentation or incision is explained by basin overspill. B) Endorheic conditions predominated during early stages of extension because rates of basin subsidence generally outpaced rates of sediment and water supply. An increase in combined sediment and water supply relative to basin subsidence allowed basins to spillover during later stages of extension (Chapter 4).

To first order, most basins in the central Apennines have a similar stratigraphic build-up with lacustrine deposits making up the lower (mostly Early Pleistocene) and thickest portion of the stratigraphy, which are topped by a relative thin layer of fluvial conglomerates (usually late Early to Middle Pleistocene in age). In general, the upper part of the stratigraphy is deeply dissected by the modern-day, basin traversing river systems (Fig. 6.3). For each individual basin, this stratigraphic build-up reflects a relative long period with endorheic conditions and mainly lacustrine sediment deposition, followed by a time interval of external drainage, fluvial sedimentation, reworking or erosion, and subsequently a period of deep fluvial incision (Chapter 4). This characteristic stratigraphy reveals a major transition from primarily deposition towards primarily sediment reworking or erosion that is associated with the progressive basin infill and integration of the drainage network. The only basin that is different to the characteristic stratigraphic record outlined here is the Fucino basin as it

has lacustrine sediments in its youngest stratigraphy and lacks major fluvial strata and deep incision (Cavinato et al., 2002; Whittaker et al., 2008).

The characteristic stratigraphic build-up of basins in the central Apennines as illustrated in figure 6.3 clearly demonstrates the most important impact of drainage integration, namely the transition from the complete storage of sediment and ponding of water towards a situation in which sediment and water is mainly exported out of the basins. This transition in turn strongly impacts on the prevailing depositional environments. However, the dataset from the Aterno River also shows that, on top of this characteristic basin stratigraphy, there is a lot of variability between the different basins (Chapter 4).

The stratigraphic variability between the basins is likely a function of many factors. However, three aspects are considered of key importance for basins in the central Apennines, first of all, the spatio-temporal pattern of drainage integration. When a basin becomes integrated with basins located further up- and downstream, it experiences a drop in base level and an increase in sediment and water supply. However, how drastic these changes are (e.g., the increase in source area or the magnitude of the base level fall) and whether the base level fall is occurring before or after sediment and water supply increase depend, to a large extent, on the relative order in which basins become integrated. The importance of the spatio-temporal pattern of drainage integration can be nicely illustrated with the Paganica-San Demetrio (PSD) basin that is located along the middle reaches of the Aterno River (Fig. 6.4a). In strong contrast to all the other basins along the Aterno River, this basin accumulated thick Gilbert delta deposits because it acted as a regional depocentre for a significant amount of time and received high sediment and water supply from a large (already mostly integrated) hinterland. If this basin would have been integrated with other basins further downstream earlier, there would not have been any trapping of sediment by the deep lake in the Paganica-San Demetrio basin and the thick delta deposits would not have been formed.

A second key factor controlling stratigraphic variability between basins in the central Apennines is the relative position of a basin along the (ultimately integrated) river system (Chapter 4). The further upstream a basin is located, the smaller the increase in source area it experiences when it becomes integrated with other basins further upstream. Therefore, the stratigraphy of far upstream-located basins (e.g., the Montereale (MTR) and Barete-Pizzoli (BPZ) basins in Fig. 6.4a) is not affected by major increases in sediment supply or abrupt deepening of lakes associated with drainage integration. The opposite applies to far downstream-located basins (e.g., the Sulmona (SUL) basin in Fig. 6.4a), for which drastic, drainage integration-induced increases in sediment and water supply are expected (Chapter 4).

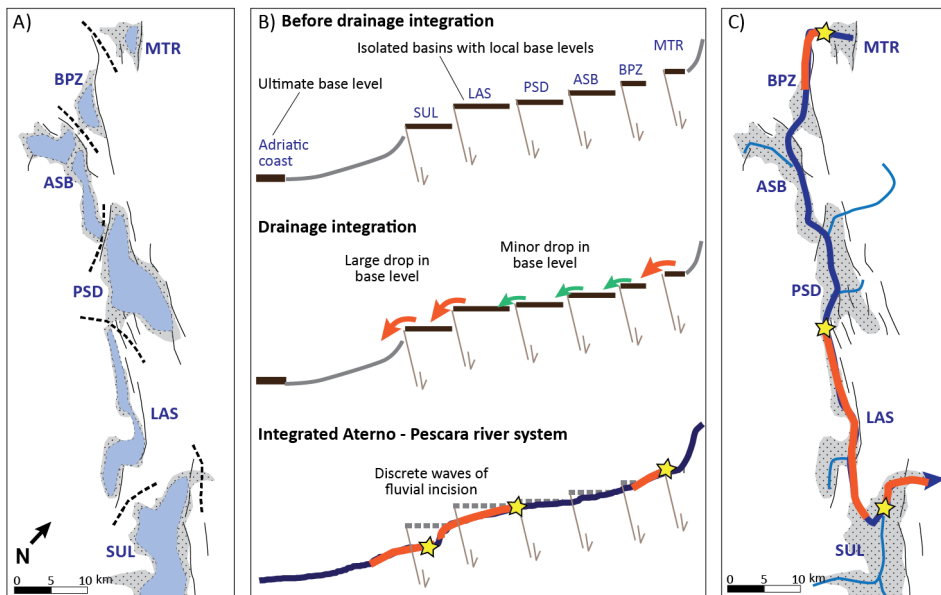


Fig. 6.4 Drainage integration along the Aterno-Pescara river system (see Fig. 8 in Chapter 4 for details). A, C) Maps of the Aterno river system, showing the situation before (A) and after (C) drainage integration. B) Schematic diagram showing the integration of the different basins along the longitudinal profile of the Aterno River. Initially, all basins were endorheic and isolated from one another, all having their own local base level (top profile). Over time the different basins spilled over and established fluvial connections with one another. Depending on the elevation difference between pairs of adjacent basins, these integration events initiated waves of deep fluvial incision (orange arrows) or minor incision (green arrows; middle profile). Only the integration events associated with large drops in base level are reflected by the Aterno longprofile as large knickzones (bottom profile). MTR = Montereale b., BPZ = Barete-Pizzoli b., ASB = l'Aquila-Scoppito-Bazzano b., PSD = Paganica-San Demetrio b., LAS = Lower Aterno-Subequana b., SUL = Sulmona basin.

A third factor that explains much of the inter-basin variability in stratigraphy is the elevation difference between adjacent basins prior to integration. A large elevation difference results in a large fall in local base level and deep fluvial incision in the upstream basin associated with integration. The downstream basin on the other hand experiences a marked increase in sediment supply because of the upstream propagating wave of deep fluvial incision. By contrast, a small elevation difference between adjacent basin floors prior to drainage integration results in a relatively small drop in base level and, in turn, more limited fluvial incision. The variability in elevation difference between basins can for instance explain why only three (instead of six) major knickzones are recognised along the Aterno river system (Fig. 6.4b; Chapter 4).

This thesis also demonstrates that overspill-driven drainage integration is important for understanding the topographic evolution of the central Apennines. First of all basin overspill can explain large convex reaches along the longitudinal river profiles that result from discrete waves of fluvial incision associated with individual drainage integration events (Fig. 6.4b,c; Chapter 4). Moreover, because drainage integration commenced in the middle or upper reaches of today's through-going river systems, the interior of the mountain range developed in isolation from the foreland area for most of the Quaternary. In combination with long-term regional uplift this allowed for the development of a large topographic disequilibrium between the mountain interior and the coastal areas (Chapter 3; see also section 7.2.3). This explains why the upper limits of most basin fills in the central Apennines are perched far above sea level, but have become deeply dissected by river systems since connections have been established with the foreland areas (Fig. 6.4b).

6.4 Mantle-related surface uplift and fault activity

Many studies suggested the potential relationship between mantle dynamics, regional uplift and extensional faulting in the central Apennines because of the correlation between topography, post-glacial (15 ± 3 ka) upper crustal strain rates, finite (2.5-3

Ma) upper crustal strain, free air gravity anomalies, advective heat flux, and low P-wave velocities in the uppermost mantle (e.g., D'Agostino and McKenzie, 1999; D'Agostino et al., 2001, 2014; Di Stefano et al., 2009; Faure Walker et al., 2012; Chiarabba and Chiodini, 2013; Faccenna et al., 2014). Chapter 5 of this thesis, however, is first in exploring the dynamic interaction between these processes for the setting of the central Apennines through numerical experiments.

The results from Chapter 5 demonstrate that mantle lithosphere removal can, first of all, explain the correlation between high topography, regional surface uplift, extensional faulting and high advective heat flux as observed in the central Apennines (e.g., Faure Walker et al., 2012; Chiodini et al., 2013). However, mantle lithosphere removal can also explain the observed low anomaly in gravimetric data as dense mantle lithosphere is replaced by light sub-lithospheric mantle (D'Agostino et al., 2001). Moreover, the model can explain the pronounced negative velocity anomaly ($\Delta V_p = -8\%$) in the upper mantle, as P-wave velocities get reduced in hot and buoyant sub-lithospheric mantle (Di Stefano et al., 2009).

Elevated topography in the central Apennines has also been explained by mantle convection exerting upwards stresses at the base of the lithosphere (Faccenna et al., 2014). However, a notable characteristic of so-called 'dynamic topography' is its low amplitude (less than a few hundred metres) and long wavelength of at least several hundred but commonly more than thousand kilometres (e.g., Braun, 2010; Molnar et al., 2015). By contrast the wavelength of regional topography in the central Apennines is only ~ 100 km. Moreover, mantle convection does not provide a mechanism for the localisation of extensional strain within this narrow zone. The results from Chapter 5 in this thesis suggest that it is more likely that mantle lithosphere removal rather than mantle convection acts as a first-order control on the localisation of surface uplift and extension in this region.

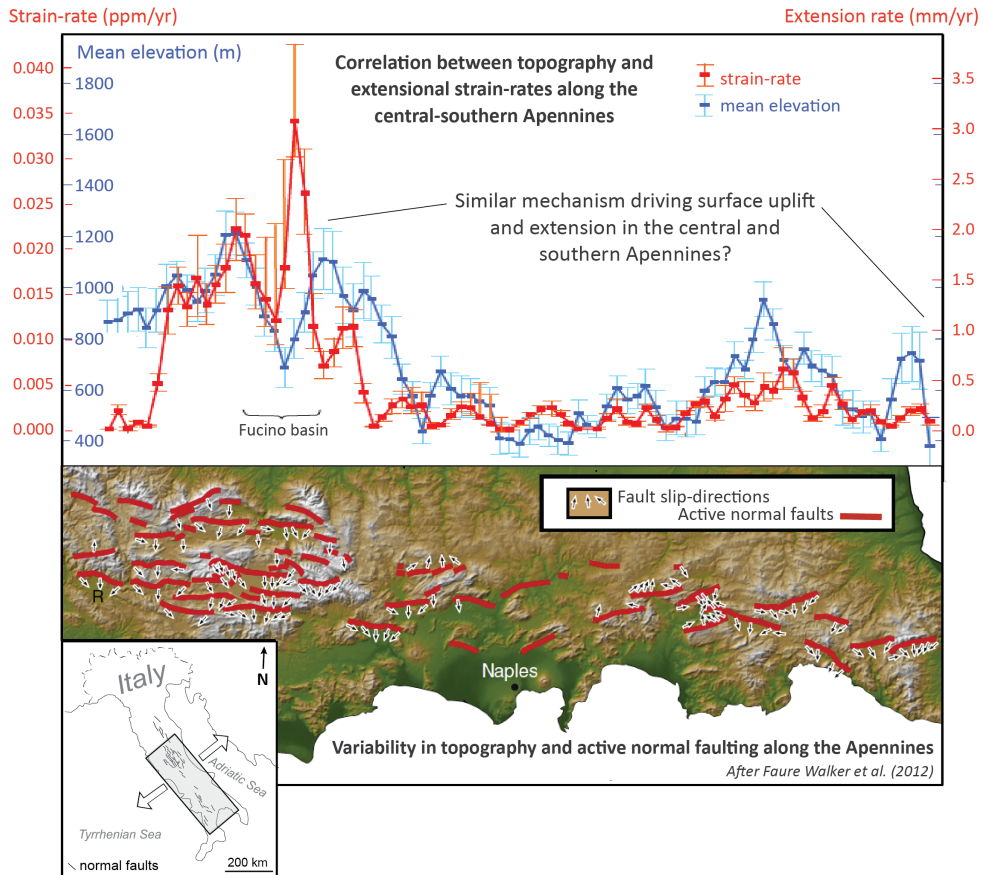


Fig. 6.5 Top panel: Spatial variation in strain-rate, extension rate and mean elevation along the strike of the Apennines. Strain-rates and extension rates are derived from post 12-18 ka fault scarps (shown in bottom panel; after Faure Walker et al., 2012).

However, a question that is not addressed in Chapter 5 is what the larger-scale context is of mantle lithosphere removal underneath the central Apennines? For instance, fault extensional strain rates also correlate with elevated topography and surface uplift in the southern part of the Apennines, though across a much narrower zone and with lower uplift and strain rates (Fig. 6.5; Faure Walker et al., 2012). Whereas the P-wave velocity anomaly underneath the central Apennines is most pronounced, velocities in the upper mantle are indeed reduced along most of the Apennines (Fig. 6.6; Di Stefano et al., 2009). This suggests that thinning of mantle lithosphere is a regional phenomenon associated with the Apennines subduction setting. Interruptions along the

Adriatic slab, for instance slab tears and detachments, may have resulted in varying degrees of lithospheric thinning and weakening, and in turn along-strike variations in topography and extensional faulting (e.g., Rosenbaum et al., 2008; Faure Walker et al., 2012; Chiodini et al., 2013).

Removal of mantle lithosphere a regional phenomenon?

Negative P-wave velocity anomaly most pronounced in the areas of the central and southern Apennines slab windows (see also Fig. 6.5)

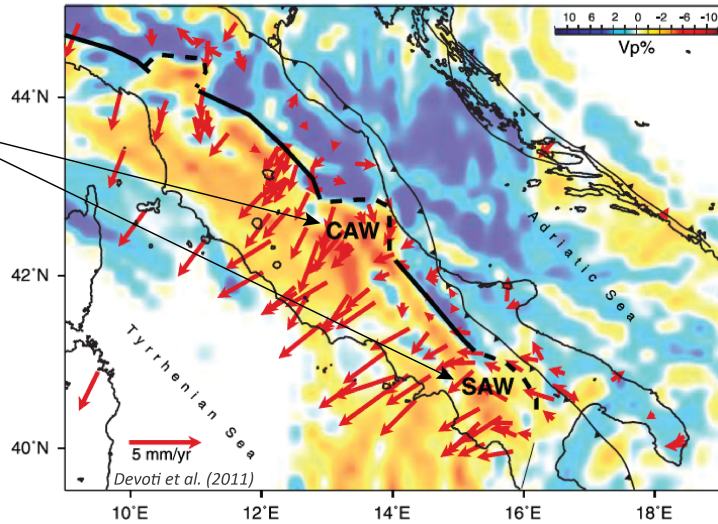


Fig. 6.6 P-wave velocities in the upper most mantle (52 km depth) computed from regional seismicity (Di Stefano et al., 2009). Red to yellow colors are negative anomalies, dark to light blue colors are positive anomalies. The red arrows plotted on top are horizontal GPS velocities (Devoti et al., 2011). This figure shows that P-wave velocities are low everywhere beneath the Apennines, but are most negative in the central and southern Apennines where so-called 'slab-windows' have been inferred (Devoti et al., 2011).

CHAPTER 7

Wider implications and future perspectives

This chapter discusses the wider implications of the main findings presented in this thesis (sections 7.1-7.3), and provides recommendations for future work (section 7.4).

7.1 Towards a process-based understanding of drainage integration in active continental rifts

7.1.1 Source-to-sink problem

Novel aspects of Chapters 3 and 4 in this thesis are the role of the drainage network itself in producing a dynamic river network evolution. Whereas conceptual models of tectono-stratigraphic evolution of rifts exist at the scale of individual fault systems or basins (e.g., Gawthorpe and Leeder, 2000; Densmore et al., 2003; Cowie et al., 2006; Whittaker et al., 2010), this study demonstrates important aspects of the regional-scale tectonic-stratigraphic development of continental rifts systems characterised by multiple active parallel fault systems and their associated basins (Fig. 7.1). This regional-scale source-to-sink perspective, or alternatively multiple-source-to-multiple-sink perspective, is considered of key importance as the histories of infilling and incision of the different basins interact with one another (Fig. 7.1; Chapters 3 and 4).

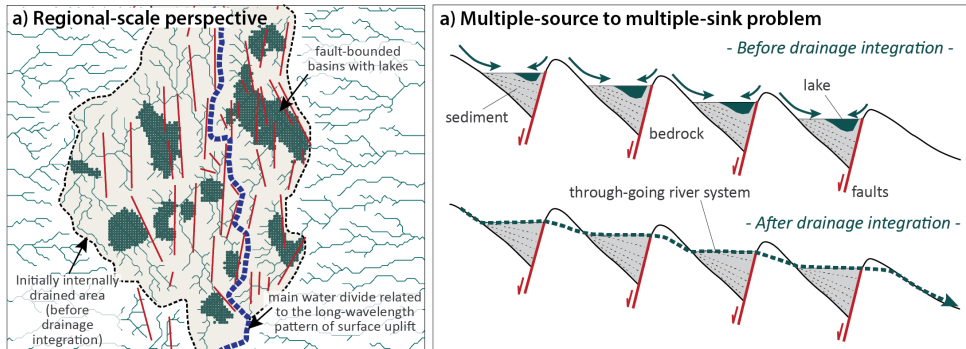


Fig. 7.1 Schematic illustration of a regional-scale (a) and multiple-source-to-multiple-sink (b) perspective that is considered of great importance for understanding long-term drainage integration in continental rifts.

7.1.2 Fluvial versus structural driving-mechanisms for drainage integration

Chapters 3 and 4 of this thesis discussed whether headward erosion or basin overspill drove drainage integration in the central Apennines. This discussion contributes to the wider debate on the relative importance of these two mechanisms that both strongly relate to developments within the fluvial realm (recent review provided by Hilgendorf et al., 2020).

In the wider tectonic-stratigraphic rift community, however, drainage integration is often also associated with the structural evolution of continental rifts. During the initial stages of fault growth, prior to fault interaction and linkage, transverse folds produce elevated topography at the boundaries between isolated fault segments, which act as along-strike topographic barriers for the drainage system. Fault linkage, however, causes these elevated areas to subside, allowing depocentres to merge and axial river systems to form (Gawthorpe and Leeder, 2000). The results from this thesis, however, suggest that fault linkage played no significant role in the establishment of through-going river systems in the central Apennines. First of all, because many basins in the central Apennines became already integrated with one another before fault linkage is estimated to have occurred (~0.8 Ma; Roberts and Michetti, 2004; Whittaker et al., 2008; Chapter 4). Secondly, many fluvial connections were clearly cut directly into bedrock spillways rather than into a depositional surface on-lapping these topographic

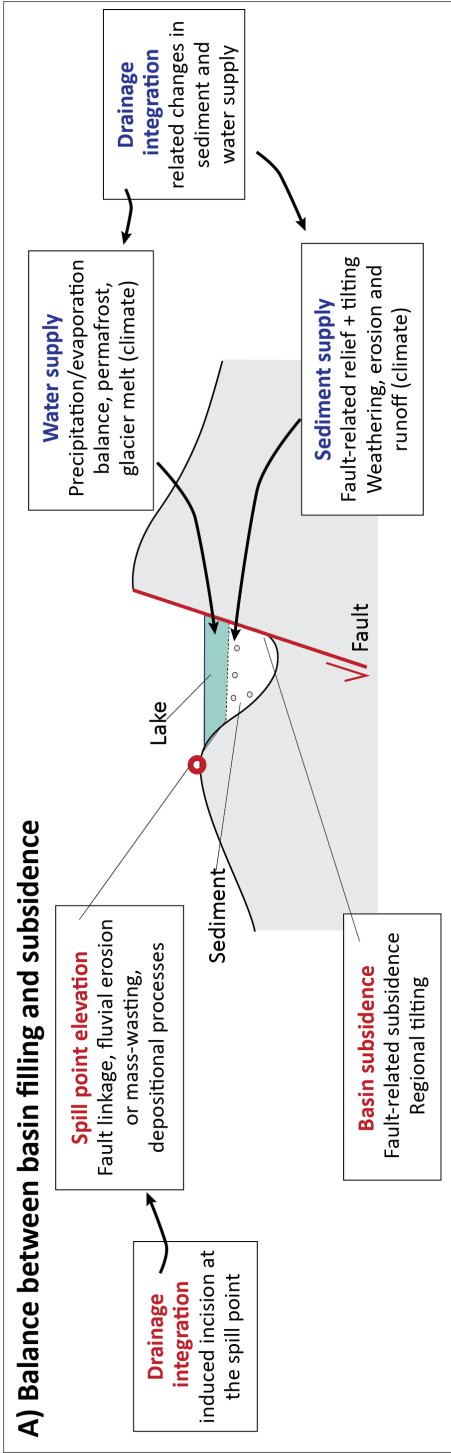
barriers. Thirdly, the surface process modelling study presented in Chapter 3 reproduced the trend of regional drainage integration also without effects from fault interaction and linkage.

Therefore, this study of the central Apennines strongly suggests that drainage integration must be considered as a mechanism of equal importance to the structural evolution of rifts. Although fault linkage favours drainage integration, these developments are not necessarily related and occurring simultaneously. In the central Apennines fault linkage mainly occurred after many basins already got fluviially integrated, whereas many through-going river systems in the Basin and Range became established long after extension ceased (e.g., Meek, 1989; Connell et al., 2005; House et al., 2008; Phillips, 2008; Larson, et al., 2014; Reheis et al., 2014).

7.1.3 Tipping the balance

One of the key findings of Chapters 3 and 4 in this thesis is the importance of the balance between the rates of sediment and water supply versus the rate of basin subsidence in controlling drainage network evolution in continental rifts (Fig. 7.2a). If basin subsidence outpaces sediment and water supply, basins become progressively more underfilled and are most likely endorheic. If sediment and water supply outpace accommodation creation, underfilled basins become progressively filled until water or sediment reaches the spillpoint allowing the basin to spill over. In the case of a continental fault-bounded basin, the accommodation space comprises its total volume up to the elevation of its spill point, irrespective of the height of the lake level. This is different from the way accommodation space is defined for the (open system of the) offshore, namely as the space that is available for sediment to accumulate below base/sea level (e.g., Allen and Allen, 2013). From the importance of the balance between basin subsidence and infilling it follows that drainage integration is a function of all factors affecting either sediment and water supply or the rate of accommodation creation, but also of changes in the elevation of the basin's spillpoint (Fig. 7.2a).

A) Balance between basin filling and subsidence



B) Tipping the balance

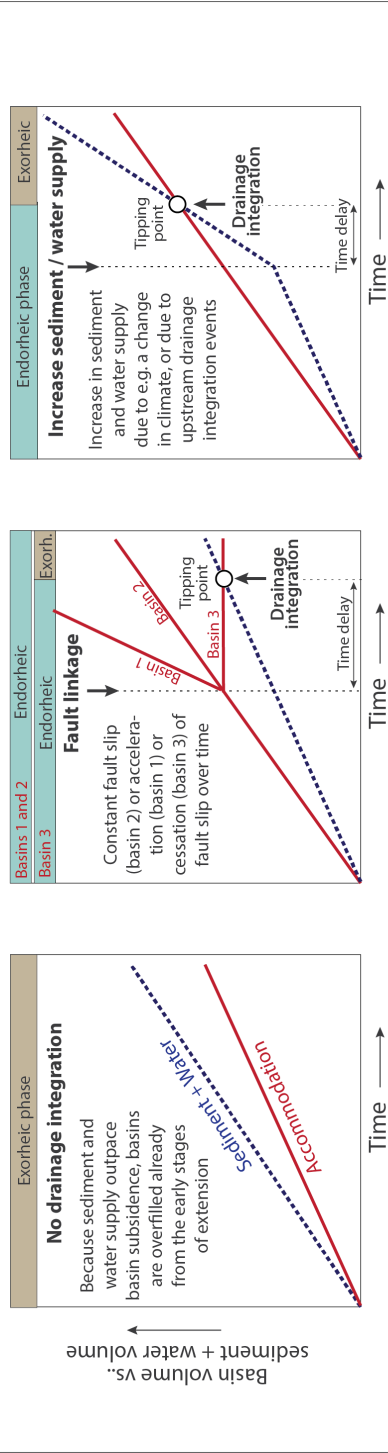


Fig. 7.2 (shown on previous page) A) Overview of the most important factors controlling the balance between basin filling and subsidence. B) Relative changes in the rates of basin filling and basin subsidence can lead to changes in the connectivity of the drainage network. These three diagrams show a few examples of potential scenarios, of different relative trajectories of the rates of basin filling (blue) and subsidence (red).

This concept of tipping the balance between underfilled and overfilled conditions is suspected to be relevant for understanding the long-term evolution of river networks in continental rifts around the globe (Fig. 7.2b). In the Basin and Range province for instance, arid climatic conditions strongly limit sediment and water supply, what may explain why the integration of many river systems could only occur after the cessation of extension (e.g., Connell et al., 2005; House et al., 2008) or required intense glacial periods for developing deep pluvial lakes that could overflow (e.g., Meek, 2019). This thesis suggests that in the central Apennines, drainage integration might have started because of the Early-Middle Pleistocene climatic transition (Chapter 4), or the more gradual long-term increase in fault-related relief (Chapter 3), that increased erosion rates and in turn the sediment supply to basins.

Returning back to truly endorheic conditions is not common in the central Apennines (Chapter 4). In order to make this happen, rapid depositional process (at least a couple of mm/yr) in the basin's spillway seems required in addition to fault slip rate acceleration. This is because in case of the reversed trend, basin subsidence not only has to outpace sediment and water supply, but also incision at the spill point imposed by the through-going river system (Fig. 7.2a). In case the Fucino basin has been temporarily externally drained and reversed towards endorheic conditions (Whittaker et al., 2008), its spillpoint may have been elevated quite rapidly because of alluvial fan progradation or activity of the NE-SW-striking Tre Monti fault (Fig. 6.2a). Other good candidate processes for blocking spillways in the Apennines are tufa (or travertine) formation that can form at a rate of several centimetres each year (e.g., downstream of the Rieti and Sulmona basins; Lombardo et al., 2001) and landslide activity (e.g., near L'Aquila). In other areas as for instance the Rio Grande Rift, damming of axial rivers occurred because of volcanic activity (e.g., Repasch et al., 2017).

7.2 The impact of drainage integration on sediment dispersal, basin stratigraphy, and transient landscape evolution

7.2.1 *Basins as ‘active’ components of landscape evolution*

Previous work has mainly focussed on the impact of fault array development on drainage network and basin stratigraphic development in continental rifts (e.g., Gawthorpe and Leeder, 2000; Densmore et al., 2003, 2004; Cowie et al., 2006; Gawthorpe et al., 2018). The results of this thesis, however, demonstrate that the evolution of individual basins and their degree of fluvial connectivity, in turn, strongly affect the long-term landscape evolution of continental rifts. Instead of ‘passively’ waiting to become captured by a headward eroding river system (e.g., D’Agostino et al., 2001; Dickinson, 2015), basins play an ‘active’ role in controlling water and sediment dispersal across the rift, the timing of spill-over events, and therefore influence the overall pace and pattern of rift-wide drainage integration. Even though the balance between basin subsidence and infilling is affected by larger-scale and longer-term developments (e.g., fault evolution, climate) or inherited conditions (e.g., bedrock lithology, inherited topography and structures), the results in this thesis highlight the importance of basins as active components in, rather than simply products of, landscape evolution in continental rifts (Chapters 3 and 4).

7.2.2 *Sediment dispersal and basin stratigraphy*

Closed endorheic basins trap all the water and sediment from their direct surrounding uplands, and potentially also from further upstream-located basins that have a drainage connection with them. As soon as a fluvial connection is established with a downstream located basin, sediment and water are no longer trapped and can be transported further downstream. Therefore the overall impact of rift-wide drainage integration is the step-wise transition from primarily local (short-distance) sediment transport and storage into an interconnected drainage system of (long-distance) sediment dispersal (Fig. 7.1b; e.g., Gawthorpe and Leeder, 2000; Meek, 2019).

Drainage integration generally also causes a transition from primarily deposition to fluvial reworking and incision (Chapters 3 and 4).

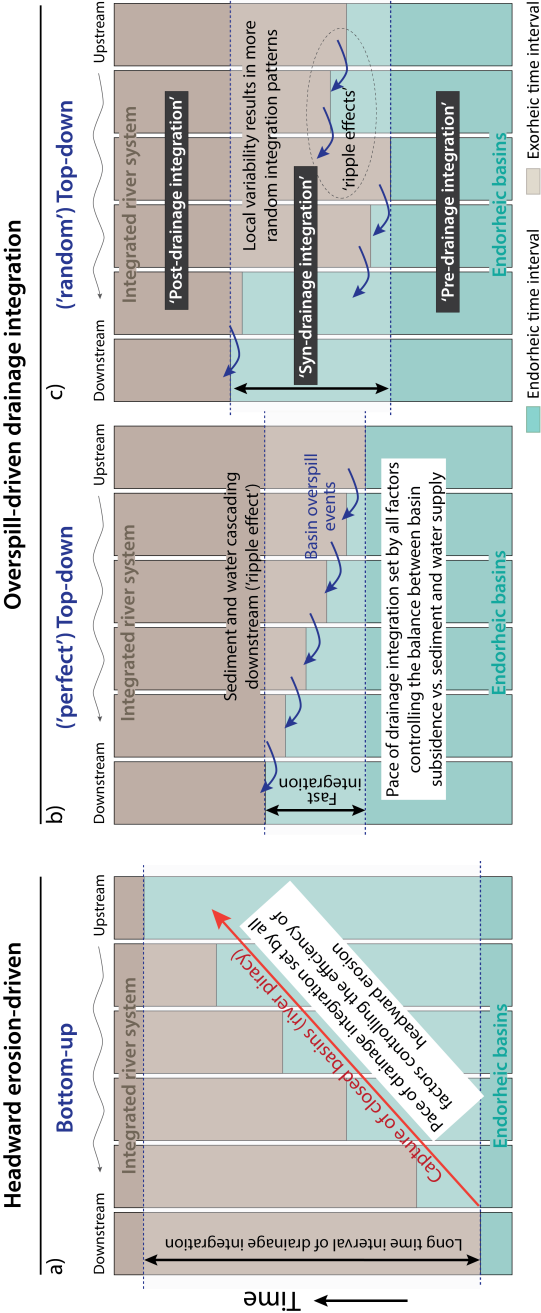


Fig. 7.3 (shown on previous page) Schematic stratigraphic columns of six adjacent fault-bounded basins that become progressively integrated with one another over time, either through headward erosion (a) or basin overflow processes (b, c). Important to note is that the stratigraphic columns are highly simplistic, and only distinguish between phases of internal (mostly lacustrine sedimentation) and external drainage (either fluvial sedimentation or deep incision). Instead of a 'perfect' top-down pattern (b), more variable patterns of drainage integration (c) can result from spatial and temporal variability in factors like (inherited) topography, (inherited) structures, drainage network, basin source area dimensions, fault activity, lithology and climate.

Overspill-driven drainage integration has been recognised for river systems in the Basin and Range Province where it tends to create clear top-down patterns of drainage integration along the full length of river systems. For instance along the Rio Grande (e.g., Repasch et al., 2017), Mojave River (e.g., Meek, 2019), and lower Colorado River (House et al., 2008), drainage integration started near their headwaters and subsequently proceeded in a downstream direction. An important finding of this thesis is, however, that the overflow of normal fault-bounded basins not necessarily produces a river system-scale top-down integration pattern *sensu stricto* (Fig. 7.3b). As demonstrated by the Aterno river dataset (Chapter 4), overflow-driven integration patterns of natural river systems can be expected to be much more complicated, in particular for tectonically active continental rifts or those with inherited complexities from pre-extensional times. In such rift systems, drainage integration can theoretically start in any basin along a river system, depending on which basin is first in tipping its balance from under- to overflowed conditions (Fig. 7.3c).

However, top-down integration patterns can still be considered characteristic for overflow-controlled drainage integration because the first overflowed basin triggers a 'ripple effect' as the release of sediment and water from each integrated basin favours the overflowing of its downstream neighbour (e.g., Meek, 2019). Therefore, even for large river systems in active continental rifts, top-down patterns of drainage integration are expected to be present across relative short distances, for instance for series of two or three neighbouring basins only. The best example from the central Apennines for this 'ripple effect' is the overflow of the Sulmona basin (~0.65 Myr) shortly after the overflow of the integrated Aterno river system across the San Venanzio gorge (~0.7 Myr; Fig. 6.2b). In other words, whereas the overall spatio-

temporal pattern of drainage integration is not necessarily ‘top-down’, top-down patterns are likely revealed across shorter distances (compare Figs. 7.3b and c).

Because of the ripple effect, overspill-driven drainage integration can be expected to proceed relative quickly compared to the relatively inefficient process of headward erosion (compare Figs. 7.3a and b; e.g., Bishop, 1995; Douglass et al., 2009). Making distinctions between pre-, syn- and post-drainage integration phases in basin stratigraphy might help unravel regional-scale effects of sediment dispersal in continental rift evolution (Fig. 7.3b,c). Whereas prior to drainage integration basin deposits are mainly local-derived, the post-drainage integration stratigraphy is characterised by the deposition of mixtures of sediment from short and long-distance transport, or by fluvial incision. During the integration phase, the number of endorheic basins progressively declines due to the increase in fluvial connectivity, and is expected to result in the most pronounced variability in between the stratigraphy of the different basins.

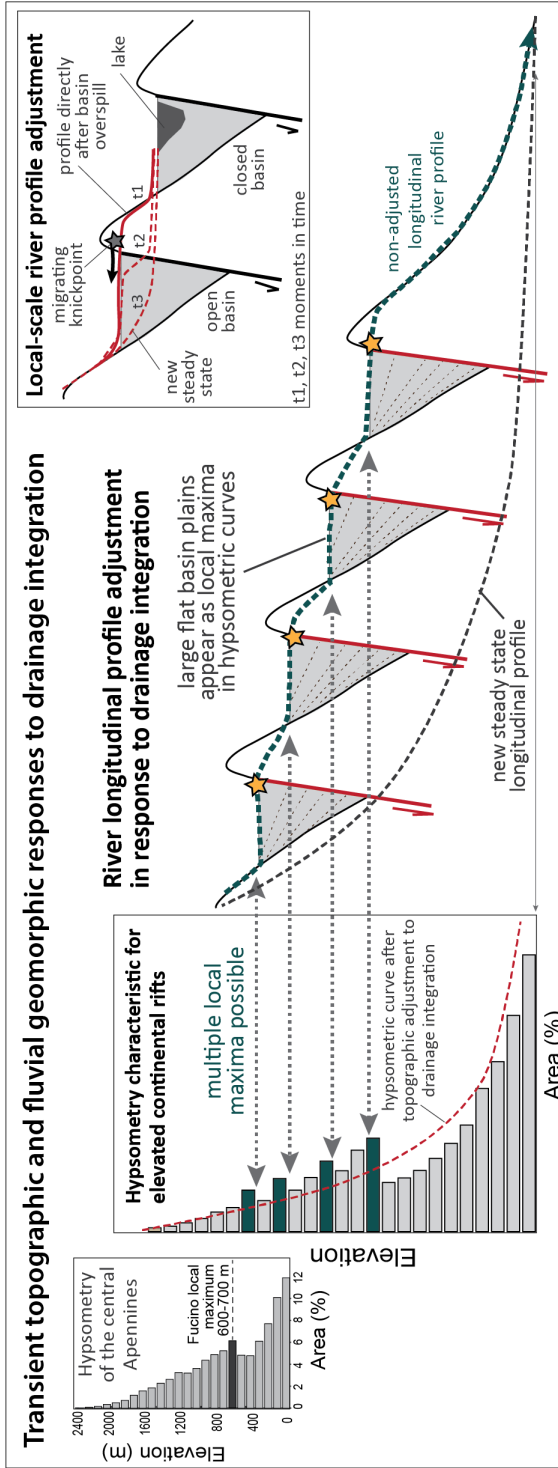
7.2.3 Transient landscape evolution

Drainage integration contributes greatly to transient landscape evolution in the central Apennines and in many other continental rifts (e.g., Connell et al., 2005; Larson et al., 2014; Repasch et al., 2017). As already summarised in section 6.3, the fluvial connectivity between basins controls the presence of local base levels, regional-scale erosion-deposition patterns and sediment dispersal, longitudinal river profile evolution and river terrace development. An aspect that has not been fully addressed is the potential impact of drainage integration on the overall topographic evolution of, in particular elevated, continental rifts. Characteristic for continental rifts that are affected by long-wavelength uplift is that significant elevation differences can develop between basins. In other words, large topographic disequilibria can develop at relative short distance between adjacent basins, but also at a regional-scale as for instance between the foreland areas and the interior of the central Apennines. Therefore, characteristic for elevated continental rifts that only recently underwent drainage

integration is the existence of local maxima in their hypsometric distributions (Fig. 7.4).

For natural systems it is challenging to distinguish between the contributions of drainage integration compared to, for instance, changes in climate and tectonics to transient landscape evolution. Therefore, the simplified numerical experiments from Chapter 3 are important as these clearly demonstrate that drainage integration itself produces a highly dynamic landscape evolution, even if both climate and tectonic forcing are constant. The fact that transient effects from drainage integration can persist in the landscape for many millions of years and that fluvial connectivity controls the propagation of tectonic and climatic signals across landscapes, suggests that drainage integration needs to be considered as an equally important factor as tectonics and climate in landscape evolution in continental rifts (Chapters 3 and 4).

Fig. 7.4 (next page) Right side of figure: Schematic illustration of river profile adjustment to drainage integration-induced drop(s) in local base level(s). At the moment of drainage integration, river profiles are characterised by convex reaches with a height that depends on the elevation difference between the basins. The river profiles adjust through the upstream propagation of these knickzones. Large (schematic) hypsometric curve in left-central part of figure: Hypsometric curve of elevated continental rifts prior to drainage integration are characterised by one or more local maxima, controlled by the elevation of the flat plains of the initially closed basins. After drainage integration these local maxima become progressively removed as the landscape geomorphically adjusts. The hypsometric profile on the far left side shows the distribution of elevations in the central Apennines (derived from 10m DEM), showing the local maxima set by the (still endorheic) Fucino basin.



7.3 Extensional faulting in areas of mantle-induced surface uplift

Dynamic surface uplift in response to mantle lithosphere thinning has been inferred for various tectonic settings around the globe (e.g., Le Pourhiet et al., 2006; Garzione et al., 2008; Göğüş and Pysklywec, 2008a). Numerous numerical and analogue modelling studies focussed on the dynamic of different mechanisms of lithosphere removal, e.g., delamination (Bird, 1979) and lithospheric dripping (Houseman, 1981), but also under what type of conditions different mechanisms occur (e.g., Göğüş and Pysklywec, 2008b). Other studies demonstrated how the different mechanisms differ in terms of surface expressions, e.g., topographic uplift or patterns of shortening versus extension (e.g., Göğüş and Pysklywec, 2008a; Göğüş et al., 2011). These modelling studies, in turn, made it feasible to deduce mechanisms of lithospheric thinning for natural systems based on field data-based reconstructions of uplift and crustal deformation (e.g., Cosentino et al., 2012; Schildgen et al., 2014).

The novelty of Chapter 5 of this thesis is that it focuses on the impact of lithospheric thinning, not only on surface uplift, but also on spatial-temporal changes in patterns of normal fault activity. Whereas previous studies already explored the impact of mantle lithosphere removal in extensional settings (e.g., Le Pourhiet et al., 2006) the model experiments in Chapter 5 allowed for the systematic analysis of patterns of fault slip distribution and slip rate variability. Moreover, this is the first modelling study motivated by the central Apennines, and can directly compare model results with first-order characteristics of this region.

Compared to previous modelling studies, the horizontal extent of mantle lithosphere removal, surface uplift and extension is very small (<150 km). The experiments in Chapter 5 demonstrate that this small scale has a number of important effects on the topography and fault development. First of all, it results in a dome-shape pattern of surface uplift rather than plateau uplift as revealed by experiments where mantle lithosphere is delaminating across much larger areas (e.g., Göğüş and Pysklywec, 2008a). Secondly, the relative small dimensions allow the stiffness of the crust to limit the total amount of isostatic uplift. Thirdly, the bending of the crust at short distance to

the narrow zone with active fault array makes plate flexure an important factor in controlling fault activity.

Isostatic uplift can result in extension in high terrain elevated at least several thousand of metres above its surroundings due to the large potential energy contrast (e.g., England and Houseman, 1989). However, Chapter 5 shows that extension does not start when regional topography is less than a thousand metres without far-field extension. Therefore, the experiments are important as they demonstrate that elevated topography and extension can be linked and both be associated with thinning of the lithosphere but do not necessarily need to have a causative relationship. For the Apennines, it has been hypothesised that both extension and uplift are driven by the same mantle-related mechanism (e.g., Faure Walker et al., 2012). Chapter 5, however, shows that removal of mantle lithosphere does not drive extension, but only localises far-field extension into the narrow zone of thermally weakened crust. These results are consistent with horizontal GPS velocities measured for the Italian Peninsula, showing far-field extension associated with the rotation of the Adriatic plate relative to Europe (e.g., D'Agostino et al., 2011; Devoti et al., 2011).

Chapter 5 also contributes to research focussing on fault development and slip rate variability. Even though the numerical experiments in Chapter 5 are only two-dimensional and therefore do not allow for along-strike fault growth, linkage and interaction, fault extension rates vary markedly over time. Therefore, also these model experiments demonstrate that slip rate variability is an essential feature of normal fault systems (e.g., Walsh and Watterson, 1991; Friedrich et al., 2003; Nicol et al., 2010; Wedmore et al., 2017). However, an interesting new insight is that the variability is revealed over much longer time-scales, namely 10^4 - 10^5 yr, than has been resolved by means of field data (e.g., Nicol et al., 2006; 2010; Cowie et al., 2017). This implies that variability in fault slip can be expected over a wide range of timescales from thousands (e.g., Cowie et al., 2017) to several hundred thousands of years (Chapter 5). The experiments suggest that this longer-term variability originates from flexure of the rift-bordering plates (Cowie et al., 2017). Furthermore, the results from Chapter 5

demonstrate the importance of fault geometry and rheology of the lower crust in controlling the distribution of extensional strain among the different active faults.

7.4 Future perspectives

7.4.1 Process-based understanding of drainage integration

The concept of overspill-driven drainage integration in continental rifts developed in this thesis needs verification on a wider dataset, both for the central Apennines, as well as for other active continental rifts (e.g., active parts of the Basin and Range, Corinth, East-African Rift). Although the research in this thesis integrated data on fault development, stratigraphy, sedimentation rates, and geomorphology, a wider range of data is available from the central Apennines that can be used for investigating drainage integration processes in higher detail. Whereas, first-order estimates of sedimentation and basin subsidence rates were used in Chapter 4, there is more detailed data available from this area on the temporal variability in sedimentation rates, fault slip rates, and climate-induced changes in discharges and erosion.

Another important advance that could be made is to compare rates of basin subsidence and infilling (as in Fig. 9 in Chapter 4) in a volumetric, rather than one-dimensional way, for individual basins separately, and to include estimates of lake volumes. This basin-by-basin approach is probably feasible for some of the major fault-bounded basins in the central Apennines with high data densities, for instance the basins around l'Aquila.

Even though headward erosion (not to be confused with the upstream propagation of knickpoints along pre-existing rivers) is not considered to be of any relevance for long-term drainage integration in the central Apennines, the general debate on the relative importance of headward erosion versus basin overspill mechanisms is clearly in need of studies that systematically constrain the efficiency of headward erosion over timescales of millions of years and under different types of climatic and tectonic conditions. This might only be feasible through landscape evolution modelling, and

requires the development of numerical algorithms that correctly describe the dynamics of the uphill propagation of incising riverheads.

7.4.2 The impact of drainage integration

The research presented in Chapters 3 and 4 of this thesis provide important new insights into the impact of drainage integration on basin stratigraphy and transient landscape evolution. However, the wealth of data that is currently available for the central Apennines allows for the analysis of the consequences of drainage integration in much higher detail. While this work mainly focused on first-order effects like for instance abrupt changes from lacustrine deposition to fluvial erosion, more detailed stratigraphic analyses may reveal important additional insights into the character of these transitions. The detailed chronostratigraphic framework that exists for the central Apennines is a critical factor in such analysis.

In order to advance our understanding of the impacts of drainage integration for continental rifts in more general, it is important to compare results from this work in more detail with studies focusing on other areas. This would allow the effects of factors like climatic conditions, lithology, or the structural and topographic build-up of the rift on drainage integration to be determined. In the Basin and Range for instance, drainage integration events often occurred through catastrophic lake outburst events that almost instantaneously removed most of the fine-grained lake sediments (e.g., Meek, 2019). By contrast, in the central Apennines drainage integration events were not as catastrophic and the lacustrine clays have been largely preserved because top layers of fluvial conglomerates protected them from erosion.

7.4.3 Normal fault activity in settings of mantle-induced surface uplift

The numerical modelling study presented in Chapter 5 was designed for exploring the impact of mantle-lithosphere removal on surface uplift and extensional faulting in the central Apennines. It demonstrates that lithospheric thinning is mainly relevant for controlling the wavelength of surface uplift and crustal weakening, and therefore, the

width of the active fault array. However, the distribution of extension among the active faults and temporal variability in their slip rates turns out to be mainly controlled by the characteristics of the fault array and crustal rheology. Therefore, for research primarily focussed on dynamic normal fault behaviour, it is recommended to continue first of all with crustal scale models. By varying the strength of the lower crust, the impact of mantle lithosphere removal-induced crustal weakening can also be indirectly tested. The experiments in Chapter 5 demonstrated that the impact of isostatic surface uplift on fault behaviour is negligible.

The results in Chapter 5 also show the importance of fault geometry in controlling dynamic fault behaviour. This suggests a major role for structural inheritance. Therefore, our understanding of fault interaction and slip rate variability can be advanced by developing modelling studies that systematically test the impact of inherited structures and associated fault geometries.

An important limitation of the experiments in Chapter 5 is the lack of surface processes. Because previous studies have demonstrated the major importance of surface processes on fault development, it is strongly recommended to include surface processes in future modelling studies investigating dynamic fault behaviour in continental rifts. As sediment dispersal occurs primarily in an along-strike direction, it is recommended to use three-dimensional crustal-scale models.

CHAPTER 8

Main conclusions

- 1) The connectivity of drainage networks in continental rifts is primarily controlled by the balance between the filling and subsidence of fault-bounded basins. Basin filling occurs through the supply of sediment and water, whereas basin volume is controlled by fault slip and changes in spill-point elevation.
- 2) Drainage integration occurs when initially underfilled and internally drained basins become overfilled with sediment and water allowing basins to overflow. Because the newly established fluvial connections allow water and sediment to cascade downstream, drainage integration predominantly follows a top-down spatial-temporal pattern. Local conditions, however, can add significant randomness to the pattern of drainage integration and even produce a reversed trend towards basin isolation.
- 3) Even if climate conditions and tectonic forcing are constant, drainage integration produces a highly dynamic landscape evolution with abrupt and pronounced changes in local base levels, the locus of erosion and deposition, sediment and water dispersal, and depositional environments. Moreover, consecutive drainage integration events produce discrete upstream migrating waves of fluvial incision and terrace formation.

- 4) Drainage integration is as important as climate and tectonics in controlling basin stratigraphy, drainage network evolution, topographic development in continental rifts and therefore needs to be considered as a factor in its own right. Drainage integration produces transient conditions that can persist for millions of years following the complete integration of the river network.
- 5) Removal of mantle lithosphere causes upwelling of hot buoyant sub-lithospheric mantle and, in turn, isostatic surface uplift. Because this additionally results in thermal weakening of the crust, far-field extension becomes localised in the area of elevated topography.
- 6) Therefore, removal of mantle lithosphere can explain active extensional faulting in areas of high topography subject to regional extension. The width of the active fault array and the length-scale of the regional topography reflect the dimensions of the area of mantle lithosphere removal.
- 7) Mantle lithosphere removal not only explains a correlation between fault strain rates, topography and surface uplift, but can also explain enhanced surface heat fluxes, negative gravity anomalies and low P-wave velocities in the upper mantle.
- 8) Fault extension rates vary over a range of 10^4 - 10^5 year timescales, which are longer time-scales of extension rate variability than previously described. This temporal variability results from fault interaction and the associated migration of the locus of activity across-strike.

References

- Allen, P.A., 2005. Striking a chord. *Nature* 434, 961-961.
- Allen, P.A., Allen, J.R., 2013. Basin analysis – Principles and application to petroleum play assessment, third ed. Wiley-Blackwell, Oxford.
- Armijo, R., Tapponnier, P., Mercier, J.L., Tong-Lin, H., 1986. Quaternary extension in southern Tibet: Field observations and tectonic implications. *J. Geophys. Res.*, 91, 13,803-13,872.
- Artoni, A., 2013. The Pliocene-Pleistocene stratigraphic and tectonic evolution of the Central sector of the Western Periadriatic Basin of Italy. *Marine Petrol. Geol.*, 42, 82-106.
- Ascione, A., Cinque, A., Miccadei, E., Villani, F., Berti, C., 2008. The Plio-Quaternary uplift of the Apennine chain: new data from the analysis of topography and river valleys in Central Italy. *Geomorphology* 102, 105-118.
- Attal, M., Cowie, P.A., Whittaker, A.C., Hopley, D., Tucker, D.E., Roberts, G.P., 2011. Testing fluvial erosion models using the transient response of bedrock rivers to tectonic forcing in the Apennines, Italy. *Journal of Geophysical Research*, 116, F02005.
- Bartonlini, C., D'Agostino, N., and Dramis, F., 2003. Topography, exhumation, and drainage network evolution of the Apennines. *Episodes*, 26, 212-216.
- Beaumont, C., Fullsack, P., and Hamilton, J., 1992. Erosional control of active compressional orogens; in: McClay, K. R., ed., *Thrust tectonics*, Chapman & Hall, London, United Kingdom, p. 1-18.
- Beaumont, C., Kooi, H. and Willett, S., 1999. Coupled tectonic-surface process models with applications to rifted margins and collisional orogens, in: *Geomorphology and Global Tectonics*, ed. M.A. Summerfield, 29-55, John Wiley and Sons Ltd.
- Becker, T.W., Lowry, A.R., Faccenna, C., Schmandt, B., Borsa, A., Yu, C., 2015. Western US intermountain seismicity caused by changes in upper mantle flow. *Nature* 524, 458-461.
- Bell, R.E., 2008. Tectonic evolution of the Corinth Rift. PhD Thesis. Faculty of Engineering, Science and Mathematics, School of Ocean and Earth Science, University of Southampton.
- Bell, R.E., Duclaux, G., Nixon, C.W., Gawthorpe, R.L., & McNeill, L.C., 2018. High-angle, not low-angle, normal faults dominate early rift extension in the Corinth Rift, central Greece. *Geology* 46, 2, 115-118.
- Beucher, R. and Huisman, R.S., 2020, *Morphotectonic Evolution of Passive Margins undergoing Active Surface Processes: Large-Scale Experiments using Numerical Models, Geochemistry, Geophysics, Geosystems*, in press.
- Bird, P., 1979. Continental delamination and the Colorado Plateau, *Journal Geophysical Research*, 84, 7561-7571.
- Byerle, B.L., Lassiter, J.C., 2012. Evidence from mantle xenoliths for lithosphere removal beneath the central Rio Grande Rift. *Earth and Planetary Science Letters*, 355-356, 82-93.
- Bialas, R.W., and Buck, W.R., 2009. How sediment promotes narrow rifting: Application to the Gulf of California. *Tectonics*, 28, TC4014.
- Bianchi-Fasani, G., Esposito, C., Petitta, M., Scarascia-Mugnozza, G., Barbieri, M., Cardarelli, E., Cercato, M., Di Fillipa, G., 2011. The Importance of Geological Models in Understanding and Predicting the Life Span of Rockslide Dams: The Case of Scanno Lake, Central Italy. In: *Natural and Artificial Rockslide Dams* (S.G. Evans, R.L. Hermanns, A. Strom & G. Scarascia-Mugnozza), Springer Science & Business Media, 133, 323-346.
- Bishop, P., 1995. Drainage rearrangement by river capture, beheading and diversion. *Progr. Physic. Geogr.*, 19, pp. 449-473.
- Bocco, G., 1991. Gully erosion: processes and models. *Progr. Physic. Geogr.*, 15, 392-406.

- Bogaart, P., Tucker, G., De Vries, J., 2003. Channel network morphology and sediment dynamics under alternating periglacial and temperate regimes: A numerical simulation study. *Geomorphology* 54, 257–277.
- Boni, C., 2000. Karst aquifers of the Central Apennines. *Hydrogéologie*, 4, pp. 49-62.
- Bordoni, P., Valensise, G., 1998. Deformation of the 125 ka marine terrace in Italy: tectonic implications. In: *Coastal tectonics* (Ed. by I.S. Stewart & C. Vita-Finzi), Geological Society, London, Spec. Publ., 146, 71–110.
- Bosi C., and Messina P., 1991. Ipotesi di correlazione fra successioni morfo-litostratigrafiche plio-pleistoceniche nell'Appennino Laziale-Abruzzese. *Studi Geol. Cam., Special Volume 2*, 257-263.
- Bosi, C., Galadini, F., Giaccio, B., Messina, P., Sposato, A., 2003. Plio-Quaternary continental deposits in the Latium-Abruzzi Apennines: The correlation of geological events across different intermontane basins. *Il Quaternario - Italian J. Quat. Sci.* 16, 55-76.
- Bosi, C., Messina, P., Moro, M., 2004. Use of allo-morphosequential units in the Quaternary geological map of the upper Aterno Valley (Central Apennines). Pasquarè G., Venturini C. (Eds.), *Mapping geology in Italy*, APAT-SELCA
- Braun, J., and Sambridge, M. (1997): Modelling landscape evolution on geological time scales: a new method based on irregular spatial discretization. *Basin Research*, 9, 27–52.
- Braun, J., 2006. Recent advances and current problems in modelling surface processes and their interaction with crustal deformation. *Geological Society, London, Special Publications*, 253, 307-325.
- Braun, J., 2010. The many surface expressions of mantle dynamics. *Nature*, 3, 825-833.
- Briant, R.M., Cohen, K.M., Cordier, S., Demoulin, A.J., Macklin, M.G., Mather, A.E., Rixhon, G., Veldkamp, T., Wainwright, J., Whittaker, A.C., 2018. Applying Pattern Oriented Sampling in current fieldwork practice to enable more effective model evaluation in fluvial landscape evolution research. *Earth Surf. Process. Landforms*, 43, pp. 2964-2980.
- Buiter, S.J.H., Huismans, R.S., and Beaumont, C., 2008. Dissipation analysis as a guide to mode selection during crustal extension and implications for the styles of sedimentary basins. *Journal of Geophysical Research*, 113, B06406.
- Burbank, D.W., and Pinter, N., 1999. Landscape evolution: the interactions of tectonics and surface processes. *Basin Research*, 11, 1-6.
- Burbank, D.W., and Anderson, R.S., 2012. *Tectonic geomorphology*. Wiley-Blackwell, Chichester, 454 pp.
- Burov, E., and Cloetingh, S., 1997. Erosion and rift dynamics: new thermomechanical aspects of post-rift evolution of extensional basins. *Earth and Planetary Science Letters*, 150, 7-26.
- Calais, E., Freed, A.M., Van Arsdale, R., Stein, S., 2010. Triggering of New Madrid seismicity by late-Pleistocene erosion. *Nature*, 466, 608-611.
- Cantalamesa, G., and Di Celma, C., 2004. Sequence response to syndepositional regional uplift: insights from high-resolution sequence stratigraphy of late Early Pleistocene strata, Periadriatic Basin, central Italy. *Sediment. Geol.*, 164, 283-309.
- Cataldi, R., Mongelli, F., Squarci, P., Taffi, L., Zito, G., Calore, C., 1995. Geothermal ranking of Italian territory. *Geothermics* 24,115–129.
- Cavinato, G.P., 1993. Recent tectonic evolution of the Quaternary deposits of the Rieti Basin (Central Apennines, Italy): Southern part. *Geol. Romana*, 29, 411-434.
- Cavinato, G.P., Cosentino, D., De Rita, D., Funicello, R., Parotto, M., 1994. Tectonic-sedimentary evolution of intrapenninic basins and correlation with the volcano-tectonic activity in Central Italy. *Mem. Descr. Carta Geol. d'Italia*, XLIX, 63-76.
- Cavinato, G. P., and De Celles, P. G., 1999. Extensional basins in tectonically bi-modal central Apennines fold-thrust belt, Italy: Response to corner flow above a subducting slab in retrograde motion, *Geology*, 27, 955-958.
- Cavinato, G.P., and Miccadei, E., 2000. Pleistocene carbonate lacustrine deposits: Sulmona Basin (Central Apennines, Italy). In: *Lake basins through space and time* (E.H. Gierlowski-Kordesch & K.R. Kelts), AAPG Studies in Geology, 46, 517-526.

Cavinato, G.P., Gliozzi, E., Mazzini, I., 2000. Two lacustrine episodes during the Late Pliocene-Holocene evolution of the Rieti basin (Central Apennines, Italy), in: Gierlowski-Kordesch, E.H., Kelts, K.R. (Eds.), *Lake basins through space and time*. AAPG Studies in Geology, 46, pp. 527-534.

Cavinato, G.P., Carusi, C., Dall'Asta, M., Miccadei, E., and Piacentini, T., 2002. Sedimentary and tectonic evolution of Plio-Pleistocene alluvial and lacustrine deposits of Fucino Basin (central Italy). *Sedimentary Geology*, 148, 29-59.

Centamore, E., and Nisio, S., 2003. Ejects of uplift and tilting in the Central-Northern Apennines, Italy. *Quat. Intern.*, 101-102, 93-101.

Chiarini, E., La Posta, E., Cifelli, F., D'Ambrogi, C., Eulilli, V., Ferri, F., Marino, M., Mattei, M., Puzilli, L.M., 2014. A multidisciplinary approach to the study of the Montereale Basin (Central Apennines, Italy). *Rend. Fis. Acc. Lincei* 25, S177-S188.

Chiarabba, C., Bagh, S., Bianchi, I., De Gori, P., Barchi, M., 2010. Deep structural heterogeneities and the tectonic evolution of the Abruzzi region (Central Apennines, Italy) revealed by microseismicity, seismic tomography, and teleseismic receiver functions. *Earth and Planetary Science Letters*, 295, 462-476.

Chiarabba, C., Chiodini, G., 2013. Continental delamination and mantle dynamics drive topography, extension and fluid discharge in the Apennines. *Geology*, 41, 715-718.

Chiodini, G., Cardellini, C., Caliro, S., Chiarabba, C., Frondini, F., 2013. Advective heat transport associated with regional Earth degassing in central Apennine (Italy). *Earth Planet. Sci. Lett.*, 373, 65-74.

Cohen, K.M., Gibbard, P.L., 2010. Global chronostratigraphical correlation table for the last 2.7 million years v. 2010. Subcommission on Quaternary Stratigraphy, International Commission on Stratigraphy: Cambridge. <http://www.quaternary.stratigraphy.org.uk/charts/>

Connell, S.D., Hawley, J.W., and Love, D.W., 2005. Late Cenozoic drainage development in the southeastern Basin and Range of New Mexico, southeasternmost Arizona, and western Texas. In: *New Mexico's ice ages: New Mexico Museum of Natural History and Science* (Lucas, S., Morgan, G. & Zeigler, K.), 125-150.

Cosentino, D., Schildgen, T.F., Cipollari, P., Faranda, C., Gliozzi, E., H, Hudáčková, N., Lucifora, S., and Strecker, M.R., 2012. Late Miocene surface uplift of the southern margin of the Central Anatolian Plateau, Central Taurides, Turkey. *GSA Bulletin*, 124, 133-145.

Cosentino, D., Asti, R., Nocentini, M., Gliozzi, E., Kotsakis, T., Mattei, M., Esu, D., Spadi, M., Tallini, M., Cifelli, F., Pennacchioni, M., Cavuoto, G., Di Fiore, V., 2017. New insights into the onset and evolution of the central Apennine extensional intermontane basins based on the tectonically active L'Aquila Basin (central Italy). *Geol. Soc. of America Bulletin*, 129, doi.org/10.1130/B31679.1.

Coward, M.P., 1990. The Precambrian, Caledonian and Variscan framework to NW Europe. *Geol. Soc. of London, Spec. Publ.*, 55, 1- 34.

Cowie, P.A., and Scholz, C.H., 1992. Physical explanation for the displacement-length relationship of faults using a post yield fracture mechanics model. *Journal of Structural Geology*, 14, 1133-1148.

Cowie, P.A., Vanneste, C., and Sornette, D., 1993. Statistical physics model for the spatio-temporal evolution of faults. *Journal Geophysical Research*, 98, 21809-21822.

Cowie, P.A., Sornette, D., and Vanneste, C., 1995. Multifractal scaling properties of a growing fault population. *Geophysical Journal International*, 122, 457-469.

Cowie, P.A., 1998. A healing-reloading feedback control on the growth rate of seismogenic faults. *Journal of Structural Geology*, 20, 1075-1087.

Cowie, P.A. (1998) Normal fault growth in three-dimensions in continental and oceanic crust. In: *Faulting and Magmatism at Mid-Ocean Ridges* (Roger Buck, W., Delaney, P.T., Karson, J.A., & Lagabriele, Y.), 325-346.

Cowie P. A., and Roberts, G. P. (2001): Constraining slip rates and spacings for active normal faults. *Journal of Structural Geology*, 23, 1901-1915.

Cowie, P. A., Attal, M., Tucker, G. E., Whittaker, A. C., Naylor, M., Ganas, A., and Roberts G. P., 2006. Investigating the Surface Process Response to Fault Interaction and Linkage Using a Numerical Modeling Approach. *Basin Research*, 18, 231-266.

- Cowie, P.A., Whittaker, A.C., Attal, M., Roberts G.P., Tucker, G.E., and Ganas, A., 2008. New constraints on sediment-flux-dependent river incision: Implications for extracting tectonic signals from river profiles. *Geology*, 36, 535-538.
- Cowie, P.A., Roberts, G.P., Bull, J., Visini, F., 2012. Relationships between fault geometry, slip-rate variability and earthquake recurrence in extensional settings. *Geophys. J. Int.* 189, 143–160.
- Cowie, P.A., Scholz, C.H., Roberts, G.P., Faure Walker, J.P., Steer, P., 2013. Viscous roots of active seismogenic faults revealed by geologic slip rate variations. *Nature Geoscience* 6, 1036–1040.
- Cowie, P.A., Phillips, R.J., Roberts, G.P., McCaffrey, K., Zijerveld, L.J.J., Gregory, L.C., Faure Walker, J., Wedmore, L.N.J., Dunai, T.J., Binnie, S.A., Freeman, S.P.H.T., Wilcken, K., Shanks, R.P., Huismans, R.S., Papanikolaou, I., Michetti, A.M., Wilkinson, M., 2017. Orogen-scale uplift in the central Italian Apennines drives episodic behaviour of earthquake faults. *Nature Sci. Rep.* 7, 44858.
- D'Agostino, N., Chamot-Rooke, N., Funicello, R., Jolivet, L., and Speranza, F., 1998. The role of pre-existing thrust faults and topography on the styles of extension in the Gran Sasso range (central Italy). *Tectonophysics*, 292, 229–254.
- D'Agostino, N., McKenzie, D., 1999. Convective support of long wavelength topography in the Apennines (Italy). *Terra Nova* 11, 234–238.
- D'Agostino, N., Jackson, J.A., Dramis F., Funicello, R., 2001. Interactions between mantle upwelling, drainage evolution and active normal faulting: an example from the central Apennines (Italy). *Geophys. J. Internat.* 147, 475-497.
- D'Agostino, N., 2009. Contemporary crustal extension in the Umbria-Marche Apennines from regional GPS networks and comparison between geodetic and seismic deformation. *Tectonophysics*, 476, 3-12.
- D'Agostino, N., Mantenuto, S., D'Anastasio, E., Giuliani, R., Mattone, M., Calcaterra, S., Gambino, P., Bonci, L., 2011. Evidence for localized active extension in the central Apennines (Italy) from global positioning system observations. *Geology* 39(4), 291-294.
- D'Agostino, N., England, P., Hunstad, I., Selvaggi, G., 2014. Gravitational potential energy and active deformation in the Apennines. *Earth Planet. Sc. Let.*, 397, 121-132.
- D'Alessandro, L., Miccadei, E., and Piacentini, T., 2003. Morphostructural elements of central–eastern Abruzzi: contributions to the study of the role of tectonics on the morphogenesis of the Apennine chain. *Quat. Internat.*, 101-102, 115-124.
- D'Alessandro, L., Miccadei, E., and Piacentini, T., 2008. Morphotectonic study of the lower Sangro River valley (Abruzzi, Central Italy). *Geomorphology*, 102, 145–158.
- D'Anastasio, E., De Martini, P.M., Selvaggi, G., Pantosti, D., Marchioni, A., and Maseroli, R., 2006. Short-term vertical velocity field in the Apennines (Italy) revealed by geodetic leveling data. *Tectonophysics*, 418, 219-234.
- De Gelder, G., Fernandez-Blanco, D., Melnick, D., Duclaux, G., Bell, R.E., Jara-Munoz, J., Armijo, R., Lacassin, R., 2019. Lithospheric flexure and rheology determined by climate cycle markers in the Corinth Rift. *Nature Scientific Reports* 9(1), 4260.
- Della Vedova, B., Bellani, S., Pellis, G., Squarci, P., 2001. Deep temperatures and surface heat flow distribution. In: Vai, G.B., Martini, I.P. (Eds.), *Anatomy of an Orogen, The Apennines and Adjacent Mediterranean Basins*. Kluwer Academic Publishers, Dordrecht, Netherlands, pp.65–76.
- De Mets, C., Gordon, R.G., Argus, D.F., Stein, S., 1990. Current plate motions. *Geophysical Journal International*, 101, 425-478.
- Densmore, A.L., Dawers, N.H., Gupta, S., Allen, P.A., Gilpin, R., 2003. Landscape evolution at extensional relay zones. *Journal of Geophysical Research*, 108, 2273.
- Densmore, A.L., Dawers, N.H., Gupta, S., Guidon, R., Goldin, T., 2004. Footwall topographic development during continental extension. *Journal of Geophysical Research*, 109, F03001.
- Devoti, R., Esposito, A., Pietrantonio, G., Pisani, A.R., Riguzzi, F., 2011. Evidence of large scale deformation patterns from PGS data in the Italian subduction boundary. *Earth and Planetary Science Letters*, 311, 230-241.
- Dickinson, W.R., 2015. Integration of the Gila River drainage system through the Basin and Range province of southern Arizona and southwestern New Mexico (USA). *Geomorphology*, 236, 1-24.

- Di Luzio, E., Mele, G., Tiberti, M.M., Cavinato, G.P., Parotto, M., 2009. Moho deepening and shallow upper crustal delamination beneath the central Apennines. *Earth Planet. Sci. Lett.*, 280, 1-12.
- Di Stefano, R., Kissling, E., Chiarabba, C., Amato, A., Giardini, D., 2009. Shallow subduction beneath Italy: Three-dimensional images of the Adriatic-European-Tyrrhenian lithosphere system based on high-quality P wave arrival times. *Journal of geophysical research*, 114, B05305.
- Douglass, J. & Schmeekle, M.W., 2007. Analogue modeling of transverse drainage mechanisms. *Geomorphology*, 84, 22-43.
- Douglass, J., Meek, N., Dorn, N.I., and Schmeekle, M.W., 2009. A criteria-based methodology for determining the mechanism of transverse drainage development, with application to the southwestern United States. *GSA Bulletin* 121, 586-598.
- Duffy, O.B., Brocklehurst, S.H., Gawthorpe, R.L., Leeder, M.R., and Finch, E., 2015. Controls on landscape and drainage evolution in regions of distributed normal faulting: Perachora Peninsula, Corinth Rift, Central Greece. *Basin Res.* 27, 473-494.
- Ebinger, C.J., and Sleep, N.H., 1998. Cenozoic magmatism throughout east Africa resulting from impact of a single plume. *Nature*, 395, 788-791.
- Elliott, J.R., Walters, R.J., England, P.C., Jackson, J.A., Li, Z., and Parsons, B., 2010. Extension on the Tibetan plateau: recent normal faulting measured by InSAR and body wave seismology. *Geophys. J. Int.*, 183, 503-535.
- England, P., Houseman, G., 1989. Extension during continental convergence, with application to the Tibetan Plateau. *Journal of Geophysical Research*, 94, 17561-17579.
- Erdoş, Z., Huisman, R. S., van der Beek, P., and Thieulot, C., 2014. Extensional inheritance and surface processes as controlling factors of mountain belt structure. *Journal of Geophysical Research: Solid Earth*, 119, 9042-9061.
- Faccenna C., Becker T.W., Lucente F.P., Jolivet L., and Rossetti F., 2001a. History of subduction and back-arc extension in the Central Mediterranean, *Geophysics Journal International*, 145, 809-820.
- Faccenna C., Funicello F., Giardini D., and Lucente F.P., 2001b. Episodic back-arc extension during restricted mantle convection in the Central Mediterranean, *Earth and Planetary Science Letters*, 187, 105-116.
- Faccenna, C., Becker, T.W., Miller, M.S., Serpelloni, E., Willett, S.D., 2014. Isostasy, dynamic topography, and the elevation of the Apennines of Italy. *Earth Planet. Sci. Lett.* 407, 163-174.
- Faure Walker, J.P., 2010. Mechanics of continental extension from Quaternary strain fields in the Italian Apennines. PhD thesis, University College London, UK, p. 379.
- Faure Walker, J.P., Roberts, G.P., Sammonds, P.R., Cowie, P.A., 2010. Comparison of earthquake strains over 10^2 to 10^4 year timescales: Insights into variability in the seismic cycle in central Apennines, Italy. *Journal of Geophysical Research*, 115, B10418.
- Faure Walker, J.P., Roberts, G.P., Cowie, P.A., Papanikolaou, I., Michetti, A.M., Sammonds, P., Wilkinson, M., McCaffrey, K.J., and Phillips, R.J., 2012. Relationship between topography and strain rate in the actively extending Italian Apennines. *Earth Planet. Sci. Lett.*, 325/326, 76-84.
- Fernández-Ibáñez, F., Pérez-Peña, J.V., Azor, A., Soto, J.I., and Azañón, J.M., 2010. Normal faulting driven by denudational isostatic rebound. *Geology*, 38, 643-646.
- Ferranti, L., Antonioli, F., Mauz, B., Amorosi, A., Dai Pra, G., Mastronuzzi, G., Monaco, C., Orru, P., Pappalardo, M., Radtke, U., Renda, P., Romano, P., Sanso, P., and Verrubi, V., 2006. Markers of the last interglacial sea-level high stand along the coast of Italy: Tectonic implications. *Quat. Internat.*, 145-146, 30-54.
- Foster, A., and Nimmo, F., 1996. Comparisons between the rift systems of East Africa, Earth and Beta Regio, Venus. *Earth and Planetary Science Letters*, 143, 183-195.
- Friedrich, A.M., Wernicke, B.P., Niemi, N.A., 2003. Comparison of geodetic and geologic data from the Wasatch region, Utah, and implications for the spectral character of Earth deformation at periods of 10 to 10 million years. *J. Geophys. Res.*, 108, B4-2199.
- Fullsack, P., 1995. An arbitrary Lagrangian-Eulerian formulation for creeping flows and its application in tectonic models. *Geophysical Journal International*, 120, 1-23.

Galadini, F., Galli, P., 2000. Active Tectonics in the Central Apennines (Italy) - Input Data for Seismic Hazard Assessment, *Natural Hazards*, 22, 225-270.

Galadini, F., Messina, P., Giacco, B. and Sposato, A., 2003. Early uplift history of the Abruzzi Apennines (Central Italy): Available geomorphological constraints, *Quaternary International*, 101-102, 125-135.

Galli, P., Giaccio, B., and Messina, P., 2010. The 2009 central Italy earthquake seen through 0.5 Myr-long tectonic history of the L'Aquila faults system. *Quat. Sci. Rev.*, 29, 3768-3789.

Galli, P., Giacco, B., Messina, P., Peronace, E., Giovanni, M.Z., 2011. Palaeoseismology of the L'Aquila faults (central Italy, 2009, Mw 6.3 earthquake): implications for active fault linkage. *Geophys. J. Internat.* 187, 1119-1134.

Garcia-Castellanos, D., Verges, J., Gaspar-Escribano, J., and Cloetingh, S., 2003. Interplay between tectonics, climate, and fluvial transport during the Cenozoic evolution of the Ebro basin (NE Iberia). *J. Geophys. Res.*, 108, B7.

Garzione, C.N., Hoke, G.D., Libarkin, J.C., Withers, S., MacFadden, B., Eiler, J., Ghosh, P., Mulch, A., 2008. Rise of the Andes. *Science*, 320, 1304-1307.

Gawthorpe, R.L., Fraser, A.J., Collier, R.E., 1994. Sequence stratigraphy in active extensional basins: implications for the interpretation of ancient basin-fills. *Marine and Petroleum Geology* 11(6), 642-658.

Gawthorpe, R.L., and Leeder, M.R., 2000. Tectono-sedimentary evolution of active extensional basins. *Basin Res.*, 12, 195-218.

Gawthorpe, R.L., Leeder, M.R., Kranis, H., Skourtsos, E., Andrews, J.E., Henstra, G.A., Mack, G.H., Muravchik, M., Turner, J.A., Stamatakis, M., 2018. Tectono-sedimentary evolution of the Plio-Pleistocene Corinth rift, Greece. *Basin Res.* 30, 448-479.

Gemmer, L., Houseman, G., 2007. Convergence and extension driven by lithospheric gravitational instability: evolution of the Alpine-Carpathian Pannonian system. *Geophys. J. Int.* 168, 1276-1290.

Geurts, A.H., Cowie, P.A., Duclaux, G., Gawthorpe, R.L., Huismans, R.S., Pedersen, V.K., Wedmore, L.N.J., 2018. Drainage integration and sediment dispersal in active continental rifts: A numerical modelling study of the central Italian Apennines. *Basin Res.* 30(5), 965-989.

Geurts, A.H., Whittaker, A.C., Gawthorpe, R.L., Cowie, P.A., 2020. Transient landscape and stratigraphic responses to drainage integration in the actively extending central Italian Apennines. *Geomorphology*, 353, 107013.

Giaccio, B., Messina, P., Sposato, A., Voltaggio, M., Zanchetta, G., Galadini, F., Gori, S., Santacroce, R., 2009. Tephra layers from Holocene lake sediments of the Sulmona Basin, central Italy: Implications for volcanic activity in Peninsular Italy and tephrostratigraphy in the central Mediterranean area. *Quat. Sci. Rev.* 28, 2710-2733.

Giaccio, B., Galli, P., Messina, P., Peronace, E., Scardia, G., Sottili, G., Sposato, A., Chiarini, E., Jicha, B., Silvestri, S., 2012. Fault and basin depocentre migration over the last 2 Ma in the L'Aquila 2009 earthquake region, central Italian Apennines. *Quat. Sci. Rev.* 56, 69-88.

Giaccio, B., Castorina, F., Nomade, S., Scardia, G., Voltaggio, M., Sagnotti, L., 2013. Revised Chronology of the Sulmona Lacustrine Succession, Central Italy. *Journal of Quaternary Science* 28, 545-551.

Giraudi, C., 1989. Lake levels and climate for the last 30,000 years in the Fucino area (Abruzzo-central Italy) - a review. *Palaeogeogr., Palaeoclim., Palaeoecol.* 70, 249-260.

Giraudi, C., Frezzotti, M., 1997. Late Pleistocene glacial events in the central Apennines, Italy. *Quat. Res.* 48, 280-290.

Gliozzi, E., Mazzini, I., 1998. Palaeoenvironmental analysis of Early Pleistocene brackish marshes in the Rieti and Tiberino intrapenninic basins (Latium and Umbria, Italy) using ostracods (Crustacea). *Palaeogeogr., Palaeoclimat., Palaeoecol.* 140, 325-333.

Göğüş O.H., and Pysklywec, R.N., 2008a. Mantle lithosphere delamination driving plateau uplift and synconvergent extension in eastern Anatolia. *Geology*, 36, 723-726.

Göğüş O.H., and Pysklywec, R.N., 2008b. Near-surface diagnostics of dripping or delaminating lithosphere. *Journal of Geophysical Research* 113, B11404.

Gögüş O.H., and Pysklywec, R.N., Corbi, F., Faccenna, C., 2011. The surface tectonics of mantle lithosphere delamination following ocean lithosphere subduction: Insights from physical-scaled analogue experiments. *Geochemistry, Geophysics, Geosystems*, 12, 5.

Gori, S., Giaccio, B., Galadini, F., Falcucci, E., Messina, P., Sposato, A., and Dramis, F., 2011. Active normal faulting along the Mt. Morrone south-western slopes (central Apennines, Italy). *International Journal of Earth Sciences*, 100, 157–171.

Gori, S., Falcucci, E., Scardia, G., Nomade, S., Guillou, H., Galadini, F., Fredi, P., 2015. Early capture of a central Apennine (Italy) internal basin as a consequence of enhanced regional uplift at the Early-Middle Pleistocene transition, in: Monegato, G., Gianotti, F., Forno, M.G. (Eds.), *The Plio-Pleistocene continental record in Italy: highlights on Stratigraphy and Neotectonics. Abstracts Volume AIQUA Congress 2015, February 24–26, Torino, Miscellanea dell'Istituto Nazionale di Geofisica e Vulcanologia (ISSN 2039-6651)*, 26, 26–27.

Gori, S., Falcucci, E., Ladina, C., Marzorati, S., and Galadini, F., 2017. Active faulting, 3-D geological architecture and Plio-Quaternary structural evolution of extensional basins in the central Apennine chain, Italy. *Solid Earth* 8, 319-337.

Gupta, S., and Cowie, P.A., 2000. Processes and Controls on the Stratigraphic Development of Extensional Basins, *Basin Res.*, 12, 185-194.

Hampel, A., Hetzel, R., Maniatis, G., Karow, T., 2009. Three-dimensional numerical modeling of slip rate variations on normal and thrust fault arrays during ice cap growth and melting. *Journal of Geophysical Research*, 114, B08406.

Head, M.J., and Gibbard, P.L., 2015. Early-Middle Pleistocene transitions: Linking terrestrial and marine realms. *Quat. Internat.* 389, 7-46.

Heidarzadeh, G., Ballato, P., Hassanzadeh, J., Ghassemi, M.R., and Strecker, M.R., 2017. Lake overspill and onset of fluvial incision in the Iranian Plateau: Insights from the Mianeh Basin. *Earth Planet. Sci. Lett.*, 469, 135-147.

Heimpel, M., and Olsen, P. A., 1996. Seismodynamical model of lithosphere deformation: development of continental and oceanic rift networks. *J. Geophys. Res.* 101, 16155–16176.

Hetzel, R., and Hampel, A., 2005. Slip rate variations on normal faults during glacial-interglacial changes in surface loads. *Nature*, 435, 81-84.

Hilgendorf, Z., Wells, G., Larson, P., Millett, J., Kohout, M., 2020. From basins to rivers: Understanding the revitalization and significance of top-down drainage integration mechanisms in drainage basin evolution. *Geomorphology*, 352, 107020.

House, P.K., Pearthree, P.A., and Perkins, M.E., 2008. Stratigraphic evidence for the role of lake spillover in the inception of the lower Colorado River in southern Nevada and western Arizona, in: Reheis, M.C., Hershler, R. & Miller, D.M. (Eds.), *Late Cenozoic Drainage History of the Southwestern Great Basin and Lower Colorado River Region: Geological and Biotic Perspectives. Geol. Soc. of America Special Paper 439*, pp. 335-353.

Houseman, G.A., and Molnar, P., 1997. Gravitational (Rayleigh-Taylor) instability of a layer with non-linear viscosity and convective thinning of continental lithosphere. *Geophys. J. Int.*, 128, 125-150.

Huismans, R.S., Buitter, S.J.H., and Beaumont, C., 2005. Effect of plastic-viscous layering and strain softening on mode selection during lithospheric extension. *J. Geophys. Res.*, 110, B02406.

Huismans, R.S., and Beaumont, C., 2011. Depth-dependent extension, two-stage breakup and cratonic underplating at rifted margins. *Nature*, 473, 74-79.

Hunstad, I., Selvaggi, G., D'Agostino, N., England, P., Clarke, P., Pierozzi, M., 2003. Geodetic strain in peninsular Italy between 1875 and 2001. *Geophysical Research Letters*, 30, 4, 1181.

Jackson, J. and Leeder, M., 1994. Drainage Systems and the Development of Normal Faults - an Example from Pleasant Valley, Nevada. *J. Struct. Geol.*, 16, 1041–1059.

Jost, A., D. Lunt, M. Kageyama, A. Abe-Ouchi, O. Peyron, P. J. Valdes, Ramstein, G. 2005. High-resolution simulations of the last glacial maximum climate over Europe: A solution to discrepancies with continental palaeoclimatic reconstructions? *Clim. Dyn.* 24, 577–590.

Kettner, A.J., Syvitski, J.P.M., 2008. Predicting discharge and sediment flux of the Po River, Italy since the Last Glacial Maximum, in: De Boer, P.L., Postma, G., Van der Zwan, C., Burgess, P.M., Kukla, P.A.

- (Eds.), *Analogue and Numerical Forward Modelling of Sedimentary Systems: From Understanding to Prediction*. Int. Assoc. of Sedimentol. Spec. Publ. 40, pp. 171–190.
- Kooi, H., and Beaumont, C., 1996. Large-scale geomorphology: classical concepts reconciled and integrated with contemporary ideas via a surface processes model. *J. Geophys. Res.*, 101, 3361–3386.
- Larson, P.H., Dorn, R.I., Palmer, R.E., Bowles, Z., Harrison, E., Kelley, S., Schmeckle, M.W., Douglass, J., 2014. Pediment response to drainage basin evolution in south-central Arizona. *Physical Geography* 35:5, 369–389.
- Larson, P.H., Meek, N., Douglass, J., Dorn, R.I., and Seong, Y.B., 2017. How rivers get across mountains: Transverse Drainages. *Annals of the American Assoc. of Geographers* 107:2, 274–283.
- Lastoria, B., Miserocchi, F., Lanciani, A., Monacelli, G., 2008. An estimated erosion map for the Aterno-Pescara river basin. *European Water* 21-22, 29–39.
- Lavecchia, G., Brozzetti, F., Barchi, M., Menichetti, M., Keller, J.V.A., 1994. Seismotectonic zoning in east-central Italy deduced from an analysis of the Neogene to present deformations and related stress fields. *Geol. Soc. America Bull.* 106, 1107–1120.
- Lavecchia, G., Ferrarini, F., Brozzetti, F., De Nardis, R., Boncio, P., Chiaraluce, L. 2012. From surface geology to aftershock analysis: Constraints on the geometry of the L'Aquila 2009 seismogenic fault system. *Ital. J. Geosci.* 131(3), 330–347.
- Leeder, M.R., and Jackson, J.A., 1993. The Interaction between normal faulting and drainage in active extensional basins, with examples from the Western United States and Central Greece. *Basin Res.*, 5, 79–102.
- Le Pourhiet, L.L., Gurnis, M., and Saleeby, J.B., 2006. Mantle instability beneath the Sierra Nevada Mountains in California and Death Valley extension, *Earth Planet. Sci. Lett.*, 251, 104–119.
- Li, Z.-H., Liu, M., Gerya, T., 2016. Lithosphere delamination in continental collisional orogens: A systematic numerical study. *J. Geophys. Res. Solid Earth*, 121, 5186–5211, doi:10.1002/2016JB013106.
- Lin, J., and Stein, R.S., 2004. Stress triggering in thrust and subduction earthquakes, and stress interaction between the southern San Andreas and nearby thrust and strike-slip faults. *J. Geophys. Res.*, 109, B02303.
- Lin, W., and Wang, Q.C., 2006. Late Mesozoic extensional tectonics in the North China block: A crustal response to sub-continental mantle removal? *Bull. Soc. Geol. Fr.*, 177, 287–297.
- Logatchev, N.A., Zorin, Y.A., 1987. Evidence and causes of the two-stage development of the Baikal rift. *Tectonophysics*, 143, 225–234.
- Loget, N., Van Den Driessche, J., 2009. Wave train model for knickpoint migration. *Geomorphology* 106, 376–382.
- Lombardo M., Calderoni G., D'Alessandro L., Miccadei E., 2001. The Travertine Deposits of the Upper Pescara Valley (Central Abruzzi, Italy): A Clue for the Reconstruction of the Late Quaternary Palaeoenvironmental Evolution of the Area, in: Visconti G., Beniston M., Iannorelli E.D., Barba D. (Eds.), *Global Change and Protected Areas. Advances in Global Change Research*, vol 9. Springer, Dordrecht.
- Lucente F.P., Margheriti L., Piromallo C., and Barruol G., 2006. Seismic anisotropy reveals the long route of the slab through the western-central Mediterranean mantle. *Earth and Planetary Science Letters*, 241, 517–529.
- Ludovisi, A., Gaino, E., Bellezza, M., and Casadei, S., 2013. Impact of climate change on the hydrology of shallow Lake Trasimeno (Umbria, Italy): History, forecasting and management. *Aquat. Ecosyst. Health & Managem.*, 16:2, 190–197.
- Macri, P., Smedile, A., Speranza, F., Sagnotti, L., Porreca, M., Mochales, T., Russo Ermolli, E., 2016. Analysis of a 150 m sediment core from the co-seismic subsidence depocenter of the 2009 Mw = 6.1 L'Aquila earthquake (Italy): Implications for Holocene-Pleistocene tectonic subsidence rates and for the age of the seismogenic Paganica fault system. *Tectonophysics* 687, 180–194.
- Magni, V., Faccenna, C., Van Hunen, J., Funicello, F., 2014. How collision triggers backarc extension: Insight into Mediterranean style of extension from 3-D numerical models. *Geology* 42, 511–514.
- Magri, D., Di Rita, F., Palombo, M.R., 2010. An Early Pleistocene interglacial record from an intermontane basin of central Italy (Scoppito, L'Aquila). *Quat. Internat.* 225, 106–113.

- Malinverno A. and Ryan W.B.F., 1986. Extension in the Tyrrhenian Sea and shortening in the Apennines as results of arc migration driven by sinking of the lithosphere, *Tectonics*, 5, 227-245.
- Mancini, M., and Cavinato, G.P., 2005. The Middle Valley of the Tiber River, central Italy: Plio-Pleistocene fluvial and coastal sedimentation, extensional tectonics and volcanism. In: Blum, M.D., Marriott, S.B., Leclair, S.F. (Eds.), *Fluvial Sedimentology VII*, Int. Ass. Sediment. Spec. Pubs, 35; Blackwell Publishing, Oxford, pp. 373-396.
- Mancini, M., D'Anastasio, E., Barbieri, M., and De Martini, P.M., 2007. Geomorphological, paleontological and $^{87}\text{Sr}/^{86}\text{Sr}$ isotope analyses of early Pleistocene paleoshorelines to define the uplift of Central Apennines (Italy). *Quaternary Research*, 67, 487-501.
- Mancini, M., Cavuoto, G., Pandolfi, L., Petronio, C., Salari, L., and Sardella, R., 2012. Coupling basin infill history and mammal biochronology in a Pleistocene intramontane basin: The case of western L'Aquila Basin (central Apennines, Italy). *Quaternary International*, 267, 62-77.
- Maniatis, G., Kurfeß, D., Hampel, A., and Heidbach, O., 2009. Slip acceleration on normal faults due to erosion and sedimentation – Results from a new three-dimensional numerical model coupling tectonics and landscape evolution. *Earth and Planetary Science Letters*, 284, 570-582.
- Meek, N., 1989. Geomorphic and hydrologic implications of the rapid incision of Afton Canyon, Mojave Desert, California. *Geology* 17, 7-10.
- Meek, N., 2019. Episodic forward prolongation of trunk channels in the Western United States. *Geomorphology*, 340, 172-183.
- Menges, C.M., 2008. Multistage late Cenozoic evolution of the Amargosa River drainage, southwestern Nevada and eastern California, in: Reheis, M.C., Hershler, R. & Miller, D.M. (Eds.), *Late Cenozoic Drainage History of the Southwestern Great Basin and Lower Colorado River Region: Geological and Biotic Perspectives*. Geol. Soc. of America Special Paper 439, pp. 39-90.
- Merritts, D., and Ellis, M., 1994. Introduction to special section on tectonics and topography. *Journal of Geophysical Research*, 99, 12135-12141.
- Miccadei, E., Piacentini, T., and Barberi, R., 2002. Uplift and local tectonic subsidence in the evolution of intramontane basins: The example of the Sulmona basin (central Apennines, Italy). *Estratto Numero Speciale 2002*, International Workshop, University of Camerino, 119-133.
- Miccadei, E., Piacentini, T., and Buccolini, M., 2017. Long-term geomorphological evolution in the Abruzzo area, Central Italy: twenty years of research. *Geologica Carpathica*, 68, 19-28.
- Miller, K.G., Kominz, M.A., Browning, J.V., Wright, J.D., Mountain, G.S., Katz, M.E., Sugerman, P.J., Cramer, B.S., Christie-Blick, N., and Pekar, S.F., 2005. The Phanerozoic Record of Global Sea-Level Change. *Science*, 310, 1293-1298.
- Miller, M.S., Agostinetti, N.P., 2012. Insights into the evolution of the Italian lithospheric structure from S receiver function analysis. *Earth Planet. Sci. Let.*, 345-348, 49-59.
- Molnar, P., and England, P.C., 1990. Late Cenozoic uplift of mountain ranges and global climate change: chicken or egg? *Nature*, 346, 29-34.
- Molnar, P., England, P.C., and Jones, C.H., 2015. Mantle dynamics, isostasy, and the support of high terrain. *Journal of Geophysical Research: Solid Earth*, 120, 1932-1957.
- Montone, P., Mariucci, M.T., Pondrelli, S., and Amato, A., 2004. An improved stress map for Italy and surrounding regions (central Mediterranean). *J. Geophys. Res.*, 109, B10410, doi:10.1029/2003JB002703.
- Moro, M., Gori, S., Falcucci, E., Saroli, M., Galadini, F., Salvi, S., 2013. Historical earthquakes and variable kinematic behaviour of the 2009 L'Aquila seismic event (central Italy) causative fault, revealed by paleoseismological investigations. *Tectonophysics* 583, 131-144.
- Mueller, K., Kier, G., Rockwell, T., Jones, C.H., 2009. Quaternary rift flank uplift of the Peninsular Ranges in Baja and southern California by removal of mantle lithosphere. *Tectonics* 28, TC5003.
- Nicol, A., Walsh, J. J., Berryman, K. R., and Villamor, P., 2006. Interdependence of fault displacement rates and paleoearthquakes in an active rift. *Geology*, 34, 865-868.
- Nicol, A., Walsh, J. J., Villamor, P., Seebeck, H., Berryman, K. R., 2010. Normal fault interactions, paleoearthquakes and growth in an active rift. *J. Struct. Geol.*, 32, 1101-1113.

- Nicoletti, P.G., Parise, M., and Miccadei, E., 1993. The Scanno rock avalanche (Abruzzi, South-Central Italy). *Boll. Soc. Geol. It.*, 112, 523-535.
- Nocentini, M., Asti, R., Cosentino, D., Durante, F., Gliozzi, E., Macerola, L., Tallini, M., 2017. Plio-Quaternary geology of L'Aquila-Scoppito Basin (Central Italy). *J. of Maps* 13:2, 563-574.
- Nocentini, M., Cosentino, D., Spadi, M., Tallini, M., 2018. Plio-Quaternary geology of the Paganica-San Demetrio-Castelnuovo Basin (Central Italy). *J. of Maps* 14:2, 411-420.
- Okada, Y., 1992. Internal deformation due to shear and tensile faults in a half-space. *Bull. Seismol. Soc. Am.*, 82(2), 1018-1040.
- Olive, J.A., Behn, M.D., Malatesta, L.C., 2014. Modes of extensional faulting controlled by surface processes. *Geophysical Research Letters*, 41, 6725-6733.
- Palombo, M.R., Mussi, M., Agostini, S., Barbieri, M., Di Canzio, E., Di Rita, F., Fiore, I., Iacumin, P., Magri, D., Speranza, F., Tagliacozzo, A., 2010. Human peopling of Italian intramontane basins: the early Middle Pleistocene site of Pagliare di Sassa (L'Aquila, central Italy). *Quat. Internat.* 223-224, 170-178.
- Papanikolaou, I.D., Roberts, G.P., Michetti, A.M., 2005. Fault scarps and deformation rates in Lazio-Abruzzo, Central Italy: Comparison between geological fault slip-rate and GPS data. *Tectonophysics*, 408, 147-176.
- Papanikolaou, I.D., and Roberts, G.P., 2007. Geometry, kinematics and deformation rates along the active normal fault system in the southern Apennines: Implications for fault growth. *Journal of Structural Geology*, 29, 166-188.
- Patacca E., Sartori R., and Scandone P., 1990. Tyrrhenian Basin and Apenninic Arcs: Kinematic relations since late Tortonian times, *Memorie della Società Geologica d'Italia*, 45, 425-451.
- Peccerillo, A., 2005. Plio-Quaternary Volcanism in Italy. Springer, Berlin, 365 pp.
- Pechlivanidou, S., Cowie, P.A., Duclaux, G., Nixon, C.W., Gawthorpe, R.L., and Salles, T., 2019. Tipping the balance: Shifts in sediment production in an active rift setting. *Geology*, [https:// doi.org /10 .1130 /G45589.1](https://doi.org/10.1130/G45589.1).
- Petit, C., Burov, E., Déverchère, J., 1997. On the structure and mechanical behaviour of the extending lithosphere in the Baikal Rift from gravity modelling. *Earth Planet. Sc. Let.*, 1997, 29-42.
- Phillips, F.M., 2008. Geological and hydrological history of the paleo-Owens River drainage since the late Miocene, in: Reheis, M.C., Hershler, R., Miller, D.M. (Eds.), *Late Cenozoic Drainage History of the Southwestern Great Basin and Lower Colorado River Region: Geological and Biotic Perspectives*. *Geol. Soc. of America Special Paper* 439, pp. 115-150.
- Piacentini, T., Miccadei, E., 2014. The role of drainage systems and intermontane basins in the Quaternary landscape of the Central Apennines chain (Italy). *Rend. Fis. Acc. Lincei* 25, S139-S150.
- Piano Agostinetti, N., and Amato, A., 2009. Moho depth and V_p/V_s ratio in peninsular Italy from teleseismic receiver functions. *Journal of Geophysical Research*, 114, B06303.
- Pinter, N., and Brandon, M.T., 1997. How erosion builds mountains. *Scientific American*, 276, 60-66.
- Pizzi, A., 2003. Plio-Quaternary uplift rates in the outer zone of the central Apennines fold-and-thrust belt, Italy. *Quat. Internat.*, 101-102, 229-237.
- Porreca, M., Smedile, A., Speranza, F., Mochales, T., Caracciolo, F.D., Di Giulio, G., Vassallo, M., Villani, F., Nicolosi, I., Carluccio, R., Amoroso, S., Macri, P., Buratti, N., Durante, F., Tallini, M., Sagnotti, L., 2016. Geological reconstruction in the area of maximum co-seismic subsidence during the 2009 Mw=6.1 L'Aquila earthquake using geophysical and borehole data. *Ital. J. Geosci.* 135, 350-362.
- Pucci, S., Villani, F., Civico, R., Pantosti, D., Del Carlo, P., Smedile, A., DeMartini, P.M., Pons-Branchu, E., Gueli, A., 2015. Quaternary geology of the Middle Aterno Valley, 2009 L'Aquila earthquake area (Abruzzi Apennines, Italy). *J. Maps* 11:5, 689-697.
- Ramrath, A., B. Zolitschka, S. Wulf, and J. F. W. Negendank, 1999. Late Pleistocene climatic variations as recorded in two Italian maar lakes (Lago di Mezzano, Lago Grande di Monticchio). *Quat. Sci. Rev.* 18, 977-992.
- Reheis, M.C., Adams, K.D., Oviatt, C.G., Bacon, S.N., 2014. Pluvial lakes in the Great Basin of the western United States - a view from the outcrop. *Quat. Sci. Rev.* 97, 33-57.

- Repasch, M., Karlstrom, K., Heizler, M., Pecha, M., 2017. Birth and evolution of the Rio Grande fluvial system in the past 8 Ma: Progressive downward integration and the influence of tectonics, volcanism, and climate. *Earth-Science Rev.* 168, 113-164.
- Roberts, G.P., Michetti, A.M., Cowie, P.A., Morewood, N.C., and Papanikolaou, I.D., 2002. Fault slip-rate variations during crustal-scale strain localisation, central Italy. *Geophysical Research Letters*, 29, 8, 1168.
- Roberts, G. P., and Micchetti, A. M., 2004. Spatial and temporal variations in growth rates along active normal fault systems: an example from Lazio-Abruzzo, central Italy. *Journal of Structural Geology*, 26, 339-376.
- Roda-Boluda, D.C., Whittaker, A.C., 2016. Normal fault evolution and coupled landscape response: examples from the Southern Apennines, Italy. *Basin Res.* 30 (1), 186-209.
- Roda-Boluda, D.C., Whittaker, A.C., 2017. Structural and geomorphological constraints on active normal faulting and landscape evolution in Calabria, Italy. *J. Geol. Soc. London* 174, 701-720.
- Rosenbaum, G., Gasparon, M., Lucente, F.P., Peccerillo, A., Miller, M.S., 2008. Kinematics of slab tear faults during subduction segmentation and implications for Italian magmatism. *Tectonics*, 27, TC2008.
- Royden, L.H., 1993. The tectonic expression slab pull at continental convergent boundaries. *Tectonics* 12(2), 303-325.
- Ruppel, C., 1995. Extensional processes in continental lithosphere. *Journal of Geophysical Research*, 100, 24187-24215.
- Santo, A., Ascione, A., Di Crescenzo, G., Miccadei, E., Piacentini, T., Valente, E., 2014. Tectonic-geomorphological map of the middle Aterno River valley (Abruzzo, Central Italy). *J. of Maps* 10:3, 365-378.
- Schildgen, T.F., Yildirim, C., Cosentino, D., Strecker, M.R., 2014. Linking slab break-off, Hellenic trench retreat, and uplift of the Central and Eastern Anatolian plateaus. *Earth-Science Reviews*, 128, 147-168.
- Scisciani, V., Tavarnelli, E., and Calamita, F., 2002. The interaction of extensional and contractional deformations in the outer zones of the central Apennines, Italy. *J. Struct. Geol.*, 24, 1647-1658.
- Serpelloni, E., Faccenna, C., Spada, G., Dong, D., Williams, S.D.P., 2013. Vertical GPS ground motion rates in the Euro-Mediterranean region: New evidence of velocity gradients at different spatial scales along the Nubia-Eurasia plate boundary. *J. Geophys. Res.: Solid Earth* 118, 1-22.
- Smith, J., 2013. Source-to-Sink Analysis of Rift Basin Tectonics and Sedimentation. PhD thesis, Manchester University, UK, p. 193.
- Sobel, E.R., Hillel, G.E., and Strecker, M.R., 2003. Formation of internally drained contractional basins by aridity-limited bedrock incision. *J. Geophys. Res.*, 108, 25-42.
- Sobolev, P. & Rundquist, D., 1999. Seismicity of oceanic and continental rifts – a geodynamic approach. *Physics of the Earth and Planetary Interiors* 111, 253-266.
- Solonenko, V.P., 1978. Seismotectonics of the Baikal rift zone. *Tectonophysics*, 45, 61-69.
- Sornette, D., Miltenberger, P., Vanneste, C., 1994. Statistical physics of fault patterns self-organised by repeated earthquakes. *Pure and Applied Geophysics*, 142, 491-527.
- Spencer, J.E., Pearthree, P.A., 2001. Headward erosion versus closed-basin spillover as alternative causes of Neogene capture of the ancestral Colorado River by the Gulf of California. *The Colorado River: Origin and Evolution: Grand Canyon, Arizona, Grand Canyon Association Monograph*, 12, 215-219.
- Stein, R.S., King, G.C.P., and Rundle, J.B., 1988. The Growth of Geological Structures by Repeated Earthquakes 2. Field Examples of Continental Dip-Slip Faults. *J. Geophys. Res.*, 93, 13,319-13,331.
- Stock, J.D., Montgomery, D.R., 1999. Geologic constraints on bedrock river incision using the stream power law. *J. Geophys. Res.* 104, 4983-4993.
- Stokes, M., Mather, A.E., and Harvey, A.M., 2002. Quantification of river-capture-induced base-level changes and landscape development, Sorbas Basin, SE Spain. *Geol. Society, London, Special Publications*, 191, 23-35.
- Tarquini, S., Isola, I., Favalli, M., Mazzarini, F., Bisson, M., Pareschi, M.T., and Boschi, E., 2007. TINITALY/01: a new Triangular Irregular Network of Italy. *Annals Geophys.*, 50, 407-425.

- Theunissen, T., and Huisman, R.S. 2019. Long-term coupling and feedback between tectonics and surface processes during non-volcanic rifted margin formation. *Journal of Geophysical Research: Solid Earth*, 124, 12,323-12,347.
- Thieulot, C., 2011. Two- and three-dimensional numerical modelling of creeping flow for the solution of geological problems. *Phys. Earth Planet. Inter.* 188, 47–68.
- Tiberti, M.M., Orlando, L., Di Bucci, D., Bernabini, M., Parotto, M., 2005. Regional gravity anomaly map and crustal model of the Central-Southern Apennines (Italy). *Journal of Geodynamics* 40, 73-91.
- Toda, S., Stein, R.S., Richards-Dinger, K. and Bozkurt, S., 2005. Forecasting the evolution of seismicity in southern California: Animations built on earthquake stress transfer. *J. Geophys. Res.*, 110, B05S16.
- Tucker, G.E., and Hancock, G.R., 2010. Modelling landscape evolution. *Earth Surf. Process. Landforms* 35, 28-50.
- Tucker, G.E., McCoy, S.W., Whittaker, A.C., Roberts, G.P., Lancaster, S.T., Phillips, R., 2011. Geomorphic significance of postglacial bedrock scarps on normal-fault footwalls. *J. Geophys. Res.* 116, F01022.
- Turpeinen, H., Hampel, A., Karow, T., Maniatis, G., 2008. Effect of ice sheet growth and melting on the slip evolution of thrust faults. *Earth Planet. Sc. Lett.*, 269, pp. 230-241.
- Turpeinen, H., Maniatis, G., Hampel, A., 2015. Slip on normal faults induced by surface processes after the cessation of regional extension – Insights from three-dimensional numerical modelling. *Geomorphology*, 237, 79-87.
- Twidale, C. R., 2004. River patterns and their meaning. *Earth Science Reviews*, 67, 159–218.
- Van der Beek, P. and Bishop, P., 2003. Cenozoic river profile development in the Upper Lachlan catchment (SE Australia) as a test of quantitative fluvial incision models. *J. Geophys. Res.*, 108, 2309.
- Vezzani, L., Ghisetti, F.C., 1998. *Carta Geologica dell’Abruzzo: scala 1:100.000*. Selca, Firenze, Italy.
- Vezzani, L., Festa, A., Ghisetti, F.C., 2010. *Geology and Tectonic Evolution of the Central-Southern Apennines, Italy: Geol. Soc. of America Spec. Paper* 469, pp. 58.
- Walsh, J.J., and Watterson, J., 1991. Geometric and kinematic coherence and scale effects in normal fault systems. Roberts, A. M., Yielding, G., and Freeman, B. (eds), *The Geometry of Normal Faults*, Geological Society Special Publication No 56, pp 193-203.
- Wedmore, L.N.J., Faure Walker, J.P., Roberts, G.P., Sammonds, P.R., McCaffrey, K.J.W., and Cowie, P.A., 2017. A 667 year record of coseismic and interseismic Coulomb stress changes in central Italy reveals the role of fault interaction in controlling irregular earthquake recurrence intervals. *J. Geophys. Res. Solid Earth*, 122, 1-21.
- Wedmore, L.N.J., Gregory, L.C., McCaffrey, K.J.W., Goodall, H., Walters, R.J., 2019. Partitioned off-fault deformation in the 2016 Norcia Earthquake captured by differential terrestrial laser scanning. *Geophysical Research Letters*, 46, 3199-3205.
- Wegmann, K.W., Pazzaglia, F.J., 2009. Late Quaternary fluvial terraces of the Romagna and Marche Apennines, Italy: Climatic, lithologic, and tectonic controls on terrace genesis in an active orogeny. *Quat. Sci. Rev.* 28, 137–165.
- Whittaker, A.C., Cowie P.A., Attal, M., Tucker G.E. and Roberts, G.P., 2007a. Bedrock channel adjustment to tectonic forcing: Implications for predicting river incision rates. *Geology*, 35, 103-106.
- Whittaker, A.C., Cowie P.A., Attal, M., Tucker G.E. and Roberts, G.P., 2007b. Contrasting transient and steady-state rivers crossing active normal faults: new field observations from the central Apennines, Italy. *Basin Research*, 19, 529-556.
- Whittaker, A.C., Attal, M., Cowie P.A., Tucker G.E. and Roberts, G.P., 2008. Decoding temporal and spatial patterns of fault uplift using transient river long-profiles. *Geomorphology*, 100, 506–526.
- Whittaker, A.C., Attal, M., and Allen, P.A., 2010. Characterising the origin, nature and fate of sediment exported from catchments perturbed by active tectonics. *Basin Res.*, 22, 809–828.
- Whittaker, A.C., 2012. How do landscapes record tectonics and climate? *Lithosphere*, 4, 2, 160-164.
- Whittaker, A.C., Boulton, S.J., 2012. Tectonic and climatic controls on knickpoint retreat rates and landscape response times, *J. Geophys. Res.*, 117, F02024.

- Willett, S.D., 1999. Orogeny and orography: The effects of erosion on the structure of mountain belts. *Journal of Geophysical Research*, 104, 28957-28981.
- Wobus, C.W., Whipple, K. X., Kirby E., Snyder, N., Johnson, J., Spyropolou, K., Crosby, B., Sheehan, D., 2006. Tectonics from topography: Procedures, promise, pitfalls. In: *Tectonics, Climate and Landscape Evolution* Eds. S. Willett, N. Hovius, M. Brandon and D Fisher, AGU special paper 398, 55-74.
- Wortel, M.J.R., Spakman, W., 2000. Subduction and slab detachment in the Mediterranean-Carpathian region. *Science*, 290, 1910-191.
- Wu, H., Guiot, J., Brewer, S., Guo, Z., 2007. Climatic changes in Eurasia and Africa at the last glacial maximum and mid-Holocene: reconstruction from pollen data using inverse vegetation modelling. *Clim. Dyn.* 29, 211-229.
- Zanchetta, G., Bini, M., Giaccio, B., Manganelli, G., Benocci, A., Regattieri, E., Colonese, A.C., Boschi, C., Biagioni, C., 2017. Middle Pleistocene (MIS14) environmental conditions in the central Mediterranean derived from terrestrial molluscs and carbonate stable isotopes from Sulmona Basin (Italy). *Paleogeography, Palaeoclimatology, Palaeoecology* 485, 236-246.
- Zwaan, F., Scheurs, G., Adam, J., 2018. Effects of sedimentation on rift segment evolution and rift interaction in orthogonal and oblique extensional settings: Insights from analogue models analysed with 4D X-ray computed tomography and digital volume correlation techniques. *Global and Planetary Change*, 171, 110-133.

Appendix I – Supplement to Chapter 3 (Paper 1)

S1 – Elastic dislocation modelling for simulating normal faulting

We simulated vertical surface deformation in response to normal faulting using the linear elastic dislocation model within the Coulomb 3.4 package (Toda *et al.*, 2005; Lin & Stein, 2004). This model considers displacement across fault planes as edge dislocations which produce stresses and strain in an elastic half-space with uniform isotropic elastic properties (Bell, 2008; Okada, 1992). In our model we consider the vertical displacements caused by slip on a simplified version of the central Apennines fault network. Total slip along the fault planes is controlled by a scaling factor γ (*'gamma'*) between fault length and fault slip. Two other important parameters that control vertical surface displacement fields in an elastic half-space are fault dip angle (*'dip'*) and fault root depth (*'root'*). As these parameters are not always known, we tested their impact on vertical surface displacement fields using a single 30 km-long fault.

For each parameter (*gamma*, *dip*, and *root*), three values (two extremes and one intermediate value) were used that correspond to published data from the central Apennines (see Table S1). According to Roberts & Michetti (2004) dip angles vary in between 50° and 70° , and therefore we have used 50, 60 and 70° as minimum, intermediate and maximum values. For γ we have used 0.04, 0.07 and 0.10 as derived from total throw/length ratios in between 0.035 and 0.083 also provided by Roberts & Michetti (2004). Fault root depth is based on the thickness of the seismogenic layer in the central Apennines, which is estimated to be in between 12 and 18 km (Boncio *et al.*, 2009; Chiarabba & Chiodini, 2013; Cowie *et al.*, 2013) and for which we have taken 15 km as the intermediate value. Using Coulomb 3.4 we have tested the impact of varying these three parameters on the vertical surface displacement field.

Table S1 – Parameters used in the elastic dislocation model Coulomb 3.4.

Parameter	Description	Values	Units
dx, dy	grid resolution	1	km
γ (<i>'gamma'</i>)	fault displacement/ length scaling	0.04, 0.07, 0.1	–
<i>'dip'</i>	fault dip angle	50, 60, 70	°
<i>'root'</i>	fault root depth	12, 15, 18	km
ν	Poisson's ratio	0.25	–
E	Young's modulus	$8 \cdot 10^{10}$	Pa
μ	Friction coefficient	0.4	–

Figure S1 shows that γ that has the largest impact on local relief across the fault plane (Fig. S1-b). The larger the value of γ , the larger fault displacement, and so the larger the fault-related relief. An increase in dip angle also leads to more local relief, as a steeper dip angle gives higher footwall uplift (Fig. S1-c). While

fault-related relief is more sensitive to changes in γ than to changes in fault dip angle (compare Figs S1-b, c), dip angle is the only parameter that affects the uplift-subsidence ratio (u/s in Figs S1-b, c, d). We observe that the higher the dip angle, the more symmetrical the uplift-subsidence ratio. Fault root depth mainly affects the average depth of the hanging wall basins (but not their maximum depth). However, it has almost no effect on relief across the fault (Fig. S1-d). Because the intermediate scenario with $\gamma = 0.07$ produces total throws which correspond best to those estimated in the field (Roberts & Michetti, 2004), we used this surface deformation field as our standard faulting scenario in most of the experiments presented in this study (Fig. 2a in the main article). Although the minimum and maximum for γ generate less or more fault-related relief, respectively, the choice of γ value within this range does not affect the main conclusions of this study.

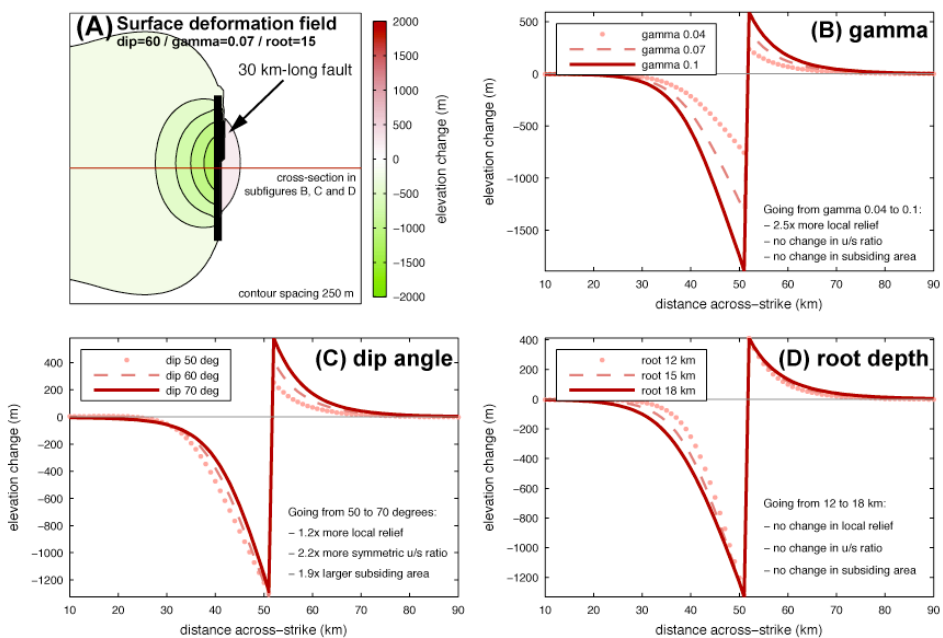


Figure S1 - Single fault experiments for exploring the impact of parameters γ , dip and $root$ on vertical surface displacement fields in Coulomb 3.4. (A) The vertical surface displacement field (in map view) produced by a single 30-km long fault, using $dip = 60^\circ$, $\gamma = 0.07$, and $root = 15$ km. The impact of different values for γ (B), dip (C), and $root$ (D) on vertical surface displacement in cross-section view.

S2 – Published data used for constraining our regional uplift function

We used four geomorphological/sedimentological markers (M1, M2, M3 and M4) for constraining our regional uplift function; a short description of each of them is provided below. These markers are from the foreland area and their localities are shown in Fig. 1b in the main article. The data described below is summarised in Table S2.

A 1.65-1.5 Ma Early Pleistocene shoreline ('M1' in Figs 1b, 2b) is continuously exposed for ca. 100 km along the Tyrrhenian side of the central Apennines (D'Agostino *et al.*, 2001; Mancini *et al.*, 2007). It has an elevation of approximately 250 ± 50 m near the centre of our study area. After correcting for sea level change, we estimate this shoreline to have been uplifted by 300 ± 80 m since its formation. Assuming uplift to have been constant over time, this shoreline provides an estimate for long-term uplift rate of 0.19 ± 0.06 mm yr⁻¹ (Table S2).

The paleoshoreline labelled 'M2' (Figs 1b, 2b) corresponds to a sea level high-stand at 125 kyr, the time of the last interglacial (MIS-5e/5.5; Ferranti *et al.*, 2006; Bordoni & Valensise, 1998). We estimated the amount of total uplift and a long-term uplift rate for 'M2', (Fig. 2b) using the same method as used for 'M1'. This shoreline is best exposed along the Tyrrhenian coast (to the West of the area shown in Fig. 1b) where it has an elevation of ca. 7-12 m at its southeast end where it is not influenced by the Latium volcanic districts. After correcting this elevation for sea level change we estimate the long-term uplift rate at the Tyrrhenian coast to be between 0-0.05 mm yr⁻¹ (Table S2).

A third estimate is provided by Sicilian (1.2-0.78 Ma) shoreface deposits ('M3' in Figs 1b, 2b), which are exposed at ca. 600-700 m on the Adriatic flank of the Maiella anticline. These sediments consist of sands and conglomerates and are organised in foresets, prograding towards the coast (Pizzi, 2003; Cantalamessa & Di Celma, 2004; Artoni, 2013). Because of poor constraints on their age and therefore a wide uncertainty range for sea level estimates, only a rough estimate for long-term average uplift rate be derived, between 0.5 and 1 mm yr⁻¹ (Table S2).

Along the central Adriatic coast there is only one MIS-5e/5.5 shoreline observation, the Fortore floodplain close to the Adriatic coastline ('M4' in Figs 1b, 2b). The floodplain has an elevation of 25 ± 3 m that suggests an average uplift rate of ca. 0.15 mm yr⁻¹ over the last ca. 125 kyr (Ferranti *et al.*, 2006; Bordoni & Valensise, 1998; Pizzi, 2003; Table S2). However, estimates of uplift rate along the central part of the Adriatic coastline are strongly variable (e.g. Cantalamessa & Di Celma, 2004; Ascione *et al.*, 2008). This is due to either i) strong spatial variability in uplift; or ii) the difficulty of dating the Pleistocene deposits in this region.

Table S2 - Data from four geomorphological/sedimentological markers (M1-M4) that we used to estimate the total amount of regional uplift and long-term averaged regional uplift rates in the Adriatic and Tyrrhenian foreland areas (Fig. 2b). References are provided in the last column. The estimated total amount of uplift is the modern-day elevation of each marker corrected for sea-level change. The long-term uplift rate is the total uplift estimate divided by the age of the marker.

Marker	Age (Ma)	Elevation today (m)	Sea-level at time of formation (m)	Estimated total uplift since formation (m)	Reconstructed long-term uplift rate (mm/yr)	References with site information
'M1' - Early Pleistocene shoreline	1.65-1.5	250±50	- 50±30 (Miller <i>et al.</i> , 2005)	300±80	0.13-0.25	D'Agostino <i>et al.</i> , 2001; Mancini <i>et al.</i> , 2007
'M2' - Last interglacial shoreline	0.125	7-12	+ 6±3 (Ferranti <i>et al.</i> , 2006)	3.5±5.5	0-0.05	Ferranti <i>et al.</i> , 2006; Bordoni & Valensise, 1998
'M3' - Sicilian shoreface deposits	1.2-0.78	650±50	- 60±40 (Miller <i>et al.</i> , 2005)	710±90	0.5-1	Pizzi, 2003; Cantalamessa & Di Selma, 2004; Artoni, 2013
'M4' - Last interglacial floodplain	0.125	25 ± 3	+ 6±3 (Ferranti <i>et al.</i> , 2006)	19±6	0.1-0.2	Ferranti <i>et al.</i> , 2006; Bordoni & Valensise, 1998

S3 – Fault-plane uplift reconstructions used for constraining our regional uplift function

In contrast to the foreland area (*Supplementary Materials S2*), it is more complicated to estimate regional uplift in the chain interior. This is because of the large impact of normal faulting and erosion in this area. A number of studies have reconstructed the pattern and amplitude of uplift by using fluvial landforms (Ascione *et al.*, 2008) or by extrapolating the peri-coastal trends in a landward direction (e.g. Pizzi, 2003). D'Agostino *et al.* (2001), on the other hand, calculated the long wavelength topography that is expected from dynamic (mantle) support based on gravity data. Whilst these separate approaches differ considerably, they all conclude that the maximum amplitude of uplift is between 800-1000 m. However, the variable approaches show marked differences in their spatial uplift patterns and lack of constraints in the highest and central portion of our model domain. Consequently, we looked for additional ways to constrain the maximum amount of uplift. For four active normal faults we estimated the amount of vertical uplift of their fault planes (Fig. S3-c). Our method relies on assumptions of the ratio of footwall uplift to hanging wall subsidence and is described below.

Hanging wall subsidence greatly exceeds footwall uplift immediately following an earthquake. However, post-seismic relaxation of the viscous-ductile lower lithosphere equalises this difference in over time. In other words, so-called uplift to subsidence ratios are initially low, typically around 1:7 or 1:8 immediately following an earthquake, but gradually increase over time during the post-seismic period. On geological time-scales uplift to subsidence ratios of 1:3 or 1:2 or even higher are observed (e.g. Stein *et al.*, 1988; Bell, 2008 and refs therein). By assuming these high uplift to-subsidence ratios for faults in the central Apennines, we are able to estimate the vertical movement of fault planes where we have both constraints on total throw of the fault, and the elevation of either the bottom or top of the (theoretical) fault plane (or footwall and hanging-wall cutoffs). The elevation of the bottom of the fault plane can be derived from the depths of fault-bounded basins. Where 'paleosurfaces' have been preserved in the footwall of a fault (i.e. erosion is believed to be negligible; Fig. S3-c and Fig. 1b in the main article), the elevation of the top of the fault plane is assumed to be equal to the height of the footwall. If we assume the pre-extensional landscape to have been close to sea level at the time extension started (see 'Geological setting' section for justification of this assumption) we can use these data to estimate the vertical movement of the fault plane. Figure S3-a explains our method, illustrated for simplicity, assuming an uplift to subsidence ratio (u/s) of 1:1.

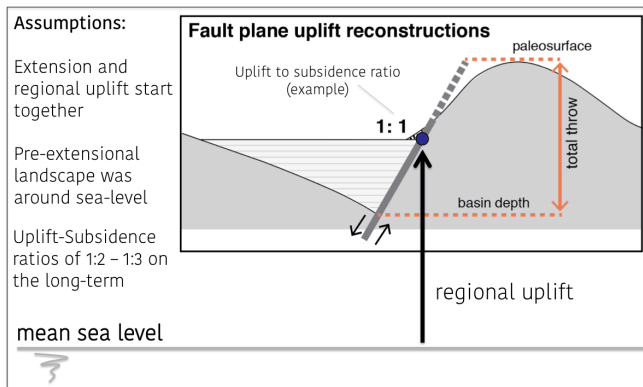


Figure S3-a - Easiest for explaining our method is to assume an uplift to subsidence ratio of 1:1 (HW subsidence equals FW uplift). This implies that the elevation of the point halfway up the fault plane represents the elevation of the surface at the time of the onset of faulting in the absence of regional uplift. However, in case of long-term regional uplift, the actual elevation of the point halfway up the fault

plane can be used to estimate the magnitude of regional uplift if some constraints exist on the initial elevation of the surface. When assuming that the central Apennines were around sea level when normal faulting initiated (e.g. Glozzi & Mazzini, 1998), this method can be used.

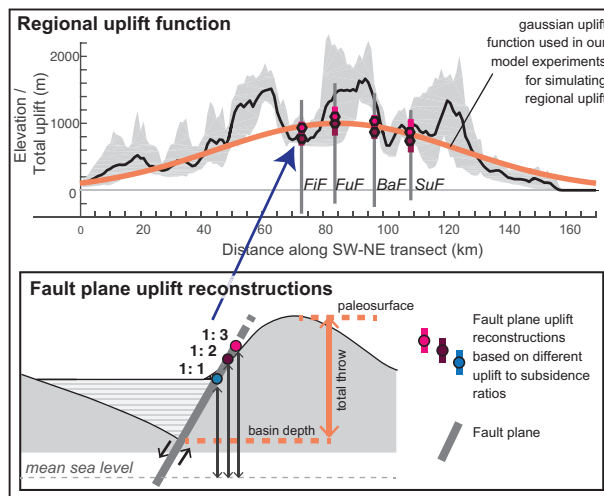


Figure S3-b - Top: Regional uplift function plotted on top of 20 km wide topographic swath (see Fig. 2b in the main article for legend). Also shown are our fault-plane uplift reconstructions for four faults assuming either a 1:2 or 1:3 uplift to subsidence ratio. Bottom: The cartoon from Fig. S3-a is shown with the addition of uplift estimates based on uplift to subsidence ratios of 1:2 and 1:3 (i.e. more realistic values than 1:1).

Figure 1b (main article) shows the localities of the four faults that we selected: the Fucino (FuF), Sulmona (SuF), Fiamignano (FiF), and Barete (BaF) faults. For all of them Roberts & Michetti (2004) provide total throw estimates (expected error <200 m). For two of them, namely the Fucino and Sulmona faults, we additionally know the depths of their basins (Cavinato *et al.* 2002; Miccadei *et al.* 2002; see Table S3). For the other two faults (Fiamignano and Barete) remnants of an old paleolandscape are observed in their footwalls. These paleosurfaces are considered to have experienced a negligible amount of erosion since the onset of extension in the region (Galadini *et al.*, 2003). Average elevations of these paleosurfaces are also given in Table S3. Assuming typical long-term uplift to subsidence ratios of 1:2 or 1:3, we calculated the likely amount of vertical uplift of the fault planes for each fault (Fig. S3-c). Although our estimates of uplift vary between ca. 750 and 1100 m (Table S3, Fig. S3-b and Fig. 2b in the main article), they are

similar or slightly higher than those suggested by other authors (e.g. Ascione *et al.*, 2008; Pizzi, 2003; D'Agostino *et al.*, 2001). From this we conclude two things: i) we believe that the similarity between our estimates and those that have previously been published justifies our method; and ii) we think that the slightly higher values of our estimates suggest that uplift experienced by the central part of our study area might be as high as 1000 m rather than the maximum of 800 m concluded by Ascione *et al.* (2008). Given that the Sangro valley studied by Ascione *et al.* (2008) lies outside the area of highest elevations, 800 m may be a minimum estimate of the uplift in the central part of our study area.

Table S3 - Data used for regional uplift reconstructions based on total throw data. Data used as input for the calculations is given in table columns 2-6 for each of the four faults defined in column 1. For two of these faults (Fucino and Sulmona) constrains on the depth of the adjacent hanging-wall basins are used. For the other two (Fiamignano and Barete) we use the elevation of paleosurfaces defined in their footwall. Assuming different uplift to subsidence ratios (1:2 and 1:3), this results in different total uplift estimates that are shown in columns 7 and 8.

Fault name	Total throw (m) (+/- 200 m)	Thickness basin-fill (m) (+/- 50 m)	Elevation basin surface (m)	Elevation basin floor (m) (+/- 50 m)	Elevation paleosurface (m) (+/- 50 m)	Total uplift (m) estimates based on two different uplift to subsidence ratios (m)	
						1:2	1:3
Fucino	1800	850	650	-200	-	1000 ± 184	1100 ± 150
Sulmona	1350	500	350	-150	-	749 ± 184	863 ± 200
Fiamignano	1700	-	-	-	1350	784 ± 117	925 ± 100
Barete	1700	-	-	-	1450	884 ± 117	1025 ± 100

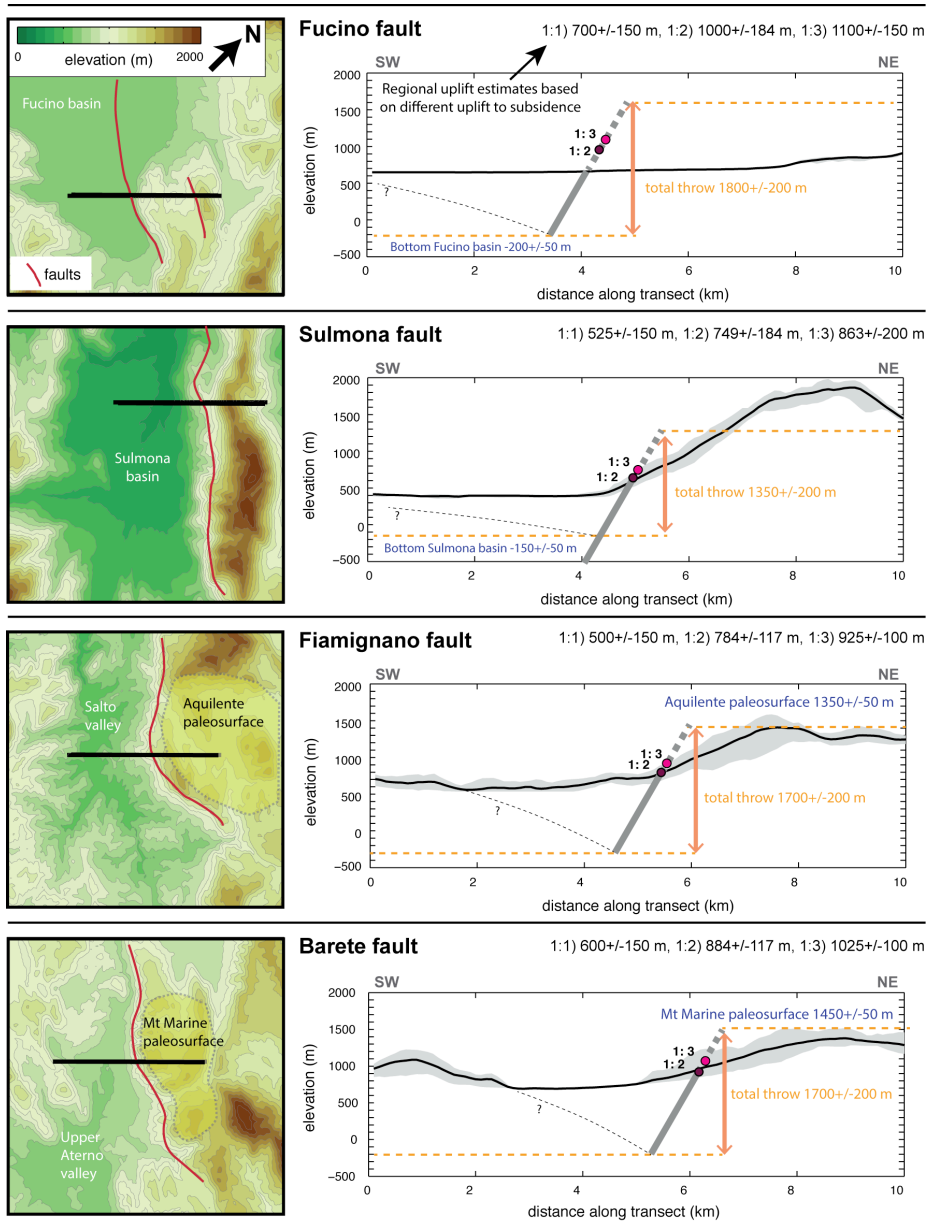


Figure S3-c – Regional uplift reconstructions for four different faults. For each fault we show a map with the fault and a 10-km long transect across them on the left. On the right we show a 5-km wide topographic swath along the transect with data used to estimate fault plane uplift over the last 3 Myr (since the onset of extension) plotted on top (see also Table S3). See Figs S3-a and S3-b for an explanation of our method for making these reconstructions.

S4 – Sensitivity analysis to erodibility parameters L_f and K_f

To test whether our findings regarding drainage integration in the central Apennines are robust, we performed a large number of experiments systematically varying the erodibility parameters K_f and L_f . Both K_f and L_f define how erosive the conditions are (e.g. both climatic and lithological effects) with higher values for K_f and lower values for L_f generating higher erosion rates and vice versa. However, as discussed in detail by Cowie *et al.* (2006), L_f additionally controls the way in which rivers respond to changes in base level, either in a more transport-limited or in a more detachment-limited manner (higher L_f values produce a more detachment-limited response). In our model setup we found that values in between 0.08 and 0.12 for K_f and values in between 30 and 70 km for L_f produce a realistic landscape evolution in the sense that at least some fluvial incision occurred (the most resistant end of the spectrum) and at least some topography was left after 3 Myr (the most erosive end of the spectrum). Within these ranges we show the final topography for nine different experiments in Fig. S4-a, including our reference model ('standard run', using $K_f = 0.10$ and $L_f = 50$ km) that is presented and discussed in the article. Importantly, even though the final topography after 3 Myr is very different when using different values for K_f and L_f (Fig. S4-a), the primary difference is due to the rate at which the landscape develops. Crucially, the main trend of landscape evolution and drainage integration that is described in the main text is robust.

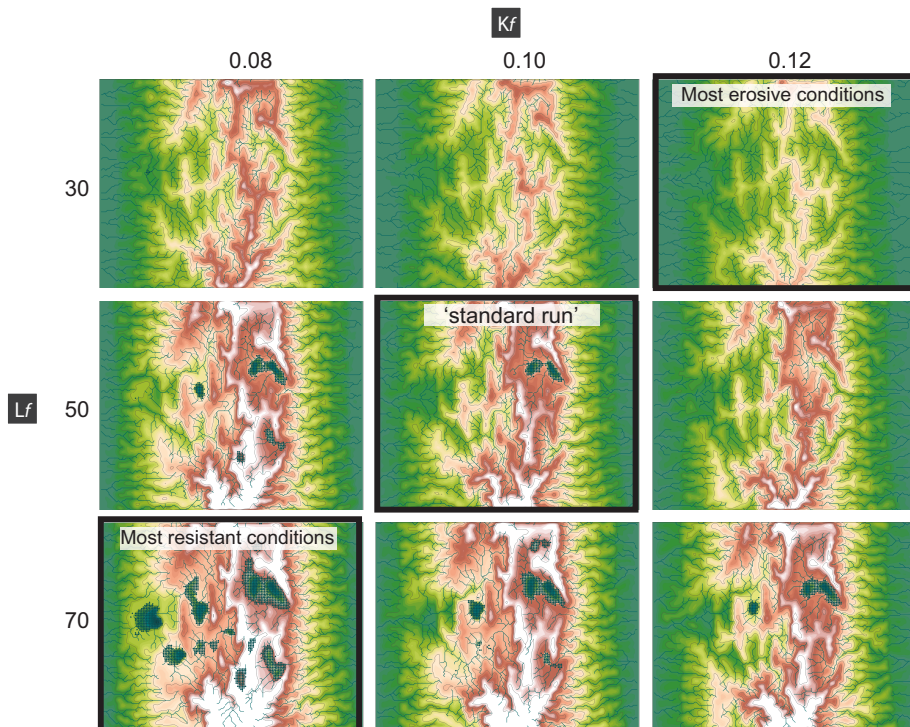


Figure S4-a – Final topography (after 3 Myr) for 9 experiments with different values for L_f and K_f .

In all our experiments overspill (basin overflowing or lake overspill) is the dominant mechanism driving drainage integration. The long-term trend of landscape evolution is shown in Fig. S4-b where we compare our reference model ($K_f = 0.10$ and $L_f = 50$ km) with our most erosive experiment ($K_f = 0.12$ and $L_f = 30$ km) and our most resistant experiment ($K_f = 0.08$ and $L_f = 70$ km). These diagrams show that under a wide range of conditions drainage integration occurs. The only difference is the rate at which lakes disappear over time and that endorheic areas shrink. The integrated (mainly published) field observations provide the constraints that lead to the choice of parameters used for the reference model shown in the main paper.

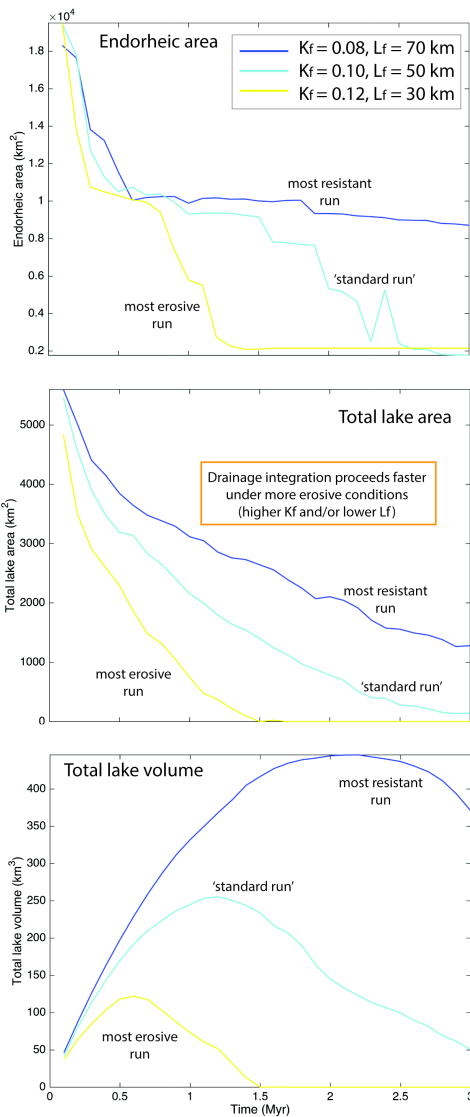


Figure S4-b – Temporal evolution for 3 different experiments (two end-members and our reference model ('standard run'), see Fig. S4-a) and three different indicators for drainage integration (endorheic area, total lake area, total lake volume). All runs show similar trends, despite proceeding at different rates.

S5 – Endorheic versus Non-endorheic type of drainage in CASCADE

An important aspect of our modelling study is what happens to the water in our surface process model CASCADE when it enters a local topographic minimum. We tested two scenarios: Endorheic drainage, where water is lost to the system after it reaches a lake, and non-endorheic drainage where 100% of water is conserved in the system all the way to the coast. Note that non-endorheic drainage is assumed in the original publication by Braun & Sambridge (1997). We discuss the arguments for assuming that truly endorheic drainage occurs in the central Apennines in the main article, but one of the key arguments is that lakes do not need an outlet but can maintain their water balance through evaporation and perhaps seepage (including karst). Moreover, in Fig. S5 we demonstrate that the characteristic topographic features of the central Apennines (Fig. 10 in the main article) and the existence of lakes for considerable amount of time can only be reproduced by means of endorheic type of drainage.

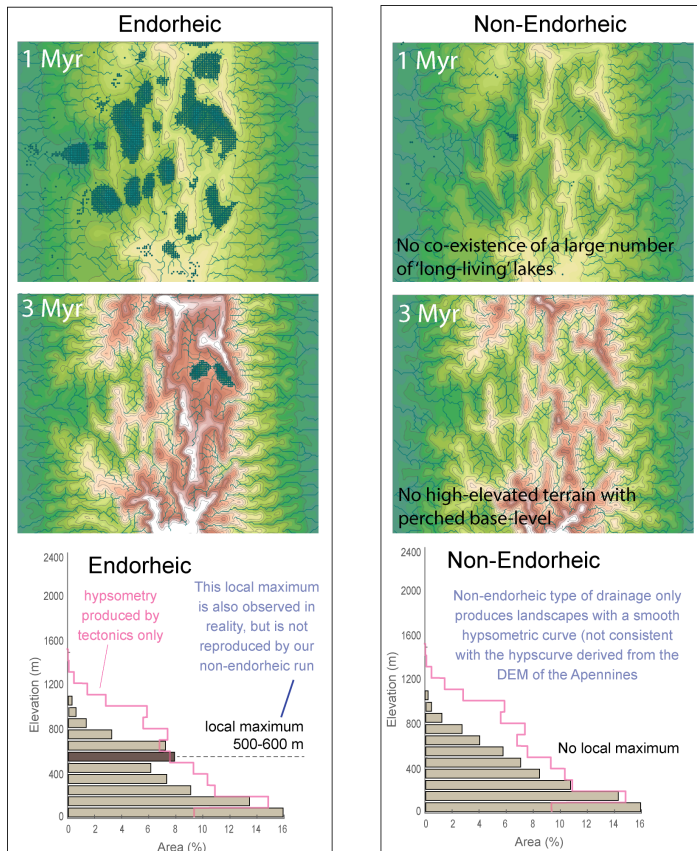


Figure S5 – Left side of the figure shows the topography after 1 Myr, the topography after 3 Myr, and the hypsometric curve of the final topography for our reference model that uses a truly endorheic type of drainage. Right hand side of the figure provides the same figures for our non-endorheic run (water 100% conserved). Comparing both experiments with the real system (e.g. Fig. 10 in the main article) shows that characteristic topographic features and widespread lake occurrence are only reproduced when using the endorheic type of drainage.

S6 – River profile concavity

In our reference model ($K_f = 0.10$ and $L_f = 50$ km) a steady state is reached after approximately 6 to 9 Myr model time. We analysed the river longitudinal profile concavities of major streams for the 9 Myr model output. The concavity varies in between ca. 0.35 and 0.6 for the large rivers penetrating into the faulted domain (e.g. streams A1-A3 in Fig. S6) which corresponds well with the concavity that is commonly observed for rivers in steady state. However, the concavity is significantly higher, namely in between ca. 0.7-0.9, for those streams crossing the mountain flanks and foreland areas only (e.g. streams B1-B4 in Fig. S6). These high concavity values can be explained by our gaussian regional uplift function (Fig. 2b in the main article) that generates progressively higher uplift rates in a landward direction. However, we do not expect these higher concavities to affect our main conclusions. We also checked the steady state (intrinsic) concavity in a block-uplift experiment (using the same values for K_f and L_f and an uniform uplift rate of 0.16 mm/yr) and these varied in between ca. 0.4 and 0.7.

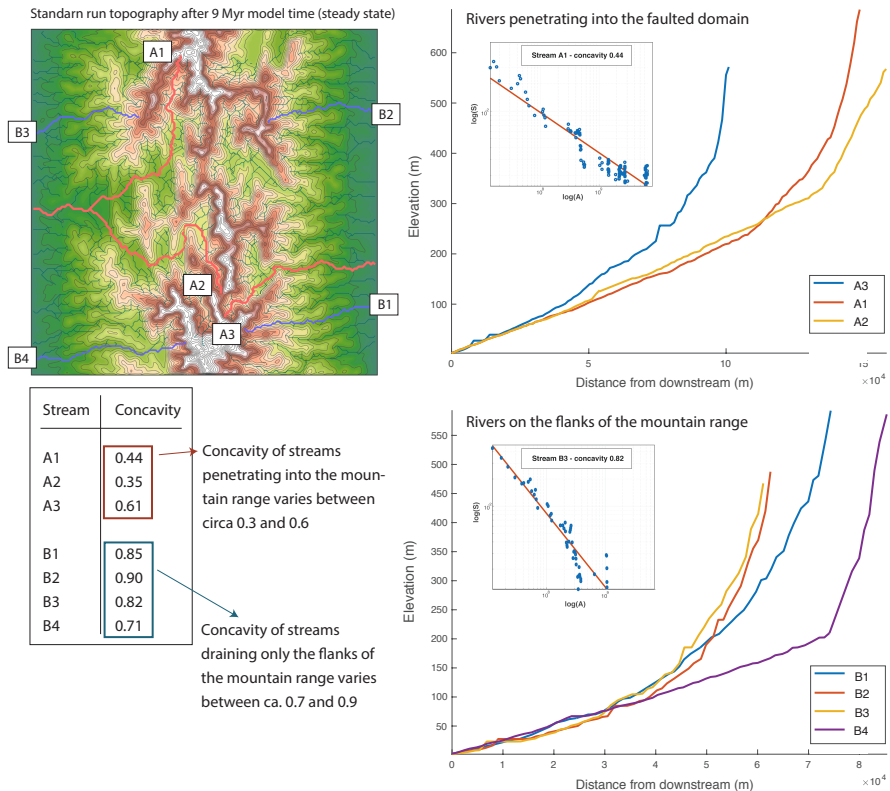


Fig. S6 – Steady state (9 Myr) topography produced by our reference model run (top left). For a few large streams (A1-A3, B1-B4) we show their longitudinal profiles on the right hand side. The inset figures show logarithmic slope-drainage area plots that we used for calculating concavities. The concavities are provided in the table in the bottom-left.

S7 – Asymmetric uplift experiment

Regional uplift in most of our model experiments is simulated by means of the symmetric uplift function shown in Fig. 2b in the main article (see also the orange curve in Fig. S7-a). However, some studies suggest the regional uplift pattern to be asymmetric (e.g. Pizzi, 2003), similar to the blue curve shown in Fig. S7-a. For evaluating the impact of the regional uplift pattern we performed an experiment in which the regional uplift is represented by an asymmetric uplift function (the blue line shown in Fig. S7-a). In figure S7-b we compare the final (3 Myr) landscape characteristics of our symmetric-uplift experiment (reference model) and our asymmetric-uplift experiment. While both experiments produce a distinctly different final topography and drainage network, the overall trend in landscape evolution is similar. Both experiments lead to the progressive fluvial integration of basins, however, the order of integration and the final drainage patterns differ. Importantly, figure S7-b clearly shows the important role of the regional uplift field in controlling the position of the main drainage divide between the Tyrrhenian and Adriatic domains. The asymmetric function produces a drainage divide and drainage pattern that differs considerably from the present-day reality.

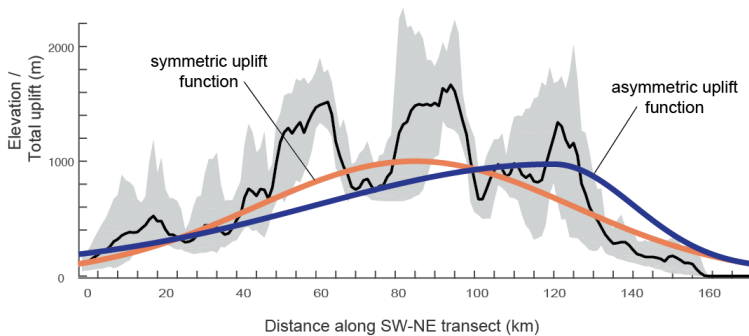
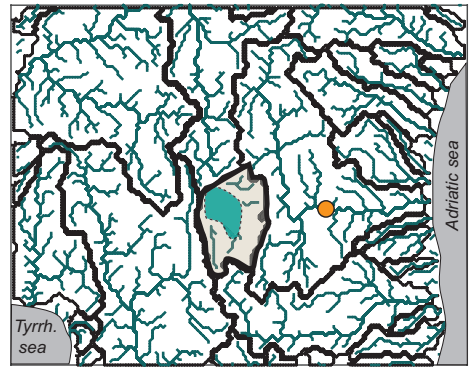
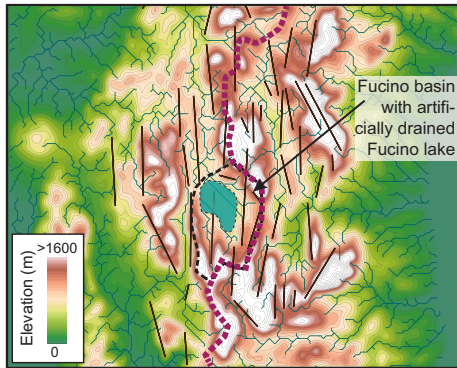
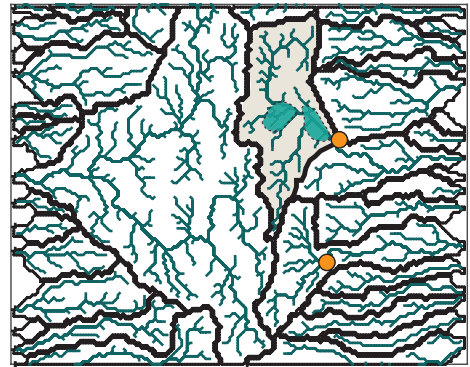
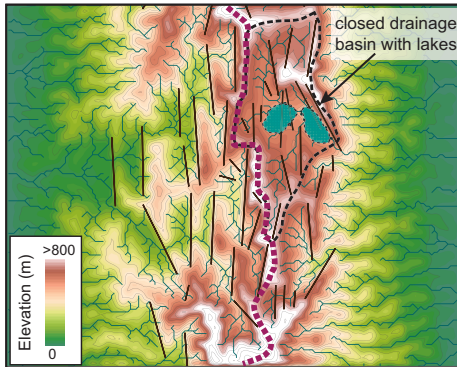


Figure S7-a – Uplift functions and topography in the central Apennines. The asymmetric uplift function (blue line) is plotted on top of NE-SW topographic swath across the central Apennines. Also shown is the symmetric uplift function (orange line) used in the reference model.

DEM Apennines



SYMMETRIC uplift



ASYMMETRIC uplift

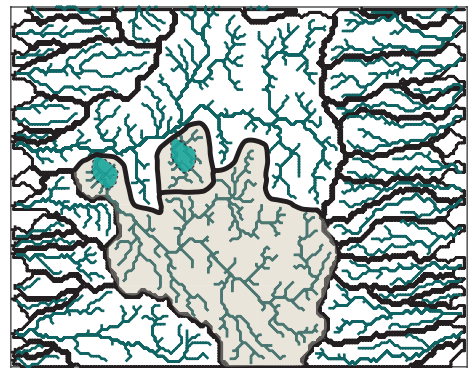
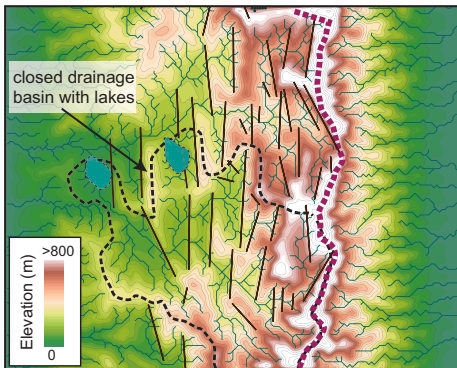


Figure S7-b – Comparing output from our asymmetric uplift experiment (2 figures at the bottom) with our reference model (symmetric uplift; 2 figures in the middle) and the DEM and drainage network of the central Apennines (2 figures at the top). On the left we show elevation, stream network, lakes, central drainage divide and the endorheic area (for legend see Fig. 3 in the main article). On the right we show the lakes, stream network, catchment geometry, endorheic area, and fluvial 'exit points' on the Adriatic side of the mountain range (orange dots).

S8 – Fault slip acceleration experiment

In most of our experiments we assume fault slip rates to be constant in time. However, as strong evidence exists that many faults in the central Apennines experienced an increase in fault slip around 1-0.5 Ma (e.g. Roberts & Michetti, 2004; Cowie & Roberts, 2001; Whittaker *et al.*, 2008) we describe here briefly the results of a fault-slip-acceleration experiment in which we increased fault slip after 2 Myr model time. Figure S8-a shows how throw accumulates over time in both our fault-slip-acceleration experiment and all our other experiments (in which fault slip rate is constant).

Long-term landscape evolution in our fault-slip-acceleration experiment follows a similar trend as in our standard series of experiments, i.e. a similar topographic development, a similar drainage network evolution, a similar long-term trend from internal to external drainage and similar patterns of sediment dispersal. However, the only major impact of fault slip acceleration is that the landscape evolution trend becomes temporally reversed when fault slip rates accelerate, i.e. after 2 Myr model time in our experiment. Because an increase of fault slip rates abruptly increases accommodation space in the subsiding basins, those basins that had previously become externally drained, now become internally drained again. In our model this is shown by the reappearance of lakes. However, this reversed trend is a transient feature, lasting only for ca. 200.000 yr model time (Fig. S8-b). After that time, erosion rates adapt to the enhanced rate at which fault-related relief is produced, and the progressive overfilling of basins and the progressive disappearance of lakes resumes (Fig. S8-b).

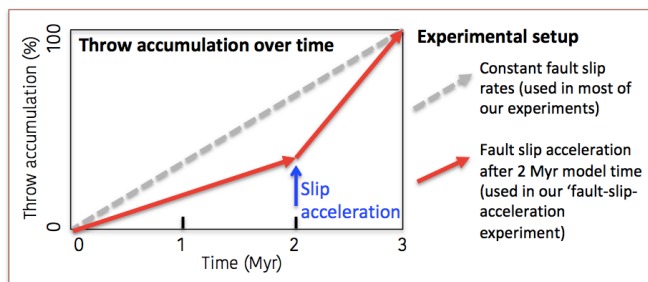


Figure S8-a – Throw accumulation over time in our fault-slip-acceleration experiment (red lines) and all our other experiments discussed in the main article text (grey dashed line). The total throw at the end of the experiments is equal in both scenarios.

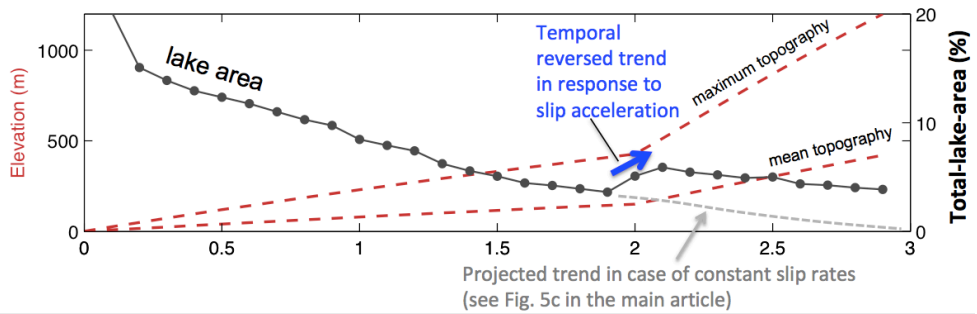


Figure S8-b – Total surface area occupied by lakes (as a percentage of the total model domain) in our fault-slip-acceleration experiment (grey curve). It shows that the long-term trend of lake disappearance becomes temporally reversed in response to an increase of fault slip rates along (all) the faults in our model. In case of constant slip rates these kind of transient reversals are absent (see Fig. 5c in the main article). However, this reversal trend is a transient feature (lasting only 100-200 kyr) as the total-lake-area starts to decline again from 2.1 Myr model time onwards. This is because the increase in fault slip rates causes an abrupt increase in the rate at which fault-related relief is produced (reflected by the mean and maximum topography curves in the diagram), which leads to an increase in erosion rates. Enhanced erosion rates, in turn, lead to an increase in sediment supply to the tectonic basins and to their progressive overfilling over time.

Appendix II – Supplement to Chapter 4 (Paper 2)

A) – Fluvial terrace morphology and the ‘endorheic-exorheic contact’

In many basins along the Aterno River we observe depositional terraces with top elevations ca. 30-150 m above the river thalweg and which seem to relate at least partly to the step-wise integration of the drainage network. These depositional terraces were formed when a long phase of predominantly aggradation in a closed basin became replaced by fluvial incision following drainage integration. Because of differences in local conditions and the timing of drainage integration between the different basins, we observe considerable variability in the ages and sedimentological characteristics of these terraces. These prominent terraces also form the upper limit of the basin fills (see Fig. 4A in the main article) and their top elevations were estimated using the approach illustrated in figure A.1 - we attempted to use only depositional terraces whose elevation relative to the Aterno River was not expected to be significantly affected by normal faulting. In figure A.2 we show the locality of the terrace remnants that we focussed on and we shortly describe their age, sedimentological characteristics and top elevation below.

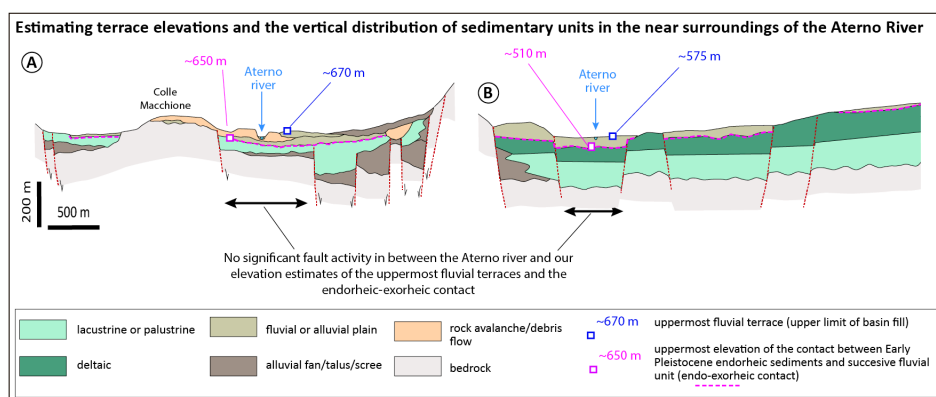


Fig. A.1. Cartoon showing our approach of selecting the area surrounding the Aterno River that is the least affected by normal fault activity. Within this area, we selected depositional terraces for constraining the upper limits of the different basin fills, and used the endorheic-exorheic contact for estimating the upper limits of the endorheic sediment and the amount of incision that occurred following drainage integration.

For the four southernmost basins, i.e. the ASB, PSD, LAS and SUL basins, cross-sections are available that provide information on their stratigraphic build-up (see Fig. 7 in the main article). In these cross-sections we identified the position of the ‘endorheic-exorheic’ contact that is located in between the endorheic (lacustrine/palustrine/deltaic) unit and the first fluvial sedimentary unit formed after drainage integration. Because drainage integration is generally followed by fluvial incision, the endorheic-exorheic contact is generally an erosional unconformity. Based on the uppermost occurrence of endorheic

sediment (and this erosional unconformity) in Fig. 7 (in the main article) we estimated the upper limit of the endorheic basin fill, which provides a minimum estimate (see also Fig. A.1 and Figs. 4A and 6 in the main article). We used the maximum amount of relief in the endorheic-exorheic contact to estimate the minimum amount of incision that occurred directly following drainage integration (see Fig. A.1 and Fig. 7 in the main article).

Monte Reale basin (MTR) – The highest fluvial depositional surface that we identified in the MTR basin is the active (Holocene) plain of the Aterno River at ca. 815 m elevation (Fig. A.1-A). This alluvial plain consists primarily of floodplain clay and silt and extends across most of the basin (Chiarini et al., 2014). Large alluvial fan systems of Early to Late Pleistocene age are identified along the footwalls of the main basin bounding faults and extend into the subsurface beneath the active plain (Chiarini et al., 2014). Chiarini et al., (2014) reconstructed a long-term Pleistocene trend of progressive incision for the MTR basin based on relict surfaces carved into the bedrock surrounding the active MTR plain, what may imply that 200-300 m of Pleistocene sediment has been removed from the MTR basin. However, because the character (depositional or erosional), origin and age of these relict surfaces are poorly constrained we used 815 m as the upper limit of the sedimentary infill in figure 4A in the main article.

Barete-Pizzoli basin (BPZ) – Pronounced terrace morphology borders the active floodplain of the Aterno River in the BPZ basin. However, the number of terraces, their characteristics and their ages are poorly constrained (Bosi et al., 2004; Piacentini and Miccadei, 2014). Moreover, the elevations of the terrace tops relative to the active riverbed seem to vary along the Aterno River, likely as a consequence of fault activity (Fig. A.2-B). All three terrace surfaces that we marked in figure A.2-B are labelled by Bosi et al., (2004) as depositional surfaces of units consisting of fluvial gravels and silts of most likely Early Pleistocene age. In the central part of the basin, i.e. in the area between the fluvial terraces marked in figure A.2-B, basin subsidence rates are highest and here the terraces surrounding the Aterno River have lower elevations and are expected to be not older than Late Pleistocene-Holocene. Overall, it is important to note that the upper limit of the sedimentary infill in the BPZ as shown in Fig. 4A in the main article is poorly constrained and should only be looked upon as a first order approximation.

L'Aquila-Scoppito-Bazzano basin (ASB) – In the ASB basin upstream of L'Aquila we identified 2 depositional terrace surfaces that together comprise the highest terrace level in this area (at ca. 650-670 m elevation; Fig. A.2-B). Both terrace remnants consist of fluvial gravels and overbank silts (called the *Fosso Vetoio Synthem* according to Nocentini et al., 2017) which were deposited most likely during the very early part of the Late Pleistocene and partly overly late Middle Pleistocene rock avalanche deposits in the Colle Macchione area (see Fig. 3A and cross-section A in Fig. 7 in the main article; Nocentini et al., 2017). The thalweg of the Aterno River lies 20-25 m below the top of this terrace level. In the area of the ASB basin downstream of L'Aquila, on the other hand, the situation is very different. Here the Aterno River has a wide active plain (at ca. 590 m elevation) that is bordered by at least one higher terrace surface at ca. 625 m elevation along the basin margin (Fig. A.2-B). These terraces are made of Early Pleistocene lacustrine sediment belonging to the *Madonna della Strada Synthem* according to Nocentini et al. (2017). However, based on the available data, we cannot exclude this terrace to be affected by normal fault

activity and therefore we used 590 m, i.e. the elevation of the active floodplain, as the upper limit of the sedimentary infill in Fig. 4A in the main article. This gives a difference of 50-100 m in the elevation of the upper limit of the sedimentary infill between the areas upstream and downstream of L'Aquila. However, we can explain such a difference by the 50-100 m thick rock avalanche deposits near L'Aquila (see cross-section B in Fig. 7 in the main article). Based on the spatial extent of this unit we argue that it temporarily blocked the Aterno River during the Middle Pleistocene and enhanced fluvial sedimentation (*Fosso Vetoio synthem* according to Nocentini et al., 2017) in the upstream part of the ASB basin. As soon as sedimentation overtopped these rock avalanche deposits, the Aterno River likely started to incise into these avalanche deposits and into the fluvial sediment upstream.

Paganica-San Demetrio basin (PSD) – Fluvial terraces have been described for the PSD basin (e.g. Santo et al., 2014). However, we believe that in most parts of the basin the terrace morphology can largely be explained by normal fault activity (see Fig. A.2-C and cross-section D in Fig. 7). Therefore, we only have an estimate of ca. 575 m elevation for the area upstream of San Demetrio which is the elevation of the active floodplain of the Aterno River. In the area downstream of San Demetrio we expect some of the terrace morphology with elevations of the order of 550-600 m to be at least partly related to the upstream propagating knickpoint (Fig. 4A in the main article).

Lower Aterno-Subequana basin (LAS) – The Aterno River is bordered by prominent terraces along both sides in the LAS basin (Fig. A.2-D; Fig. 5A in the main article). Even though we expect these high terraces all to be associated with drainage integration, their top elevation varies considerably along the Aterno River, i.e. between ca. 550 and 600 m. We can explain this variability by spatial differences in the thickness of alluvial fan and mass-wasting deposits and by spatial differences in fault activity. Even though we marked quite extensive terrace surfaces in Fig. A.2-D, we primarily estimated the elevation of these terraces based on the elevation of the break in slope along the terrace edges (closest to the Aterno River).

Sulmona basin (SUL) – The highest fluvial terrace in the SUL basin is the so-called '*Terraza Alta di Sulmona*'. In the central part of the basin, i.e., furthest away from alluvial fan systems along the basin margins, this terrace has a top elevation of the order of ca. 400 m (Fig. A.2-D; cross-section G in Fig. 7 in the main article). The uppermost ca. 50 m of this terrace comprises fluvial gravel that was deposited between ca. 530 and 135 ka. Underneath the fluvial gravel lies fine-grained lacustrine sediment that dates back to the time period before drainage integration occurred, i.e. before ca. 650 ka.

Figure A.2 (Next page). Detailed topographic maps (10 m DEM and hillshade) of (A) the MTR basin, (B) the BPZ and ASB basins, (C) the PSD basin, and (D) parts of the LAS and SUL basins. All maps show the active normal faults (based on Roberts and Michetti (2004) and Nocentini et al. (2018)), and the fluvial terraces that were used for estimating the highest occurrence of basin sediment.

B) – Sedimentation rate estimates

For the Early(-to-Middle) Pleistocene lacustrine units from the L'Aquila-Scoppito-Bazzano (ASB), Paganica-San Demetrio (PSD), Lower Aterno-Subequana (LAS) and Sulmona (SUL) basins we calculated long-term average sedimentation rates based on the thickness of these units and constraints on the time period during which they were formed (see table below). Thereby we assumed lacustrine sedimentation to have started ca. 3 Ma (Cosentino et al., 2017). The sediment thicknesses were extracted from the available stratigraphic cross-sections (Fig. 7 in the main article), but also from descriptions of the different units from the relevant literature (e.g. Miccadei et al., 2002; Mancini et al., 2012; Giaccio et al., 2012; Pucci et al., 2015; Nocentini et al., 2017, 2018). These values give minimum long-term average sedimentation rates in the order of **0.10-0.17 mm yr⁻¹** that we used in figure 9 in the main article.

	Timing of drainage integration (Ma)	(Minimum preserved) thickness endorheic (lacustrine) sediments (m)	(Minimum) sedimentation rate during endorheic phase (mm/yr)
Monte reale (MTR) Chiarini et al., 2014	Poorly constrained, most likely late Early Pleistocene or early Middle Pleistocene	~100 m in eastern sub-basin	~0.04-0.05 in case we assume drainage integration to have occurred sometime between 1.2 - 0.7 Ma
Barete-Pizzoli (BPZ) Bosi et al., 2004	Poorly constrained, sometime during the Early Pleistocene	Unconstrained	Unconstrained
L'Aquila-Scoppito-Bazzano (ASB) Nocentini et al., 2017	~1.2-1.1 Ma	~200-250 m	0.10-0.14
Paganica-San Demetrio (PSD) Santo et al., 2014; Pucci et al., 2015; Nocentini et al., 2018	~0.7 Ma	~400 m	~0.17
Lower Aterno-Subequana (LAS) Gori et al., 2015, 2017	~0.8-0.7 Ma	~300-350 m	0.13-0.16
Sulmona (SUL) Miccadei et al., 2002 Giaccio et al., 2009, 2013; Zanchetta et al., 2017	~0.65 Ma	~350-400 m (?), the depth of the bottom of the endorheic unit is uncertain (Miccadei et al., 2002)	0.15-0.17

C) – Landscape response time calculations

As we explain in the main article, the large convex reach along the Aterno longitudinal profile upstream of the Sulmona basin and San Venanzio gorge was likely formed because of drainage integration between the Lower Aterno-Subequana basin and the Sulmona basin, around 0.7 Ma (Fig. 4A-C in the main article). For this convex reach we calculated how fast its upper limit (what we call the knickpoint) has been propagating upstream since drainage integration occurred. Assuming that the knickpoint has an elevation of ca. 550-575 m, provided convex reach lengths of ca. 30-35 km. These distances give an average knickpoint migration rate C_E of the order of **43-50 mm yr⁻¹**. Because this migration rate depends on the distribution of drainage area upstream of the knickpoint, we normalised it by the square root of drainage area A following the approach of Whittaker and Boulton (2012):

$$\psi_A = \frac{C_E}{\sqrt{A}} \quad \text{Eq. D-1}$$

By assuming a unit stream power model, this equation provides a normalised knickpoint migration rate parameter ψ_A of **1.4-1.7 · 10⁻⁶ yr⁻¹**. Hereby A is the drainage area upstream of the knickpoint, which is 850-950 km², depending on whether we assume a knickpoint elevation of 550 or 575 m. We extracted A from the DEM-derived drainage network (shown in Fig. 4B in the main article).

Then, we used this normalised knickpoint migration parameter to estimate the total time t_E it takes for this knickpoint to reach the headwaters of the Aterno River. Therefore we calculated the knickpoint migration rate at each point along the full length of the Aterno River upstream of this knickpoint $(C_E)_i$ using the area upstream of this point A_i . Therefore we extracted drainage area A and distance L data from the longitudinal profile derived from the 10 m resolution DEM (Tarquini et al., 2007; Fig. 4A in the main article).

$$(C_E)_i = \psi_A \cdot \sqrt{A_i} \quad \text{Eq. D-2}$$

For each small increment in distance upstream of the knickpoint we calculated how much time it takes for the knickpoint to propagate across this distance dx_i . By summing all these short time intervals for the full length of the river upstream of the knickpoint L we retrieved the total time period it takes for the knickpoint to reach the headwaters of the river.

$$t_E = \sum_{i=0}^L \frac{dx_i}{(C_E)_i} \quad \text{Eq. D-3}$$

Using this approach we estimate that a time period of ca. **2.5-3.1 Myr** is required for the 'San Venanzio knickpoint' to reach the headwaters of the Aterno river (ca. 5 km distance from the drainage divide).

Appendix III – Supplement to Chapter 5 (Paper 3)

Appendix A – Methodology

The table below shows the model parameter values that we used in our reference model (see also Fig. 2 in the main article). For model description, see main article text.

Table A-1) Model parameter values:

Parameter	Symbol	Value
Rheological parameters Wet Quartz (Gleason and Tullis, 1995) - Upper crust, lower crust, fault zones		
Reference density (at T = 0°C)	ρ	2800 kg · m ⁻³
Power law exponent	n	4.0
Activation energy	Q	222.815 · 10 ³ J · mol ⁻¹
Activation volume	V	3.1 · 10 ⁻⁶ m ³ · mol ⁻¹
Pre-exponential scaling factor	A	8.574 · 10 ⁻²⁸ Pa ⁻ⁿ · s ⁻¹
Crustal scaling factor	f_c	1
Heat capacity	C_p	803.5
Thermal conductivity	k	2.25 · 10 ⁻⁶ m ² · s ⁻¹
Heat productivity	H	0.846 · 10 ⁻⁶ W · m ⁻³
Rheological parameters Wet Olivine (Karato and Wu, 1993) – Mantle lithosphere, weak mantle lithosphere, sub-lithospheric mantle		
Reference density (at T = 0°C)	ρ	3300 kg · m ⁻³
Power law exponent	n	3.0
Activation energy	Q	429.83 · 10 ³ J · mol ⁻¹
Activation volume	V	15 · 10 ⁻⁶ m ³ · mol ⁻¹
Pre-exponential scaling factor	A	1.393 · 10 ⁻¹⁴ Pa ⁻ⁿ · s ⁻¹
Mantle lithosphere scaling factor	f_{mt}	5
Sublithospheric mantle scaling factor	f_{slm}	1
Weak mantle lithosphere scaling factor	f_{wml}	0.02
Heat capacity	C_p	681.82
Thermal conductivity	k	2.25 · 10 ⁻⁶ m ² · s ⁻¹
Heat productivity	H	0
Other rheological parameters		
Angle of internal friction	$\phi(\varepsilon)$	15°
Cohesion	C	20 · 10 ⁶ Pa
Universal gas constant	R	8.3144 J · mol ⁻¹ · °C ⁻¹
Initial and Boundary conditions		
Surface temperature	T_0	0°C
Initial LAB temperature	T_l	1330°C
Model base temperature	T_b	1520°C
Initial thermal anomaly at LAB		200 x 15 km
Crustal thickness		35 km
Base of mantle lithosphere		125 km
Extension velocity	v_e	3 mm · yr ⁻¹ (in total for both boundaries)
Top boundary condition		Stress free surface
Side boundary condition		Free slip, normal velocity = $v_e/2$
Basal boundary condition		Free slip, zero normal velocity
Model resolution		500 x 500 m in the upper crust

Fault extension rates & fault plane elevation

We used the Lagrangian grid output from our models to estimate the amount of extension across each fault zone at approximately 600 m below the surface (see Fig. A-1). For every 2000 year of model output, we track the distance between two grid points located in either the hanging- or footwall of each fault. While the fault zones are only 1.5 km wide, we took grid points at initially 6 km distance from one another to be certain that all the deformation related to fault activity was included. Figure A-1 shows the deformation of the Lagrangian grid for one of our thermo-mechanical models with symmetric fault geometry (TM-2; see Appendix B). As examples, we also zoom-in to two faults (faults 2 and 6) with very different amounts of deformation, showing the two grid points for which we tracked their coordinates through time.

We used the vertical coordinates of the same Lagrangian grid points as metrics for the elevation of the hanging- and footwalls of each fault. Because the elevation of these grid points is not only affected by movement along the fault plane, but also by regional uplift and block rotation, we additionally also analysed changes in their average elevation ('midpoint elevation, see Fig. 2 in the main article).

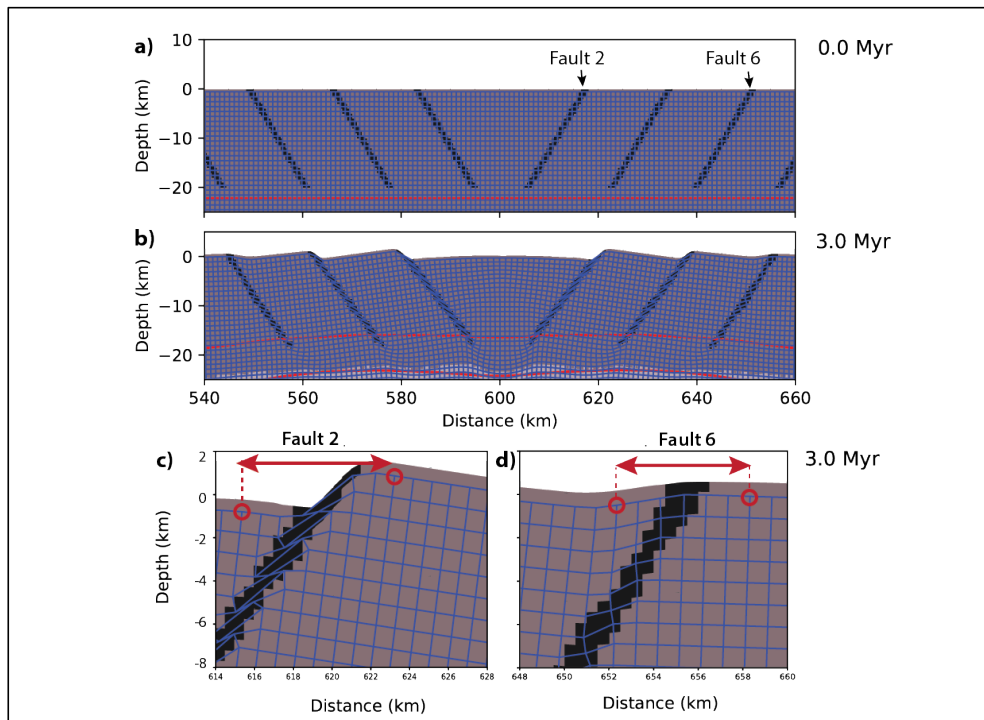


Fig. A-1) Example of Lagrangian grid output from model TM-2, at the onset of the experiment (a) and after 3 Myr (b,c,d). For faults 2 and 6 we show in more detail how the grid looks like after 3 Myr in (c) and (d). These figures show that the grid is strongly extended across fault 2 (c) but almost no extension has occurred across fault 6 (d).

Isostatically compensated topography

We calculated the isostatically compensated topography of our reference model as follows. First we integrated the density field down to the base of the mantle lithosphere, i.e., down to 125 km depth, and subtracted the weight of each column from the weight of a reference column (we took a column at 40 km distance from model boundaries) in order to get the 'residual mass'. Assuming that the residual mass is extra crustal material added to the top of our crust and assuming a crustal density of 2800 kg/m³, we calculated the amount of residual topography for each 500 m column in our model. Finally, we subtracted the residual topography from the actual topography in order to get the isostatic topography (see Fig. A-2).

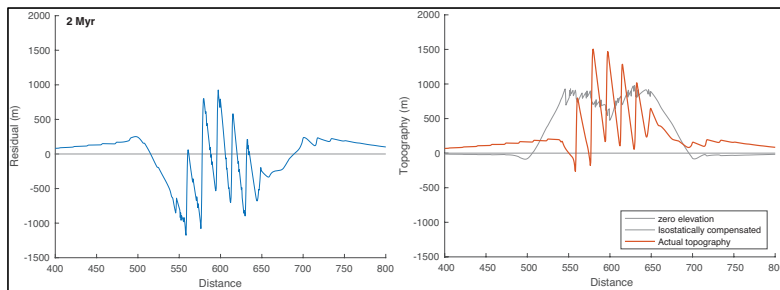


Fig. A-2) Example of the residual topography (left panel) that we used to calculate the isostatically compensated topography (right panel).

Power spectral analysis

We investigated the dominant timescales of variability observed in our fault extension rates by calculating the Fourier transform for each time series. For instance, for all the extension rate time series shown in figure 6a in the main article, we calculated the Fourier transform and plotted the power spectra as shown in figure 6c (see also Fig. A-3 below). We calculated the Fourier transform in Matlab, by means of the following piece of code:

```
% Calculating the Fourier transform for timeseries X (time interval T):  
  
X = ER(3,:); % Selecting the extension rate series for one fault  
           % For instance fault #3 from reference model TM-1  
  
dt = 0.002; % timestep length (2000 yr)  
Fs = 1/dt;  % frequency (0.0005 sample per year)  
  
y = fft(X); % Fourier transform  
n = length(X); % number of samples  
f = (0:n-1)*(Fs/n); % frequency range  
  
power = abs(y).^2/n; % power of the DFT  
  
figure  
subplot(2,1,1)  
plot(T,X)  
axis tight  
ylabel('Extension rate (mm/yr)')  
xlabel('Time (Myr)')  
  
subplot(2,1,2)  
plot(f,power,'linewidth',2)  
xlim([0 25])  
ylim([0 0.6])  
ylabel('Power')  
xlabel('Frequency (1/Myr)')
```

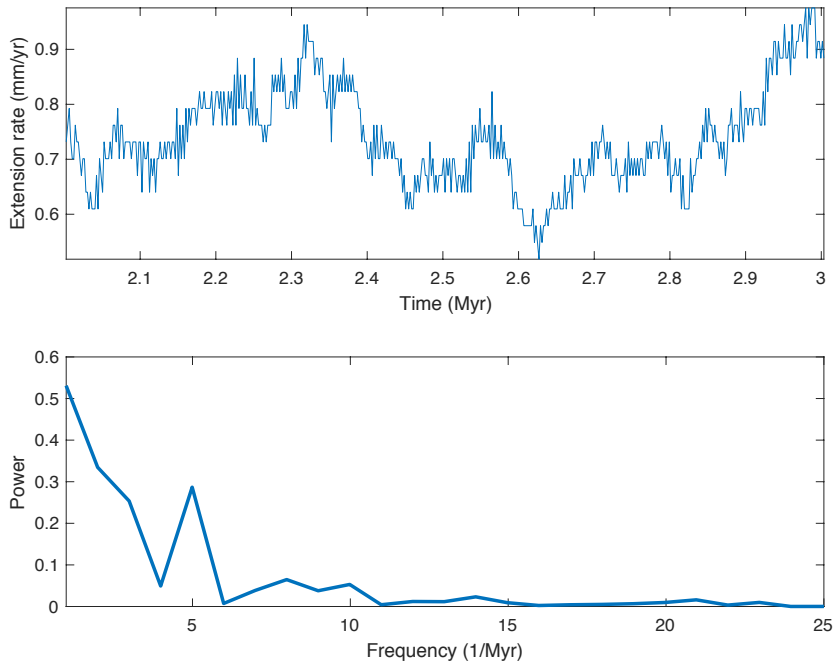


Fig. A-3) Example of an extension rate time series (top panel) for which we calculated a power spectrum (bottom panel) by means of the Matlab code provided on previous page.

Appendix B – Overview numerical experiments

The findings presented in this study are based on a large number (>100) of numerical modelling experiments. Here, we provide an overview of only those experiments that are discussed or referred to in the main article text. We used three different types of model setups as illustrated in figure B-1 below. All our experiments were performed by means of the code FANTOM (Thieulot, 2011), however, we used the code to test three different types of models (see Fig. B-1). In most of our experiments we convectively removed mantle lithosphere and solved both for mechanics and temperature (Thermo-Mechanical models TM1 – TM10; see Fig. B-1 and Table B-1). In these experiments, mantle lithosphere removal produced regional uplift and strong localisation of extension within a narrow zone in the model centre. In order to evaluate the role of mantle convection, temperature effects and the non-linear viscous model, we also performed a series of mechanical model experiments with a linear viscous lower crust (Mechanical models M1 – M5; see Fig. B-1 and Table B-1). In this mechanical model we still generate regional uplift, however, this time by means of a density difference rather than through the convective removal of weak mantle lithosphere. To investigate in more detail the dynamic fault behaviour that we observed, we also run a number of very simplistic 2-layered crustal-scale extensional models in which we varied fault geometry and the viscosity of the linear viscous lower crust (Crustal-scale models C1-C6; see Fig. B-1 and Table B-1).

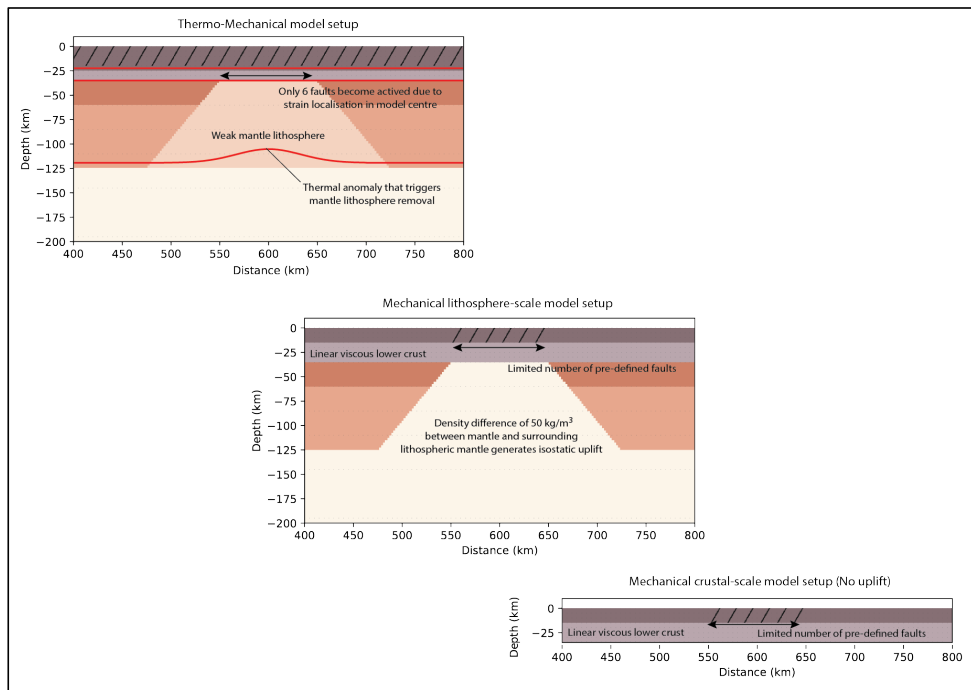


Fig. B-1) Three different type of model setups that we used for evaluating to contribution of different aspects inherent to an extensional setting affected by mantle lithosphere removal.

Table B-1) Overview model experiments (more details provided in Appendices C and D):

Exp.	Description	V_e (mm yr ⁻¹)	Fault geometry	Other changes compared to reference model *
Thermo-mechanical lithosphere-scale models				
TM-1	Reference (TM-) model	3	60 west-dipping faults	
TM-2	Symmetric fault geometry	3	60 faults, but E or W-dipping towards model centre	
TM-3	Low far-field extension rate	1.5	60 west-dipping faults	
TM-4	High far-field extension rate	6	60 west-dipping faults	
TM-5	Lateral shift in fault positions	3	60 west-dipping faults, but shifted 5 km towards the west	
TM-6	Stronger faults	3	60 west-dipping faults	Fault zone friction angle 7° instead of 2°
TM-7	1 fault	3	One west-dipping fault	
TM-8	2 faults – asymmetric	3	Two west-dipping faults	
TM-9	2 faults – symmetric	3	Two faults, dipping towards model centre	
TM-10	Without far-field extension	0	60 west-dipping faults	
Mechanical lithosphere-scale models with linear viscosity				
M-1	60 faults, weak lower crust (Reference M-Model)	3	60 west-dipping faults	LC viscosity 10 ¹⁹
M-2	6 faults, weak lower crust	3	6 west-dipping faults	LC viscosity 10 ¹⁹
M-3	6 faults, strong lower crust	3	6 west-dipping faults	LC viscosity 10 ²⁰
Crustal-scale mechanical models with linear viscosity (no dynamic uplift)				
C-1	6 faults, strong lower crust (Reference C-Model)	3	6 west-dipping faults	LC viscosity 10 ²⁰
C-2	6 faults, strong lower crust, symmetric	3	6 faults dipping towards model centre	LC viscosity 10 ²⁰
C-3	6 faults, weak lower crust	3	6 west-dipping faults	LC viscosity 10 ¹⁹
C-4	2 faults, strong lower crust	3	2 west-dipping faults	LC viscosity 10 ²⁰
C-5	2 faults, weak lower crust	3	2 west-dipping faults	LC viscosity 10 ¹⁹
C-6	2 faults, weak lower crust, symmetric	3	2 faults dipping towards model centre	LC viscosity 10 ¹⁹
C-7	2 faults, weak lower crust	3	2 west-dipping faults	LC viscosity 10 ¹⁹ , Von Mises

* In the final column we describe the differences (other than extension velocity and fault geometry as these are given in columns 3 and 4) between the experiments compared to the reference experiment of the group of models to which it belongs, i.e. compared to either experiment TM-1, M-1, or C-1.

Appendix C – Thermo-Mechanical model experiments

Here we briefly describe the thermo-mechanical modelling experiments listed in Table B-1. In nine of them (TM-1-9) there is fault activity and for these experiments we compare the patterns of faulting and fault dynamics in figures C-4 to C-8 on the next pages. First, we provide a bit more details on the evolution of our reference model (TM-1) which is the main model being discussed in our article.

Reference model TM-1

Long-wavelength topography - The parameters used for this model are provided in Appendix A and results from this model are in detail discussed in the main article text (see Figs. 2-6, 7a, 8, 10a-b in the main article). In figure C-1 below we show the long-wavelength topography that we calculated by means of a Gaussian filter with window size varying between 100-150 km. The left panel shows that the long-wavelength topography reaches 600-700 m after 0.5 Myr. Because of crustal extension, the height of the long-wavelength topography gradually declines from 0.5 Myr onwards and reaches 520-600 m after 3 Myr (right panel) using the same window size range of 100-150 km.

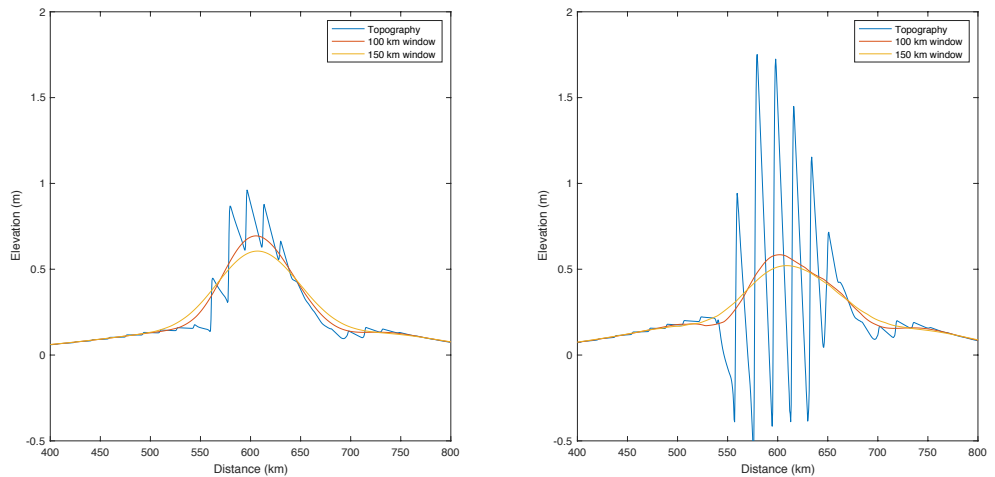


Fig. C-1) Long-wavelength topography calculated by means of a Gaussian filter with different window sizes after 0.5 Myr (left panel) and 3 Myr (right panel) for our reference model TM-1.

Isostatically compensated topography - Because of the rapid removal of mantle lithosphere, the actual topography is lower than the isostatically compensated topography during early stages of the experiments (Fig. C-2). Around ca. 0.5 Myr, the first footwall crests get above the isostatically compensated topography (Fig. C-2a). At later stages, most of the footwalls are reaching above the isostatically compensated topography, while the hanging walls remain below it (Fig. C-2b).

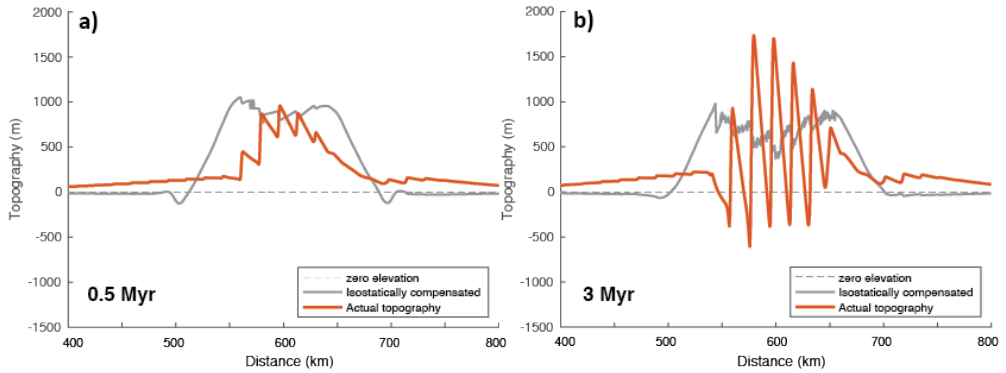


Fig. C-2) Topography after 0.5 (a) and 3 Myr (b) of our reference model TM-1, together with the isostatically compensated topography.

Fault plane elevation – We calculated the elevation of our fault planes with time using the elevations of gridpoints of the Lagrangian grid in the hanging- and footwall of each fault (see Appendix A). The midpoint elevation (average of the hanging- and footwall elevation) of all 6 active fault planes increases rapidly the first ~0.5 Myr and most of them keep a fairly constant elevation during the remaining part of the experiment (Fig. C-3 a). East flank faults 2 and 4, however, experience significant subsidence following 0.5 Myr. Overall, no correlations exist between our fault extension rates and (the rate of change in) fault plane elevation (Fig. C-3 b, c).

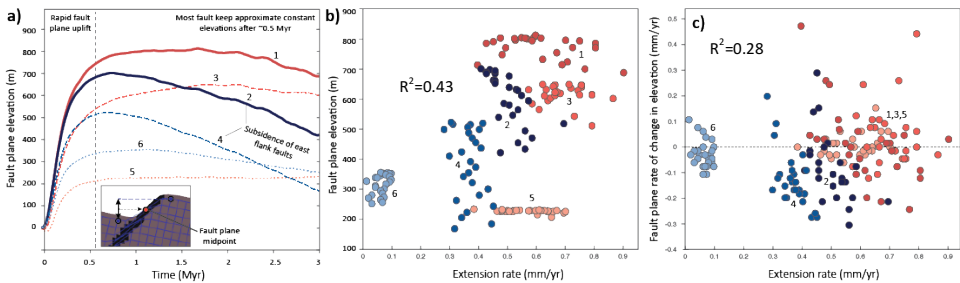


Fig. C-3) a) Elevation of fault plane midpoints over time for each active fault in our reference model TM-1. b,c) Rate of change in fault plane midpoint elevation plotted against extension rates for every 100 kyr time step in between 0.5 and 3 Myr.

Varying fault geometry and the number of faults - TM-2, -7, -8, -9

Experiments TM-2, -7, -8, and -9, are similar to reference model TM-1 except from the geometry of the pre-defined faults zones. Model TM-2 also has faults across the full width of the model, however, has a symmetric fault geometry with all faults dipping towards the model centre. Similar as in model TM-1, only the 6 central most faults become activated due to weakening and thinning of the lithosphere in the model centre. In experiment TM-7 we only pre-defined one single west-dipping fault in order to investigate whether its extension rate also reveals temporal variability as we observe is most of our experiments. However, as shown in figure C-6, its extension rate is highly constant and continuously 3 mm/yr. Experiments TM-8 and -9 both have two faults. In experiment TM-8 both faults dip westward, while they dip towards the model centre in experiment TM-9.

Varying extension velocity – TM-3, -4

Experiments TM-3 and -4 are similar to experiment TM-1 except from the rate of far-field extension that we apply to the model boundaries. The extension rate is 1.5 and 6 mm/yr in TM-3 and TM-4, respectively.

Lateral variations in fault positions – TM-5

In order to investigate the sensitivity of our pattern of fault activity to the exact position of our pre-defined fault zones we performed an experiment in which we shifted all faults towards the west with 5 km, which is approximately one third of the fault spacing. This experiment shows that fault position does not affect the patterns of fault activity and temporal variability in extension rates significantly (see Figs. C-5,6,7). Lateral changes in fault zone positions do affect, however, the importance of the outermost located faults, i.e. west flank fault 5 and east flank fault 6, as these are located near the edges of the area of mantle lithosphere removal.

Varying fault strength – TM-6

In this model we used an internal friction angle of 7° instead of 2° for our fault zone material. This increases the strength of the fault zones relative to the surrounding crust.

No far-field extension – TM-10

We performed a ‘zero-far-field-extension’ experiment that has a similar setup as our reference model (TM-1), however, without any extension imposed along our model boundaries. This experiment demonstrates the height and shape of the regional (dome-shaped) topography that develops in response to mantle lithosphere removal only, without any additional effects from fault activity as is the case for our reference model (see Fig. 3e, f in the main article). The maximum height of the dome-shaped topography after 3 Myr is of the order of 650 m. The wavelength of this regional topography is approximately 100 km, which is similar to the width of the zone of mantle lithosphere removal. Another interesting finding of this experiment is that the amount of regional topography itself is not sufficient for activating our faults. A

small rate of far-field extension is needed for generating fault activity, as demonstrated by our reference model TM-1 in which we use an extension velocity of 3 mm yr^{-1} but also when we halve the extension rate down to 1.5 mm yr^{-1} (TM-3).

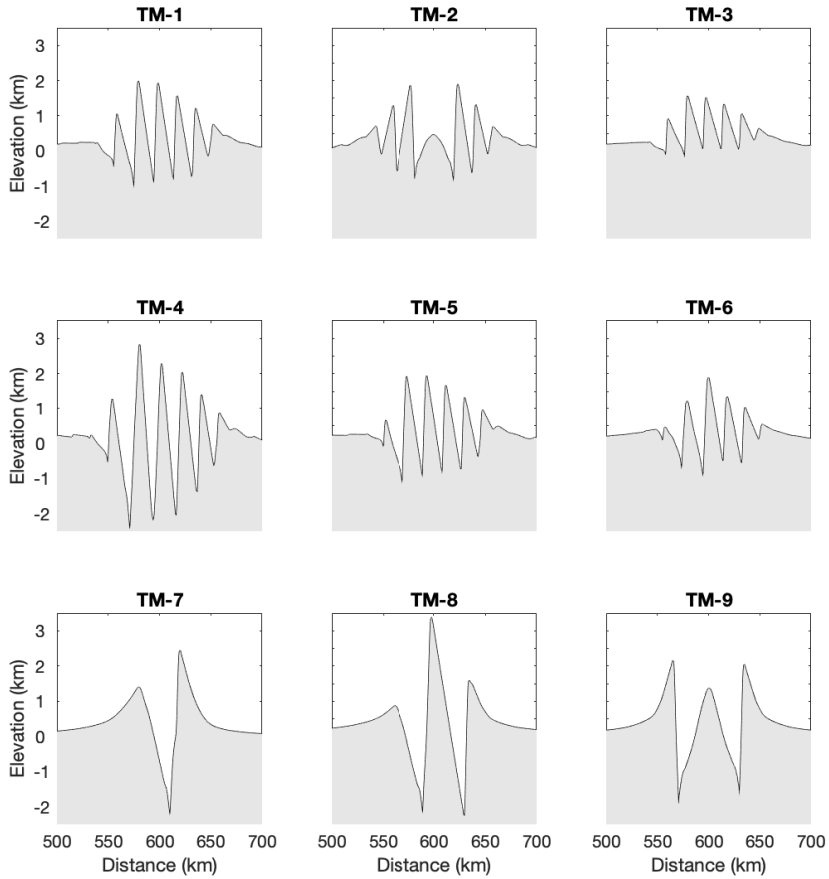


Fig. C-4) Final topography (after 3 Myr) for all the thermo-mechanical models (see also Table B-1).

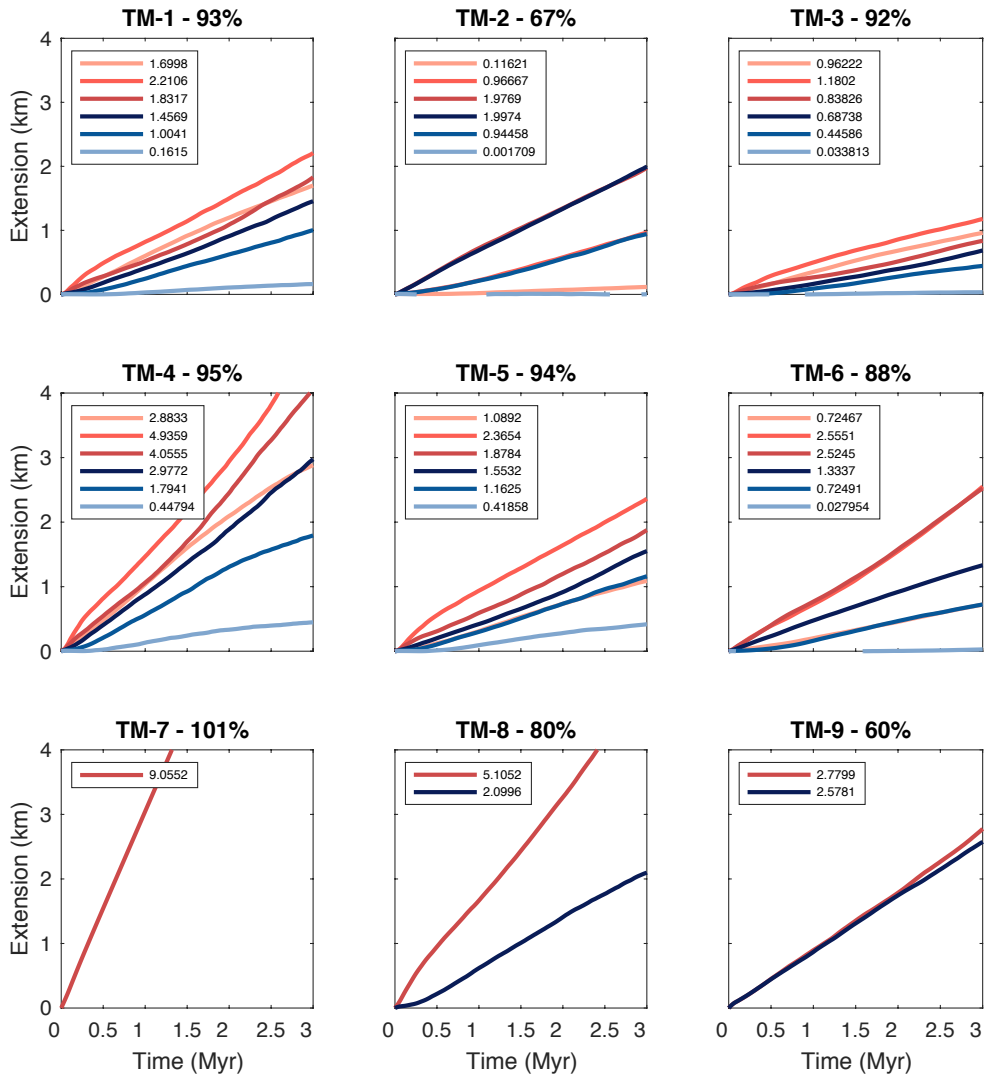


Fig. C-5) Extension accumulation for each individual fault over time for all the thermo-mechanical models (see also Table B-1). For fault color-coding see figure 5 in the main article text. The final total amount of extension for each fault is given in the legend. The percentage provided in the title of each graph shows how much extension of the total amount of (far-field) extension is accommodated by all faults together. For instance in case of reference model TM-1, 93% of all the extension is accommodated by fault activity.

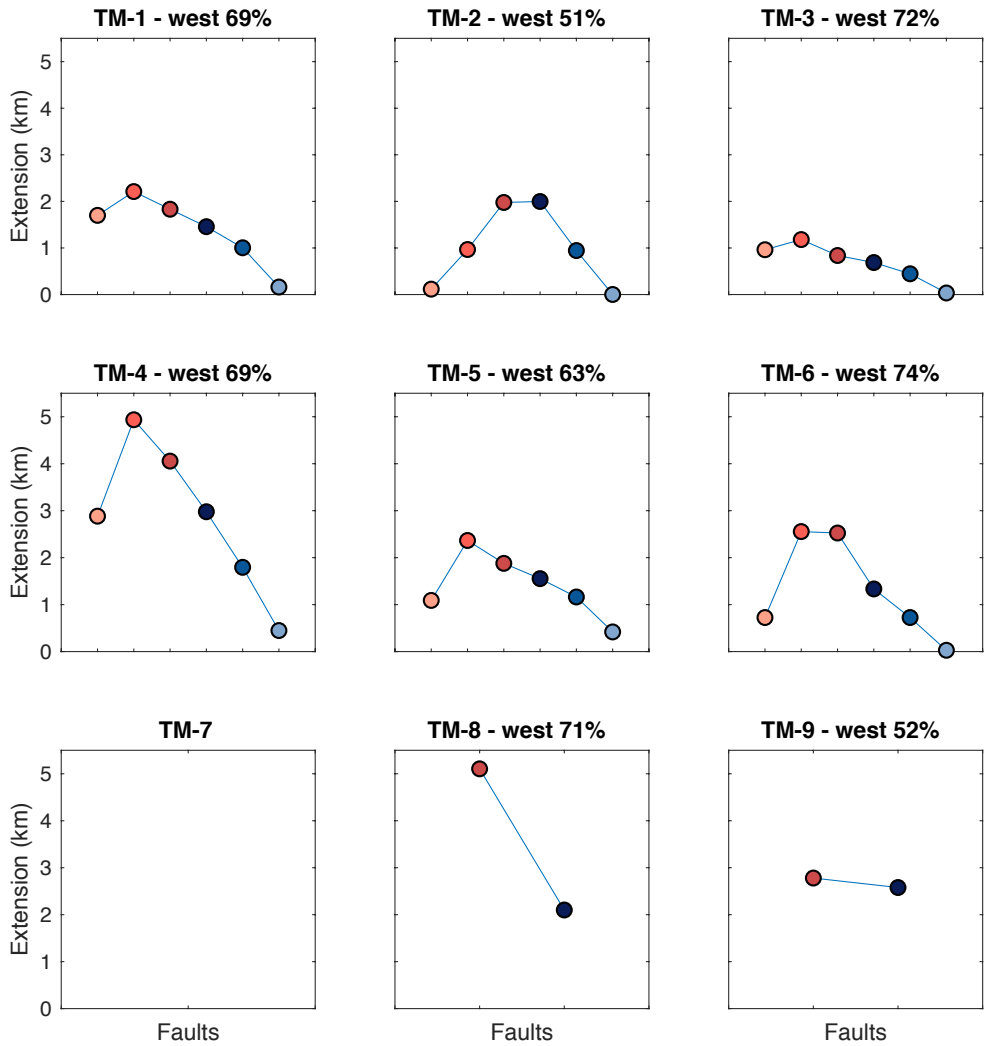


Fig. C-6) Fault activity distribution patterns based on the final (3 Myr) amount of extension. The percentage provided in the title of each graph shows how much extension of the total amount of fault-accommodated extension is accommodated by only the west flank faults, i.e. the red or reddish coloured faults in each plot.

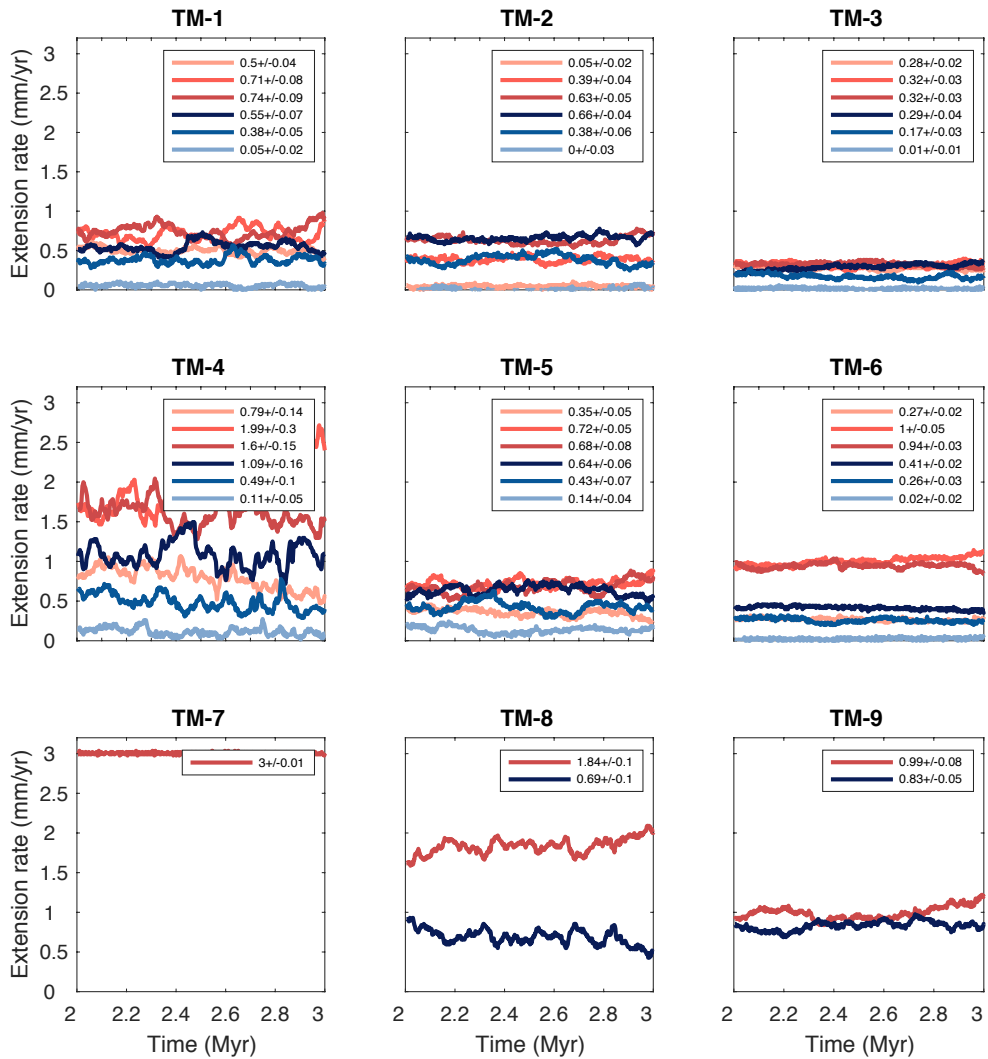


Fig. C-7) Extension rates between 2 and 3 Myr, that is the period that rapid surface uplift has largely ceased. The mean and standard deviation of these signals is provided in the legend of each plot.

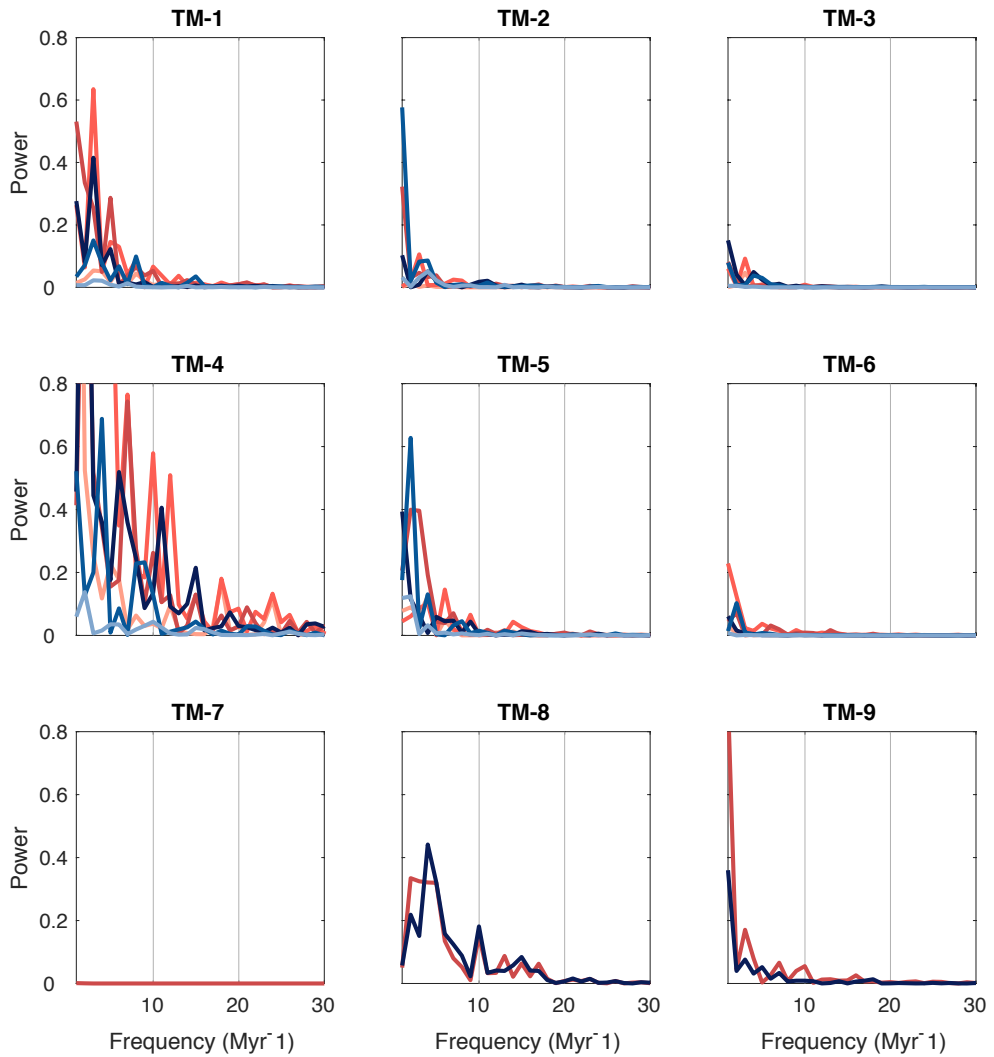


Fig. C-8) Power spectra resulting from Fourier transform analysis for each fault extension rate time series for the time-interval between 2 and 3 Myr, that is the period that rapid surface uplift has largely ceased (see Appendix A for methodology).

Appendix D – Mechanical model experiments

Lithosphere-scale mechanical models M-1, -2, -3

The geometric setup of mechanical model M-1 is similar to our thermo-mechanical reference model TM-1, as shown in figure B-1 in Appendix B. However, in the mechanical lithosphere-scale models (M-1,-2,-3) we do not have weak mantle lithosphere material getting convectively removed, we have asthenosphere material in the lithospheric gap from the start. Because we reduced the density of this asthenosphere material to 3250 (instead of 3300 kg/m³), we still create a mantle buoyancy effect and regional uplift. In these models there is no temperature-dependency, the upper crust has a rigid plastic rheology (Mohr-Coulomb yield criterion) and the lower crust, mantle lithosphere and asthenosphere have linear viscous rheology (Newtonian).

As illustrated in figure D-1 below, regional uplift occurs very fast (already during the first 100 kyr), followed by a gradual decrease in mean elevation due to extensional faulting (see figures from M-1 and M-2). Because we do not temperature effects in these models, the degree of strain localisation is less compared to model TM-1 so many more faults become activated in model M-1. To allow comparison of fault dynamics with the thermo-mechanical models we therefore also performed mechanical experiments in which we only pre-defined 6 faults only, either with relative weak lower crust with a viscosity of $\eta = 10^{19}$ (M-2) or a relative strong lower crust ($\eta = 10^{20}$; M-3).

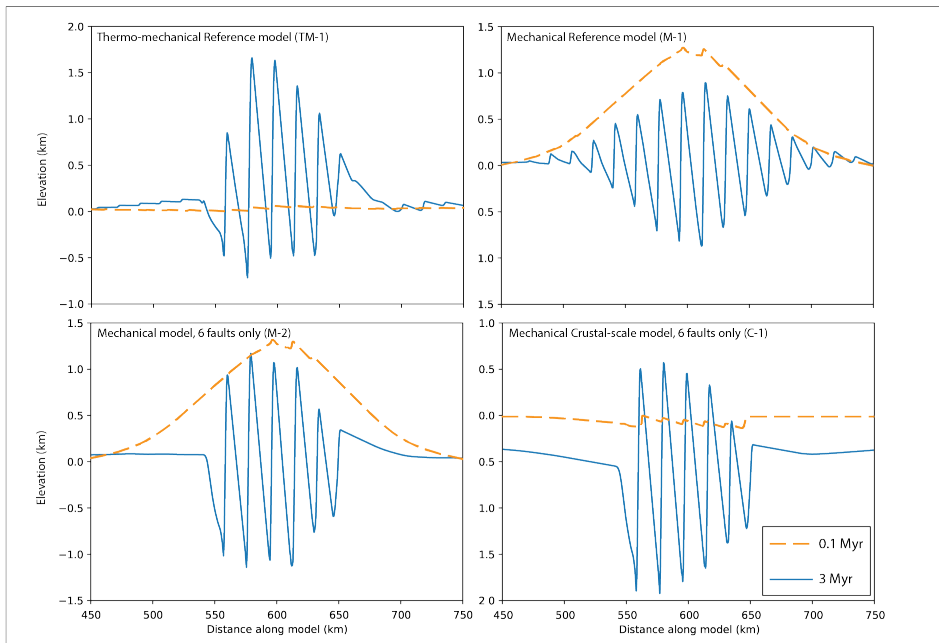


Fig. D-1) Topographic evolution of models TM-1, M-1, M-2 and C-1 for demonstrating the main differences between them.

Crustal-scale mechanical models with six faults – C-1, -2, -3

Our crustal-scale models consist of 2 layers; a rigid-plastic upper crustal layer bonded to a linear viscous lower crustal layer (see also Fig. B-1). Between the different crustal-scale models we vary the number of faults, their dip direction and the strength of the lower crust. Models C-1 and C-2 both have a relative strong lower crust ($\eta = 10^{20}$) and 6 pre-defined fault zones, either dipping towards the west (in case of model C-1) or dipping towards the model centre (in case of model C-2). Model C-3 has a similar asymmetric fault geometry as model C-1 but now with a relative weak lower crust ($\eta = 10^{19}$).

Crustal-scale mechanical models with 2 faults – C-4, -5, -6, -7

Model C-4 and C-5 are both characterised by two west-dipping faults. In model C-4 we used a relative strong lower crust ($\eta = 10^{20}$), and in model C-5 a relative weak lower crust ($\eta = 10^{19}$). Model C-6 has a relative weak lower crust ($\eta = 10^{19}$) and a symmetric fault geometry with two faults dipping towards the model centre. In model C-7 we used 'von Mises' yield criterion in the plastic upper crustal layer to make the deformation independent of the depth-related increase in vertical stress.

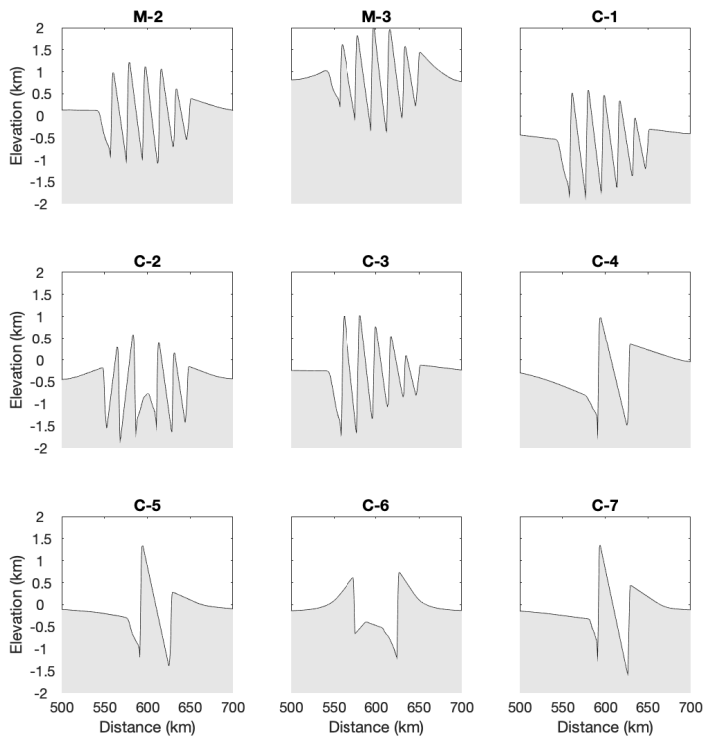


Fig. D-2) Final topography (after 3 Myr) for mechanical models at lithosphere-scale (M-2, M-3) or crustal-scale (C-1 to C-7) (see also Table B-1 for an overview).

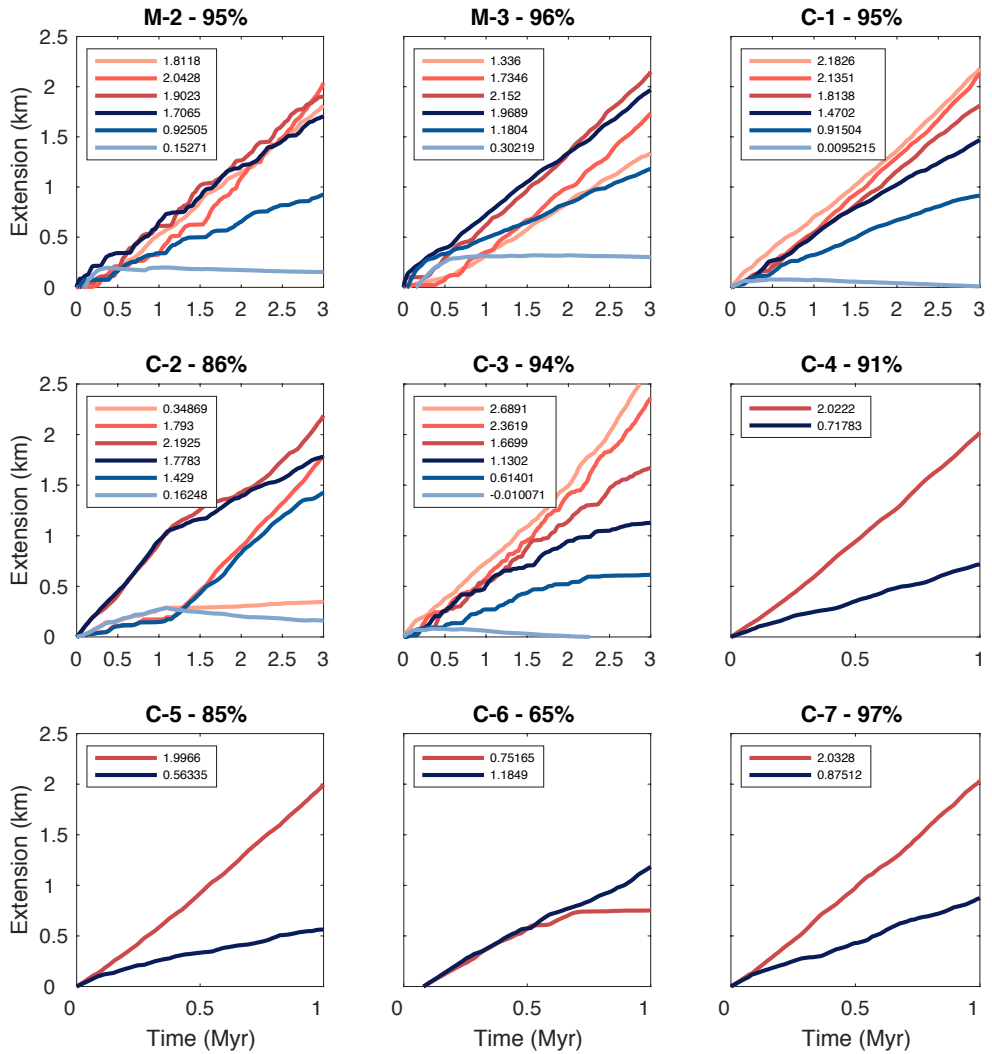


Fig. D-3) Extension accumulation for each individual fault over time mechanical models at lithosphere-scale (M-2, M-3) or crustal-scale (C-1-C-7) (see also Table B-1). For fault color-coding see figure 5 in the main article text. The final total amount of extension for each fault is given in the legend. The percentage provided in the title of each graph shows how much extension of the total amount of (far-field) extension is accommodated by all faults together. For instance in case of model M-2, 95% of all the extension is accommodated by fault activity.

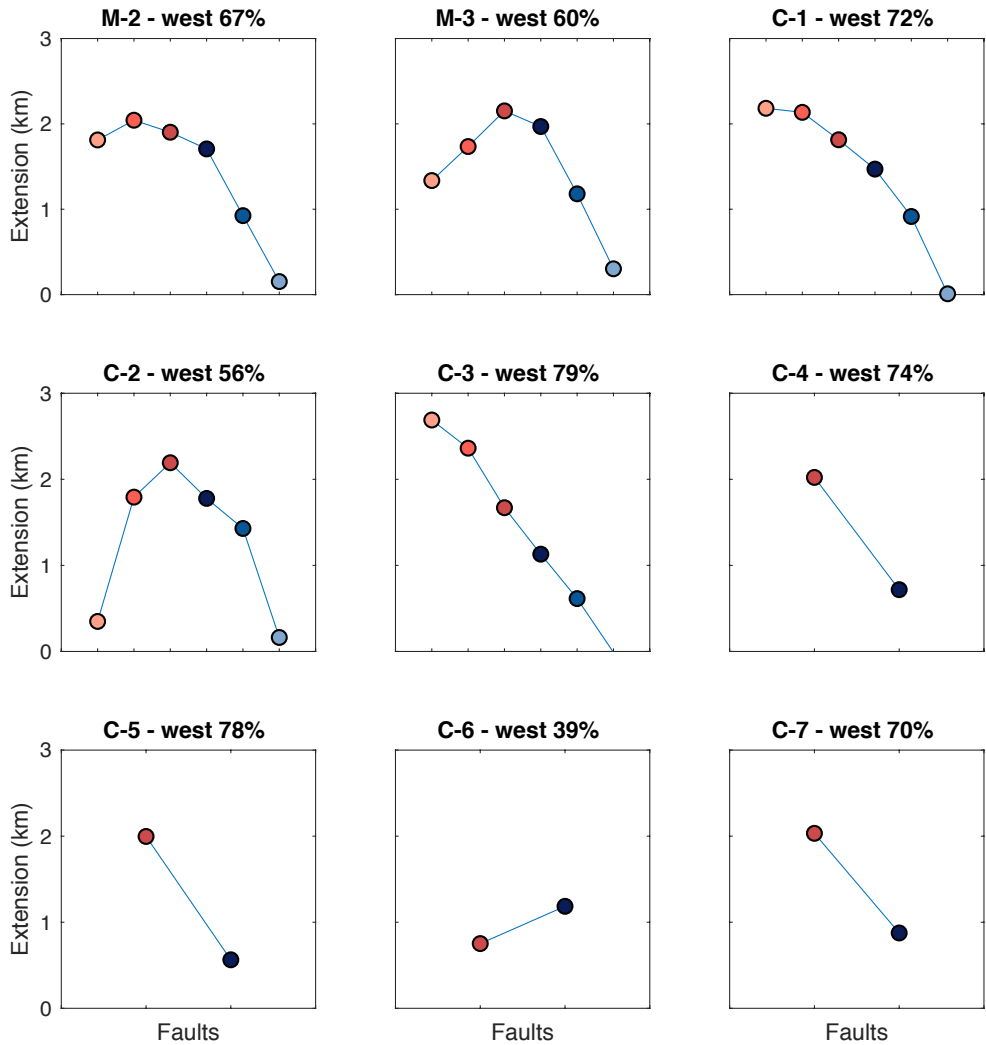


Fig. D-4) Fault activity distribution patterns based on the final amount of extension, which is after 3 Myr in case of experiments M2, M3, C-1, C-2, and C-3 and is after 1 Myr for all the other experiments. The percentage provided in the title of each graph shows how much extension of the total amount of fault-accommodated extension is accommodated by only the west flank faults, i.e. the red or reddish coloured faults in each plot.

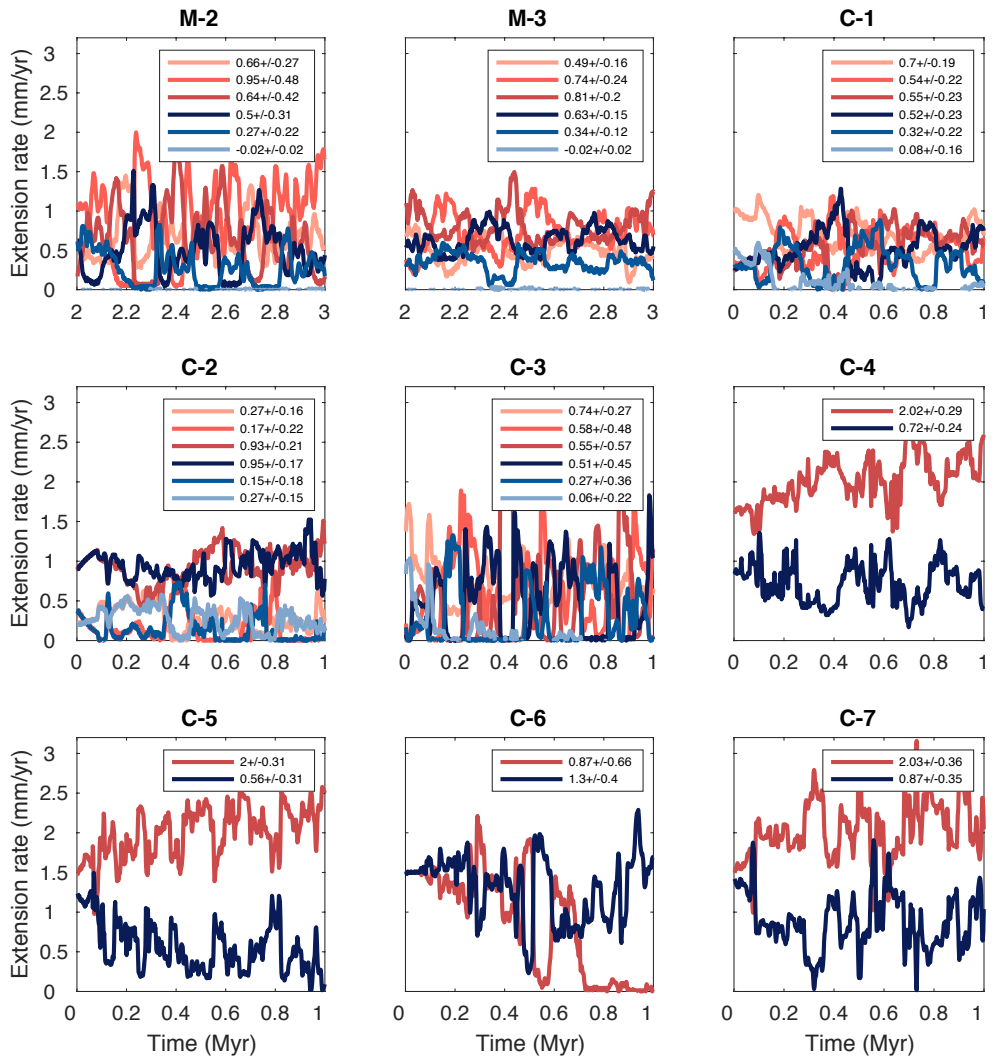


Fig. D-5) Extension rates for all the individual active faults. For the lithosphere-scale models we show the extension rates between 2 and 3 Myr, that is the period that rapid surface uplift has largely ceased. The mean and standard deviation of these signals is provided in the legend of each plot.

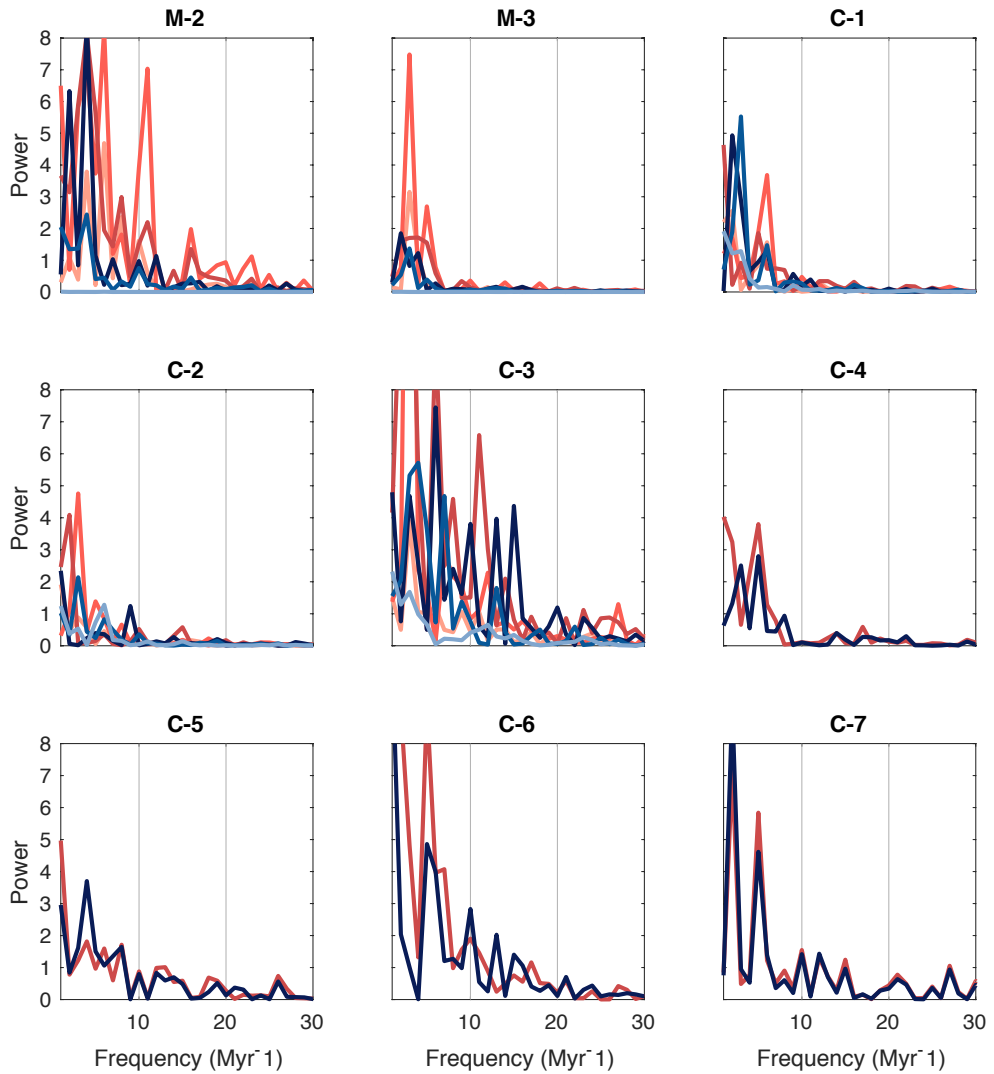


Fig. D-6) Power spectra resulting from Fourier transform analysis for each fault extension rate time series (see Appendix A for methodology). For models M-2 and M-3, only data from the time-interval between 2 and 3 Myr was used, that is the period that rapid surface uplift has largely ceased. For all other (crustal-scale) models we used the data from 0-1 Myr because these models do not have regional uplift.

Appendix E – Energy dissipation analysis crustal-scale model

To evaluate the dynamic fault behaviour in our models we performed energy dissipation analysis for a 2-layered crustal-scale mechanical model with a linear viscous lower crustal layer and only 2 pre-defined west-dipping faults (Fig. E-1a; Model C-5 in Appendix B and D). We used this model with relative weak lower crust ($\eta = 10^{19}$) because the amplitude of the variability in the fault extension rates is very pronounced in this model (Fig. E-1b).

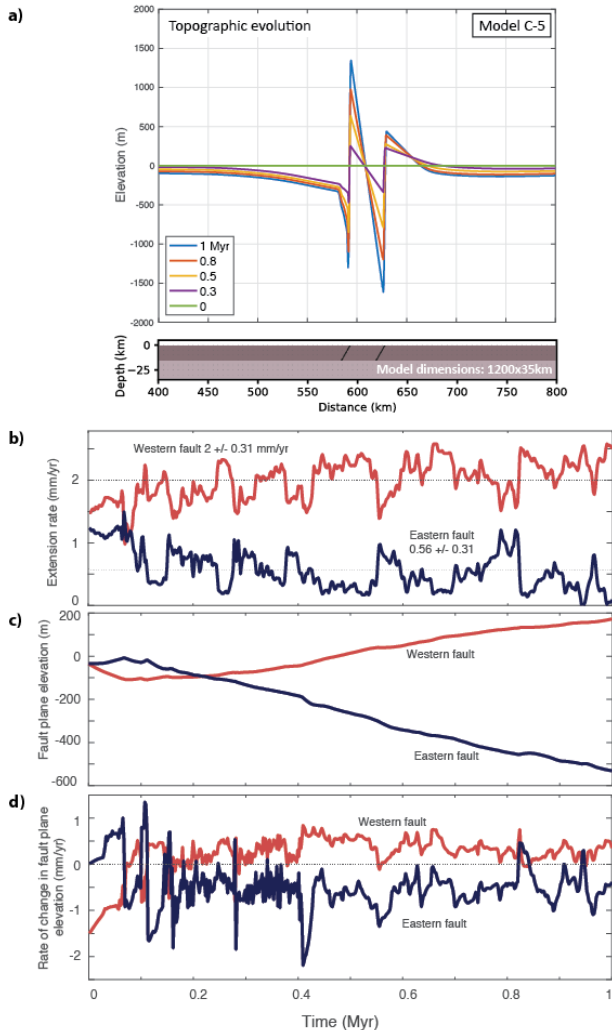


Fig. E-1: a) Model setup and topographic development for experiment C-5. b) Extension rates for the eastern and western fault. c) Elevation of the fault planes, based on the average elevation of their footwall and hanging wall ('fault plane midpoint elevation', see also Appendix A), showing the long-term uplift and subsidence of the western and eastern fault planes, respectively. d) The rate of change in fault plane elevation, so the time derivative of the time series shown in subfigure c).

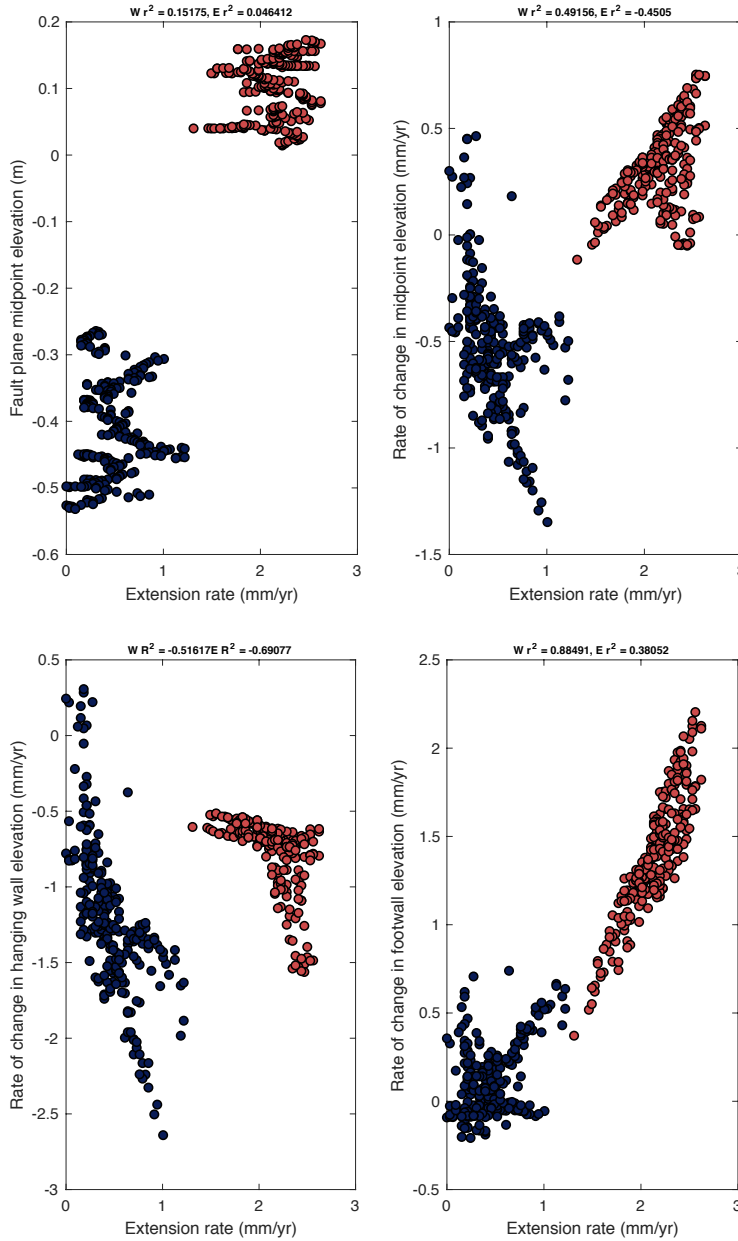


Fig. E-2: Top panels: Extension rates plotted against fault plane mid point elevation (top left panel) and its time derivative (top right panel) for both the western and eastern faults from model C-5 (0.5-1 Myr time interval, see fig. E-1). Correlation coefficients R^2 for the western (W) and eastern (E) faults are provided above the figures. Bottom panels: Extension rates plotted against rate of change in hanging wall (bottom left panel) and footwall elevations (bottom right panel) for both the western (red) and eastern (blue) faults from model C-5. R^2 for the western (W) and eastern (E) faults are provided above the figures, showing a reasonable correlation between extension rate and rate of change in hanging wall elevation for the eastern fault ($R^2 = -0.69$; bottom left panel) and a strong correlation between extension rate and rate of change in footwall elevation for the western fault ($R^2 = 0.88$; bottom right panel).

Internal energy dissipation for different parts of the lower and upper crust and the gravitational rate of work were calculated following a similar approach as Huisman et al. (2005) and Buitter et al. (2008). According to Buitter et al. (2008), the mechanical energy balance in the systems that we model is defined as:

$$\dot{W}_b = \dot{W}_I + \dot{W}_G$$

in which \dot{W}_b is the rate at which energy is supplied to the system, \dot{W}_I is the rate at which energy is used or dissipated because of internal deformation (internal dissipation), and \dot{W}_G is the gravitational rate of work. The rate of internal energy dissipation \dot{W}_I is defined as (Malvern, 1969):

$$\dot{W}_I = \frac{1}{2} \int \sigma \cdot \dot{\epsilon} \cdot dU$$

in which σ and $\dot{\epsilon}$ are the stress and strain rate tensors, respectively. We integrated the product between them over six different volumes U. For both the eastern and western flanks of our models, we integrated over a proximal and distal region in the plastic (upper-crustal) domain and a single region in the viscous (lower-crustal) domain (Fig. E-3). Important to note is that the distal plastic and viscous domains (Pw_dist, Pe_dist, Vw, Ve; see Fig. E-3) extend all the way to the left or right model boundaries, while the proximal plastic domains only extend up to ~15 km from the most western or eastern faults (Pw_prox, Pe_prox). We also calculated the internal dissipation for the central located rotating crustal block in between both faults (Fig. E-3). Across the proximal domains of the west- and east flanks we also calculated the gravitational rate of work \dot{W}_G by integrating the vertical surface velocity V_{surf} across distance l that is shown in figure E-3:

$$\dot{W}_G = \frac{1}{2} \rho g h \int_0^l V_{surf} dx$$

in which ρ is the crustal density (2850 kg/m³), g is the gravitational acceleration (9.81 m/s²), and h is the thickness of the crust (35 km). The rates of dissipation are shown in figure E-4, and in figure E-5 we tested the correlation between the different data.

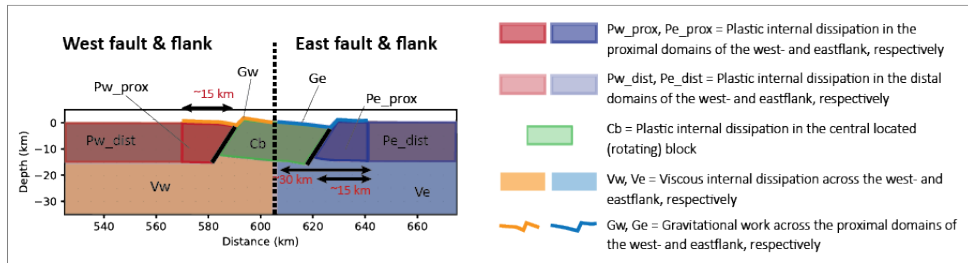


Figure E-3: Dimensions of the model domains for which we calculated internal energy dissipation in the plastic domain (Pe_{prox} , Pe_{dist} , Pw_{prox} , Pw_{dist} , Cb) and viscous domain of our models (Vw , Ve). We also show the distances across we calculated the rate of gravitational work (Ge , Gw).

Also in this simple crustal-scale model with only two west-dipping faults, the western fault generally has a higher long-term average extension rate than the eastern fault (Fig. E-1b). The extension rates of the western and eastern fault are respectively 2.0 ± 0.31 and 0.56 ± 0.31 mm/yr and both faults experience marked changes over time. Some of the variability may relate to changes in fault surface areas that change by $\pm 5\%$ over time, producing variations in fault strength along the fault plane and over time (Fig. E-4b). However, because the variations in fault surface area do not correlate with extension rate (Fig. E-5) we do not expect these ‘numerical asperities’ to be a great importance for the fault interaction that we observe.

Figure E-4c-g show the energy dissipation rates for the different domains illustrated in figure E-3. These figures show that the amount of gravitational work (Fig. E-4c) is greater than the amounts of internal energy dissipation in the different domains by one or two orders of magnitude (Fig. E-4d-g). However, no correlation exists between the fault extension rates and the rate of gravitational work, also not with internal dissipation in any of the other domains (Fig. E-5).

In the main article we argue that the tendency of the west located fault(s) to dominate in terms of fault activity is because it takes more energy to bend the eastern plate than the western plate. If we sum the internal dissipation rates of the proximal and distal domains of each plate for this simple crustal-scale model we find that the long-term average dissipation rate is indeed slightly higher in the east, namely ~ 2.6 W/m versus ~ 2.3 W/m. As both faults are located at similar elevation and do not differ in terms of gravitational potential energy, this implies that it takes slightly more energy to deform the eastern plate than the western plate. This can explain the dominance of west-located faults over east-located faults in case of a dominant westward dip direction, irrespective of whether extension is accompanied by regional uplift. An even stronger east-west asymmetry in our thermo-mechanical experiments during the early stage of rapid regional uplift (e.g. see Fig. 5b in the main article) can be explained by the fact that bending of the eastern plate in response to both regional uplift and fault slip occurs in a similar direction, accumulating even more flexure-induced stress compared to the western plate where flexure in response to regional uplift and fault slip work in opposite directions.

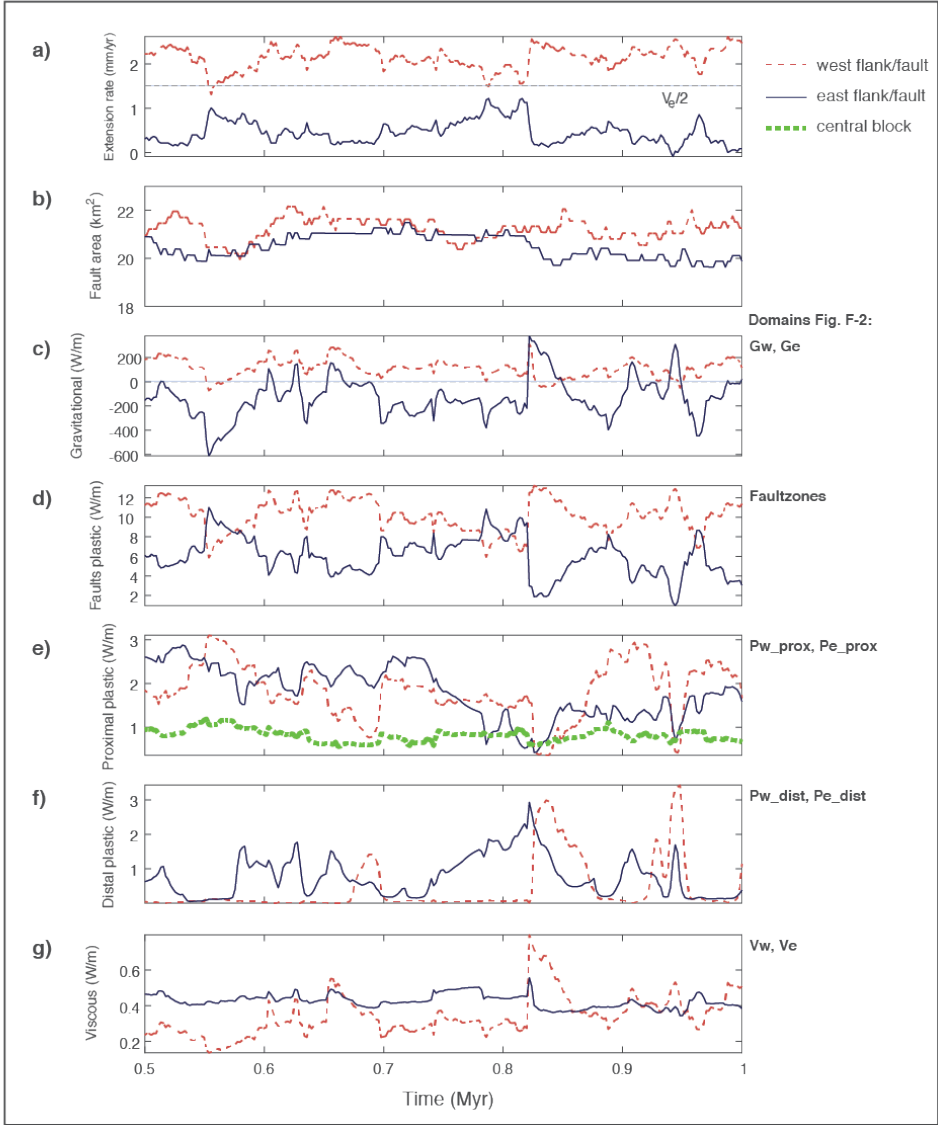


Figure E-4: Results from energy dissipation analysis for model C-5.

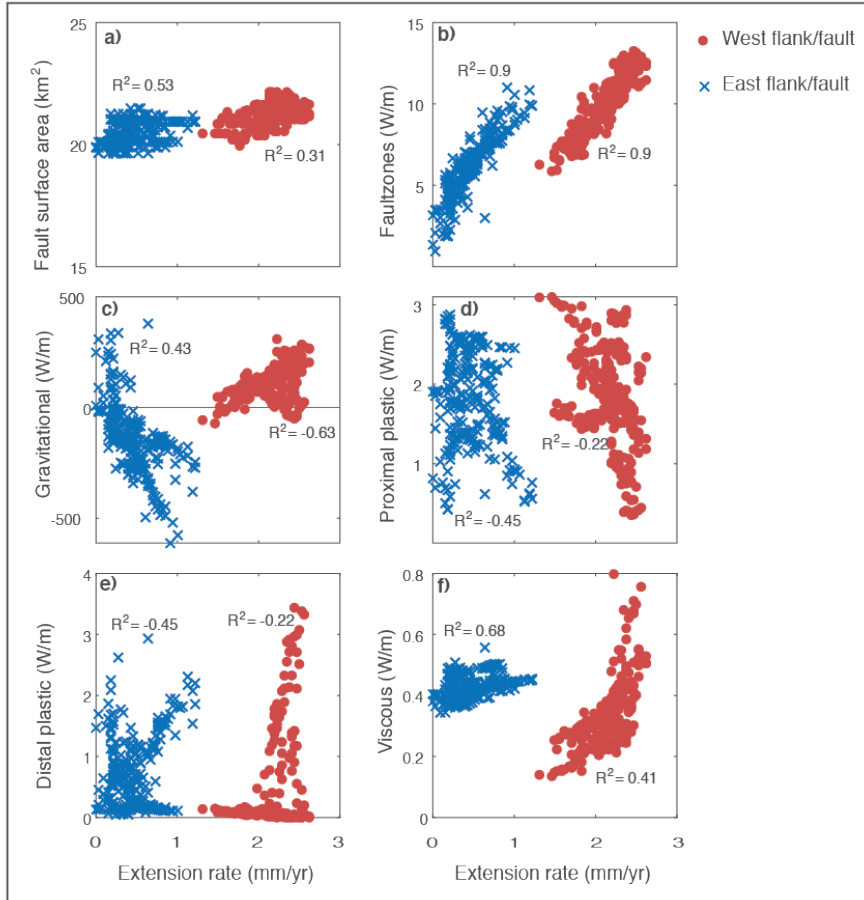


Figure E-5: Correlation plots for the different energy dissipation domains for model C-5, for testing the correlation with the fault extension rates.

References

- Buiter, S.J.H., Huismans, R.S., Beaumont, C., 2008. Dissipation analysis as a guide to mode selection during crustal extension and implications for the styles of sedimentary basins. *J. Geophys. Res.*, 113, B06406.
- Cowie, P.A., Roberts, G.P., Bull, J., Visini, F., 2012. Relationships between fault geometry, slip-rate variability and earthquake recurrence in extensional settings. *Geophys. J. Int.* 189, 143–160.
- Gleason, G. C., Tullis, J., 1995. A flow law for dislocation creep of quartz aggregates determined with the molten-salt cell. *Tectonophysics*, 247, 1–23.
- Huismans, R.S., Buiter, S.J.H., Beaumont, C., 2005. Effect of plastic-viscous layering and strain softening on mode selection during lithospheric extension. *J. Geophys. Res.*, 110, B02406.
- Karato, S., Wu, P., 1993. Rheology of the upper mantle. *Science*, 260, 771–778.
- Malvern, L. E., 1969. *Introduction to the Mechanics of a Continuous Medium*. Prentice-Hall, Upper Saddle, N. J., 713 pp.
- Thieulot, C., 2011. Two- and three-dimensional numerical modelling of creeping flow for the solution of geological problems. *Phys. Earth Planet. Inter.* 188, 47–68.

**Errata for
'The interplay between surface processes and
tectonics in the actively extending central Italian
Apennines'**

Anneleen H. Geurts



Thesis for the degree philosophiae doctor (PhD)
at the University of Bergen

_13/05/2020 Anneleen Geurts
(date and sign. of candidate)

A rectangular box containing a handwritten signature in blue ink. The signature appears to be 'Birthe Gedecke'.

(date and sign. of faculty)

Errata

Page 3 Here a full page has been added with the text: “I dedicate this work to the memory of my supervisor, Patience Cowie.” Including a picture.

Page 7,8 In the Contents list, page numbering has been changed in order to have it consistent with the thesis in its new format (book size instead of A4).

Subheadings of Chapters 3 and 4 have been added to the Contents list. In the first submitted version of the thesis, these subheadings were not included because then still the Journal copies of these two published articles (in A4 format) were used.

Mistakes in the Contents list: The subheadings of Chapter 6 were not consistent with those used in the main text:

- 6.2) ‘The central Apennines continental rift’ is corrected into: ‘Drainage integration: patterns and driving mechanisms’
- 6.3) ‘Surface processes and normal fault activity in continental rifts’ is corrected into: ‘Implications of overspill-driven drainage integration’
- 6.4) ‘Research aims and approach’ is corrected into: ‘Mantle-related surface uplift and fault activity’

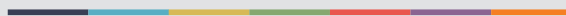
At the end of the Contents list, I have added the words ‘Paper 1’, ‘Paper 2’, and ‘Paper 3’ to the headings of the Appendix I, II and III in order to make clear which papers these appendices belong to.

Pages 41-130 In Chapters 3 and 4 (the published articles), figures and (sub-)section numbers have been modified in order to have the numbering consistent with the remaining part of the thesis. For instance, instead of Figs. 1,2,3,... (Journal numbering format) the figures in these chapters have now become: Figs. 3.1, 3.2, 3.3, etc. and Figs. 4.1, 4.2, 4.3, etc., in Chapters 3 and 4, respectively.

Across the full document: To some of the figure captions, the words ‘(shown on previous page)’ or ‘(shown on next page)’ have been added in case the figure caption didn't fit on the same page as the figure itself.



Graphic design: Communication Division, UIB / Print: Skjipes Kommunikasjon AS



uib.no

ISBN: 9788230867235 (print)
9788230849323 (PDF)